Universität Stuttgart

Quantum Simulator for Spin-Orbital Magnetism

Von der Fakultät Mathematik und Physik der Universität Stuttgart zur Erlangung der Würde eines Doktors der Naturwissenschaften (Dr. rer. nat.) genehmigte Abhandlung.

vorgelegt von

Adam Bühler

aus Stuttgart-Bad Cannstatt

Hauptberichter:	Prof. Dr. H. P. Büchler
Mitberichter:	Prof. Dr. G. Wunner
Prüfungsvorsitz:	Prof. Dr. T. Pfau

Tag der mündlichen Prüfung: 03.02.2016

Institut für Theoretische Physik III

Universität Stuttgart

2015

Abstract

In this dissertation we focus on many-body phenomena on a quantum level. In particular fermionic quantum gases in a temperature regime approaching absolute zero. Ultracold quantum gases have proven to be a versatile framework for Theorists and Experimentalists to probe many-body quantum mechanics. They also serve to quantum simulate solid state problems in a clean and controllable environment. The use of optical lattices include the advantage of tuning the required lattice structure nearly at will and lack the experimental shortcomings compared to the solid state, like the presence of lattice dislocations. The relevant lattice parameters can be easily tuned without changing the setup. In recent years many goals within theory and experiments of ultracold quantum gases in optical lattices were achieved. This emphasizes the significance of ongoing research with ultracold quantum gases on optical lattices.

We present two aspects of modern theory of ultracold quantum gases in optical lattices. On the one hand, we implement orbital physics in a setup of optical lattices and on the other, we find elusive Majorana fermions in a setup with ultracold fermionic gases. Both aspects are well-known in solid state systems, but did not make the step towards ultracold quantum gases so far. We propose and investigate setups to quantum simulate these challenges in the framework of optical lattices.

The first part of this work concerns the implementation of orbital physics in optical lattices. The orbital structure of atoms reveals novel phenomena in solid state systems. This raises the interest in creating optical lattice systems exhibiting analog behavior, as dictated by the orbitals in the solid state. We derive the microscopic Hamiltonian for a p-orbital system and investigate it in detail. For this Hamiltonian we perform a mean-field treatment and discover novel phase transitions including a possible tricritical point. In the analysis of the strong coupling regime we find an additional phase transition towards an antiferromagnet and then extend the mean-field phase diagram. Concluding the investigations is a proposal of an experimental setup to achieve orbital physics with state-of-the-art experimental tools.

The second part of this work considers Majorana modes and p-wave superfluids. Majorana modes are not only present in high-energy physics, but also in

condensed matter systems. Here we demonstrate a setup in order to simulate Majorana modes and p-wave superfluids in optical lattices. We derive an effective Hamiltonian and investigate it on a mean-field level as well as give the mean-field phase diagram. It contains a rich manifold of different p-wave phases. In addition, we extend our investigations to topological properties of our system and provide the topological phase diagram. We discover the special phenomena that the mean-field and topological phase transitions are decoupled in our system. The proposed system is suited to have Majorana modes at vortices and dislocations, which are injected into the system in controllable experimental manner. We conclude the considerations by giving a protocol for braiding in order to demonstrate non-Abelian statistics of Majorana modes.

Zusammenfassung

In dieser Dissertation konzentrieren wir uns auf Vielteilchenphänomene auf der Quantenebene. Im Besonderen auf fermionische Quantengase in der Nähe des absoluten Nullpunktes. Ultrakalte Quantengase haben bewiesen ein vielseitiger Rahmen für Theoretiker und Experimentatoren zu sein, um Vielteilchen-Quantenmechanik zu testen als auch darzulegen. Ebenso dienen sie dazu Probleme der Festkörperphysik in einer sauberen und kontrollierbaren Umgebung auf der Quantenebene zu simulieren. Die Verwendung von optischen Gittern hat den Vorteil, die benötigten Gitterstrukturen fast nach belieben einzustellen. Ihnen fehlen die experimentellen Mängel im Vergleich zur Festkörperphysik, wie beispielsweise das Vorhandensein von Gitterfehlstellen. Ohne einen Aufbau zu wechseln können relevante Gitterparameter leicht geändert werden. In den letzten Jahren haben ultrakalte Quantengase in optischen Gittern viele Ziele erreicht. Dies betont die Wichtigkeit weiterhin Forschung mit ultrakalten Quantengasen in optischen Gittern fortzuführen.
Wir stellen zwei Aspekte moderner Theorie ultrakalter Quantengase in optischen Gittern vor. Einerseits implementieren wir Orbitalphysik in einen Aufbau optischer Gitter und andererseits finden wir schwer fassbare Majorana Fermionen in einem Aufbau mit ultrakalten fermionischen Gasen. Beide Aspekte sind wohlbekannt in Festkörpersystemen, haben jedoch seither nicht den erfolgreichen Schritt in Richtung ultrakalter Quantengase geschafft. Wir schlagen Systeme vor, um diese Herausforderungen im Rahmen von optischen Gittern auf einer Quantenebene zu simulieren und untersuchen diese.
Der erste Teil dieser Arbeit behandelt die Implementierung orbitaler Physik in optischen Gittern. Die orbitale Struktur der Atome eröffnet neuartige Phänomene in Festkörpersystemen. Dies steigert das Interesse Systeme optischer Gitter zu erzeugen, die ein vergleichbares Verhalten besitzen, wie es durch die Orbitale im Festkörper vorgegeben wird. Wir leiten den mikroskopischen Hamiltonian für ein System mit p-Orbitalen her, um Orbitalphysik in optischen Gittern im Detail zu untersuchen. Weiter führen wir eine Mean-Field-Behandlung durch und entdecken dabei neuartige Phasenübergänge mit einem möglichen trikritischen Punkt. Mittels der Analyse des stark wechselwirkenden Bereichs finden wir einen weiteren Phasenübergang zum Antiferromagnet und erweitern

damit das Mean-Field-Phasendiagramm. Die Untersuchungen schließen wir mit einem Vorschlag eines experimentellen Aufbaus ab, um Orbitalphysik mittels modernster experimenteller Techniken zu erreichen.
Der zweite Teil dieser Arbeit behandelt Majorana Moden und p-Wellen Supraflüssigkeiten. Majorana Moden gibt es nicht nur in der Hochenergiephysik, sondern können auch in Systemen kondensierter Materie simuliert werden. Wir legen hier einen Aufbau dar, um Majorana Moden und p-Wellen Supraflüssigkeiten zu simulieren. Wir leiten einen effektiven Hamiltonian her und untersuchen ihn auf einer Mean-Field-Ebene. Ebenfalls geben wir das Mean-Field-Phasendiagramm an. Es beinhaltet ein reiches Angebot an verschiedenen p-Wellen Phasen. Zusätzlich erweitern wir unsere Untersuchungen auf topologische Eigenschaften unseres Systems und liefern das topologische Phasendiagramm. Dabei entdecken wir das besondere Phänomen, dass in unserem System die Mean-Field- und topologischen Phasenübergänge entkoppelt sind. Das vorgeschlagene System eignet sich um Majorana Moden an Vortices und Gitterfehlstellen zu bekommen. Die Gitterfehlstellen werden auf kontrollierbare experimentelle Weise in das System gebracht. Wir schließen unsere Betrachtungen durch eine Vorschrift um nicht-Abelsche Statistik der Majorana Moden nachzuweisen.

CONTENTS

LIST OF FIGURES

CHAPTER

ONE

INTRODUCTION

Solid state research is essential in modern physics and reveals novel as well as interesting phenomena. Especially magnetism in metals engages physicists since many years [1, 2]: Properties like ferromagnetism [3–8], diamagnetism [9] and antiferromagnetism [10, 11]. Intense research went into the theoretical understanding and classifications of magnetic structures [12–14]. A challenging task is the theoretical description of these discoveries, e.g. the antiferromagnetic order within some solids [15] via the superexchange mechanism [16, 17]. Especially the introduction by J. Hubbard [18] of a simple model describing electrons in the tight-binding limit in metals revolutionized the description of a large class of solids. A major success of this Hamiltonian was the prediction of phase transitions, like the superfluid to Mott Insulator transition essential in metals [19]. In recent years the orbital structure of solid state systems becomes more important leading to novel orbital orderings [20] and exotic phases [21]. Up to now, many of these phenomena are not yet fully understood [22, 23] and demand for an definitive answer, for example high-temperature superconductivity [24–26].

At the turn of the millennium an idea was proposed, implementing the Hubbard model for a gas of ultracold bosons into a controllable environment, namely optical lattices [27, 28]. Shortly after this proposal the prime example of phase transitions in solids, the superfluid to Mott Insulator transition, was experimentally achieved for ultracold bosons in an optical lattice setup [29].

This was the first major step of quantum simulating solid state problems in a controllable setup of optical lattices [30]. Furthermore, the first steps towards ultracold gases of fermions were proposed [31] in order to set up an actual quantum simulator for solid state problems. As in metals, the Hubbard model was also implemented in an optical lattice framework [32]. More and more solid state properties, known from previous investigations in metals, became accessible in optical lattices: including the Fermi surface [33], antibunching of fermions [34], even pairing of fermions and superfluidity [35]. Recently even the Mott Insulator phase transition was revealed in optical lattices [36–38]. The goals for theory and experiments are currently simulating magnetic properties within ultracold gases in optical lattices, such as ferromagnetism [39, 40] and the superexchange mechanism [41, 42], relevant to antiferromagnetism in optical lattices [43–50]. These pioneering experiments show that ultracold fermionic gases indeed are able to quantum simulate magnetic behavior in optical lattice setups [51–54].

Ultracold fermions in optical lattices demonstrated to be a framework in order to quantum simulate the solid state in a controllable experimental environment. In this work we take this framework to a new level and investigate two different branches for fermions in optical lattices. On the one hand we start to bridge the – still open – gap of orbital physics within optical lattices and on the other we explore a path towards quantum simulating a setup delivering Majorana modes and p-wave superfluids in an optical lattice system.

In the first part of this work we explain how orbital physics can be implemented into the framework of optical lattices. Previous work was so far restricted to s-orbital systems. The orbital structure of atoms is essential for novel mechanisms in solid state systems. Here we propose a setup for p-orbital physics as a first step towards the goal of simulating d-orbital problems in an optical lattice. In the investigation we discover interesting mechanisms as well as novel phase transitions. Hereby we pave the path towards the possible realization of orbital physics in ultracold fermionic gases.

In the second part of this work we focus on another novelty of solid state systems, namely Majorana modes. We design an optical lattice setup revealing p-wave superfluids as well as Majorana modes at vortices and lattice dislocations. In our investigation we discover that the mean-field and topological phase

transitions are decoupled. In addition, our setup can be used to implement a braiding protocol to demonstrate non-Abelian statistics of Majorana modes. Creating and detecting Majorana fermions is essential for a reliable quantum register and thus quantum computer.
This work is structured as follows: In chapter 2 we briefly present the general concepts of this work. Chapter 3 gives the in-depth analysis of the implementation of orbital physics in an optical lattice setup. The investigations regarding the Majorana modes in the fermionic p-wave system is given in chapter 4. Supplementary material to the individual chapters are presented in the appendix.

CHAPTER

TWO

GENERAL CONCEPTS

The general concepts consider the rudimentary basics for the following chapters in a brief manner. For each topic we give additional references for further reading. Section 2.4 is presented in more detail since the two main chapters rely on this concept.

2.1. Optical Lattices

Optical lattices are frequently used in experiments with ultracold gases to trap neutral atoms [55]. They are created by counter propagating a set of lasers to create the required lattice structure, see fig. 2.1. A set of two counter propagating lasers create a structure, which directly relates to a one-dimensional lattice. If an additional pair of counter propagating lasers is set perpendicular to the previous setup, the resulting structure reveals a two-dimensional lattice system. In this work we focus on two-dimensional setups. For the common experimental setup, every lattice site is positive of the created two-dimensional lattice, see fig. 2.2a) [30]. We refer to this configuration as *positive optical lattice*. If an additional set of Raman lasers is used, a modulation of the sign for each lattice site is achieved, as proposed in [57]. Here every other lattice site is negative and we will refer to this as *negative optical lattice*, see fig. 2.2b) for an illustration. For details regarding optical lattices see [30, 56].

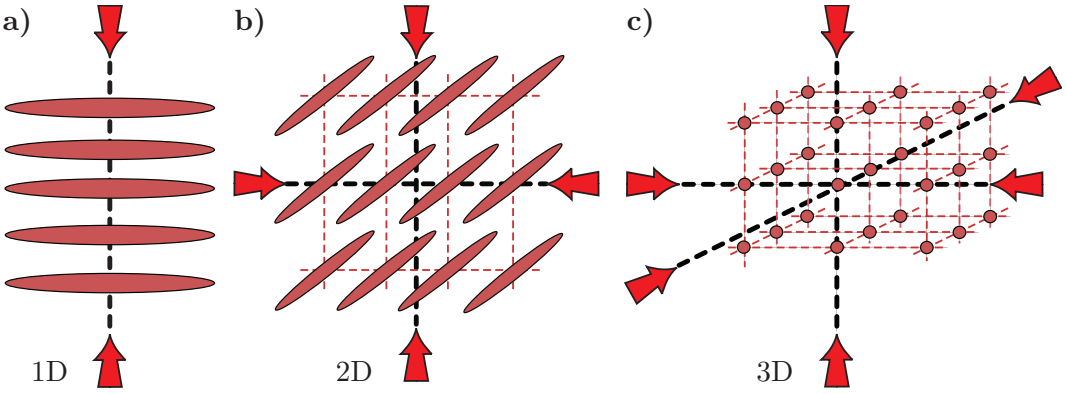

Fig. 2.1 Counter propagating lasers produce a landscape of different possible optical lattices. **a)** Two lasers create a one-dimensional lattice. **b)** Four lasers (two counter propagating and the other two perpendicular) produce an array of two-dimensional tubes. Here a two-dimensional plane can be created, thus a two-dimensional lattice. **c)** Six counter propagating lasers result in a three-dimensional lattice. For additional details see [30, 53, 56].

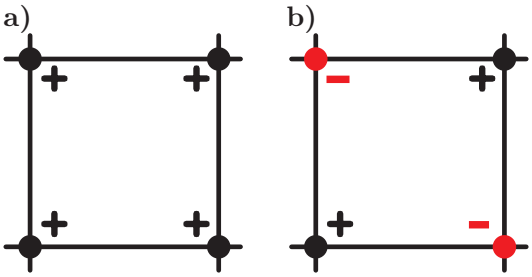

Fig. 2.2 Two-dimensional square lattice, created by two sets of counter propagating laser pairs. **a)** Positive optical lattice. **b)** Negative optical lattice, where every other site is negative.

2.2. Alkaline-Earth Atoms and Magic Wavelength

Atoms located in the second group of the periodic table of elements are named alkaline-earth metals, see fig. A.1. They have a closed s-wave orbital shell and fermionic as well as bosonic isotopes. The special feature characterizing alkaline-earth atoms is the highly forbidden transition between the $^1S_0$ ground state and the $^3P_0$ excited state, see fig. 2.3. This transition is called *optical clock transition* [58], it can be measured with high precision [59–62] and is used for a wide range of setups including as an application for state-insensitive light

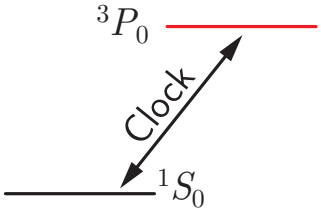

Fig. 2.3 Simplified illustration of the clock transition of alkaline-earth atoms between the $^1S_0$ ground state and the $^3P_0$ excited state.

traps [63], measuring density-dependent collisional frequency shifts [64], optical tuning of the scattering length [65] and more [66–68]. For further reading regarding selection rules and forbidden transitions see [69–72].
If the alkaline-earth atoms are trapped in an optical lattice [58, 73], the transition frequency ν for atoms in the $^1S_0$ ground state to the $^3P_0$ excited state is given by

$$\nu(\lambda_L, \mathbf{e}_L) = \nu_0 + \nu_{ac} \approx \nu_0 - \frac{\Delta\alpha(\lambda_L, \mathbf{e}_L)}{2\varepsilon_0 ch} I + \mathcal{O}\big(I^2\big) \ , \tag{2.1}$$

where ν_0 is the unperturbed transition frequency, ν_{ac} the ac Stark shift due to the perturbation of the lasers [71], ε_0 is the permittivity of free space, c the speed of light, h Planck's constant, $\mathbf{e}_L$ the polarization vector and I is the lattice laser intensity. The difference between the ac polarizabilities of the upper (excited) and lower (ground) state is

$$\Delta\alpha(\lambda_L, \mathbf{e}_L) = \alpha_u(\lambda_L, \mathbf{e}_L) - \alpha_l(\lambda_L, \mathbf{e}_L) \ , \tag{2.2}$$

and depends on the polarization vector as well as the lattice laser wavelength λ_L. The goal is to set the difference $\Delta\alpha(\lambda_L, \mathbf{e}_L)$ to zero, in order to transfer the ground state atoms to the excited state with the unperturbed transition frequency ν_0 and have the transition to be independent of the lattice laser intensity I. This is achieved by adjusting the polarization vector and setting the laser wavelength to the *magic wavelength* λ_m [58, 73, 74], where $\Delta\alpha(\lambda_m, \mathbf{e}_L) = 0$ can be achieved. Thus, if the lattice laser is set to match the magic wavelength, a second laser can be used to excite atoms through the forbidden transition into the meta-stable $^3P_0$ state. This state decays slowly with a finite lifetime of $\Gamma_0^{-1} \approx 150\,\mathrm{s}$ [73]. Commonly used for experiments are Strontium $^{87,88}Sr$, Ytterbium ^{171}Yb and Calcium ^{43}Ca. A possible candidate is also Mercury ^{199}Hg [58, 73].

The discovery of the magic wavelength mechanism opened up a new road of experiments and theoretical calculations, like implementing a many-body spin system in an optical lattice clock [75], quantum computing with alkaline-earth atoms [76] or the application of alkaline-earth atoms as quantum registers [77]. Experimentally it was even possible to cancel the cold-collision-shift and inelastic scattering in optical clock setups [78], determine the nuclear spin effects [79] and even suppress the collisional shifts in lattice clocks [80]. Theoretically many-body treatments were applied to the collisional frequency shifts in alkaline-earth system [81]. The next major step was achieved, by implementing SU(N) symmetric models with a setup of alkaline-earth atoms [82–84].
On the other hand, it is also possible to tune the polarizabilities to match the *anti-magic wavelength* λ_{am}, such that the polarizabilities are opposite for the ground and excited state, leading to off-resonant lattices [85–87].

2.3. Hubbard Model

In 1963 J. Hubbard introduced a simple model to describe fermions on a lattice in a solid [18]. The Hamiltonian reads

$$\mathrm{H} = -\sum_{\langle i,j\rangle,s} t_{ij}\, c^{\dagger}_{js} c_{is} + U \sum_{i} n_{i\uparrow} n_{i\downarrow} - \mu \sum_{i} n_i \,, \tag{2.3}$$

where the summation runs over all lattice sites i and nearest neighbors j of our two-dimensional systems, t_{ij} is the hopping amplitude for the fermions between sites i and j, $c^{(\dagger)}_{i,s}$ is the annihilation (creation) operator for a fermion with spin $s =\uparrow,\downarrow$. Note, it is also possible to adapt the Hubbard Hamiltonian for bosons, then the it is called *Bose-Hubbard Hamiltonian* [27]. The on-site interaction is U, the chemical potential μ and the particle number operator is n_i. Even though this Hamiltonian has a simple form, it nevertheless describes the principle mechanisms of fermions on a lattice. For vanishing interaction $U = 0$, the system is in a Fermi liquid state, where the fermions are delocalized over the whole lattice. On the other hand, for vanishing hopping $t = 0$, the fermions are localized and thus are in a Mott insulating state [88, 89]. The phase transition between the Fermi liquid and Mott Insulator is subject of intense research over the last years [19]. Despite its simple form, the Hubbard

Hamiltonian incorporates interesting physics [90, 91] and serves as starting point for many approaches and problems in the solid state framework [92, 93]. In addition, the Hubbard Hamiltonian also describes the basic mechanisms of bosons [27, 28, 41, 94] and fermions [32, 33, 44, 53, 95–99] in optical lattices.

Quantum Phase Transitions

Phase transitions play an important role in all areas of physics. For classical phase transitions, temperature is a crucial quantity and serves as a control parameter to drive the transitions. Thus, *thermal* fluctuations are omnipresent [19, 23, 100–102]. On the other hand, for quantum phase transitions, the temperature is zero, i.e. $T = 0$, such that fluctuations are solely due to *quantum* fluctuations. Here the order parameters for the phase transitions are independent of temperature. Relevant tuning parameters can be the interaction strength among the considered atoms, a magnetic field, external pressure etc. A prominent example of a quantum phase transition is the superfluid to Mott Insulator transition in an optical lattice [29, 35, 36, 38]. For further reading regarding quantum phase transitions, see [22, 30, 56, 103, 104].

2.4. Strong Coupling Limit and Schrieffer-Wolff Transformation

The Hubbard model describes the mechanisms of fermions on a lattice. In the limit for vanishing hopping ($t = 0$) or interaction ($U = 0$), the evaluation of the ground state properties is straightforward [18, 91, 105]. If the parameter regimes becomes comparable ($t \sim U$) the situation changes and the analysis becomes challenging [19, 88].
The question now arises, if and how the Hubbard model can describe the strong coupling limit ($U \gg t$) and the ground state in this limit. We therefore investigate the strong coupling limit and derive the corresponding Hamiltonian. We start from the previously introduced Hubbard Hamiltonian (2.3) with

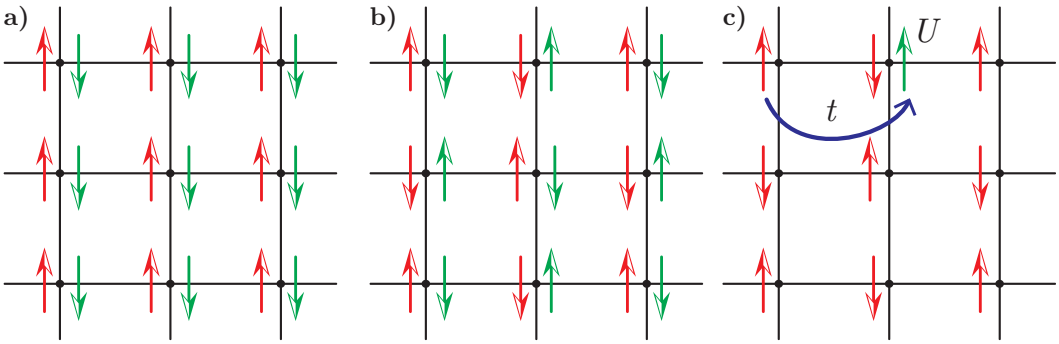

Fig. 2.4 Possible ground state configurations in the strong coupling limit. Two possible configurations are given in red and green. **a)** Ferromagnetic configuration: either every site on the lattice is spin up or down. **b)** Antiferromagnetic order: every other site up and down, respectively. **c)** Hopping process in the antiferromagnetic configuration resulting in an energy penalty $U \gg t$. Further details are given in the text.

vanishing chemical potential ($\mu = 0$)

$$\mathrm{H} = -\sum_{\langle i,j\rangle,s} t_{ij}\, c^{\dagger}_{js} c_{is} + U \sum_{i} n_{i\uparrow} n_{i\downarrow}\,, \tag{2.4}$$

where the summations are over all lattice sites i and nearest neighbors j, where s is the spin, t_{ij} the hopping strengths between sites i and j, U the on-site interaction strength, $c^{(\dagger)}_{is}$ the annihilation (creation) operator and n_{is} the particle number operator. In the strong coupling limit, the kinetic part of the Hubbard Hamiltonian is a weak perturbation to the system. To derive an effective Hamiltonian, we first have to specify the system. We consider a square lattice with lattice spacing a and sites $N \gg 1$. For vanishing hopping, the ground state of the system is obtained when the interaction energy vanishes. At half-filling, there is always one fermion per site with either spin up or down, since both cases have in the same energy. This freedom results in a large degeneracy for the ground state of 2^N possibilities with general form

$$|\psi_i\rangle = c^{\dagger}_{i\uparrow}\,|0\rangle \qquad \text{or} \qquad |\psi_i\rangle = c^{\dagger}_{i\downarrow}\,|0\rangle\,. \tag{2.5}$$

In fig. 2.4 we give illustrations for the different possible ground state configu-

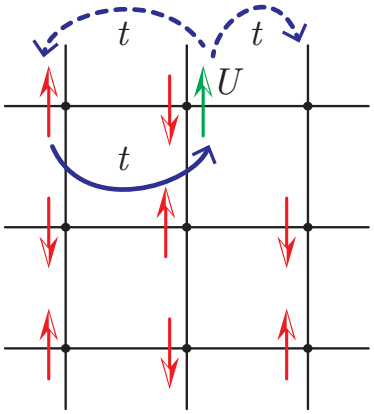

Fig. 2.5 Second order hopping process where the first process produces an energy penalty U and the second process again leaves only one fermion per site. The second process can either lead back to the initial site or to a neighboring site. Further details are given in the text.

rations and the resulting degeneracy with respect to the Hubbard Hamiltonian in the $t = 0$ case. If we allow weak hopping, the ferromagnetic configuration in fig. 2.4a) prohibits hopping due to the Pauli principle. Here hopping can only be induced via hole doping or spin flip processes. On the other hand, in the antiferromagnetic case of fig. 2.4b) nearest neighbor hopping processes are possible, although here the hopping results in an on-site interaction U and thus hopping is penalized by $U \gg t$, see fig. 2.4c). The question then is, how this energy penalty can be circumvented. This is only possible if the initial and final state again only has one fermion per site. Thus, the single fermion in the final state avoids the interaction energy U. This process is of second order, since there are two hopping processes involved, see fig. 2.5. These second order processes are of a virtual nature, since actual hopping of fermions would result in a large energy penalty $U \gg t$. The virtual hopping process reduces the energy of the system and thus reveals the nature of the ground state in the strong coupling limit. The next step is to derive the Hamiltonian in the strong coupling limit describing the virtual processes.

To derive a Hamiltonian, which solely describes virtual second order and no first order processes, we have to perform a canonical transformation also known as *Schrieffer-Wolff transformation* [106–109], a mathematical review can be found in [110]. This canonical transformation is commonly used in strong coupling approaches. The prominent example is the $t - J$ model, the strong coupling limit of the Hubbard model [105, 111–118].

In the strong coupling limit we are interested in double-occupied lattice sites.

Double-occupancies set the energy scale of the system. Each double-occupancy contributes an interaction energy of U. Therefore we decompose the total Hilbert space $\mathcal{H}$ into a direct sum of the Hilbert spaces of double-occupied sites

$$\mathcal{H} = \mathcal{H}_0 \oplus \mathcal{H}_1 \oplus \ldots \oplus \mathcal{H}_N \,, \tag{2.6}$$

where the index m of $\mathcal{H}$ gives the number of double-occupied sites. Next, we consider the involved states and how the projectors P_m act on them. The projectors project onto corresponding double-occupied state and annihilate the remaining states. We denote the total state as $|\psi\rangle$ and by $|\psi_m\rangle$ all the states having m double-occupied sites such that

$$|\psi\rangle = \sum_{m=0}^{N} |\psi_m\rangle \,, \quad P_m\,|\psi\rangle = |\psi_m\rangle \,, \quad \text{and} \quad |\psi_m\rangle \in \mathcal{H}_m \,. \tag{2.7}$$

Note that the projectors have the property $P_m^2 = P_m$. The projected Hubbard Hamiltonian (2.4) operating in the subspaces is

$$\mathrm{H} = \sum_{m=0}^{N-1} [P_m\,\mathrm{H}\,P_m + P_m\,\mathrm{H}\,P_{m+1} + P_{m+1}\,\mathrm{H}\,P_m] + P_N\,\mathrm{H}\,P_N \,. \tag{2.8}$$

Here we follow the approach given in [105, 111]. We modify this approach with respect to the possible double-occupancies and only consider the projectors P_0, P_1 and P_2. This simplification is justified, since in our later work - section 3.5 and section 4.2.3 - we only consider systems with such configurations.
After the projection onto the different subspaces we expand the Hamiltonian perturbatively

$$\mathrm{H}_\varepsilon := \mathrm{H}_0 + \varepsilon\,\mathrm{H}_1 + \varepsilon^2\,\mathrm{H}_2 \,, \tag{2.9}$$

where ε is the small dimensionless perturbation parameter and serves to collect the different orders in ε. The unperturbed part of the Hamiltonian is

$$\mathrm{H}_0 := P_0\,\mathrm{H}\,P_0 + P_1\,\mathrm{H}\,P_1 + P_2\,\mathrm{H}\,P_2 \,. \tag{2.10}$$

The first H_1 and second H_2 order perturbation is

$$\mathrm{H}_1 := P_0\,\mathrm{H}\,P_1 + P_1\,\mathrm{H}\,P_0 \,, \quad \mathrm{H}_2 := P_1\,\mathrm{H}\,P_2 + P_2\,\mathrm{H}\,P_1 \,, \tag{2.11}$$

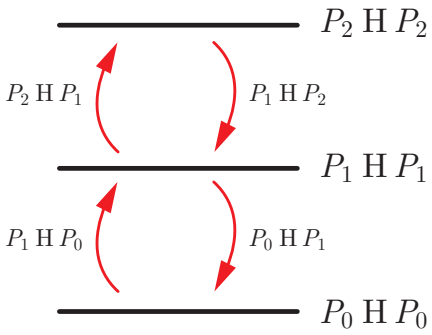

Fig. 2.6 Different processes as described by the expanded Hamiltonian (2.9), the unperturbed part (2.10), the first and second order processes (2.11).

and H is the initial Hamiltonian of interest. The Hamiltonian $P_0\,\mathrm{H}\,P_0$ provides an energy contribution of the order of the hopping amplitude $\sim t_{ij}$, where $P_1\,\mathrm{H}\,P_1$ provides an energy of the order of the interaction strength $\sim U$ and $P_2\,\mathrm{H}\,P_2$ of $\sim 2U$, with respect to $P_0\,\mathrm{H}\,P_0$. This energy scale is much larger than the hopping amplitude. In fig. 2.6 we give an illustration of the different processes.

To transform the Hamiltonian H_ε into a form which gets rid of the first order processes and only contains second order virtual ones, we introduce an unitary transformation

$$U = e^{-i\varepsilon S}\,, \tag{2.12}$$

in order to transform the expanded Hamiltonian as

$$\tilde{\mathrm{H}} := U\,\mathrm{H}_\varepsilon\,U^\dagger = e^{-i\varepsilon S}\,\mathrm{H}_\varepsilon\,e^{i\varepsilon S}\,, \tag{2.13}$$

where S is the generator with $S = S^\dagger$. The central idea of the generator S is to find a condition, such that the first order processes can be eliminated from the projected Hamiltonian. The goal thus is to only have processes of the form $P_0\,\mathrm{H}\,P_0$ and $P_0\,\mathrm{H}\,\ldots\,\mathrm{H}\,P_0$.

Next, we expand the two exponentials up to second order

$$e^{\mp i\varepsilon S} = 1 \mp i\varepsilon S + \frac{(\mp i\varepsilon S)^2}{2} + \ldots \approx 1 \mp i\varepsilon S - \frac{1}{2}\,\varepsilon^2 S^2\,. \tag{2.14}$$

Now we insert the expanded functions into Hamiltonian $\tilde{\mathrm{H}}$ (2.13) and obtain

$$\begin{aligned}\tilde{\mathrm{H}} &= \left(1 - i\varepsilon S - \frac{1}{2}\,\varepsilon^2 S^2\right)\,\mathrm{H}_\varepsilon\,\left(1 + i\varepsilon S - \frac{1}{2}\,\varepsilon^2 S^2\right) \\ &= \left(1 - i\varepsilon S - \frac{1}{2}\,\varepsilon^2 S^2\right)\left(\mathrm{H}_0 + \varepsilon\,\mathrm{H}_1 + \varepsilon^2\,\mathrm{H}_2\right)\left(1 + i\varepsilon S - \frac{1}{2}\,\varepsilon^2 S^2\right).\end{aligned} \tag{2.15}$$

We sort the expanded equation in orders of the perturbation parameter ε and neglect all higher contributions than second order. The remaining orders of ε can be brought into the form

$$\begin{aligned}\tilde{\mathrm{H}} &= \mathrm{H}_0 + \varepsilon\,\left(\mathrm{H}_1 + i\,[\mathrm{H}_0, S]\right) + i\varepsilon^2\,[\mathrm{H}_1, S] \\ &\qquad + \frac{\varepsilon^2}{2}\,\left(-\mathrm{H}_0\,S^2 + 2S\,\mathrm{H}_0\,S - S^2\,\mathrm{H}_0\right) + \varepsilon^2\,\mathrm{H}_2 \\ &= \mathrm{H}_0 + \varepsilon\,\left(\mathrm{H}_1 + i\,[\mathrm{H}_0, S]\right) + \frac{\varepsilon^2}{2}\,\left(2i\,[\mathrm{H}_1, S] - [[\mathrm{H}_0, S], S] + 2\mathrm{H}_2\right),\end{aligned} \tag{2.16}$$

where $[\mathrm{H}_0, S] = \mathrm{H}_0\,S - S\,\mathrm{H}_0$ denotes the commutator relation. To get rid of the first order processes, we directly find that

$$\mathrm{H}_1 + i\,[\mathrm{H}_0, S] \stackrel{!}{=} 0\,, \quad \Rightarrow \quad [\mathrm{H}_0, S] = i\mathrm{H}_1\,. \tag{2.17}$$

Here it important to stress, that now we have computed a condition for the generator S. Fulfilling this condition via the correct derivation of S, cancels the first order processes, as intended at the beginning.
Inserting the condition (2.17) into the perturbed Hamiltonian (2.16) then reveals the transformed Hamiltonian

$$\tilde{\mathrm{H}} = \mathrm{H}_0 + \frac{\varepsilon^2}{2}\,\left(i\,[\mathrm{H}_1, S] + 2\mathrm{H}_2\right)\,. \tag{2.18}$$

It solely consists of zero and second order processes. The next task is to determine the generator S, such that $[\mathrm{H}_1, S]$ describes virtual second order processes. The additional Hamiltonian H_2 describes real second order processes, i.e. no virtual second processes. In the following we are only interested in the lowest possible energy scale and hence neglect H_2, since here the energy contribution is of the order of $\sim 2U$ with respect to $P_0\,\mathrm{H}\,P_0$. At this point

we set the perturbation parameter to one, $\varepsilon = 1$, because we performed the required sorting of the different perturbative contributions.
We thus derive the generator S. The details are found in [111, 114]. We project the condition (2.17) onto the Hilbert subspaces using the general projectors P_μ and P_ν

$$P_\mu \,\mathrm{H}\, P_\nu \,(1-\delta_{\mu,\nu}) + i P_\mu \,\mathrm{H}\, P_\mu \,(P_\mu \,S\, P_\nu) - i\,(P_\mu \,S\, P_\nu)\; P_\nu \,\mathrm{H}\, P_\nu = 0\,. \tag{2.19}$$

In the case for $\mu = \nu$, the above equation directly yields

$$P_\mu \,\mathrm{H}\, P_\mu \,(P_\mu \,S\, P_\mu) = (P_\mu \,S\, P_\mu)\, P_\mu \,\mathrm{H}\, P_\mu \;\Rightarrow P_\mu \,S\, P_\mu = \gamma P_\mu\,, \tag{2.20}$$

with γ being an arbitrary constant. On the other hand, for $\mu \neq \nu$ we have

$$P_\mu \,\mathrm{H}\, P_\mu \,(P_\mu \,S\, P_\nu) - (P_\mu \,S\, P_\nu)\, P_\nu \,\mathrm{H}\, P_\nu = i P_\mu \,\mathrm{H}\, P_\nu\,. \tag{2.21}$$

Adapting the obtained expression for the generator S to our scenario, we find

$$P_0 \,S\, P_1 = -i\,\frac{P_0 \,\mathrm{H}\, P_1}{P_1 \,\mathrm{H}\, P_1 - P_0 \,\mathrm{H}\, P_0} \quad \text{and} \quad P_1 \,S\, P_0 = i\,\frac{P_1 \,\mathrm{H}\, P_0}{P_1 \,\mathrm{H}\, P_1 - P_0 \,\mathrm{H}\, P_0}\,. \tag{2.22}$$

Inserted into eq. (2.18) we find for the transformed Hamiltonian $\tilde{\mathrm{H}}$ the relation

$$\tilde{\mathrm{H}} = P_0 \,\tilde{\mathrm{H}}\, P_0\,, \quad \text{with} \quad P_0 \,\tilde{\mathrm{H}}\, P_0 = P_0 \,\mathrm{H}\, P_0 - P_0 \,\mathrm{H}\, P_1 \,\mathrm{H}\, P_0 \; U^{-1}\,. \tag{2.23}$$

The main task within the degenerate perturbation theory is to find the explicit form of the expression $P_0 \,\mathrm{H}\, P_1 \,\mathrm{H}\, P_0$. For details regarding the derivation of the canonical transformed Hamiltonian see [105, 107–109, 111, 114, 117, 118].
In Dirac notation, we can derive the matrix elements of the generator S as

$$\langle m|S|n\rangle = i\,\frac{\langle m|\mathrm{H}_1|n\rangle}{E_m - E_n}\,, \tag{2.24}$$

where $\{|n\rangle, |\tilde{n}\rangle\}$ being many-body eigenstates of H_0 and $|m\rangle$ are the virtual intermediate states. The corresponding energies are $E_n, E_{\tilde{n}}, E_m$. The transformed Hamiltonian is

$$\tilde{\mathrm{H}} = \mathrm{H}_0 - \frac{1}{2}\sum_{m,n,\tilde{n}} |n\rangle\langle\tilde{n}|\,\langle n|\mathrm{H}_1|m\rangle\langle m|\mathrm{H}_1|\tilde{n}\rangle \left(\frac{1}{E_m - E_{\tilde{n}}} - \frac{1}{E_n - E_m}\right)\,. \tag{2.25}$$

For the energy denominators we know, that the energy of the initial and final state is of the order of t_{ij} and no interaction strength contribution is present. At the intermediate state there is one double-occupancy, resulting in an energy contribution of order $t_{ij} + U$. The energy difference thus reduces to

$$E_m - E_n \sim (t_{ij} + U) - t_{ij} = U\,, \tag{2.26}$$

and hence the denominator of eq. (2.23) for the virtual processes.

The $t - J$ Hamiltonian

After the canonical transformation, the Hubbard Hamiltonian (2.4) takes the form

$$\begin{aligned}
\mathrm{H}_{tJ} = &-P_0 \sum_{\langle i,j\rangle,s} t_{ij}\, c^\dagger_{js} c_{is}\, P_0 \\
&+ \sum_{\langle i,j\rangle} J_{ij} \left[\vec{S}_i \cdot \vec{S}_j - \frac{1}{4} \sum_{s,s'} n_{is}\,(1 - n_{i\bar{s}})\, n_{js'}\,(1 - n_{j\bar{s}'}) \right] \\
&+ \sum_{i,j,k,s} \frac{t_{ij}\, t_{jk}}{U} \Big[c^\dagger_{is}\,(1 - n_{i\bar{s}})\, n_{j\bar{s}}\,(1 - n_{js})\, c_{ks}\,(1 - n_{k\bar{s}}) \\
&\qquad\qquad - c^\dagger_{is}\,(1 - n_{i\bar{s}})\, \vec{S}_j^{-s}\, c_{k\bar{s}}\,(1 - n_{ks}) \Big]\,,
\end{aligned} \tag{2.27}$$

with $J_{ij} = 2t_{ij}^2/U$ and $\bar{s} \neq s$. This is the well-known $t - J$-model [111, 119], describing the strong coupling limit of the Hubbard model. In this form it also incorporates three-site processes only relevant away from half-filling, see fig. 2.7. Here $\vec{S}_i$ is the spin operator with components $\vec{S}_i = \left(c^\dagger_{i\uparrow} c_{i\downarrow}\,,\, c^\dagger_{i\downarrow} c_{i\uparrow}\,,\, \left(n_{i\uparrow} - n_{i\downarrow}\right)/2 \right)$, see [107, 108, 116, 120, 121]. In the case of half-filling and without the three-site terms, the kinetic part of the Hamiltonian H_{tJ} drops out and we obtain the well-known form

$$\mathrm{H}_{tJ} = \sum_{\langle i,j\rangle} \frac{2t_{ij}^2}{U} \left(\vec{S}_i \cdot \vec{S}_j - \frac{1}{4} \right)\,, \tag{2.28}$$

of the antiferromagnetic, isotropic Heisenberg model. The $t - J$ Hamiltonian describes the virtual processes within the antiferromagnetic ground state.

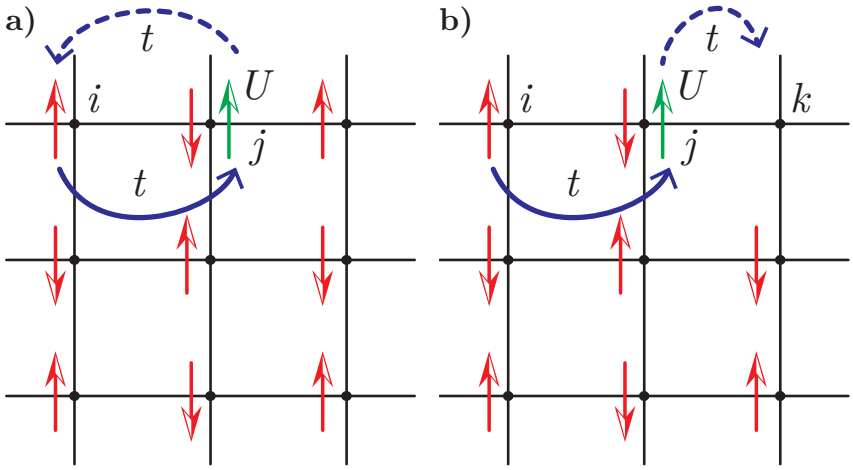

Fig. 2.7 Possible processes in the strong coupling regime of the Hubbard model, described by the $t - J$ model. **a)** Virtual two-site process, where the initial site equals the final site. **b)** Three-site process with initial site i, intermediate site j and final site k.

CHAPTER

THREE

QUANTUM SIMULATOR FOR SPIN-ORBITAL MAGNETISM

Cold gases experiments pave the way of understanding solid state problems better by designing setups, which simulate the basic mechanisms in the solid without having the problems of accessibility in an experiment. They have demonstrated key properties of solid state systems, but so far lacked achieving orbital physics in optical lattices. Orbitals provide interesting mechanisms and novel physics, especially d-orbitals. Here we propose a design in order to give the possibility of simulating p-orbitals within a cold gases experiment, as a first step towards d-orbitals, and investigate the phase diagram [122].

3.1. Introduction

Spin and orbital physics are essential in solid state systems and are the key ingredients for interesting and novel phenomena including exchange interactions in magnetic substances [123], the Jahn-Teller effect and magnetism [124], orbital physics in transition-metal oxides [125] and orbital order in Mott Insulators [126]. Observing these phenomena within an experiment is a challenging task, given the experimental restrictions.
Experiments with ultracold gases in optical lattices do not suffer restrictions like solid state experiments and they delivered promising results, see chapter 1.

Optical lattices made the transition to fermionic atoms to make a major step towards quantum simulating the solid state systems [36, 38] and even probe magnetic phase transitions [51], which makes optical lattice experiments an ideal testing ground for solid state physics.
This paved the way for the approach, how to implement orbital physics into optical lattice systems. Theoretical proposals suggested to use alkaline-earth atoms and their inherent meta-stable state to simulate orbital behavior [76, 82]. Recently it was shown, that alkaline-earth atoms indeed serve as candidates to simulate orbital physics [83, 84].
The next step is to actually use the optical lattice system to simulate p-orbital behavior in a convenient lattice system. For this task, there are several possibilities. Theoretical proposals suggested filling the lowest energy band to reach the higher p-band [127, 128]. Alternatively, ground state atoms can be excited into a higher meta-stable state, ideally in the p-band [129]. This has been theoretically analyzed in detail [130]. The excitation to the higher band can also be achieved by sweeping through a Feshbach resonance [33, 131]. These experiments then lead to intense theoretical calculations [132], and even a theoretical proposal to implement p-orbital physics for different optical lattice structures [133, 134]. Another scheme is to shake the optical lattice periodically to excite the atoms into the p-band [135–139]. Very recently a review of the progresses in orbital physics within optical lattices was published [140].

Another road is to engineer an optical lattice setup, where the physics of the p-orbitals can be intrinsically achieved through the lattice itself. Here we propose a lattice setup to simulate the behavior of p-orbitals. We use an anisotropic optical lattice system, which provides anisotropic hopping strengths for different directions within the lattice. The lattice system is filled with cold fermionic atoms having two spin states as well as a meta-stable excited state, e.g. alkaline-earth atoms. In addition, the system is sensitive to the internal states involved, see fig. 3.1. The fermionic atoms remain in the lowest Bloch band and can interact through the s-wave channel. For further details see the experimental proposal in section 3.7. The analysis even for this simple model reveals a rich phase diagram with interesting mechanisms. Our proposal is feasible with the current experimental techniques, circumvents the problems and shortcomings of previous approaches and delivers an testing playground,

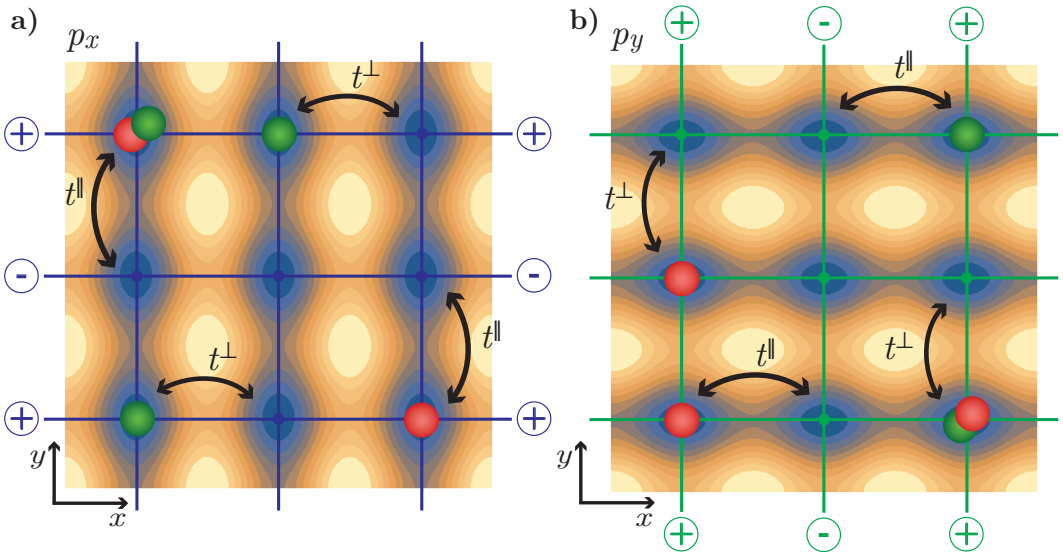

Fig. 3.1 Anisotropic bipartite two-dimensional optical lattice system with anisotropic hopping strengths $t^\parallel$ and $t^\perp$. The lattice system is sensitive to the internal states of the used alkaline-earth atoms. The lattice system is shifted out of plane for sake of visualization and each lattice is addressed to one internal state. The different colors of the cold fermionic atoms represent the different spin states $\uparrow, \downarrow$. **a)** Optical lattice configuration to simulate the mechanisms of the p_x-orbital, where **b)** is rotated by $\pi/4$ with respect to the previous optical lattice and used to simulate the p_y-orbital behavior. Further details are given in the text and see section 3.7 for an detailed description.

as well as a controllable environment, for orbital physics within optical lattices.

The next sections are structured as follows: In section 3.2 we give the Hamiltonian of our system and the basic setup we use throughout our investigations. We begin in section 3.3 with a preliminary analysis to find interesting features of our system, to then extend the investigation in section 3.4 to a mean-field analysis for all fillings and small temperature influences. Section 3.5 considers the strong coupling limit for the half-filling scenario in detail. A sketch of the phase diagram is given in section 3.6, whereas section 3.7 concludes the investigations by an experimental proposal. In section 3.8 we give an outlook and conclusion.

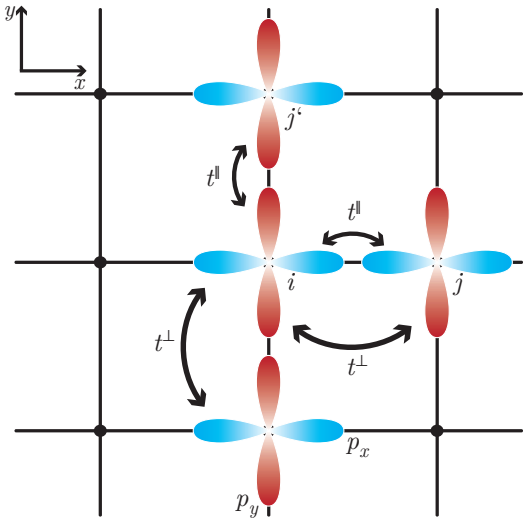

Fig. 3.2 Principle lattice setup to simulate with the optical lattice system. Two-dimensional square lattice, where each lattice site i holds a p_x- and p_y-orbital, indicated as blue and red, respectively. In addition, the possible hopping scenarios are given, the perpendicular $t^{\perp}$ and parallel hopping $t^{\parallel}$ with $t^{\parallel} > t^{\perp}$. For further details, see text.

3.2. Hamiltonian and Basic Setup

We start by giving the p-orbital lattice configuration that we simulate with the introduced optical lattice system. The lattice configuration is a two-dimensional square lattice, where each lattice site contains a p_x- and p_y-orbital. Each $p_{x,y}$-orbital can be occupied by a fermion with up or down spin $s = \uparrow, \downarrow$. There are two relevant hopping mechanisms throughout the lattice, the parallel hopping $t^{\parallel}$ and the perpendicular hopping $t^{\perp}$, see fig. 3.2. As in common solid state systems, the parallel hopping $t^{\parallel}$ is larger than the perpendicular hopping $t^{\perp}$. See the experimental proposal for the implementation of the p-orbital setup. The Hamiltonian for this setup is

$$\mathrm{H} = \mathrm{H}_{kin} + \mathrm{H}_{int}\,, \tag{3.1}$$

with the kinetic part H_{kin} and the interaction part H_{int}. A detailed derivation of Hamiltonian (3.1) is given in the appendix B.2.

3.2.1. Kinetic Hamiltonian

We begin our discussion with the kinetic part of Hamiltonian (3.1), which is

$$\mathrm{H}_{kin} = -\sum_{\alpha s}\Bigg\{ t^{\parallel} \sum_{\langle i,j\rangle_{\alpha}^{\parallel}} \left(c_{j\alpha s}^{\dagger} c_{i\alpha s} + \mathrm{h.c.} \right) + t^{\perp} \sum_{\langle i,j\rangle_{\alpha}^{\perp}} \left(c_{j\alpha s}^{\dagger} c_{i\alpha s} + \mathrm{h.c.} \right) + \mu \sum_{i} c_{i\alpha s}^{\dagger} c_{i\alpha s} \Bigg\}, \tag{3.2}$$

here the sums run over the orbitals $\alpha = p_x$, p_y, spins $s = \uparrow, \downarrow$, all lattice sites i and nearest neighbors j. The chemical potential is denoted by μ. The fermionic operator $c_{i\alpha s}^{(\dagger)}$ annihilates (creates) a fermion on lattice site i and orbital $\alpha = p_x\,, p_y$ with spin $s = \uparrow, \downarrow$. In the following we abbreviate the labeling of the orbitals $\alpha = p_x$, p_y by $\alpha = x$, y. To avoid confusion with vector components, we write vector components $\gamma = x$, y, z as exponents and the label for the corresponding orbitals α as indices on the quantities. Note that the sum of the nearest neighbors j crucially depends on the considered orbital α. For the parallel hopping components the summation index is $\langle i, j\rangle_{\alpha}^{\parallel}$. The nearest neighbor j for a p_x-orbital for parallel hopping is in x-direction, whereas it is in y-direction for a p_y-orbital. The perpendicular components are summed by $\langle i, j\rangle_{\alpha}^{\perp}$. Here the nearest neighbor j for the p_x-orbital is in y-direction and for the p_y-orbital in x-direction, see fig. 3.2 for details. The introduced bipartite optical lattice system considers the different signs encountered by the hopping strengths, in addition the sign can be gauged away, such that $t^{\parallel}$, $t^{\perp} > 0$. The dispersion relation for the kinetic part of the p_x-orbital and one spin direction is

$$\varepsilon_{\mathbf{k}xs} = -2\left[t^{\parallel} \cos\left(k^x\, a\right) + t^{\perp} \cos\left(k^y\, a\right) \right] - \mu\,, \tag{3.3}$$

where a is the lattice spacing. The remaining dispersion relations are of analog form as the above and we thus encounter four energy bands in the system. The density of states $g_{n\alpha s}(E)$ can be calculated through

$$g_{n\alpha s}(E) = \frac{1}{N} \sum_{\mathbf{k}} \delta(E - \varepsilon_{n\mathbf{k}\alpha s})\ , \tag{3.4}$$

where n is the energy band, E is the energy, N the number of lattice sites and $\varepsilon_{n\mathbf{k}\alpha s}$ the dispersion relation of the problem, as in standard literature [107, 141]. Here we restrict our considerations and calculations to the lowest energy band n and neglect higher contributions. The analytic expression for the density of states for a 2D rectangular lattice system [142] can be adapted to fit the p-orbital system for the individual orbitals and spin directions as

$$g(\epsilon) = \frac{1}{2t^{\parallel}\,\pi^2\,\sqrt{t^{\perp}/t^{\parallel}}}\,K\left[\frac{\sqrt{\left(1+t^{\perp}/t^{\parallel}\right)^2-(\epsilon/2)^2}}{2\sqrt{t^{\perp}/t^{\parallel}}}\right], \tag{3.5}$$

where $K[x]$ is the complete elliptic integral of first kind and $\epsilon = E/t^{\parallel}$, see [142]. The relation holds for $2\left(1+t^{\perp}/t^{\parallel}\right) \geq \epsilon \geq 2\left(1-t^{\perp}/t^{\parallel}\right)$ or $2\left(-1+t^{\perp}/t^{\parallel}\right) \geq \epsilon > -2\left(1+t^{\perp}/t^{\parallel}\right)$. For the region $2\left(1-t^{\perp}/t^{\parallel}\right) \geq \epsilon \geq 2\left(-1+t^{\perp}/t^{\parallel}\right)$ we have

$$g(\epsilon) = \frac{1}{t^{\parallel}\,\pi^2\,\sqrt{\left(1+t^{\perp}/t^{\parallel}\right)^2-(\epsilon/2)^2}}\,K\left[\frac{2\sqrt{t^{\perp}/t^{\parallel}}}{\sqrt{\left(1+t^{\perp}/t^{\parallel}\right)^2-(\epsilon/2)^2}}\right]. \tag{3.6}$$

The density of states for one orbital and one spin direction is shown in fig. 3.3a) with the two van Hove singularities at $\epsilon = \pm 1$. The two peaks are due to the two hopping parameters $t^{\parallel}$, $t^{\perp}$ with $t^{\perp}/t^{\parallel} = 1/2$. If we set $t^{\parallel} = t^{\perp}$, the two peaks merge into one van Hove singularity, as in the common tight-binding scenario [107]. In addition, we give the particle density in fig. 3.3b), where the influence of the two van Hove singularities can be observed at $\mu/t^{\parallel} = \pm 1$. For different values of the hopping strengths, the van Hove singularities would appear for different energies than illustrated in our case. The behavior of the density of states at the van Hove singularities can be described as

$$g(\epsilon) \sim -\frac{1}{2}\ln\left[\epsilon - 2\left(1-\frac{t^{\perp}}{t^{\parallel}}\right)\right], \tag{3.7}$$

which transforms into the common logarithmic expression $g(\epsilon) \sim -\frac{1}{2}\ln\epsilon$ for the common tight-binding scenario, where $t^{\parallel} = t^{\perp}$. The detailed calculation for the behavior of the density of states near the van Hove singularities can be found in sec. B.4. For the p_y-orbital we obtain the analogous relations.

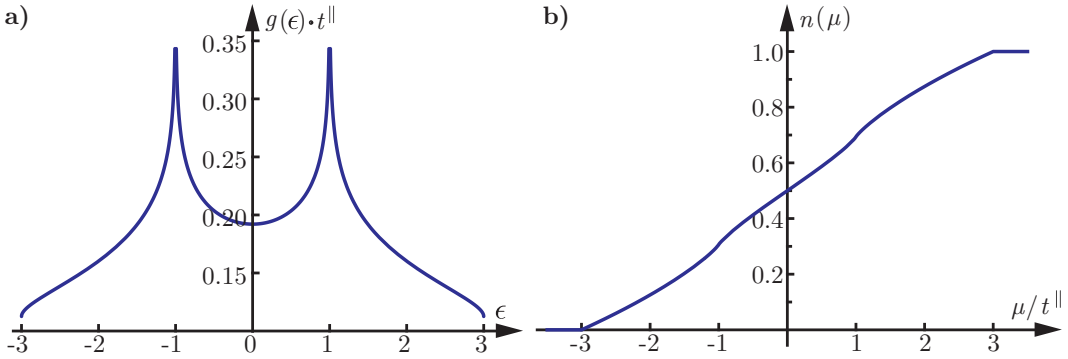

Fig. 3.3 a) Density of states for the dispersion relation eq. (3.3) with $t^{\perp}/t^{\parallel} = 1/2$. The two characteristic peaks at $\epsilon = E/t^{\parallel} = \pm 1$ are the van Hove singularities of the system, due to the two different hopping strengths. The behavior of the density of states near the van Hove singularities is given in eq. (3.7). **b)** Particle density depending on the chemical potential $\mu/t^{\parallel}$ for $t^{\perp}/t^{\parallel} = 1/2$, for one spin direction and orbital. The influence of the van Hove singularities can be observed at the kinks at $\mu/t^{\parallel} = \pm 1$.

3.2.2. Interaction Hamiltonian

The interaction part of the Hamiltonian (3.1) is composed out of two parts

$$\mathrm{H}_{int} = \mathrm{H}_{intra} + \mathrm{H}_{inter} \,, \tag{3.8}$$

the intra-orbital interaction part

$$\mathrm{H}_{intra} = U \sum_i \left(n_{ix\uparrow}\, n_{ix\downarrow} + n_{iy\uparrow}\, n_{iy\downarrow} \right) \,, \tag{3.9}$$

corresponds to the on-site interaction term within the Hubbard model, where the number operator for site i and orbital p_α is $n_{i\alpha} = n_{i\alpha\uparrow} + n_{i\alpha\downarrow}$; and the inter-orbital part

$$\mathrm{H}_{inter} = V \sum_i \left[T^+_{i\uparrow}\, T^+_{i\downarrow} + T^-_{i\uparrow}\, T^-_{i\downarrow} - 2 \left(\vec{S}_{ix} \cdot \vec{S}_{iy} - \frac{1}{4}\, n_{ix}\, n_{iy} \right) \right] \,. \tag{3.10}$$

The intra-orbital interaction strength is U and identical for the p_x- and p_y-orbital, respectively, whereas the inter-orbital interaction strength is V, i.e. the

interaction strength between the p_x- and p_y-orbital. The orbital operators T^{γ}_{is} are introduced in analogy to the spin operators, as part of an orbital vector

$$\vec{T}_{is} = \left(T^x_{is}\,, T^y_{is}\,, T^z_{is}\right)\,, \qquad\qquad T^{\gamma}_{is} = \frac{1}{2}\sum_{\alpha,\beta} c^{\dagger}_{i\alpha s}\,\sigma^{\gamma}_{\alpha\,\beta}\,c_{i\beta s}\,, \tag{3.11}$$

here γ indicates the component of the orbital operator and α, β the corresponding $p_{\alpha,\beta}$ orbital. The Pauli spin matrix is σ^{γ} with $\gamma = x, y, z$. As for the spin operators, the quantization axis of the orbital operators is chosen to be the z-axis and then behave as

$$T^z_{is}|\alpha, s\rangle_i = \begin{cases} \frac{1}{2} & \text{if } |y, s\rangle_i \\ -\frac{1}{2} & \text{if } |x, s\rangle_i \\ 0 & \text{if } |x, s; y, s\rangle_i \quad \text{and} \quad |x, \bar{s}; y, \bar{s}\rangle_i \end{cases}\,, \tag{3.12}$$

where $|\alpha, s\rangle_i$ describes a state on lattice site i with orbital α occupied by a spin s and $\bar{s} \neq s$. In analogy to the common spin algebra, the orbital operators follow the commutation relation

$$\left[T^{\gamma_1}_{is}\,,\, T^{\gamma_2}_{is}\right] = i\,\varepsilon^{\gamma_1\gamma_2\gamma_3}\,T^{\gamma_3}_{is}\,, \tag{3.13}$$

where $\varepsilon^{\gamma_1\gamma_2\gamma_3}$ is the totally anti-symmetric tensor with $\varepsilon^{xyz} = +1$. Next, we introduce the raising and lowering orbital operator through

$$T^{\pm}_{is} = T^x_{is} \pm i\,T^y_{is}\,. \tag{3.14}$$

These operators then act as

$$\begin{aligned} &T^{+}_{is}\,|x, s\rangle_i = |y, s\rangle_i\,, && T^{+}_{is}\,|y, s\rangle_i = 0\,, \\ &T^{-}_{is}\,|y, s\rangle_i = |x, s\rangle_i\,, && T^{-}_{is}\,|x, s\rangle_i = 0\,, \\ &T^{\pm}_{is}\,|\alpha, \bar{s}\rangle_i = 0\,. \end{aligned} \tag{3.15}$$

Thus, the orbital raising and lowering operator flips the occupied orbital, but conserves the spin.
The spin operators $\vec{S}_{i\alpha}$ are defined through

$$\vec{S}_{i\alpha} = \left(S^x_{i\alpha}\,,\, S^y_{i\alpha}\,,\, S^z_{i\alpha}\right)\,, \qquad\qquad S^{\gamma}_{i\alpha} = \frac{1}{2}\sum_{s,s'} c^{\dagger}_{i\alpha s}\,\sigma^{\gamma}_{s\,s'}\,c_{i\alpha s'}\,, \tag{3.16}$$

with $\gamma = x, y, z$, α the p_α-orbital and the spin index $s, s' = \uparrow, \downarrow$. They describe the spin degrees of freedom and only act on the spin of the corresponding state. In contrast to the orbital operators, here the orbital occupancy is conserved.

Interaction Strengths

Our setup is well described within the tight-binding regime, such that we can use the well established approach of Wannier functions [18, 27] and apply it for the p_α-orbitals. The interaction parameters U and V can then be given in terms of Wannier functions w_α as

$$\begin{aligned} U &= g \int \mathrm{d}\mathbf{r}\, |w_\alpha(\mathbf{r})|^4 \,, \\ V &= g \int \mathrm{d}\mathbf{r}\, |w_x(\mathbf{r})|^2 \, |w_y(\mathbf{r})|^2 \,, \end{aligned} \tag{3.17}$$

where $g = 4\pi\hbar^2 a_s/m$, a_s is the s-wave scattering length, m the atomic mass and $\alpha = x, y$. Next, we calculate the ratio of the two interaction strengths V/U. We can estimate the ratio V/U by a Gaussian approximation for the Wannier functions, where the p_x-orbital experiences a confinement in y-direction and the p_y-orbital in x-direction. The ratio V/U becomes

$$\frac{V}{U} = \sqrt{2} \Bigg/ \sqrt{1 + \frac{\sigma^{x\,4} + \sigma^{y\,4}}{2\,\sigma^{x\,2}\,\sigma^{y\,2}}} \,, \tag{3.18}$$

with σ^γ being the size of the Gaussian in γ-direction. For further details to the interaction potentials see sec. B.2 and sec. B.3.

3.2.3. Full Hamiltonian

After the separate investigations, we can combine both parts and give the full Hamiltonian of interest

$$\begin{aligned} \mathrm{H} = &- \sum_{\alpha s} \left\{ t^{\parallel} \sum_{\langle i,j \rangle^{\parallel}_{\alpha}} \left(c^\dagger_{j\alpha s} c_{i\alpha s} + \mathrm{h.c.} \right) + t^{\perp} \sum_{\langle i,j \rangle^{\perp}_{\alpha}} \left(c^\dagger_{j\alpha s} c_{i\alpha s} + \mathrm{h.c.} \right) \right\} \\ &- \mu \sum_{i\alpha s} c^\dagger_{i\alpha s} c_{i\alpha s} + U \sum_i \left(n_{ix\uparrow}\, n_{ix\downarrow} + n_{iy\uparrow}\, n_{iy\downarrow} \right) \\ &+ V \sum_i \left[T^+_{i\uparrow}\, T^+_{i\downarrow} + T^-_{i\uparrow}\, T^-_{i\downarrow} - 2 \left(\vec{S}_{ix} \cdot \vec{S}_{iy} - \frac{1}{4}\, n_{ix}\, n_{iy} \right) \right] . \end{aligned} \tag{3.19}$$

3.3. Preliminary Investigations

As a motivation we focus on a single lattice site and analyze the Hamiltonian (3.1) in the half-filling case for the weak coupling regime. Hence, there are two fermions present and no hopping is possible, thus the kinetic part of the Hamiltonian is not relevant here. The idea is to get a first glance of possible mechanisms and phases appearing in our system. In the following sections we then extend and deepen these investigations.

In our system we encounter two sets of degrees of freedom, namely two degrees for spin and two for the orbitals. The two fermions on the single lattice site are coupled through the addition of angular momenta within the Clebsch-Gordan framework and the Pauli principle, i.e. the constraint of a total anti-symmetric wave function. Thus, we are left with six possible states, which fulfill the requirements. We can classify them as spin singlet/triplet states, labeled as $|S_i\rangle$, $|T_i\rangle$, and orbital triplet/singlet states. The possible spin triplet states are

$$\begin{aligned}
|T_1\rangle &= c^\dagger_{ix\uparrow}\, c^\dagger_{iy\uparrow}|0\rangle\,, \\
|T_2\rangle &= c^\dagger_{ix\downarrow}\, c^\dagger_{iy\downarrow}|0\rangle\,, \\
|T_3\rangle &= \frac{1}{\sqrt{2}}\left(c^\dagger_{ix\uparrow}\, c^\dagger_{iy\downarrow} + c^\dagger_{ix\downarrow}\, c^\dagger_{iy\uparrow}\right)|0\rangle\,,
\end{aligned} \tag{3.20}$$

whereas all spin triplets states are orbital singlet states. The spin singlet and orbital triplet states are

$$\begin{aligned}
|S_1\rangle &= \frac{1}{\sqrt{2}}\left(c^\dagger_{ix\downarrow}\, c^\dagger_{ix\uparrow} + c^\dagger_{iy\downarrow}\, c^\dagger_{iy\uparrow}\right)|0\rangle\,, \\
|S_2\rangle &= \frac{1}{\sqrt{2}}\left(c^\dagger_{ix\downarrow}\, c^\dagger_{ix\uparrow} - c^\dagger_{iy\downarrow}\, c^\dagger_{iy\uparrow}\right)|0\rangle\,, \\
|S_3\rangle &= \frac{1}{\sqrt{2}}\left(c^\dagger_{ix\uparrow}\, c^\dagger_{iy\downarrow} - c^\dagger_{ix\downarrow}\, c^\dagger_{iy\uparrow}\right)|0\rangle\,.
\end{aligned} \tag{3.21}$$

All states are given to act on the vacuum state $|0\rangle$. See fig. 3.4 for an illustration of the different coupling possibilities. Details to the different coupling mechanisms are in section B.5.

We calculate the interaction energy of Hamiltonian (3.1) in first order pertur-

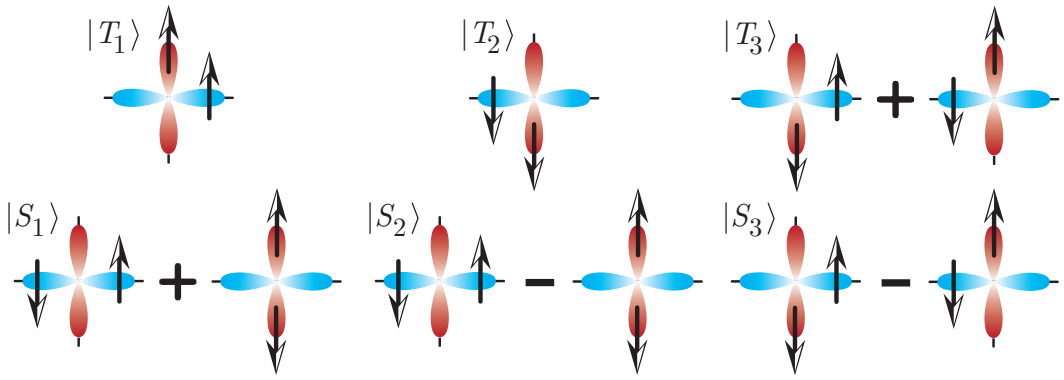

Fig. 3.4 Possible configurations of two fermions and a single lattice site. We present the possible configurations of the degrees of freedom determined through the Clebsch-Gordan framework. There are six different possible states, as illustrated. The spin triplet states $|T_i\rangle$ as given in eq. (3.20) are in the top row of the figure. The spin singlet states $|S_i\rangle$ are as in eq. (3.21) and are given in the lower row.

bation theory and compute for the spin singlet states

$$\langle S_{1,2}|\mathrm{H}_{int}|S_{1,2}\rangle = (U \pm V)\ , \qquad \langle S_3|\mathrm{H}_{int}|S_3\rangle = 2\,V\,. \tag{3.22}$$

The calculation reveals a linear energy contribution with interactions. The computations for the spin triplet configuration directly gives

$$\langle T_i|\mathrm{H}_{int}|T_i\rangle = 0\,, \tag{3.23}$$

and thus no contribution of the interaction Hamiltonian to the energy. We can conclude, that for vanishing interaction and a single site, the system has Fermi liquid behavior. Increasing the interaction will lead to a competition between hopping $t^{\parallel}$, $t^{\perp}$ and interaction U, V. For stronger interactions we expect a spontaneous magnetization of the system and thus a phase transition towards a magnetic phase. These preliminary investigations give us reasons to analyze our Hamiltonian (3.1) in more detail. We therefore extent the investigations to all fillings and make use of a mean-field treatment.

3.4. Mean-Field Analysis

We are interested in magnetic phases in the system, as motivated before. There are two principle approaches for a mean-field treatment of the system, either the spin imbalance approach – in analogy to the Stoner ferromagnetism [6] – or the orbital imbalance approach. In the orbital approach the imbalance of the filling of the two orbitals is analyzed and thus an orbital instability. In this section we focus on the spin instability. The orbital imbalance approach was done in a different work [143].

3.4.1. Mean-Field Treatment

We treat the Hamiltonian (3.1) in the mean-field manner in order to analyze the behavior of the system for all fillings. The Hamiltonian takes the form

$$\begin{aligned} \mathrm{H} = \mathrm{H}_{kin} + \mathrm{H}_{intra} - 2\,V \sum_i \left(S^z_{ix} \cdot S^z_{iy} - \frac{1}{4}\, n_{ix}\, n_{iy} \right) \\ - g_J\, \mu_\mathrm{B}\, H \sum_i \left(S^z_{ix} + S^z_{iy} \right) , \end{aligned} \tag{3.24}$$

where for the spin operators $\vec{S}_{ix,y}$ only the z-component is relevant and can be given as

$$S^z_{i\alpha} = \frac{1}{2} \left(n_{i\alpha\uparrow} - n_{i\alpha\downarrow} \right) . \tag{3.25}$$

Note, we have chosen the z-axis as quantization axis of the problem. The kinetic Hamiltonian H_{kin} is of equation (3.2) and the intra-orbital interaction Hamiltonian H_{intra} is of equation (3.9). Here we have included a Zeeman shift, where the external magnetic field points along the z-direction, with g_J being the Landé factor, μ_B the Bohr magneton and H the external magnetic field. The Landé factor can be computed through

$$g_J = 1 + \frac{J\,(J+1) - L\,(L+1) + S\,(S+1)}{2J\,(J+1)} , \tag{3.26}$$

where J is the total angular momentum, L the orbit and S the spin momentum [71]. The orbital operators in Hamiltonian (3.19) can be neglected, since

they do not influence the spin imbalance within the orbitals.
For the mean-field treatment we use the standard approach

$$n_{i\alpha s} = \langle c^\dagger_{i\alpha s} c_{i\alpha s}\rangle + \Big(n_{i\alpha s} - \langle c^\dagger_{i\alpha s} c_{i\alpha s}\rangle\Big) = \bar{n}_{\alpha s} + (n_{i\alpha s} - \bar{n}_{\alpha s}) \;, \tag{3.27}$$

with $\bar{n}_{i\alpha s}$ being the mean-particle density and $\bar{n}_{i\alpha s} = \bar{n}_{\alpha s}\,\forall\, i$. This simplification is well justified, since we only assume a global mean-particle density $\bar{n}_{\alpha s}$ and no local deviations of the mean-particle density. Be aware, in the proceeding steps we indicate the particle number operators as $n_{i\alpha s}$, i.e. by using an i in the index of n, and write $\bar{n}_{\alpha s}$, i.e. without the site label in the index, as the mean-particle density.
Inserting the mean-field approach decouples the Hamiltonian (3.24). The interaction part of the mean-field Hamiltonian H_{MF} is

$$\begin{aligned}\mathrm{H}_{MF,\,int} = &\sum_{i\alpha s} \left\{n_{i\alpha s}\left(U\,\bar{n}_{\alpha\bar{s}} + V\,\bar{n}_{\alpha'\bar{s}}\right)\right\} \\ &- \sum_i \left[U \sum_\alpha \bar{n}_{\alpha\uparrow}\bar{n}_{\alpha\downarrow} + V \sum_s \bar{n}_{xs}\bar{n}_{y\bar{s}}\right] \;,\end{aligned} \tag{3.28}$$

with $\alpha, \alpha' = x, y$ and $\alpha' \neq \alpha$, for the spin index we have $s = \uparrow, \downarrow$ and $s \neq \bar{s}$. The second part of the above Hamiltonian is the mean-field energy shift. Within the mean-field approach, we have neglected terms of the form $(n_{i\alpha s} - \bar{n}_{\alpha s})\,\left(n_{i\beta s'} - \bar{n}_{\beta s'}\right)$, since their contribution is small. The mean-field treatment of the kinetic Hamiltonian as well as Zeeman shift is straightforward and we will include these terms in the final form of the mean-field Hamiltonian.
Next, we introduce the mean-field parameters

$$\bar{n}_\alpha = \bar{n}_{\alpha\uparrow} + \bar{n}_{\alpha\downarrow} \,, \qquad m_\alpha = \bar{n}_{\alpha\uparrow} - \bar{n}_{\alpha\downarrow} \,, \tag{3.29}$$

where m_α is the magnetization and serves as the order parameter within the system, $\bar{n}_\alpha$ is the total mean-particle density. We express the mean-field interaction Hamiltonian (3.28) through the new parameters by using

$$\bar{n}_{\alpha\uparrow} = \frac{1}{2}\left(\bar{n}_\alpha + m_\alpha\right) \;, \quad \bar{n}_{\alpha\downarrow} = \frac{1}{2}\left(\bar{n}_\alpha - m_\alpha\right) \;, \quad \bar{n}_{\alpha\uparrow}\bar{n}_{\alpha\downarrow} = \frac{1}{4}\left(\bar{n}_\alpha^2 - m_\alpha^2\right) \;, \tag{3.30}$$

and obtain

$$\begin{aligned}\mathrm{H}_{MF,\,int} = \sum_{i\alpha} \Bigg\{ & n_{i\alpha\uparrow} \left[\frac{U}{2} \left(\bar{n}_\alpha - m_\alpha \right) + \frac{V}{2} \left(\bar{n}_{\alpha'} - m_{\alpha'} \right) \right] \\ & + n_{i\alpha\downarrow} \left[\frac{U}{2} \left(\bar{n}_\alpha + m_\alpha \right) + \frac{V}{2} \left(\bar{n}_{\alpha'} + m_{\alpha'} \right) \right] \Bigg\} \\ & - \sum_i \left\{ \frac{U}{4} \left(\bar{n}_x^2 + \bar{n}_y^2 - m_x^2 - m_y^2 \right) + \frac{V}{2} \left(\bar{n}_x \bar{n}_y - m_x m_y \right) \right\} . \end{aligned} \tag{3.31}$$

Combining the kinetic part as well as Zeeman shift to the interaction part, we have the mean-field Hamiltonian as

$$\begin{aligned}\mathrm{H}_{MF} = \mathrm{H}_{kin} + \sum_{i\alpha} \Bigg\{ & n_{i\alpha\uparrow} \left[\frac{U}{2} \left(\bar{n}_\alpha - m_\alpha \right) + \frac{V}{2} \left(\bar{n}_{\alpha'} - m_{\alpha'} \right) - \frac{g_J}{2} \mu_\mathrm{B} H \right] \\ & + n_{i\alpha\downarrow} \left[\frac{U}{2} \left(\bar{n}_\alpha + m_\alpha \right) + \frac{V}{2} \left(\bar{n}_{\alpha'} + m_{\alpha'} \right) + \frac{g_J}{2} \mu_\mathrm{B} H \right] \Bigg\} + E_0 \,, \end{aligned} \tag{3.32}$$

where E_0 is the mean-field energy shift.

3.4.2. Fourier Transformation and Energy Scales

Now, we Fourier transform the whole mean-field Hamiltonian (3.32) by using the standard relations

$$c_{i\alpha s}^\dagger = \frac{1}{\sqrt{N}} \sum_{\mathbf{k}} e^{-i\mathbf{k}\mathbf{x}_i} \, c_{\mathbf{k}\alpha s}^\dagger \,, \qquad c_{i\alpha s} = \frac{1}{\sqrt{N}} \sum_{\mathbf{k}} e^{i\mathbf{k}\mathbf{x}_i} \, c_{\mathbf{k}\alpha s} \,, \tag{3.33}$$

where N is the number of lattice sites. The mean-field Hamiltonian becomes

$$\begin{aligned}\mathrm{H}_{MF} = \sum_{\mathbf{k}\alpha} \Bigg\{ & n_{\mathbf{k}\alpha\uparrow} \left[\varepsilon_{\mathbf{k}\alpha\uparrow} + \frac{U}{2} \left(\bar{n}_\alpha - m_\alpha \right) + \frac{V}{2} \left(\bar{n}_{\alpha'} - m_{\alpha'} \right) - \frac{g_J}{2} \mu_\mathrm{B} H \right] \\ & + n_{\mathbf{k}\alpha\downarrow} \left[\varepsilon_{\mathbf{k}\alpha\downarrow} + \frac{U}{2} \left(\bar{n}_\alpha + m_\alpha \right) + \frac{V}{2} \left(\bar{n}_{\alpha'} + m_{\alpha'} \right) + \frac{g_J}{2} \mu_\mathrm{B} H \right] \Bigg\} \\ & - N \left[\frac{U}{4} \left(\bar{n}_x^2 + \bar{n}_y^2 - m_x^2 - m_y^2 \right) - \frac{V}{2} \left(\bar{n}_x \bar{n}_y - m_x m_y \right) \right] , \end{aligned} \tag{3.34}$$

with $\varepsilon_{\mathbf{k}\alpha s}$ being the dispersion relations of eq. (3.3), $\alpha, \alpha' = x, y$, $\alpha \neq \alpha'$ and $s = \uparrow, \downarrow$. The next step is to determine the mean-particle densities $\bar{n}_\alpha = \bar{n}_{\alpha\uparrow} + \bar{n}_{\alpha\downarrow}$ and magnetizations $m_\alpha = \bar{n}_{\alpha\uparrow} - \bar{n}_{\alpha\downarrow}$ self-consistently, where we allow a small temperature influence such that $\epsilon_F = E_F/t^{\parallel} \gg k_\mathrm{B}T_F/t^{\parallel}$. In order to perform these calculations, we clarify the energy scales involved. We know, that the mean-particle density is much larger than the magnetization, i.e. $\bar{n}_\alpha \gg m_\alpha$, and the applied magnetic field is small, compared to $\bar{n}_\alpha$. To this end, we absorb the contributions of the large mean-particle densities into new Fermi energies

$$E_{F,x} = E'_{F,x} + \frac{1}{2}\left(U\bar{n}_x + V\bar{n}_y\right), \quad E_{F,y} = E'_{F,y} + \frac{1}{2}\left(U\bar{n}_y + V\bar{n}_x\right), \tag{3.35}$$

with $E'_{F,\alpha}$ being the old Fermi energy. Then we assume, that the chemical potential μ is close to the Fermi energy such that

$$\mu_\alpha = E_{F,\alpha} + \Delta\mu_\alpha(m_\alpha, m_{\alpha'}, H, T) \ , \tag{3.36}$$

where the deviation $\Delta\mu_\alpha(m_\alpha, m_{\alpha'}, H, T)$ is small and depends on the magnetization, magnetic field H and temperature T. Absorbing the large mean-particle density contributions leads to modified dispersion relations. They can then be written as

$$\begin{aligned} E_{\mathbf{k}\alpha\uparrow} &= \varepsilon'_{\mathbf{k}\alpha\uparrow} - \frac{1}{2}\left(Um_\alpha + Vm_{\alpha'}\right) - \Delta\mu_\alpha - \frac{g_J}{2}\mu_\mathrm{B}H \ , \\ E_{\mathbf{k}\alpha\downarrow} &= \varepsilon'_{\mathbf{k}\alpha\downarrow} + \frac{1}{2}\left(Um_\alpha + Vm_{\alpha'}\right) - \Delta\mu_\alpha + \frac{g_J}{2}\mu_\mathrm{B}H \ , \end{aligned} \tag{3.37}$$

with $\varepsilon'_{\mathbf{k}\alpha s}$ being the dispersion relation including the mean-particle density shift. In addition, we illustrate in fig. 3.5 the different energy scales, since we need the different levels for the proceeding computations.

3.4.3. Mean-Particle Density

We calculate the mean-particle density $\bar{n}_\alpha$ and magnetization m_α self-consistently, as given in eq. (3.29) and use

$$\bar{n}_{\alpha s} = \frac{1}{2}\int_{-\infty}^{\infty} \mathrm{d}\varepsilon \, g_\alpha(\varepsilon)\, f_{\alpha s}(\varepsilon) \ . \tag{3.38}$$

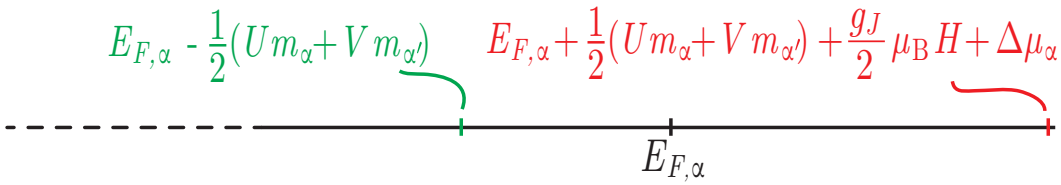

Fig. 3.5 Involved energy scales of the mean-field analysis. The Fermi energy $E_{F,\alpha}$ is the shifted energy as given in eq. (3.35). Additional shifts in the Fermi energy result from the magnetizations m_α, magnetic field H and the deviation $\Delta\mu_\alpha$, resulting in a lower or higher energy than $E_{F,\alpha}$.

For the density of states it holds $g_{\alpha s}(\varepsilon) = \frac{1}{2}\, g_\alpha(\varepsilon)$ and $f_{\alpha s}(\varepsilon)$ is the Fermi-Dirac distribution function. To tackle the integrals, we apply the Sommerfeld expansion, as given in sec. B.1,

$$\int_{-\infty}^{\infty} g(\epsilon)\, f(\epsilon)\, \mathrm{d}\epsilon \approx \int_{-\infty}^{\mu} g(\epsilon)\, \mathrm{d}\epsilon + \frac{\pi^2}{6}\,(k_\mathrm{B}T)^2\, g'(\mu)\ , \tag{3.39}$$

where $g(\epsilon)$ is the density of states and $f(\epsilon)$ is the Fermi-Dirac distribution. The second term involves the temperature dependence as well as the derivative of g with respect to ϵ at the position μ.
We then begin the computations with the mean-particle density of the p_x-orbital

$$\begin{aligned}
\bar{n}_x = \bar{n}_{x\uparrow} + \bar{n}_{x\downarrow} &= \frac{1}{2}\int_{-\infty}^{\infty} \mathrm{d}\varepsilon\, g_x(\varepsilon)\, f_{x\uparrow}(\varepsilon) + \frac{1}{2}\int_{-\infty}^{\infty} \mathrm{d}\varepsilon\, g_x(\varepsilon)\, f_{x\downarrow}(\varepsilon) \\
&\approx \frac{1}{2}\left\{\int_{-\infty}^{\mu_{x\uparrow}} g_x(\varepsilon)\, \mathrm{d}\varepsilon + \frac{\pi^2}{6}\,(k_\mathrm{B}T)^2\, g_x'\big(\mu_{x\uparrow}\big)\right\} \\
&\quad + \frac{1}{2}\left\{\int_{-\infty}^{\mu_{x\downarrow}} g_x(\varepsilon)\, \mathrm{d}\varepsilon + \frac{\pi^2}{6}\,(k_\mathrm{B}T)^2\, g_x'\big(\mu_{x\downarrow}\big)\right\} \\
&= \frac{1}{2}\int_{-\infty}^{\bar{E}_{F,x}+\Delta\mu_x} g_x(\varepsilon)\, \mathrm{d}\varepsilon + \frac{1}{2}\int_{-\infty}^{\bar{\bar{E}}_{F,x}+\Delta\mu_x} g_x(\varepsilon)\, \mathrm{d}\varepsilon \\
&\quad + \frac{1}{2}\,\frac{\pi^2}{6}\,(k_\mathrm{B}T)^2\left[g_x'\big(\bar{E}_{F,x}+\Delta\mu_x\big) + g_x'\big(\bar{\bar{E}}_{F,x}+\Delta\mu_x\big)\right]\ .
\end{aligned} \tag{3.40}$$

Here we have introduced

$$\begin{aligned}
\bar{E}_{F,x} &= E_{F,x} + \frac{1}{2}\,(U m_x + V m_y + g_J \mu_\mathrm{B} H)\ , \\
\bar{\bar{E}}_{F,x} &= E_{F,x} - \frac{1}{2}\,(U m_x + V m_y + g_J \mu_\mathrm{B} H)\ ,
\end{aligned} \tag{3.41}$$

for sake of convenience. Next, we split the limits of the integrals and add a zero to the equation to obtain

$$\begin{aligned}\bar{n}_x = &\frac{1}{2}\int_{-\infty}^{E_{F,x}} g_x(\varepsilon)\,\mathrm{d}\varepsilon + \frac{1}{2}\int_{E_{F,x}}^{\bar{E}_{F,x}} g_x(\varepsilon)\,\mathrm{d}\varepsilon + \frac{1}{2}\int_{\bar{E}_{F,x}}^{\bar{E}_{F,x}+\Delta\mu_x} g_x(\varepsilon)\,\mathrm{d}\varepsilon \\ &+ \frac{1}{2}\int_{-\infty}^{\bar{\bar{E}}_{F,x}} g_x(\varepsilon)\,\mathrm{d}\varepsilon + \frac{1}{2}\int_{\bar{\bar{E}}_{F,x}}^{\bar{\bar{E}}_{F,x}+\Delta\mu_x} g_x(\varepsilon)\,\mathrm{d}\varepsilon \pm \frac{1}{2}\int_{\bar{\bar{E}}_{F,x}}^{E_{F,x}} g_x(\varepsilon)\,\mathrm{d}\varepsilon \\ &+ \frac{1}{2}\frac{\pi^2}{6}\left(k_\mathrm{B}T\right)^2\left[g_x'\big(\bar{E}_{F,x}+\Delta\mu_x\big) + g_x'\big(\bar{\bar{E}}_{F,x}+\Delta\mu_x\big)\right]\,. \end{aligned} \tag{3.42}$$

The first term in the first and second line of eq. (3.42) can be reduced to $\int_{-\infty}^{E_{F,x}} g_x(\varepsilon)\,\mathrm{d}\varepsilon$. We then carry out the integrations and find

$$\begin{aligned}\bar{n}_x = \bar{n}_{0x} &+ \frac{1}{2}\Big[G_x(\varepsilon)\Big]_{E_{F,x}}^{\bar{E}_{F,x}} - \frac{1}{2}\Big[G_x(\varepsilon)\Big]_{\bar{\bar{E}}_{F,x}}^{E_{F,x}} \\ &+ \frac{1}{2}\Big[G_x(\varepsilon)\Big]_{\bar{E}_{F,x}}^{\bar{E}_{F,x}+\Delta\mu_x} + \frac{1}{2}\Big[G_x(\varepsilon)\Big]_{\bar{\bar{E}}_{F,x}}^{\bar{\bar{E}}_{F,x}+\Delta\mu_x} \\ &+ \frac{1}{2}\frac{\pi^2}{6}\left(k_\mathrm{B}T\right)^2\left[g_x'\big(\bar{E}_{F,x}+\Delta\mu_x\big) + g_x'\big(\bar{\bar{E}}_{F,x}+\Delta\mu_x\big)\right]\,, \end{aligned} \tag{3.43}$$

with $\bar{n}_{0x}$ being the magnetization- and magnetic field-free mean-particle density and $G_x(\varepsilon)$ is the integrated density of states.

We are interested in small magnetizations m_α, therefore we can expand the integrated density of states $G_x(\varepsilon)$ around the Fermi energy $E_{F,x}$ up to third order in m_α. In addition, we expand G_x around $\bar{E}_{F,x}$ and $\bar{\bar{E}}_{F,x}$ up to first order in $\Delta\mu_x$ as well as the temperature dependent part in orders of $\Delta\mu_x$.

After a straightforward calculation we have

$$\begin{aligned}\bar{n}_x = \bar{n}_{0x} &+ \frac{1}{2}\left\{\frac{1}{4}\left(Um_x + Vm_y\right)^2 g_x'\left(E_{F,x}\right) + \frac{\pi^2}{6}\left(k_\mathrm{B}T\right)^2 \bar{g}_x'\left(E_{F,x}\right)\right\} \\ &+ \frac{1}{2}\Delta\mu_x\left\{\bar{g}_x\left(E_{F,x}\right) + \frac{\pi^2}{6}\left(k_\mathrm{B}T\right)^2 \bar{g}_x''\left(E_{F,x}\right)\right\}\,, \end{aligned} \tag{3.44}$$

where we have introduced

$$\begin{aligned}\bar{g}_x\big(E_{F,x}\big) &= g_x\left(\bar{E}_{F,x}\right) + g_x\left(\bar{\bar{E}}_{F,x}\right)\,, \\ \bar{g}_x'\left(E_{F,x}\right) &= g_x'\left(\bar{E}_{F,x}\right) + g_x'\left(\bar{\bar{E}}_{F,x}\right)\,, \\ \bar{g}_x''\left(E_{F,x}\right) &= g_x''\left(\bar{E}_{F,x}\right) + g_x''\left(\bar{\bar{E}}_{F,x}\right)\,. \end{aligned} \tag{3.45}$$

Be aware, only the linear contribution of the magnetic field is relevant, see section B.6.3 for details. This is due to direct comparison of the principle form of the energy functional of the Ginzburg-Landau theory of phase transitions [100, 101], where only the linear order in the magnetic field is relevant.
Although we have $T \neq 0$ and $H \neq 0$, we still can assume, that $\bar{n}_x - \bar{n}_{0x} \approx 0$ [144], such that we can calculate $\Delta\mu_x$ to be

$$\Delta\mu_x = -\frac{\frac{1}{4}\left(Um_x + Vm_y\right)^2 g_x'\left(E_{F,x}\right) + \frac{\pi^2}{6}\left(k_\mathrm{B}T\right)^2 \bar{g}_x'\left(E_{F,x}\right)}{\bar{g}_x\left(E_{F,x}\right) + \frac{\pi^2}{6}\left(k_\mathrm{B}T\right)^2 \bar{g}_x''\left(E_{F,x}\right)} \,. \tag{3.46}$$

The calculation for the mean-particle density of the p_y-orbital can be done analogously and is found in detail in appendix B.6.1. The result for $\Delta\mu_y$ thus is

$$\Delta\mu_y = -\frac{\frac{1}{4}\left(Um_y + Vm_x\right)^2 g_y'\left(E_{F,y}\right) + \frac{\pi^2}{6}\left(k_\mathrm{B}T\right)^2 \bar{g}'\left(E_{F,y}\right)}{\bar{g}_y\left(E_{F,y}\right) + \frac{\pi^2}{6}\left(k_\mathrm{B}T\right)^2 \bar{g}_y''\left(E_{F,y}\right)} \,, \tag{3.47}$$

with

$$\begin{aligned}
\bar{g}_y\left(E_{F,y}\right) &= g_y\left(\bar{E}_{F,y}\right) + g_y\left(\bar{\bar{E}}_{F,y}\right) \,, \\
\bar{g}_y'\left(E_{F,y}\right) &= g_y'\left(\bar{E}_{F,y}\right) + g_y'\left(\bar{\bar{E}}_{F,y}\right) \,, \\
\bar{\bar{g}}_y''\left(E_{F,y}\right) &= g_y''\left(\bar{E}_{F,y}\right) + g_y''\left(\bar{\bar{E}}_{F,y}\right) \,,
\end{aligned} \tag{3.48}$$

and in analogy to the p_x-orbital calculation, the introduced Fermi energy abbreviations are

$$\begin{aligned}
\bar{E}_{F,y} &= E_{F,y} + \frac{1}{2}\left(Um_y + Vm_x + g_J\mu_\mathrm{B}H\right) \,, \\
\bar{\bar{E}}_{F,y} &= E_{F,y} - \frac{1}{2}\left(Um_y + Vm_x + g_J\mu_\mathrm{B}H\right) \,.
\end{aligned} \tag{3.49}$$

3.4.4. Magnetization

With the deviations $\Delta\mu_{x,y}$ calculated, we can now perform the computations of the corresponding magnetizations of the system. We start with the p_x-orbital. The magnetization is given by

$$m_x = \bar{n}_{x\uparrow} - \bar{n}_{x\downarrow} = \frac{1}{2}\int_{-\infty}^{\infty} g_x(\varepsilon)\, f_{x\uparrow}(\varepsilon)\,\mathrm{d}\varepsilon - \frac{1}{2}\int_{-\infty}^{\infty} g_x(\varepsilon)\, f_{x\downarrow}(\varepsilon)\,\mathrm{d}\varepsilon \,. \tag{3.50}$$

We again apply the Sommerfeld expansion eq. (3.39) to compute

$$\begin{aligned}
m_x \approx{}& \frac{1}{2}\left\{\int_{-\infty}^{\mu_{x\uparrow}} g_x(\varepsilon)\,\mathrm{d}\varepsilon + \frac{\pi^2}{6}\left(k_\mathrm{B}T\right)^2 g_x'\big(\mu_{x\uparrow}\big)\right\} \\
&- \frac{1}{2}\left\{\int_{-\infty}^{\mu_{x\downarrow}} g_x(\varepsilon)\,\mathrm{d}\varepsilon + \frac{\pi^2}{6}\left(k_\mathrm{B}T\right)^2 g_x'\big(\mu_{x\downarrow}\big)\right\} \\
={}& \frac{1}{2}\int_{-\infty}^{E_{F,x}} g_x(\varepsilon)\,\mathrm{d}\varepsilon + \frac{1}{2}\int_{E_{F,x}}^{\bar{E}_{F,x}} g_x(\varepsilon)\,\mathrm{d}\varepsilon + \frac{1}{2}\int_{\bar{E}_{F,x}}^{\bar{E}_{F,x}+\Delta\mu_x} g_x(\varepsilon)\,\mathrm{d}\varepsilon \\
&- \frac{1}{2}\int_{-\infty}^{\bar{\bar{E}}_{F,x}} g_x(\varepsilon)\,\mathrm{d}\varepsilon - \frac{1}{2}\int_{\bar{\bar{E}}_{F,x}}^{\bar{\bar{E}}_{F,x}+\Delta\mu_x} g_x(\varepsilon)\,\mathrm{d}\varepsilon \pm \frac{1}{2}\int_{\bar{\bar{E}}_{F,x}}^{E_{F,x}} g_x(\varepsilon)\,\mathrm{d}\varepsilon \\
&+ \frac{1}{2}\frac{\pi^2}{6}\left(k_\mathrm{B}T\right)^2\left[g_x'\big(\mu_{x\uparrow}\big) - g_x'\big(\mu_{x\downarrow}\big)\right]\,. \qquad (3.51)
\end{aligned}$$

Performing the integrations reveals

$$\begin{aligned}
m_x ={}& \frac{1}{2}\Big[G_x(\varepsilon)\Big]_{\bar{\bar{E}}_{F,x}}^{\bar{E}_{F,x}} + \frac{1}{2}\Big[G_x(\varepsilon)\Big]_{\bar{E}_{F,x}}^{\bar{E}_{F,x}+\Delta\mu_x} - \frac{1}{2}\Big[G_x(\varepsilon)\Big]_{\bar{\bar{E}}_{F,x}}^{\bar{\bar{E}}_{F,x}+\Delta\mu_x} \\
&+ \frac{1}{2}\frac{\pi^2}{6}\left(k_\mathrm{B}T\right)^2\left[g_x'\big(\mu_{x\uparrow}\big) - g_x'\big(\mu_{x\downarrow}\big)\right]\,. \qquad (3.52)
\end{aligned}$$

Next, we expand the integrated density of states in orders of m_α up to third order. In addition we expanded $G_x(\varepsilon)$ around $\bar{E}_{F,x}$ and $\bar{\bar{E}}_{F,x}$ in orders of $\Delta\mu_x$. The straightforward computation reveals

$$\begin{aligned}
m_x ={}& \frac{1}{2}\Big\{\left(Um_x + Vm_y + g_J\mu_\mathrm{B}H\right) g_x\big(E_{F,x}\big) \\
&+ \frac{1}{4!}\left(Um_x + Vm_y\right)^3 g_x''\big(E_{F,x}\big)\Big\} \\
&+ \frac{1}{2}\Delta\mu_x\left\{\bar{\bar{g}}_x\big(E_{F,x}\big) + \frac{\pi^2}{6}\left(k_\mathrm{B}T\right)^2\bar{\bar{g}}_x''\big(E_{F,x}\big)\right\} \\
&+ \frac{1}{2}\frac{\pi^2}{6}\left(k_\mathrm{B}T\right)^2\bar{\bar{g}}_x'\big(E_{F,x}\big)\,, \qquad (3.53)
\end{aligned}$$

with

$$\begin{aligned}
\bar{\bar{g}}_x\big(E_{F,x}\big) &= g_x\big(\bar{E}_{F,x}\big) - g_x\big(\bar{\bar{E}}_{F,x}\big)\,, \\
\bar{\bar{g}}_x'\big(E_{F,x}\big) &= g_x'\big(\bar{E}_{F,x}\big) - g_x'\big(\bar{\bar{E}}_{F,x}\big)\,, \\
\bar{\bar{g}}_x''\big(E_{F,x}\big) &= g_x''\big(\bar{E}_{F,x}\big) - g_x''\big(\bar{\bar{E}}_{F,x}\big)\,. \qquad (3.54)
\end{aligned}$$

We simplify the magnetization (3.53) further by using the expansions of the modified density of states $\bar{\bar{g}}_x\big(E_{F,x}\big)$, given in sec. B.6.2. This directly computes

$$\begin{aligned} m_x = \frac{1}{2}\Big\{ & \left(Um_x + Vm_y + g_J\mu_\mathrm{B}H\right) g_x\big(E_{F,x}\big) \\ & + \frac{1}{4!}\left(Um_x + Vm_y\right)^3 g_x''\big(E_{F,x}\big) \\ & + \frac{\pi^2}{6}\left(k_\mathrm{B}T\right)^2 \left[\left(Um_x + Vm_y + g_J\mu_\mathrm{B}H\right) g_x''\big(E_{F,x}\big)\right] \Big\} \\ & + \frac{1}{2}\Delta\mu_x \left\{\left(Um_x + Vm_y + g_J\mu_\mathrm{B}H\right) g_x'\big(E_{F,x}\big)\right\} . \end{aligned} \tag{3.55}$$

The next step is to insert the deviation $\Delta\mu_x$ of eq. (3.46) into the magnetization. To the deviation $\Delta\mu_x$ we have also applied the expansions of sec. B.6.2, leading to the magnetization

$$\begin{aligned} m_x = & \frac{1}{2}\left(Um_x + Vm_y + g_J\mu_\mathrm{B}H\right) g_x\big(E_{F,x}\big) \\ & \times \left\{1 - \frac{\pi^2}{6}\left(k_\mathrm{B}T\right)^2 \left[\frac{g_x'^2\big(E_{F,x}\big)}{g_x^2\big(E_{F,x}\big)} - \frac{g_x''\big(E_{F,x}\big)}{g_x\big(E_{F,x}\big)}\right]\right\} \\ & + \frac{3}{2}\frac{1}{4!}\left(Um_x + Vm_y\right)^3 \left[\frac{g_x''\big(E_{F,x}\big)}{3} - \frac{g_x'^2\big(E_{F,x}\big)}{g_x\big(E_{F,x}\big)}\right] . \end{aligned} \tag{3.56}$$

The calculation for the magnetization of the p_y-orbital is found in detail in appendix B.6.3. The final form is

$$\begin{aligned} m_y = & \frac{1}{2}\left(Um_y + Vm_x + g_J\mu_\mathrm{B}H\right) g_y\big(E_{F,y}\big) \\ & \times \left\{1 - \frac{\pi^2}{6}\left(k_\mathrm{B}T\right)^2 \left[\frac{g_y'^2\big(E_{F,y}\big)}{g_y^2\big(E_{F,y}\big)} - \frac{g_y''\big(E_{F,y}\big)}{g_x\big(E_{F,y}\big)}\right]\right\} \\ & + \frac{3}{2}\frac{1}{4!}\left(Um_y + Vm_x\right)^3 \left[\frac{g_y''\big(E_{F,y}\big)}{3} - \frac{g_y'^2\big(E_{F,y}\big)}{g_y\big(E_{F,y}\big)}\right] . \end{aligned} \tag{3.57}$$

We are now able to generalize the expressions for the magnetizations from above and find the self-consistency equations for our system

$$\begin{aligned} m_\alpha = & \frac{1}{2}\left(Um_\alpha + Vm_{\alpha'} + g_J\mu_\mathrm{B}H\right) g_\alpha\big(E_{F,\alpha}\big)\ \xi\big(T, E_{F,\alpha}\big) \\ & + \frac{3}{2}\frac{1}{4!}\left(Um_\alpha + Vm_{\alpha'}\right)^3 \zeta\big(E_{F,\alpha}\big) , \end{aligned} \tag{3.58}$$

with $\alpha \neq \alpha'$ and we have introduced

$$\begin{aligned}\xi\big(T, E_{F,\alpha}\big) &:= 1 - \frac{\pi^2}{6}\left(k_\mathrm{B}T\right)^2 \left[\frac{g_\alpha'^2\big(E_{F,\alpha}\big)}{g_\alpha^2\big(E_{F,\alpha}\big)} - \frac{g_\alpha''\big(E_{F,\alpha}\big)}{g_\alpha\big(E_{F,\alpha}\big)}\right] \\ &= 1 - \frac{\pi^2}{6}\left(k_\mathrm{B}T\right)^2 \Lambda\big(E_{F,\alpha}\big) \\ \zeta\big(E_{F,\alpha}\big) &:= \left[\frac{g_\alpha''\big(E_{F,\alpha}\big)}{3} - \frac{g_\alpha'^2\big(E_{F,\alpha}\big)}{g_\alpha\big(E_{F,\alpha}\big)}\right], \end{aligned} \tag{3.59}$$

for sake of convenience.
We directly see from equation (3.58), that we encounter two scenarios: one where we are interested in the mechanism for vanishing magnetic field and the other with finite H. In the following we investigate both scenarios, determine the instabilities and solve for the magnetizations.

3.4.5. Vanishing Magnetic Field

We investigate equation (3.58) for the magnetic field-free system, i.e. $H = 0$. We begin with the instability condition and present the mean-field phase diagram. Then we evaluate the transition temperature for the involved phase transitions as well as analyze the order of them. This section is concluded by solving for the magnetization and plotting them for different parameter regimes.

Instability Condition and Eigenvalues

For the instability only the linear contribution of equation (3.58) is relevant. It can be transformed into a tensor representation

$$\begin{pmatrix} m_x \\ m_y \end{pmatrix} = \frac{1}{2}\begin{pmatrix} U g_x\big(E_{F,x}\big)\,\xi\big(T, E_{F,x}\big) & V g_x\big(E_{F,x}\big)\,\xi\big(T, E_{F,x}\big) \\ V g_y\big(E_{F,y}\big)\,\xi\big(T, E_{F,y}\big) & U g_y\big(E_{F,y}\big)\,\xi\big(T, E_{F,y}\big) \end{pmatrix}\begin{pmatrix} m_x \\ m_y \end{pmatrix}. \tag{3.60}$$

We determine the following eigenvalues

$$\lambda_{1,2} = \frac{U}{4}\Big[g_x\big(E_{F,x}\big)\,\xi\big(T,E_{F,x}\big) + g_y\big(E_{F,y}\big)\,\xi\big(T,E_{F,y}\big)\Big] \times \left[1 \pm \sqrt{1 + \frac{4g_x\big(E_{F,x}\big)\,g_y\big(E_{F,y}\big)\,\xi\big(T,E_{F,x}\big)\,\xi\big(T,E_{F,y}\big)\,(V^2-U^2)}{U^2\left(g_x\big(E_{F,x}\big)\,\xi\big(T,E_{F,x}\big) + g_y\big(E_{F,y}\big)\,\xi\big(T,E_{F,y}\big)\right)^2}}\right]. \tag{3.61}$$

Next, we make the assumption that the density of states for the individual orbitals are the same and the corresponding Fermi energies are also identical, such that

$$\begin{aligned} & g_x\big(E_{F,x}\big) = g_y\big(E_{F,y}\big) = g(E_F)\ , \\ \Rightarrow\ & \xi\big(T,E_{F,x}\big) = \xi\big(T,E_{F,y}\big) = \xi(T,E_F)\ . \end{aligned} \tag{3.62}$$

The eigenvalues (3.61) then reduce to

$$\lambda_{1,2} = \frac{1}{2}\,g(E_F)\,\xi(T,E_F)\,[U \pm V]\ . \tag{3.63}$$

These eigenvalues lead to two instability conditions

$$1 = \frac{1}{2}\,g(E_F)\,\xi(T,E_F)\,[U+V]\ , \tag{3.64a}$$

$$\text{and} \qquad 1 = \frac{1}{2}\,g(E_F)\,\xi(T,E_F)\,[U-V]\ , \tag{3.64b}$$

which are the desired self-consistency equations of our system. They can be tuned through the interaction strengths U, V and the density of states $g(E_F)$ via the Fermi energy.
Fulfilling one of these equations signals an instability of the system and thus triggers a phase transition. The principle structure of the appearing phase is indicated through the eigenvectors of the system. We obtain the eigenvectors as

$$\mathrm{EV}_1 = \begin{pmatrix}1\\1\end{pmatrix} \ \vee\ \begin{pmatrix}-1\\-1\end{pmatrix}, \qquad \mathrm{EV}_2 = \begin{pmatrix}1\\-1\end{pmatrix} \ \vee\ \begin{pmatrix}-1\\1\end{pmatrix}. \tag{3.65}$$

The first eigenvector EV_1 shows that for the first eigenvalue λ_1 the majority of spins are $\uparrow$ in both orbitals or $\downarrow$. This relates to the common ferromagnetic

configuration with the spins pointing ↑ or ↓. For the second eigenvector EV_2, to the second eigenvalue λ_2, we find an alternating ordering with the majority of spins within the p_x-orbitals being ↑ and ↓ within the p_y-orbitals or vice versa. Here we encounter a ferromagnetic phase with orbital symmetry breaking. The details of the eigenvalue problem is found in appendix B.6.4.

Mean-Field Phase Diagrams

For both situations of instabilities we give the mean-field phase diagrams in fig 3.6. The axes of the diagrams are $Ug(\epsilon_F)$ and $Vg(\epsilon_F)$, to have a filling-independent phase diagram. In addition, we have introduced the reduced Fermi energy $\epsilon_F = E_F/t^{\parallel}$.
The order parameter for the first instability (3.64a) can be given as $m = m_x + m_y$, where for the second instability (3.64b) it is $\tilde{m} = m_x - m_y$. We find the ferromagnetic phase transition with order parameter m to be the dominant transition, since increasing the interaction strengths U, V always leads towards the instability. On the other hand, the instability leading to the ferromagnetic phase with orbital symmetry breaking and order parameter $\tilde{m}$ is the sub-leading phase transition. Here the interaction strength V always has to be weaker than the intra-interaction strength U in order to trigger the phase transition towards the ferromagnetic phase with orbital symmetry breaking, see fig. 3.6.
Therefore, the dominant phase transition with order parameter m is pre-empted. In contrast, the sub-leading phase transition with $\tilde{m}$ is suppressed.

Transition Temperatures

Next, we analyze the transition temperatures for the phase transitions. The self-consistency equations (3.64a) and (3.64b) can be rearranged as

$$\xi(T, E_F) = \frac{2}{g(E_F)\,[U \pm V]}\,. \tag{3.66}$$

Then using the definition (3.59) directly gives

$$k_{\mathrm{B}} T_c = \frac{\sqrt{6}}{\pi\sqrt{\Lambda(\epsilon_F)}} \sqrt{1 - \frac{2}{g(\epsilon_F)\,[U \pm V]}}\,, \tag{3.67}$$

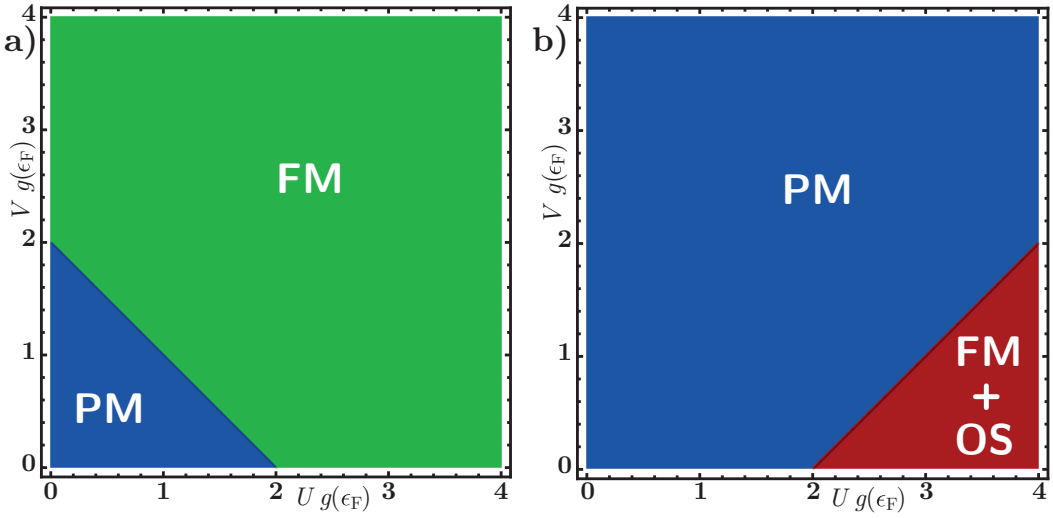

Fig. 3.6 Mean-field phase diagrams: The axes are chosen to be $Ug(\epsilon_F)$ and $Vg(\epsilon_F)$. The region in blue and marked with "PM" represents the paramagnetic phase with $m = 0$. The region in green with "FM" label is the ferromagnetic phase, the region in red with "FM + OS" label is the phase with ferromagnetic order as well as orbital symmetry breaking, both phases have a finite magnetization with m, $\tilde{m} \neq 0$. **a)** Shows the phase diagram for the first instability (3.64a), where the eigenvectors are $m_x = m_y$. **b)** Shows the phase diagram for the second instability (3.64b), where the eigenvectors are $m_x = -m_y$. Here we observe, that the transition towards the ferromagnetic phase with orbital symmetry breaking is suppressed in comparison to the previous case of $m_x = m_y$.

with $\Lambda(\epsilon_F) = g'^2(\epsilon_F)/g^2(\epsilon_F) - g''(\epsilon_F)/g(\epsilon_F)$ and the reduced Fermi energy ϵ_F, as before. The function $\Lambda(\epsilon_F)$ is plotted in fig. 3.7 and is negative in a large range for the reduced Fermi energy ϵ_F.

We give the transition temperature in fig. 3.8 for the reduced temperature $k_B T/t^{\parallel}$ and the dominant ferromagnetic phase transition with $(U+V)/t^{\parallel}$. In addition, we chose different values for the reduced Fermi energy $\epsilon_F > 0$. We find, that for values of the reduced Fermi energy up to $\epsilon_F \approx 2.36$ the phase transition is of first order. At the critical reduced value $\epsilon_{F\,crit} \approx 2.37$ the order of the transition changes to two. We sketch this critical line within the figure in black and dashed. For values $\epsilon_F > 2.37$ the phase transition is of second

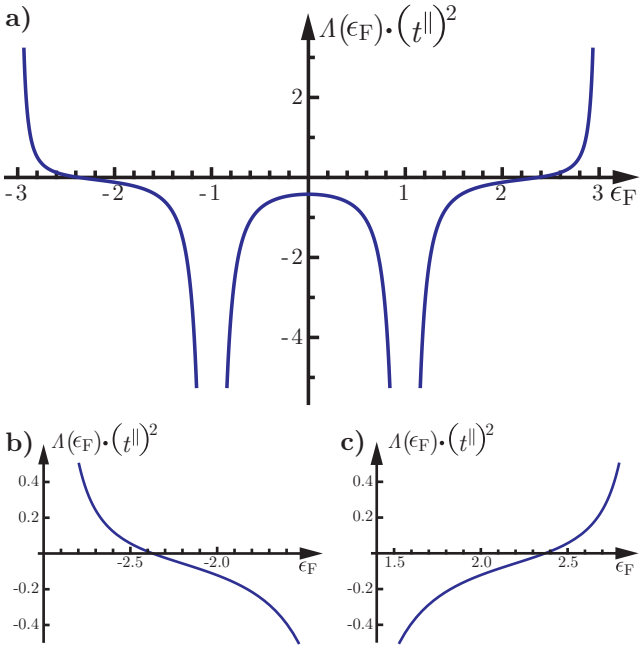

Fig. 3.7 a) Function $\Lambda(\epsilon_F)$ of eq. (3.59). The hopping ratio is $t^{\perp}/t^{\parallel} = 1/2$. For most of the range of the reduced Fermi energies ϵ_F the function $\Lambda(\epsilon_F)$ is negative and diverges at the van Hove singularities at $\epsilon_F = \pm 1$. **b)** Here we give the left section of the function $\Lambda(\epsilon_F)$ with the zero crossing at $\epsilon_F \approx -2.37$. **c)** Right section of $\Lambda(\epsilon_F)$ with the zero crossing at $\epsilon_F \approx 2.37$.

order. This is also resembled in the well-known form of the paramagnet to ferromagnet transition temperature [141, 144–146]. Increasing the values of ϵ_F up to $\epsilon_F \approx 3.0$ reduces the ferromagnetic phase. It eventually vanishes for $\epsilon_F = 3.0$ and only the paramagnetic phase prevails.
Plotting the transition temperature for the sub-leading phase transition with order parameter $\tilde{m}$, over the interaction strength $(U - V)/t^{\parallel}$ and the same values of ϵ_F reveals the analogous figure as for the dominant transition. In addition, the change of the order of the phase transition also occurs for the same reduced Fermi energy ϵ_F, hence we neglect giving this plot.

Order of Phase Transitions

In the investigation of the linear contribution of the order parameter of the self-consistency equation (3.58) we discovered two instabilities in the system leading to two phase transitions. There is the dominant phase transition from a paramagnet to a ferromagnet with order parameter m and there is the sub-leading phase transition from the paramagnet to a ferromagnetic phase with orbital symmetry breaking.
Next, we analyze the order of these phase transitions. Here we refer to the

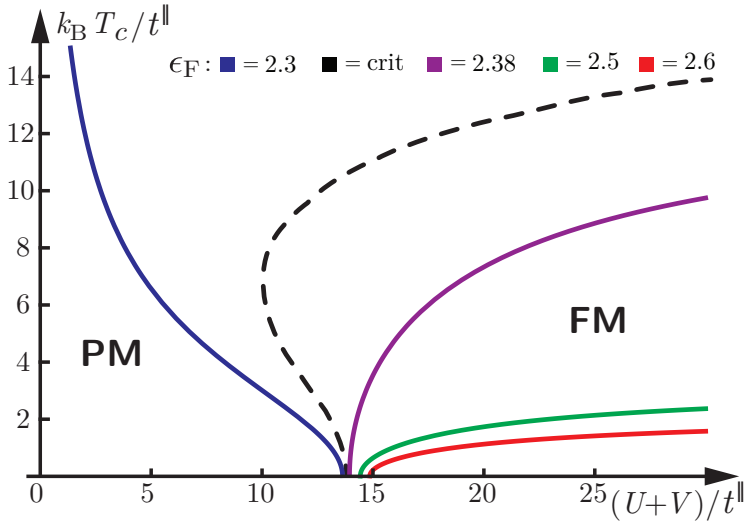

Fig. 3.8 Transition temperature for the dominant phase transition with order parameter m. The axes are the reduced transition temperature $k_B T_c/t^{\parallel}$ and interaction strengths $(U+V)/t^{\parallel}$. Plotted are different values of the reduced Fermi energy ϵ_F. For $\epsilon_F < 2.37$ the phase transition is of first order. At the critical value $\epsilon_{F\,crit} \approx 2.37$ the order of the transition changes to two, indicated by the black dashed line. For $\epsilon_F > 2.37$ the transition takes the form of the well-known paramagnet to ferromagnet transition.

Ginzburg-Landau theory of phase transitions, the corresponding energy functional and especially the minimizing condition of the order parameter [100, 101]. Our self-consistency equation (3.58) is exactly of the minimizing form. From the Ginzburg-Landau theory we know, that the cubic contribution of the order parameter in the self-consistency equation determines the order of the phase transition and the stability of the new phase. Applying the results of the discussion of the different orders of the phase transition within the Ginzburg-Landau framework to our system we find, that the cubic contribution has to be positive for a first order transition, where the new phase is unstable, and negative for a second order transition, where the new phase can be stabilized. Within our system only the function $\zeta(E_F)$ can change the sign and thus the order of the phase transition. We give the function $\zeta(\epsilon_F)$ in fig. 3.9 for the relevant range of the reduced Fermi energy ϵ_F. We find, that it is positive for values of ϵ_F up to $\epsilon_F \approx \pm 1.7$ and has its zero crossing at $\epsilon_F = \pm 1.7$. For

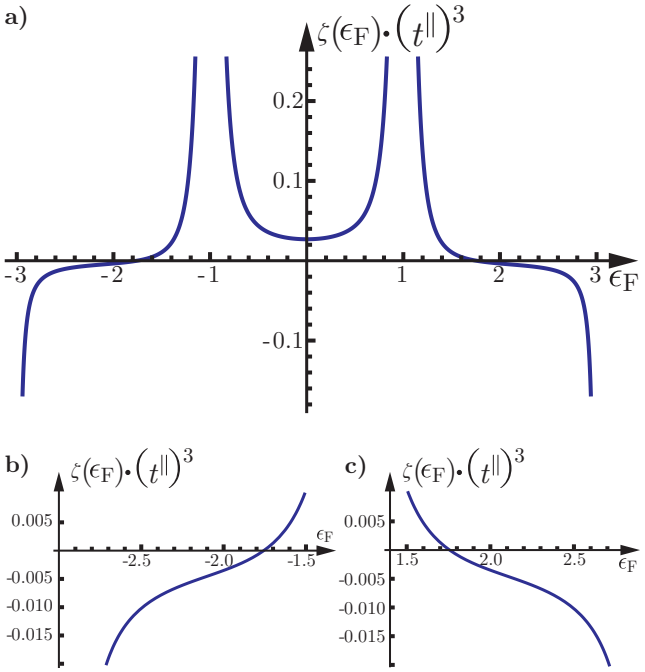

Fig. 3.9 a) Function $\zeta(\epsilon_F)$ of eq. (3.59), with reduced Fermi energy ϵ_F. It diverges at the two van Hove singularities at $\epsilon_F = \pm 1$ and is positive for values of $\epsilon_F \approx -1.7$ to $\epsilon_F \approx 1.7$. At the zero crossing, $\epsilon_F = \pm 1.7$, the function becomes negative indicating a possible change in the order of the phase transition. **b)** Zoom of the left part of $\zeta(\epsilon_F)$ and its zero crossing, **c)** of the right part.

values $\epsilon_F > 1.7$ ($\epsilon_F < -1.7$) the function is negative, indicating that here the transition can become of second order, where before, it was of first order. Comparing this result with the behavior of the transition temperature eq. (3.67) and its plot fig. 3.8, we see that the conditions do not match. Thus, the sign change of $\zeta(\epsilon_F)$ only indicates a possible change of the order of the phase transition. In addition, we have to consult the $\Lambda(\epsilon_F)$ function in fig. 3.7, since it also influences the critical value of the reduced Fermi energy $\epsilon_{F\,crit}$. The function $\Lambda(\epsilon_F)$ has its zero crossing at $\epsilon_F \approx \pm 2.37$ and for values $\epsilon_F > 2.37$ it is positive. Exactly for these values ϵ_F the transition temperature takes the well-known form of the paramagnet to ferromagnet phase transition, which is of second order [144]. Hence, the tricritical point [100] is at $\epsilon_{F\,crit} \approx \pm 2.37$, where the phase transition becomes of second order and the new phase can be stabilized.

Solutions of Magnetization

To verify the result regarding the order of the phase transitions, we investigate the system further. In addition, we check the assumption of the small

and slowly increasing magnetization, which is essential in our mean-field approach. We therefore insert the two eigenvectors (3.65) into the self-consistency equations (3.58) and solve for the two order parameters. The self-consistency equations take the form

$$m = \frac{1}{2}\,(U+V)\,g(E_F)\,\xi(T,E_F)\;m + \frac{3}{2}\,\frac{1}{4!}\,(U+V)^3\,\zeta(E_F)\;m^3\,,$$

and

$$\tilde{m} = \frac{1}{2}\,(U-V)\,g(E_F)\,\xi(T,E_F)\;\tilde{m} + \frac{3}{2}\,\frac{1}{4!}\,(U-V)^3\,\zeta(E_F)\;\tilde{m}^3\,. \tag{3.68}$$

The two equations can be solved for m, $\tilde{m}$ and thus reveal

$$m_1 = 0\,, \qquad m_{2,3} = \pm\sqrt{\frac{1-\frac{1}{2}\;(U\pm V)\,g(E_F)\,\xi(T,E_F)}{\frac{3}{2}\,\frac{1}{4!}\,(U\pm V)^3\,\zeta(E_F)}}\,, \tag{3.69}$$

where the plus sign within the interaction strengths $(U+V)$ relates to the order parameter m and the minus sign in $(U-V)$ to $\tilde{m}$. In fig. 3.10 we plot the non-zero solutions for the dominant order parameter m for two different temperatures and different reduced Fermi energies ϵ_F. For the values ϵ_F we restrict the plot to the $\epsilon_F > 0$ sector, since the $\epsilon_F < 0$ sector reveals the analog behavior. This is based on the symmetry of the density of states $g(\epsilon_F)$ and the functions $\Lambda(\epsilon_F)$, $\zeta(\epsilon_F)$. In addition, we plot the solutions for values of ϵ_F larger than the critical reduced Fermi energy $\epsilon_{F\,crit} \approx 2.37$, in order to be in the region of the second order phase transition and to then compare the behavior of the solutions for two different temperatures. Again we neglect the plot for the sub-leading order parameter $\tilde{m}$, since we obtain an analogous plot with the analog behavior.

We analyze the possible solutions m_i. There is always the solution $m_1 = 0$, which corresponds to the paramagnetic phase. The additional solutions for the magnetizations $m_{2,3}$ can be tuned through the interaction strengths U, V, the density of states via the Fermi energy E_F and the temperature T. These solutions appear, as soon as the instability conditions (3.64a), (3.64b) are fulfilled and mark the appearing phases with finite magnetization. Either the ferromagnetic phase or the ferromagnetic phase with orbital symmetry breaking. The solutions for the magnetization $m_{2,3}$ increase smoothly and are small, as

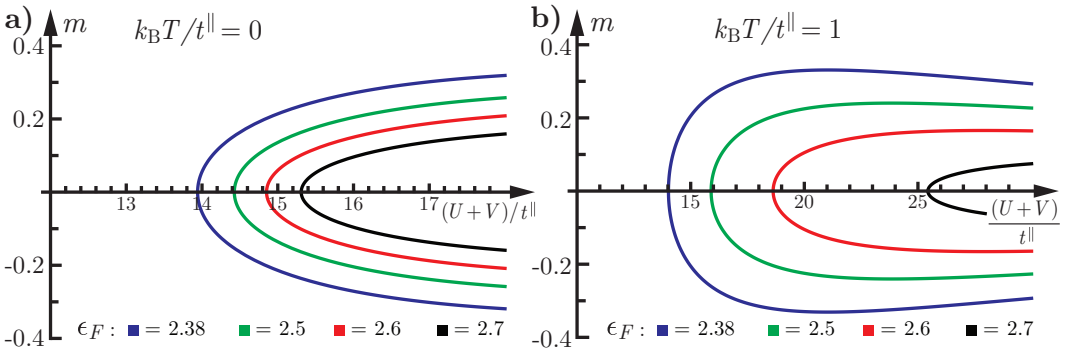

Fig. 3.10 Plotted are the solutions for the magnetization $m_{2,3}$ of eq. (3.69), for different reduced Fermi energies $\epsilon_F > 0$ as given within the plot and two different reduced temperatures $k_B T/t^{\parallel}$, depending on the reduced interaction strengths $(U+V)/t^{\parallel}$. The reduced Fermi energies are chosen to be beyond the tricritical point at $\epsilon_{F\,crit} \approx 2.37$. The hopping parameters are $t^{\perp}/t^{\parallel} = 1/2$. **a)** Zero temperature magnetization. **b)** Solutions for the magnetization at $k_B T/t^{\parallel} = 1$. Here the critical interaction strengths for the $m \neq 0$ solutions are increased compared to the zero temperature case. See text for further details.

required for the mean-field analysis. For increasing ϵ_F, increased interaction strengths are required to trigger the phase transition, as can be observed in the figure 3.10. On the other hand, increasing the temperature of the system, shifts the critical interaction strengths to larger values, in comparison to the zero temperature scenario. In addition we find, that increasing the interaction strength U, V further, reduces the magnetization again. For large interaction strengths the denominator in eq. (3.69) grows faster than the nominator.
In the beginning of the mean-field derivation – in the stage of the expansions and simplifications – we assumed a small magnetization as well as a smooth growth through the tuning parameters. These assumptions are well justified by comparison with fig. 3.10.

3.4.6. Finite Magnetic Field

In the preceding investigations, we have turned the magnetic field off, i.e. $H = 0$. Next, we turn it on and thus apply a small magnetic field in z-direction to the

system. We are interested in the instability of the system under the influence of the magnetic field. The section is concluded by solving the self-consistency equation for the magnetizations and plotting the solutions.

Instability Condition and Susceptibility

Here, again, we begin the considerations with the linear contribution of the magnetization for the analysis of the instability. The tensor representation of the linear self-consistency equations is

$$\begin{aligned}\begin{pmatrix} m_x \\ m_y \end{pmatrix} = \frac{1}{2}\, g_J \mu_\mathrm{B} H \begin{pmatrix} g_x\left(E_{F,x}\right) \xi\left(T, E_{F,x}\right) \\ g_y\left(E_{F,y}\right) \xi\left(T, E_{F,y}\right) \end{pmatrix} \\ + \frac{1}{2} \begin{pmatrix} U g_x\left(E_{F,x}\right) \xi\left(T, E_{F,x}\right) & V g_x\left(E_{F,x}\right) \xi\left(T, E_{F,x}\right) \\ V g_y\left(E_{F,y}\right) \xi\left(T, E_{F,y}\right) & U g_y\left(E_{F,y}\right) \xi\left(T, E_{F,y}\right) \end{pmatrix} \begin{pmatrix} m_x \\ m_y \end{pmatrix}.\end{aligned} \tag{3.70}$$

For the magnetic field-free part we use the determined eigenvalues (3.61) and insert them, to find

$$\begin{pmatrix} m \\ \tilde{m} \end{pmatrix} = \frac{1}{2}\, g_J \mu_\mathrm{B} H \begin{pmatrix} g_x\left(E_{F,x}\right) \xi\left(T, E_{F,x}\right) \\ g_y\left(E_{F,y}\right) \xi\left(T, E_{F,y}\right) \end{pmatrix} + \begin{pmatrix} \lambda_1 & 0 \\ 0 & \lambda_2 \end{pmatrix} \begin{pmatrix} m \\ \tilde{m} \end{pmatrix}, \tag{3.71}$$

where the order parameters are m, $\tilde{m}$. Next, we apply the simplification of equal filling and density of states (3.62) and have

$$\begin{pmatrix} 0 \\ 0 \end{pmatrix} = \frac{1}{2}\, g_J \mu_\mathrm{B} H g(E_F)\, \xi(T, E_F) \begin{pmatrix} 1 \\ 1 \end{pmatrix} + \begin{pmatrix} \lambda_1 - 1 & 0 \\ 0 & \lambda_2 - 1 \end{pmatrix} \begin{pmatrix} m \\ \tilde{m} \end{pmatrix}, \tag{3.72}$$

with the eigenvalues $\lambda_{1,2}$ being now of eq. (3.63).
We are interested in the behavior of the system through the application of the magnetic field. Therefore we calculate the magnetic susceptibility, revealing

$$\chi = \frac{\frac{1}{2}\, g_J\, \mu_\mathrm{B}^2\, g(E_F)\, \xi(T, E_F)}{1 - \frac{1}{2} g(E_F)\, \xi(T, E_F)\, (U \pm V)}. \tag{3.73}$$

We directly discover, the susceptibility diverges for the same condition as the instabilities (3.64a), (3.64b). Driving the system towards the diverging susceptibility can be done through the density of states $g(E_F)$ and its Fermi energy

E_F, the interaction strengths U, V as well as the temperature T.
The presence of the magnetic field influences the configurations of the magnetizations, depending on the sign of H and its strength. For a finite magnetic field, we find a finite magnetization m_α even before reaching the self-consistency condition. Then, fulfilling the instability condition reveals additional solutions for the magnetizations. Details to the calculation of the susceptibility and a plot for different parameters is in the appendix B.6.5.

Solutions of Magnetization

In order to obtain more insight into the behavior of the system with an applied magnetic field, we solve the self-consistency equation (3.58) with the two order parameters $m = m_x + m_y$ and $\tilde{m} = m_x - m_y$ inserted. We again use the simplification of identical density of states $g(E_F)$ eq. (3.62). The self-consistency equation with the applied magnetic field then reduces to

$$0 = m \left[1 + \frac{\frac{3}{2}\,\frac{1}{4!}\,(U \pm V)^3\,\zeta(E_F)}{\frac{1}{2}\,(U \pm V)\,g(E_F)\,\xi(T, E_F) - 1}\, m^2 \right] + \frac{\frac{1}{2}\,g_J\,\mu_\mathrm{B}\,g(E_F)\,\xi(T, E_F)\,H}{\frac{1}{2}\,(U \pm V)\,g(E_F)\,\xi(T, E_F) - 1}\,, \tag{3.74}$$

where the equation with $U + V$ holds for the dominant order parameter m and $U - V$ for the sub-leading order parameter $\tilde{m}$. The three solutions of the magnetization for the dominant order parameter m are given in fig. 3.11 for different reduced Fermi energies $\epsilon_F > 0$, temperatures $k_\mathrm{B}T/t^{\|}$, and magnetic fields $g_J\,\mu_\mathrm{B}\,H/t^{\|}$. We only give the $\epsilon_F > 0$ sector, because the $\epsilon_F < 0$ sector produces the analog behavior. In appendix B.6.6 we show the details of the solution of eq. (3.74).

From the plot and its investigation we find, that applying the small magnetic field always leads to finite solutions for the magnetization m, even for no interaction present. Increasing the interaction strength increases the value of the magnetization as well. As soon as the critical interaction strength is reached, a bifurcation is revealed, where one solution branch of the magnetization splits into two solutions, one with increased magnetization, the other solution dropping to $m \to 0$ – the paramagnetic solution of the system. If the interaction strength

is increased further, the magnetization is reduced again, as before, for the vanishing magnetic field scenario 3.4.5.
Increasing the magnetic field, $g_J\,\mu_\mathrm{B}\,H/t^{\parallel} = 0.1 \rightarrow 0.3$, leads to a larger initial gap between the two solutions for the magnetization – see fig. 3.11a) $\rightarrow$ c) and fig. 3.11b) $\rightarrow$ d) – as well as a larger critical interaction strength for the bifurcation to appear. On the other hand, increasing the temperature, $k_\mathrm{B}T/t^{\parallel} = 0 \rightarrow 1$ – see fig. 3.11a) $\rightarrow$ b) and fig. 3.11c) $\rightarrow$ d) – shifts the individual bifurcations for the different reduced Fermi energies apart of each other and to larger interaction strengths.
Hence, as soon as a magnetic field is present, there is always a transition from a paramagnet towards a phase with finite magnetization m, $\tilde{m} \neq 0$. Reaching the critical interaction strength then leads to a bifurcation and additional solutions for the magnetization, revealing again the possible paramagnetic solution. In this scenario the phase transition is of first order.
To conclude, even for an applied magnetic field, the assumption of a small and smoothly growing magnetization holds, as required by the mean-field approach.

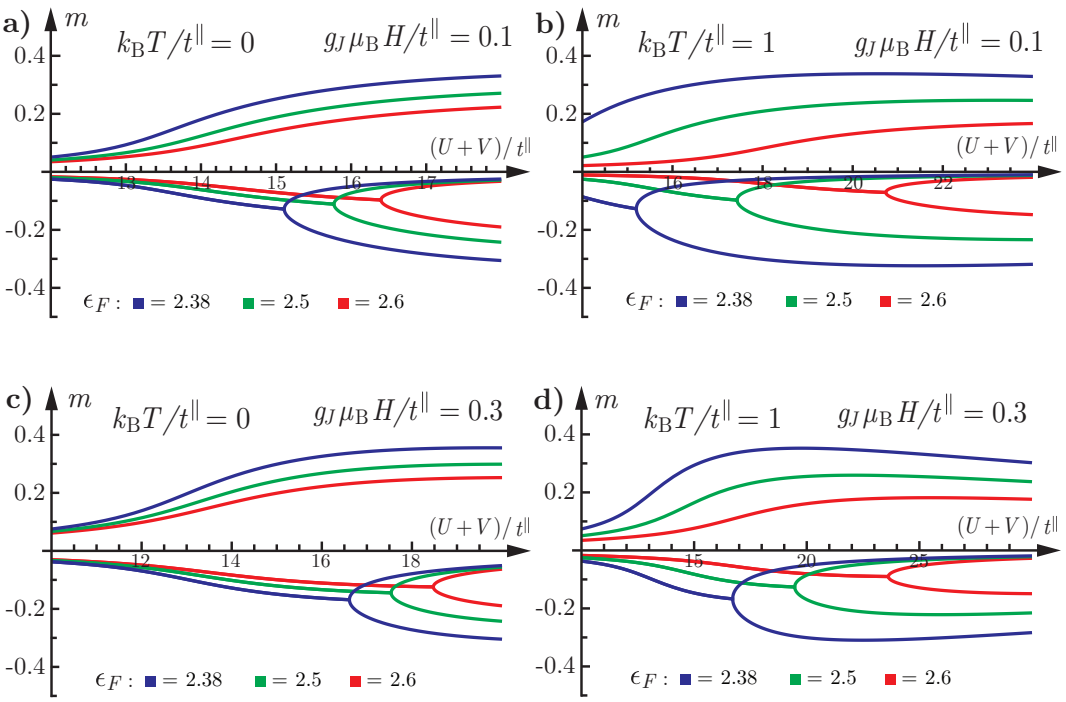

Fig. 3.11 Solutions of the magnetization with an applied magnetic field for equation (3.74). We give the magnetization over the reduced interaction strength $(U+V)/t^{\parallel}$, for the dominant phase transition with order parameter m. For a finite magnetic field, there are always finite solutions for the magnetization m, even before the instability condition is fulfilled. At the critical interaction strength, one magnetization experiences a bifurcation, this then leads to three possible solutions again. We plot two different temperatures $k_\mathrm{B}T/t^{\parallel} = 0, 1$; two different magnetic fields $g_J\,\mu_\mathrm{B}H/t^{\parallel} = 0.1, 0.3$; for the same three different reduced Fermi energies $\epsilon_F > 0$ as before. Increasing the magnetic field increases the required critical interaction strength. On the other hand, going to larger temperatures separates the individual solutions and increases the critical interaction strength. From left to right [a) $\rightarrow$ b); c) $\rightarrow$ d)], the temperature is increased, where from top to bottom [a) $\rightarrow$ c); b) $\rightarrow$ d)], the magnetic field is increased. Further details are given in the text.

3.5. Strong Coupling

We increase the interaction strength further to reach the strong coupling limit, where $U, V \gg t^{\parallel}, t^{\perp}$, investigate the behavior of the system and focus on half-filling. For strong coupling, we are in the Mott insulating regime and are interested in only two fermions per lattice site, thus half-filling. These two fermions couple to a spin-1 moment on each lattice site, to reduce the interaction energy penalty. From the single site analysis of section 3.3 we know, that the spin triplet state configuration $|T_i\rangle$ (3.20) is favored for such increased interaction strengths. We expand the analysis around the spin triplet states $|T_i\rangle$, which serve as the ground state in perturbation theory. The kinetic part of the Hamiltonian (3.1) is treated as a perturbation to the interaction part H_{int} and provides virtual hopping processes.

3.5.1. Preliminary Investigation

The degeneracy of the half-filled ground state, constructed through the spin triplet states $|T_i\rangle$, is 3^N, where N is the number of lattice sites. Each one of the two fermions can occupy one of the orbitals, respectively. Here both spins can be up or down, in addition the configuration $\uparrow\downarrow + \downarrow\uparrow$ is also possible, see fig. 3.4. This configuration is possible for every lattice site, resulting in the exponential degeneracy. Based on this degeneracy of the half-filled ground state, we refer to the canonical perturbation theory, as in the derivation of the $t - J$ model [111, 147, 148], also see to section 2.4.
In order to begin the derivation of the strong coupling Hamiltonian, we investigate the different energy scales involved for a single site and focus on the interaction part of the Hamiltonian (3.19). The half-filled strong coupling ground state energy thus is

$$\mathrm{H}_{int}|T_i\rangle = E_i|T_i\rangle = 0\,, \tag{3.75}$$

where the spin triplets $|T_i\rangle$ are of equation (3.20). For an additional fermion on the single lattice site, the interaction energy increases to $E_1 = U + V$, since one of the orbitals experiences a double-occupancy. For a fully filled lattice site with four fermions on site, the interaction energy is $E_2 = 2\,(U + V)$. To summarize the energy scales we find

- $E_0 = 0$: ground state energy for the half-filled scenario.
- $E_1 = U + V$: first "excited" state, where one of the orbitals becomes double-occupied, through a hopping process of a neighboring fermion, hence there are three fermions on site.
- $E_2 = 2\,(U + V)$: second "excited" state, here another hopping process occurred, resulting in a fully filled site with four fermions.

The different interaction energies E_i can be calculated for each spin triplet state by adjusting the state for the additional fermions present, respectively. This computation then is straightforward.

3.5.2. Decomposition of Hilbert Space

Next, we extend the single lattice site analysis to our N lattice site system. For the further derivation, we split the Hilbert space into double-occupied subspaces, as presented in detail in section 2.4. The Hilbert space then takes the form

$$\mathcal{H} = \mathcal{H}_0 \oplus \mathcal{H}_1 \oplus \mathcal{H}_2 \oplus \ldots \oplus \mathcal{H}_N\,, \tag{3.76}$$

where $\mathcal{H}$ is the total Hilbert space and $\mathcal{H}_m$ refers to the number of double-occupancies $0, 1, 2, \ldots N$ of the lattice sites. At this point, we introduce the projectors P_m to the different Hilbert subspaces

- $P_0 \rightarrow$ projecting onto an empty or single-occupied subspace $\mathcal{H}_0$,
- $P_m \rightarrow$ projecting onto an m times double-occupied subspace $\mathcal{H}_m$.

Now we investigate which relevant processes can appear within our system and make use of the projectors, where H is the full Hamiltonian (3.19),

1. $P_0\,\mathrm{H}\,P_0$: hopping process from a single-occupied site i into an empty neighboring site j; here the initial site i can contain one fermion or be half-filled.

2. $P_1 \, \mathrm{H} \, P_0$: process, where a fermion of site i hops into a neighboring site j in order to make one orbital of that site j double-occupied; the neighboring site j then contains three fermions.

3. $P_0 \, \mathrm{H} \, P_1$: inverse process of the previous one; a fermion of the double-occupied orbital in site i hops into an empty or single-occupied site j. If the process is into a single-occupied site j, the hopping must occur into the other orbital, e.g. hopping into $p_x \Rightarrow p_y$ can be occupied be a fermion and vice versa.

4. $P_1 \, \mathrm{H} \, P_1$: process, where the hopping occurs between a single double-occupied orbital in site i and a single-occupied site j to make the corresponding orbital double-occupied.

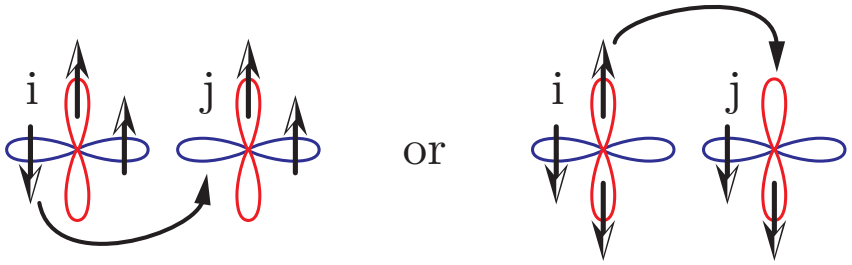

Fig. 3.12 Two illustrations for the possible hopping process $P_1 \, \mathrm{H} \, P_1$, as given in the text.

5. $P_2 \, \mathrm{H} \, P_1$: here the initial lattice site i has a single double-occupied orbital and the hopping process makes the neighboring lattice site j fully filled with two double-occupied orbitals.

6. $P_1 \, \mathrm{H} \, P_2$: inverse process of the previous hopping scenario; the initial lattice site i has two double-occupied orbitals and the process makes the neighboring site j to have an orbital double-occupied, where initially the neighboring site had two fermions.

7. $P_2 \, \mathrm{H} \, P_2$: the process starts with a fully filled site i and the hopping into the neighboring site j afterwards becomes fully filled; here the hopping can only occur, if the corresponding orbital of site j was not occupied.

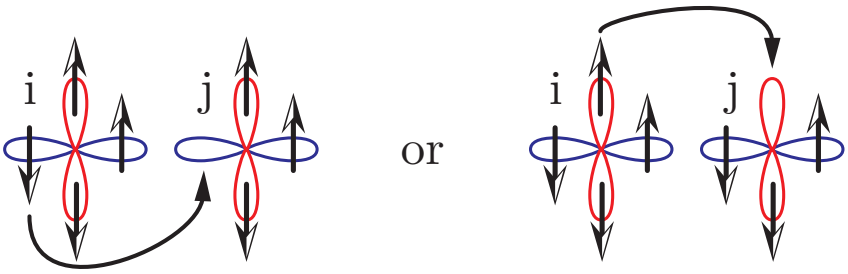

Fig. 3.13 Hopping process $P_2\,\mathrm{H}\,P_2$ for two examples.

For details regarding the representation of the decomposed Hamiltonian, see section 2.4.

3.5.3. Derivation of Effective Hamiltonian

After the description of the processes, we need to evaluate the corresponding representations of the projected Hamiltonian. The details of the representations are found in appendix B.7.1. From section 2.4 of the general concepts we know, that finding the transformed Hamiltonian describing the virtual processes reduces to an evaluation of the contribution $P_0\,\mathrm{H}\,P_1\,\mathrm{H}\,P_0$. This part of the Hamiltonian is

$$\begin{aligned} P_0\,\mathrm{H}\,P_1\,\mathrm{H}\,P_0 = \Bigg[&- P_0 \sum_{\alpha s} \Bigg\{ t^{\parallel} \sum_{\langle i,j\rangle^{\parallel}_{\alpha}} \left(c^{\dagger}_{j\alpha s} c_{i\alpha s} + \mathrm{h.c.} \right) \\ &\qquad + t^{\perp} \sum_{\langle i,j\rangle^{\perp}_{\alpha}} \left(c^{\dagger}_{j\alpha s} c_{i\alpha s} + \mathrm{h.c.} \right) \Bigg\} P_1 \Bigg] \\ \times \Bigg[&- P_1 \sum_{\alpha s} \Bigg\{ t^{\parallel} \sum_{\langle i,j\rangle^{\parallel}_{\alpha}} \left(c^{\dagger}_{j\alpha s} c_{i\alpha s} + \mathrm{h.c.} \right) \\ &\qquad + t^{\perp} \sum_{\langle i,j\rangle^{\perp}_{\alpha}} \left(c^{\dagger}_{j\alpha s} c_{i\alpha s} + \mathrm{h.c.} \right) \Bigg\} P_0 \Bigg] . \end{aligned} \tag{3.77}$$

Next, we analyze the different possible processes. To avoid confusion, we relabel the sums, such that the initial lattice sites are labeled by i, the intermediate

sites are j and the final sites k. In addition, we introduce an additional spin label s', where $\bar{s}' \neq s'$. The contribution then takes the form

$$
\begin{aligned}
P_0\,\mathrm{H}\,P_1\,\mathrm{H}\,P_0 = \Bigg[& -\sum_{\langle j,k\rangle^{\parallel}_{\alpha},s} \Big\{ P_0\; t^{\parallel}\, c^{\dagger}_{kxs} c_{jxs}\; n_{jx\bar{s}}\,(1 - n_{jys}\, n_{jy\bar{s}}) \\
& \quad + P_0\; t^{\parallel}\, c^{\dagger}_{kys} c_{jys}\; n_{jy\bar{s}}\,(1 - n_{jxs}\, n_{jx\bar{s}}) \Big\} \\
& - \sum_{\langle j,k\rangle^{\perp}_{\alpha},s} \Big\{ P_0\; t^{\perp}\, c^{\dagger}_{kxs} c_{jxs}\; n_{jx\bar{s}}\,(1 - n_{jys}\, n_{jy\bar{s}}) \\
& \quad + P_0\; t^{\perp}\, c^{\dagger}_{kys} c_{jys}\; n_{jy\bar{s}}\,(1 - n_{jxs}\, n_{jx\bar{s}}) \Big\} \Bigg] \\
\times \Bigg[& -\sum_{\langle i,j\rangle^{\parallel}_{\alpha},s'} \Big\{ (1 - n_{jys'}\, n_{jy\bar{s}'})\, n_{jx\bar{s}'}\; t^{\parallel}\, c^{\dagger}_{jxs'} c_{ixs'}\; P_0 \\
& \quad + (1 - n_{jxs'}\, n_{jx\bar{s}'})\, n_{jy\bar{s}'}\; t^{\parallel}\, c^{\dagger}_{jys'} c_{iys'}\; P_0 \Big\} \\
& - \sum_{\langle i,j\rangle^{\perp}_{\alpha},s'} \Big\{ (1 - n_{jys'}\, n_{jy\bar{s}'})\, n_{jx\bar{s}'}\; t^{\perp}\, c^{\dagger}_{jxs'} c_{ixs'}\; P_0 \\
& \quad + (1 - n_{jxs'}\, n_{jx\bar{s}'})\, n_{jy\bar{s}'}\; t^{\perp}\, c^{\dagger}_{jys'} c_{iys'}\; P_0 \Big\} \Bigg]
\end{aligned}
\tag{3.78}
$$

To evaluate the processes further, we expand the above equation and make use of the fermionic property $n^2_{i\alpha s} = n_{i\alpha s}$. In addition, we only consider virtual processes, where the initial site is also the final site and neglect three site processes $i \to j \to k$, see fig. 3.14. All combinations have to be investigated carefully and checked, if they can contribute or not.

After the straightforward evaluation of all terms, we are left with

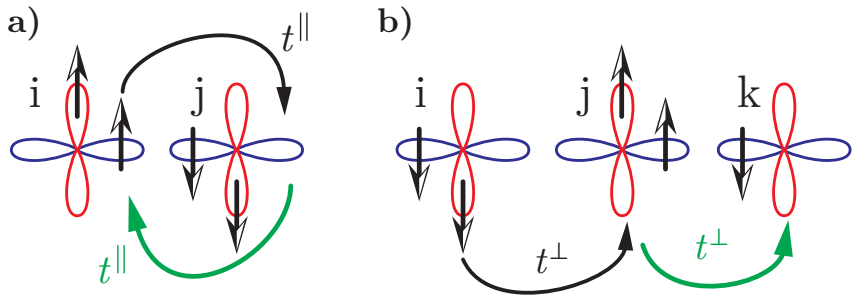

Fig. 3.14 Two illustrations of possible hopping processes of eq. (3.78). **a)** Virtual hopping process, where the initial site i is also the final site. **b)** Three site hopping process, with the initial site i, the intermediate site j and final site k.

$$
\begin{aligned}
&P_0\,\mathrm{H}\,P_1\,\mathrm{H}\,P_0 \\
&= t^{\parallel\,2} \sum_{\langle i,j\rangle^{\parallel}_{\alpha},s} \Big[P_0 \left(n_{ixs}\, n_{jx\bar{s}} - c^{\dagger}_{ixs} c_{ix\bar{s}}\, c^{\dagger}_{jx\bar{s}} c_{jxs} \right) (1 - n_{jys}\, n_{jy\bar{s}})\, P_0 \\
&\qquad + P_0 \left(n_{iys}\, n_{jy\bar{s}} - c^{\dagger}_{iys} c_{iy\bar{s}}\, c^{\dagger}_{jy\bar{s}} c_{jys} \right) (1 - n_{jxs}\, n_{jx\bar{s}})\, P_0 \Big] \\
&+ t^{\perp\,2} \sum_{\langle i,j\rangle^{\perp}_{\alpha},s} \Big[P_0 \left(n_{iys}\, n_{jy\bar{s}} - c^{\dagger}_{iys} c_{iy\bar{s}}\, c^{\dagger}_{jy\bar{s}} c_{jys} \right) (1 - n_{jxs}\, n_{jx\bar{s}})\, P_0 \\
&\qquad + P_0 \left(n_{ixs}\, n_{jx\bar{s}} - c^{\dagger}_{ixs} c_{ix\bar{s}}\, c^{\dagger}_{jx\bar{s}} c_{jxs} \right) (1 - n_{jys}\, n_{jy\bar{s}})\, P_0 \Big] .
\end{aligned}
\tag{3.79}
$$

To reduce the projected expression further, we introduce the spin representation for the operators

$$
S^{\gamma}_{i\alpha} = \frac{1}{2} \sum_{s,s'} c^{\dagger}_{i\alpha s}\, \sigma^{\gamma}_{s\,s'}\, c_{i\alpha s'} \,, \tag{3.80}
$$

as in equation (3.16). The expression for the virtual processes then becomes

$$\begin{aligned} P_0\,\mathrm{H}\,P_1\,\mathrm{H}\,P_0 = -2t^{\parallel\,2}\sum_{\langle i,j\rangle^{\parallel}}\Bigg[&P_0\Big(\vec{S}_{ix}\cdot\vec{S}_{jx}-\frac{1}{4}\,n_{ix}\,n_{jx}\Big)\big(1-n_{jy\uparrow}\,n_{jy\downarrow}\big)P_0 \\ &+P_0\Big(\vec{S}_{iy}\cdot\vec{S}_{jy}-\frac{1}{4}\,n_{iy}\,n_{jy}\Big)\big(1-n_{jx\uparrow}\,n_{jx\downarrow}\big)P_0\Bigg] \\ -2t^{\perp\,2}\sum_{\langle i,j\rangle^{\perp}}\Bigg[&P_0\Big(\vec{S}_{iy}\cdot\vec{S}_{jy}-\frac{1}{4}\,n_{iy}\,n_{jy}\Big)\big(1-n_{jx\uparrow}\,n_{jx\downarrow}\big)P_0 \\ &+P_0\Big(\vec{S}_{ix}\cdot\vec{S}_{jx}-\frac{1}{4}\,n_{ix}\,n_{jx}\Big)\big(1-n_{jy\uparrow}\,n_{jy\downarrow}\big)P_0\Bigg]. \end{aligned} \tag{3.81}$$

In our setup, the denominator U of expression (2.23) is $U+V$. Then we can give the whole transformed Hamiltonian as

$$\begin{aligned} &P_0\,\tilde{\mathrm{H}}\,P_0 = P_0\,\mathrm{H}\,P_0 - P_0\,\mathrm{H}\,P_1\,\mathrm{H}\,P_0/\,(U+V) \\ &= -P_0\sum_{\alpha s}\Bigg\{t^{\parallel}\sum_{\langle i,j\rangle^{\parallel}_{\alpha}}\Big(c^{\dagger}_{j\alpha s}c_{i\alpha s}+\mathrm{h.c.}\Big)+t^{\perp}\sum_{\langle i,j\rangle^{\perp}_{\alpha}}\Big(c^{\dagger}_{j\alpha s}c_{i\alpha s}+\mathrm{h.c.}\Big)\Bigg\}P_0 \\ &\quad+J^{\parallel}\sum_{\langle i,j\rangle^{\parallel}_{\alpha}}\Bigg\{P_0\left(\vec{S}_{ix}\cdot\vec{S}_{jx}-\frac{1}{4}\,n_{ix}\,n_{jx}\right)\left(1-n_{jy\uparrow}\,n_{jy\downarrow}\right)P_0 \\ &\qquad\qquad+P_0\left(\vec{S}_{iy}\cdot\vec{S}_{jy}-\frac{1}{4}\,n_{iy}\,n_{jy}\right)\left(1-n_{jx\uparrow}\,n_{jx\downarrow}\right)P_0\Bigg\} \\ &\quad+J^{\perp}\sum_{\langle i,j\rangle^{\perp}_{\alpha}}\Bigg\{P_0\left(\vec{S}_{iy}\cdot\vec{S}_{jy}-\frac{1}{4}\,n_{iy}\,n_{jy}\right)\left(1-n_{jx\uparrow}\,n_{jx\downarrow}\right)P_0 \\ &\qquad\qquad+P_0\left(\vec{S}_{ix}\cdot\vec{S}_{jx}-\frac{1}{4}\,n_{ix}\,n_{jx}\right)\big(1-n_{jy\uparrow}\,n_{jy\downarrow}\big)P_0\Bigg\}, \end{aligned} \tag{3.82}$$

where we have introduced the two coupling strengths for the virtual processes as

$$J^{\parallel}=\frac{2\,t^{\parallel\,2}}{U+V}\,,\qquad\text{and}\qquad J^{\perp}=\frac{2\,t^{\perp\,2}}{U+V}\,. \tag{3.83}$$

When analyzing the transformed Hamiltonian, we have to keep in mind, that an additional factor of 2 comes about, when the sum over i and $j^{\parallel,\perp}$ is carried out.

3.5.4. Effective Hamiltonian

We can reduce the form of the transformed Hamiltonian (3.82) further, since we restrict our system to half-filling. For half-filling the kinetic part of Hamiltonian (3.82) directly drops out. In addition we can neglect the projectors P_0 and the operator contributions $(1 - n_{j\alpha s}\, n_{j\alpha \bar{s}})$.
After the analysis we find the effective Hamiltonian H_{SC} of the strong coupling limit as

$$\mathrm{H}_{SC} = \sum_{\alpha} \Bigg[J^{\parallel} \sum_{\langle i,j \rangle_{\alpha}^{\parallel}} \Big(\vec{S}_{i\alpha} \cdot \vec{S}_{j\alpha} - \frac{1}{4}\, n_{i\alpha} n_{j\alpha} \Big) + J^{\perp} \sum_{\langle i,j \rangle_{\alpha}^{\perp}} \Big(\vec{S}_{i\alpha} \cdot \vec{S}_{j\alpha} - \frac{1}{4}\, n_{i\alpha} n_{j\alpha} \Big) \Bigg] . \tag{3.84}$$

The summation i runs over all lattice sites. The summation of the nearest neighbors j, again, crucially depends on the considered orbital α, indicated by the summation indices $\langle i,j \rangle_{\alpha}^{\parallel,\perp}$. For the parallel components $\langle i,j \rangle_{\alpha}^{\parallel}$, the p_x-orbitals have nearest neighbors in x-direction and the p_y-orbitals in y-direction. On the other hand, the p_x-orbitals have their nearest neighbors in y-direction for the perpendicular components $\langle i,j \rangle_{\alpha}^{\perp}$ and the p_y-orbitals in x-direction. Note, for half-filling the particle number operator $n_{i\alpha}$ is fixed, since there are always two fermions per site and one per orbital.
In the appendix B.7.2 we investigate the effective Hamiltonian H_{SC} for a two-site model. We directly see, since $J^{\parallel,\perp} > 0$, the ground state for the strong coupling system is an antiferromagnet, as in the well-known Heisenberg scenario [141, 144, 145, 149]. Extending the investigation of the two-site model towards our N lattice system, we find an antiferromagnetic order to minimize the effective Hamiltonian H_{SC}. In fig. 3.15 we illustrate a possible ordering of three lattice sites within the system.

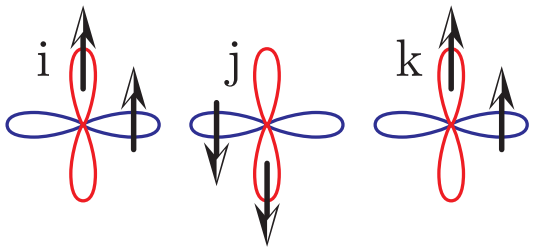

Fig. 3.15 Possible ordering of the half-filled strong coupling case, demonstrated for three lattice sites i, j, k. Each lattice site represents a spin triplet configuration. The overall order reveals an antiferromagnet.

3.5.5. Effective Hamiltonian in Spin-1 Representation

The effective Hamiltonian H_{SC} (3.84) describes the coupling of the Hilbert subspaces

$$\left(\mathcal{H}_{1/2} \otimes \mathcal{H}_{1/2}\right)_i \otimes \left(\mathcal{H}_{1/2} \otimes \mathcal{H}_{1/2}\right)_j = (\mathcal{H}_0 \oplus \mathcal{H}_1)_i \otimes (\mathcal{H}_0 \oplus \mathcal{H}_1)_j \ . \quad (3.85)$$

The next step is to find a reduced representation of the effective Hamiltonian H_{SC}. From our previous investigations we know, that the initial ground state was a spin triplet $|T_i\rangle$ for every lattice site i. In the strong coupling limit the ground state is described by an antiferromagnetic order. Thus the $(\mathcal{H}_0)_i$ subspace is not relevant for the reduced representation and we neglect these contributions.
In order to reduce the effective Hamiltonian further, we introduce spin-1 operators as

$$\vec{S}_i = \vec{S}_{ix} + \vec{S}_{iy} \, . \quad (3.86)$$

This allows us to transform the effective Hamiltonian (3.84) and bring it to a reduced form. The detailed introduction of the spin-1 operator representation is in appendix B.7.3. These new operators allow us to write the effective Hamiltonian H_{SC} in the form

$$\mathrm{H}_J = \frac{1}{4}\left(J^{\parallel} + J^{\perp}\right) \sum_{\langle i,j \rangle} \left(\vec{S}_i \cdot \vec{S}_j - \frac{1}{4} n_i \, n_j\right) \ , \quad (3.87)$$

where the operators $\vec{S}_i$ are now operators of the spin-1 representation, n_i is the particle number operator. Note, here the summation runs over all lattice sites

i and all nearest neighbors j. This Hamiltonian H_J now couples the subspaces

$$(\mathcal{H}_1)_i \otimes (\mathcal{H}_1)_j = (\mathcal{H}_0 \oplus \mathcal{H}_1 \oplus \mathcal{H}_2)_{ij} \ . \tag{3.88}$$

Thus, in this scenario there are additional coupling mechanisms possible, into a singlet, triplet and quintet. The representation of these additional couplings are also found in appendix B.7.3. Analyzing the reduced effective Hamiltonian H_J (3.87) for these possible configurations, we discover the singlet to reveal the lowest energy contribution.
In analogy to the well-known $t-J$ model [111, 147, 148], we find a transition towards an antiferromagnetic order. An antiferromagnetic configuration minimizes the energy and thus the effective Hamiltonian.
Hence, within the strong coupling regime, we encounter an additional magnetic phase transition.

3.6. Phase Diagram

To summarize the investigations we sketch the full phase diagram for our system in units of reduced chemical potential $\mu/t^{\parallel}$ and interaction strengths $(U+V)/t^{\parallel}$ for the zero temperature limit, see fig. 3.16. We focus on the case for vanishing magnetic field, $H=0$, and again the dominant order parameter $m = m_x + m_y$. In addition, we sketch a phase boundary for the sub-leading order parameter $\tilde{m} = m_x - m_y$ colored in yellow. For the hopping strengths we have chosen the ratio $t^{\perp}/t^{\parallel} = 1/2$.

3.6.1. Description of Phases

The different colors within the phase diagram represent the different phases of the system: the Fermi liquid regime with its paramagnetic phase is blue and labeled by "PM, FL"; the ferromagnetic phase is shown in green and has the "FM" label; red and labeled as "AF" is the Mott insulating regime, where the order is antiferromagnetic. The black line separating the phases serves as a sketch of the phase boundary between the paramagnetic and ferromagnetic phase and corresponds to the dominant order parameter m. On the other hand, the yellow line illustrates the phase boundary for the sub-leading order

parameter $\tilde{m}$. Here the transition is from the paramagnetic to ferromagnetic phase with orbital symmetry breaking. For the case of a dashed (dashed dotted) line the phase transition is of first order and becomes of second order, when the line becomes bold. Note, we give the phase diagram for the $\mu/t^{\parallel} > 0$ sector, since the $\mu/t^{\parallel} < 0$ case is symmetric to it and reveals the analog phases and their transitions.

3.6.2. Phase Transitions for Dominant Order Parameter

At half-filling, $\mu/t^{\parallel} = 0$, we observe two magnetic phase transitions. For small interactions the system is in a paramagnetic phase. Increasing the interaction strengths leads to a first order phase transition to a ferromagnet, characterized by a finite magnetization $m \neq 0$. The black dashed line between the two phases indicates the transition to be of first order. For large interaction strengths, a further phase transition takes place and the system becomes a Mott Insulator, where the spins order into a singlet and thus an antiferromagnet. Here it is important to stress, that the antiferromagnetic order is extended throughout the whole lattice system, where it can be characterized by two sublattices A, B, see [107, 141, 150]. The transition point towards the antiferromagnetic phase for a cold fermionic system in an optical lattice is at $U/t \sim 10$, see [151]. Be aware, in [151] they have just considered the common Hubbard interaction U, an isotropic hopping t and solely an s-orbital configuration. Nevertheless, the antiferromagnetic transition point of $U/t \sim 10$ serves as a good estimate even for our system and we thus sketch the antiferromagnetic phase starting from this value, $U/t \sim 10$.
At $\mu/t^{\parallel} = 1$ the van Hove singularity appears for the chosen hopping strengths and drives the phase transition to a ferromagnet even for very weak interactions, also see fig. 3.3. Hence, close to the van Hove singularity, the system strongly drives towards the ferromagnetic order.
For increasing chemical potentials $\mu/t^{\parallel} > 1$ we only discover the paramagnet to ferromagnet phase transition, where the phase transition is still of first order, shown by the black dashed line separating the two phases. At the critical value $\mu_{crit}/t^{\parallel} \approx 2.37$ the order of the paramagnetic to ferromagnetic phase transition changes to second order. This is illustrated by the bold black line between

the phases. For details regarding the critical value $\mu_{crit}/t^{\parallel}$ compare to the behavior of the transition temperature fig. 3.8 as well as the solutions for the magnetization fig. 3.10.

3.6.3. Phase Transitions for Sub-Leading Order Parameter

In addition to the order parameter m – it only considers spin imbalance instabilities and its corresponding phases – we also have sketched the phase boundary of the additional order parameter $\tilde{m} = m_x - m_y$ for a small and fixed value of the interaction strength V. The phase boundary is indicated by the dashed dotted yellow line within the phase diagram fig. 3.16. In contrast to the dominant order parameter, here the phase transition takes place between a paramagnetic phase and a phase with ferromagnetic order as well as orbital symmetry breaking. This transition is again of first order up to the critical value $\mu_{crit}/t^{\parallel} \approx 2.37$, where the transition becomes of second order. The second order transition is marked by the bold yellow line within the diagram.
For the $\tilde{m}$ order parameter the system requires larger absolute interaction strengths to trigger the phase transition towards the ferromagnetic and orbital symmetry breaking phase, compared to the previous scenario.
The influence of the van Hove singularity remains as before. Additional details of the phase boundaries and the tricritical point, we leave to further discussions.

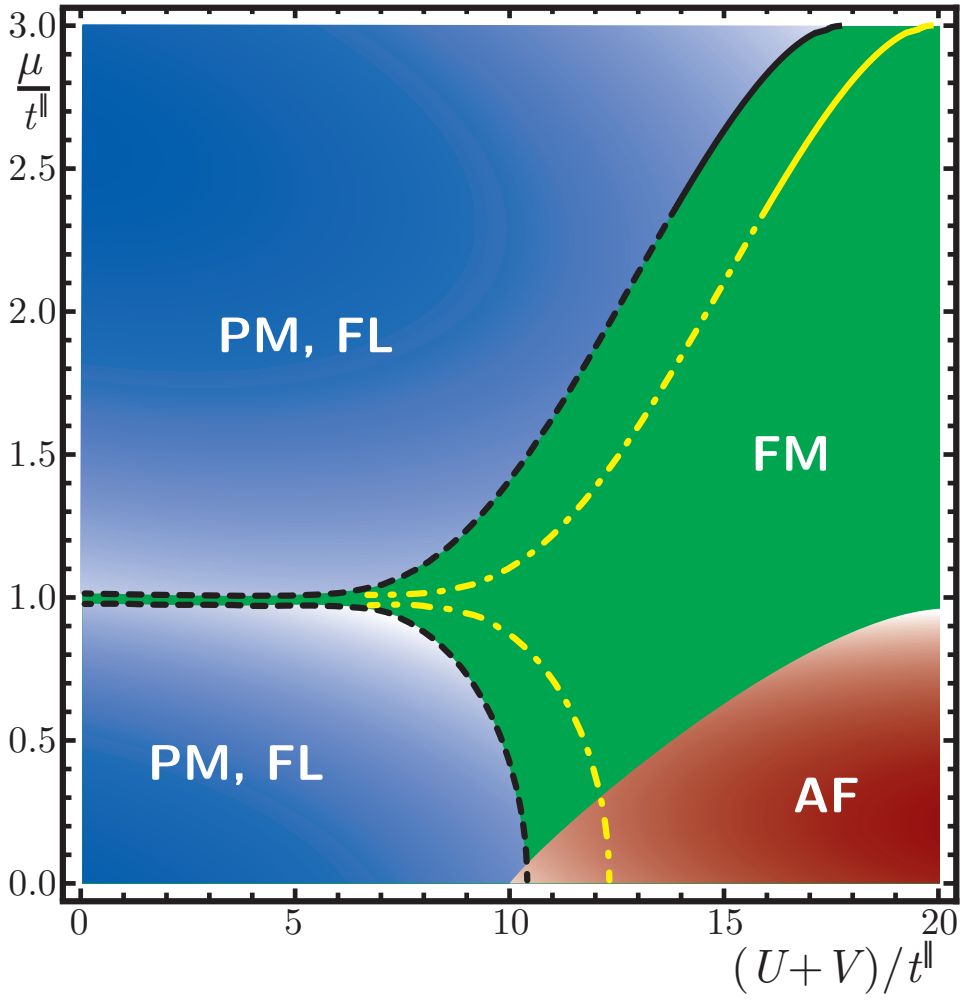

Fig. 3.16 Zero temperature phase diagram for vanishing magnetic field. The axes are the reduced chemical potential $\mu/t^{\parallel}$ and interaction strengths $(U+V)/t^{\parallel}$ for hopping strengths $t^{\perp}/t^{\parallel} = 1/2$ and the dominant order parameter m. The different colors represent the different phases within the system: blue with label "PM, FL" gives the Fermi liquid with paramagnetic order; green and "FM" is the ferromagnetic phase with $m \neq 0$; red, labeled with "AF", the antiferromagnetic phase. The dashed (dashed dotted) line separating the phases indicates a first order transition. The bold line marks the transition of second order. The dashed dotted line in yellow gives the phase boundary for the sub-leading order parameter $\tilde{m}$ for the paramagnetic to phase with ferromagnetic order and orbital symmetry breaking. The phase boundary for the sub-leading order parameter $\tilde{m}$ is given for a small and fixed value of V. Further details see text.

3.7. Experimental Proposal

We propose an optical lattice setup to realize the theoretically discussed system. The main idea is to simulate the physics of the orbitals through internal states of the involved fermionic atoms.
The two anisotropic optical lattices have the same structure and have different lattice depths in x- and y-direction, see fig. 3.17. The optical lattices are created in the standard procedure of counter propagating lasers, where the system is strongly confined in z-direction, in order to produce 2D planes. We create two 2D planes and rotate them by an angle of $\pi/4$ with respect to each other.
The next important step is to create a spin-dependent optical lattice system. Prominent candidates here are alkaline-earth atoms such as ^{87}Sr, with the long-lived meta-stable $^3P_0$ state, see section 2.2. The spin-dependent optical lattices are tuned to the magic wavelength condition [58, 63, 73], where one optical lattice is prepared to match the $^1S_0$ state, the other for the meta-stable $^3P_0$ state. In addition, the lattices are bipartite, indicated in fig. 3.17 through the alternating signs.
The optical lattices are tuned to have different lattice depths for x- and y-direction to achieve the anisotropic hopping strengths $t^{\parallel}$ and $t^{\perp}$. Note, if different laser strengths are required, it is possible to use the mirror technique introduced in [152]. For details regarding the magic wavelength or bipartite optical lattice see the general concepts, section 2.1 and 2.2.
The light assisted inelastic two body loss channels in alkaline-earth setups – between $^1S_0$ - $^3P_0$ atoms or two atoms in the excited $^3P_0$ state – are theoretically [81, 153] and experimentally well-known [78, 154, 155]. If these inelastic processes can be suppressed, our system thus becomes feasible in the near future.
In fig. 3.17a) we sketch the principle setup of the optical lattice system, where we have shifted the two lattices out of plane, for sake of visualization. This optical lattice system then can be used to simulate the behavior of the p_x- and p_y-orbitals. The lower optical lattice is addressed to match the ground state of the alkaline-earth atoms, where the upper optical lattice is tuned to the magic wavelength, such that it can be occupied by alkaline-earth atoms in the meta-stable state $^3P_0$. The anisotropic hopping strengths $t^{\parallel}$ and $t^{\perp}$ are tuned

via the different lattice depths. The different spin configurations $s = \uparrow, \downarrow$ are indicated by the different colors, red relates to spin up and green to spin down. We give the top view of each optical lattice in fig. 3.17b), where the anisotropic, as well as bipartite, nature of the optical lattices is observed. The lattices are again shifted out of plane. The different signs represent the bipartite lattice sites. In addition, we mark two directions in the figure, where we cut along the optical lattice system in order to illustrate the different mechanisms in fig. 3.17c) and d). The different colors for the fermions again relate to the color code introduced in fig. 3.17a).
In fig. 3.17c) and d) we show the cuts through the optical lattice system along direction 1 and 2 as indicated in fig. 3.17b), with all relevant quantities as parallel hopping $t^{\parallel}$, perpendicular hopping $t^{\perp}$, the intra-orbital interaction strength U and the inter-orbital interaction strength V. The two lattices are shifted out of plane as well, for sake of visualization.

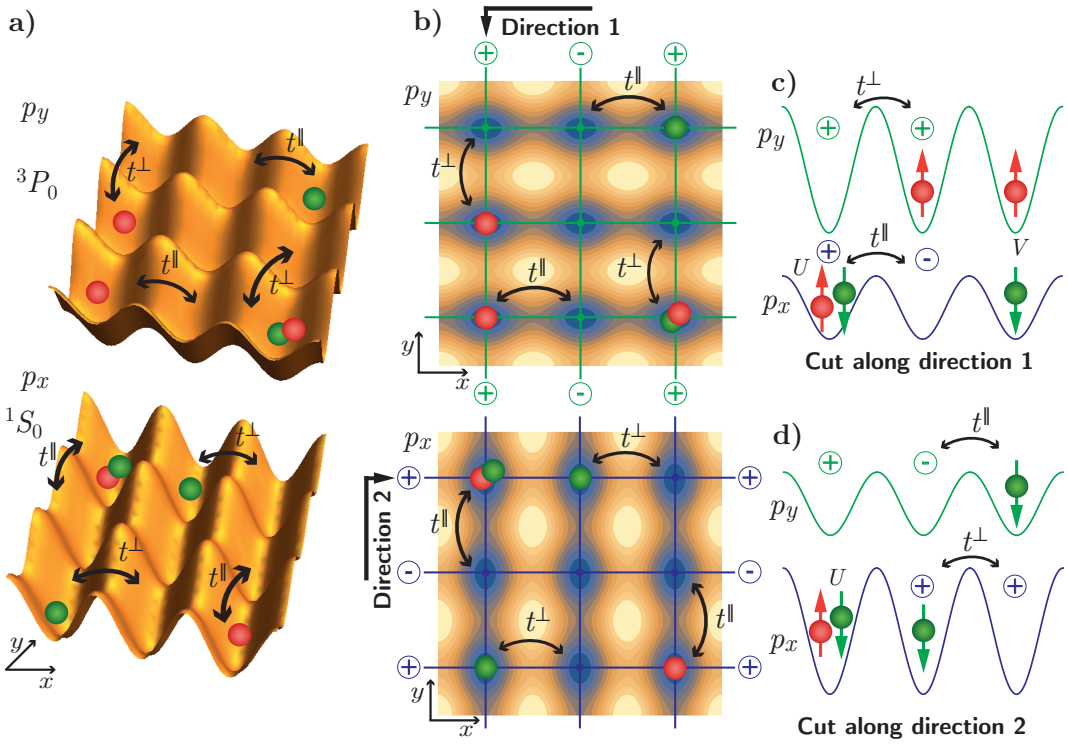

Fig. 3.17 Principle optical lattice setup for the two internal states of the alkaline-earth atoms, with the bipartite, as well as anisotropic, lattice structure. The optical lattices are shifted out of plane. The different internal states of the alkaline-earth atoms are red for spin up and green for spin down. The parallel hopping strength is given by $t^{\parallel}$ and the perpendicular as $t^{\perp}$. **a)** Total view of the optical lattices, showing all essential features. **b)** Top view for both lattices, to focus on the bipartite and anisotropic nature of the lattice as well as give the directions for the cut along the system. **c)** and **d)** Cut along direction 1 and 2, respectively. Here the two possible interaction strengths – intra-orbital U and inter-orbital V – can be visualized. For further details see text.

3.8. Conclusion and Outlook

To conclude, we have demonstrated how our simple model can be used to create a quantum simulator for spin-orbital magnetism. It can be realized within experimental progress in the near future. Our system shows promising steps incorporating orbital physics in the framework of optical lattices without the shortcomings of solid state systems. It paves the way towards d-orbital physics in optical lattices and the glimpse of solving open solid state mysteries in a controllable environment.

Even for this simple model we discovered a rich phase diagram of competing phases – most of spin-1 configuration – as well as a possible tricritical point for the phase transitions. In addition, we found a phase with potential orbital ordering.

We derived the microscopic Hamiltonian from the general second quantized Hamiltonian, for the present p_α-orbital system and investigated it in-depth. The kinetic part of the Hamiltonian is influenced by two van Hove singularities, which are due to the anisotropic hopping strengths $t^{\parallel}$ and $t^{\perp}$. The interaction part delivers two interaction strengths, an intra-orbital interaction U, comparable to the well-known Hubbard interaction, as well as an inter-orbital interaction V, considering the interaction between the p_x- and p_y-orbital.

From the preliminary investigations for a single-site model we found the system to experience a possible phase transition for increasing interaction strengths. We extended these investigations in a mean-field analysis and discovered various possible phase transitions. One phase transition is from a paramagnet towards a ferromagnet with finite magnetization. Another phase transition is towards a ferromagnet with orbital symmetry breaking. The latter phase transition is suppressed in contrast to the pre-empted well-known paramagnet to ferromagnet transition. In addition, we analyzed the temperature, as well as the influence of an external magnetic field.

Then we extended the calculations and evaluated the strong coupling limit for the half-filled case. Here we derived an effective Hamiltonian in analogy to the well-known $t - J$ scenario. In this large interaction limit the ground state is an antiferromagnet.

After these investigations we were able to sketch the phase diagram of our

system for the dominant order parameter and discovered its richness with respect to the transitions. We even found a possible tricritical point in the phase diagram.
The proposed optical lattice system and its sensitivity for internal states can thus be used to simulate the behavior of the p_x- and p_y-orbital. This setup then allows us to create a quantum simulator to simulate the intrinsic behavior of the different orbitals within the solid state Hamiltonian (3.1) and opens the path for a better understanding of the mechanisms of solid state systems in the toolbox of cold gases experiments.

So far, we were only interested in spin imbalance instabilities and their corresponding phases. For the sub-leading phase transition we found a possible orbital ordering. Thus, the next step is to investigate orbital instabilities. To this end it is necessary to introduce a new set of order parameters as $m = m_x + m_y$ – the common magnetization – $\bar{m} = m_x - m_y$ – the magnetization with orbital symmetry breaking – and $O = n_x - n_y$ – the pure orbital symmetry order parameter. This setup was investigated recently [143].
For the new set of order parameters it is also recommended to extend the analysis to an energy functional approach. This then covers all scenarios for all potential phase transitions. The investigation of the orbital imbalance instability then would shed light into the mechanisms of the phase transitions and reveal the potential of our simple model.
An additional step for further investigations would be to analyze the spin-1 Hamiltonian of the strong coupling regime in more detail and find additional transitions for this limit.

CHAPTER

FOUR

MAJORANA MODES AND *P*-WAVE SUPERFLUIDS

The interest in non-Abelian phases of matter increased in recent years due to developments in the research area of p-wave superconductors. One prime example supporting non-Abelian quasiparticles is the $p_x + ip_y$-wave superconductor in 2D as it also exhibits Majorana modes in vortices. This superconductor can serve as a blueprint of fractional topological order. On the other hand, Kitaev proposed Majorana wires to be an ideal playground to understand the physics of Majorana modes. In this chapter we demonstrate the transition from the Majorana wire setup by Kitaev [156] to a two-dimensional p-wave superconductor system [157] within cold atomic gases in an optical lattice.
The central idea is the coupling of orbital degrees of freedom with strong s-wave interactions in order to create p-wave interactions. In the following we demonstrate that our approach supports Majorana modes at edge dislocations in the optical lattice and we describe a protocol to pinpoint the non-Abelian statistics within a cold atomic gas experiment.

We begin with a short introduction to the basic concepts essential for the further investigations. Then a brief overview on the research fields of topological and superconducting phases is given and their shortcomings with respect to possible experimental realizations are discussed. The features of cold atomic gases are highlighted to pave a path towards p-wave superfluidity and its possible quantum simulation. Afterwards we explain in detail our system and focus on our calculations.

4.1. Basic Concepts

In the following we briefly review the basic concepts of Majorana fermions in condensed matter physics. We then comment on non-Abelian statistics of Majorana modes. Finally we illustrate the main idea of the Bogoliubov-de Gennes Hamiltonian and its transformation.

4.1.1. Majorana Fermions and non-Abelian Statistics

In our presentation of the Majorana fermions and their properties, we follow the road given in [158]. The special feature of Majorana fermions is that the particle is its own anti-particle. In terms of operators this reads

$$\gamma_i = \gamma_i^\dagger \,, \tag{4.1}$$

where $\gamma_i^{(\dagger)}$ annihilates (creates) a Majorana fermion at site i. The operators obey the anti-commutation relation

$$\left\{\gamma_i, \gamma_j^\dagger\right\} = \gamma_i\,\gamma_j^\dagger + \gamma_j^\dagger\,\gamma_i = \delta_{ij}\,. \tag{4.2}$$

Fermion operators $c_i^{(\dagger)}$ can be constructed out of two of the introduced Majorana operators such that

$$c_1^\dagger = \frac{1}{\sqrt{2}}\left(\gamma_{A,1} + i\gamma_{B,2}\right)\,, \qquad c_1 = \frac{1}{\sqrt{2}}\left(\gamma_{A,1} - i\gamma_{B,2}\right)\,. \tag{4.3}$$

Conversely, the Majorana operators can be expressed through the fermionic operators

$$\gamma_{A,1} = \frac{1}{\sqrt{2}}\left(c_1^\dagger + c_1\right)\,, \qquad \gamma_{B,2} = \frac{1}{i\sqrt{2}}\left(c_1^\dagger - c_1\right)\,. \tag{4.4}$$

The Majorana operator γ_i thus changes the number of fermions between even and odd. The operator for the fermion parity of a single fermion mode c_1 can be defined as

$$P = 1 - 2\,c_1^\dagger c_1 = 2i\,\gamma_{A,1}\gamma_{B,2}\,. \tag{4.5}$$

It takes the eigenvalues $+1$ for an empty state and -1 for an occupied one.

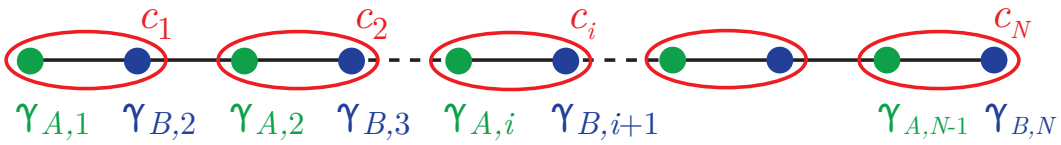

Fig. 4.1 Kitaev chain in 1D with N lattice sites. The fermions are marked in red and described by the operators c_i (4.3). They can be constructed from two Majorana operators (4.4), figure adapted from [158].

In 2001, A. Kitaev introduced a toy model [156] to implement Majorana fermions. The model is a p-wave superconducting system of a one-dimensional chain of spinless fermions. The Hamiltonian is of the form

$$\mathrm{H} = -\sum_{i=1}^{N-1} \left(t\, c_i^\dagger c_{i+1} + \Delta\, e^{i\phi}\, c_i c_{i+1} + \mathrm{h.c.} \right) - \mu \sum_{i=1}^{N} c_i^\dagger c_i \,, \tag{4.6}$$

where t is the hopping strength, $\Delta e^{i\phi}$ the superconducting order parameter, μ the chemical potential and N the number of lattice sites, see also fig. 4.1. We consider a special parameter set for the Hamiltonian, namely $\mu = 0$ and $t = \Delta$. The Hamiltonian then becomes

$$\begin{aligned} \mathrm{H} &= -t \sum_{i=1}^{N-1} \left(c_i^\dagger c_{i+1} + e^{i\phi}\, c_i c_{i+1} + \mathrm{h.c.} \right) \\ &= -t \sum_{i=1}^{N-1} \left(e^{i\phi/2}\, c_i + e^{-i\phi/2}\, c_i^\dagger \right) \left(e^{i\phi/2}\, c_{i+1} - e^{-i\phi/2}\, c_{i+1}^\dagger \right) . \end{aligned} \tag{4.7}$$

Next, we introduce the operators

$$\gamma_{B,i} = \frac{1}{\sqrt{2}} \left(e^{i\phi/2}\, c_i + e^{-i\phi/2}\, c_i^\dagger \right) , \quad \gamma_{A,i} = \frac{1}{i\sqrt{2}} \left(e^{i\phi/2}\, c_i - e^{-i\phi/2}\, c_i^\dagger \right) , \tag{4.8}$$

which are again Majorana fermions and obey the relation (4.1), as can be easily checked. The Hamiltonian (4.7) then reads

$$\mathrm{H} = -2it \sum_{i=1}^{N-1} \gamma_{B,i}\, \gamma_{A,i+1} \,. \tag{4.9}$$

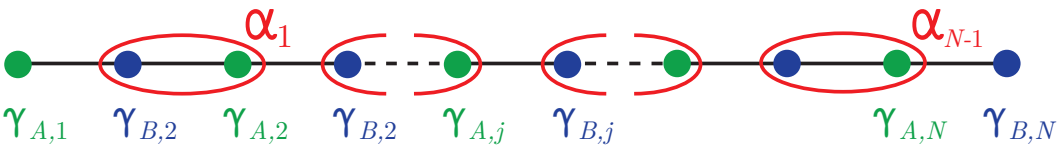

Fig. 4.2 Kitaev chain in 1D with N lattice sites. The Majorana fermions are labeled by $\gamma_{A,i}$ and $\gamma_{B,i}$. They then form a new quasiparticle α_i, which is again a fermion. The two Majorana fermions at the beginning $\gamma_{A,1}$ and the end of the chain $\gamma_{B,N}$ are unpaired. The figure is adapted from [158].

Now we are able to define an alternative fermion operator through

$$\alpha_i = \frac{1}{\sqrt{2}} \left(\gamma_{A,i+1} + i\gamma_{B,i} \right) , \tag{4.10}$$

where we have combined the two Majorana fermions $\gamma_{B,i}$ and $\gamma_{A,i+1}$ and we find

$$i\gamma_{B,i}\,\gamma_{A,i+1} = \frac{1}{2} - \alpha_i^\dagger \alpha_i \,. \tag{4.11}$$

The Hamiltonian (4.9) can be written as

$$\mathrm{H} = 2t \sum_{i=1}^{N-1} \alpha_i^\dagger \alpha_i - (N-1)\, t \,, \tag{4.12}$$

also see fig. 4.2. We can directly observe, that all pairs $\left(\gamma_{B,i}\,,\,\gamma_{A,i+1}\right)$ for $i = 1, 2, ..., N-1$ give new fermions described by α_i. The Majorana fermions at the beginning of the chain $\gamma_{A,1}$ and the end $\gamma_{B,N}$ are unpaired.

The ground-state of the 1D chain $|g\rangle$ then is the state where $\alpha_i|g\rangle = 0$ for all i and thus

$$\mathrm{H}|g\rangle = -\,(N-1)\, t\, |g\rangle \,. \tag{4.13}$$

Since we have two degenerate Majorana modes with $\gamma_{A,1}$ and $\gamma_{B,N}$, which are absent from the Hamiltonian (4.12), we can define a zero-energy fermion $\alpha_0 = \frac{1}{\sqrt{2}} \left(\gamma_{A,1} + i\gamma_{B,N} \right)$. We directly find $\langle g|\alpha_0|g\rangle = 0$ and obtain a relation for the operators $\gamma_{A,1}$, $\gamma_{B,N}$ acting on $|g\rangle$ such as

$$\langle g|\gamma_{A,1}\gamma_{B,N}|g\rangle = \left\langle g \middle| \frac{1 - 2\alpha_0^\dagger \alpha_0}{2i} \middle| g \right\rangle = \begin{cases} +\frac{i}{2} & \text{for} \quad \alpha_0^\dagger \alpha_0 = 1 \\ -\frac{i}{2} & \text{for} \quad \alpha_0^\dagger \alpha_0 = 0 \end{cases} . \tag{4.14}$$

The eigenvalue is determined by the number parity of the ground-state $|g\rangle$. The ground state manifold of the introduced 1D chain, the Kitaev model, is doubly degenerate and is characterized by different parities. The state $|g\rangle$ has even parity and $\alpha_0 |g\rangle$ has odd. The stable double degeneracy indicates that the Kitaev model is topologically non-trivial and thus promises interesting features and applications on the boundary of condensed matter physics and quantum information theory.
For further details and research see [156, 159–168].

Non-Abelian Statistics

A group G is called Abelian, if the elements a, b within the group commute

$$ab = ba\,, \quad \text{for all} \quad a,\, b \in G\,. \tag{4.15}$$

Thus, non-Abelian statistics means

$$ab \neq ba\,. \tag{4.16}$$

Majorana fermions follow non-Abelian statistics, i.e. they "know" by which path they were commuted, in contrast to bosons and fermions, see fig. 4.3. The non-Abelian statistic of Majorana modes is best demonstrated via the fusion process after braiding two modes. For further reading regarding non-Abelian statistics and anyons see [169].
Details to Abelian statistics can be found in literature regarding Algebra [170, 171] or specialized books for group theory [172–174].

4.1.2. Bogoliubov-de Gennes Hamiltonian

The BCS theory was developed to describe superconductivity on a microscopic level [24, 175]. Within a mean-field approach the well-known BCS Hamiltonian is of the form

$$\mathrm{H_{BCS}} = \sum_{\mathbf{k}\sigma} \xi_{\mathbf{k}}\, c^{\dagger}_{\mathbf{k}\sigma} c_{\mathbf{k}\sigma} - \sum_{\mathbf{k}} \left(\Delta^{*}_{\mathbf{k}}\, c_{-\mathbf{k}\downarrow} c_{\mathbf{k}\uparrow} + \Delta_{\mathbf{k}}\, c^{\dagger}_{\mathbf{k}\uparrow} c^{\dagger}_{-\mathbf{k}\downarrow} \right) + \text{const.}\,, \tag{4.17}$$

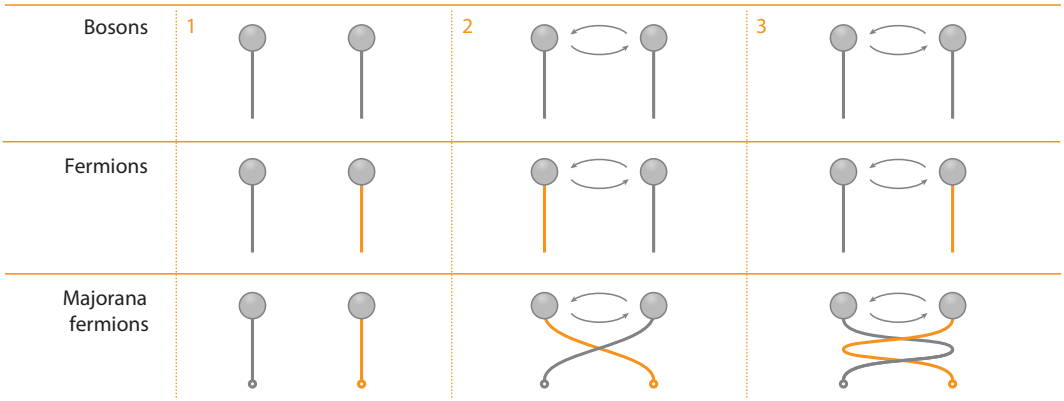

Fig. 4.3 Bosons, fermions and Majorana fermions are compared with respect to their behavior under braiding. For bosons it holds $|\Psi_a\Psi_b\rangle = |\Psi_b\Psi_a\rangle$. For fermions $|\Psi_a\Psi_b\rangle = -|\Psi_b\Psi_a\rangle = |\Psi_a\Psi_b\rangle$. Majorana fermions do not follow the preceding mechanisms. Interchanging positions results in intertwining the paths of the Majorana fermions, which gives rise to non-Abelian statistics. The figure is taken and adapted from [164].

where $\xi_{\mathbf{k}} = \epsilon_{\mathbf{k}} - \mu$, with $\epsilon_{\mathbf{k}}$ being the dispersion relation, μ the chemical potential, $\Delta_{\mathbf{k}}$ the superconducting gap order parameter, $c^{(\dagger)}_{\pm\mathbf{k}\sigma}$ the fermionic annihilation (creation) operator and σ is the spin $\uparrow\downarrow$. The Hamiltonian describes pure, homogeneous superconductors. Diagonalizing reveals the excitation spectrum

$$E_{\mathbf{k}} = \pm\sqrt{\xi_{\mathbf{k}}^2 + |\Delta_{\mathbf{k}}|^2}\,. \tag{4.18}$$

Since the theory is on a mean-field level, the gap parameter then has to be determined self-consistently [175].

The situation and equations become more challenging if a spatially inhomogeneous superconductor is considered. For this case, the superconducting order parameter becomes spatially variable and has to be described by Δ_{ij}, where ij is the position of the edge between sites i and j. Examples for such situations are dirty superconductors, if a vortex core is present, a lattice dislocation, near an interface with another material, and a configuration of two superconducting materials sandwiching a normal material (SNS) [175, 176].

Diagonalizing Hamiltonian (4.17) in $\mathbf{k}$-space is no longer possible because of the position dependency of the gap parameter Δ_{ij}.

In order to tackle this problem we introduce the *Bogoliubov-de Gennes Hamiltonian* defined in position space

$$\mathrm{H_{BdG}} = -\sum_{\langle i,j\rangle,\sigma} t_{ij}\, c^{\dagger}_{j\sigma} c_{i\sigma} + \sum_{i,j}\left(\Delta^{*}_{ij}\, c_{i\downarrow} c_{j\uparrow} + \Delta_{ij}\, c^{\dagger}_{j\uparrow} c^{\dagger}_{i\downarrow}\right) - \mu \sum_{i\sigma} c^{\dagger}_{i\sigma} c_{i\sigma}\,, \tag{4.19}$$

where t_{ij} is the hopping parameter to nearest neighbor sites and μ is the chemical potential. The Hamiltonian $\mathrm{H_{BdG}}$ can be diagonalized efficiently by introducing quasi-particle operators $\alpha^{(\dagger)}_{i\sigma}$ [176]. In addition, the gap parameter Δ_{ij} has to be determined accordingly. Depending on the considered system, the gap parameter Δ_{ij} can be spin-dependent. These additional contributions make the required diagonalization of the system more complicated. On the other hand, based on symmetry arguments or further assumptions, the Bogoliubov-de Gennes Hamiltonian can also be simplified to make the calculations manageable. For additional insight into the microscopic theory of homogeneous and inhomogeneous superconductors see [149, 175–178].

4.2. p-Wave Analysis

Topological phases supporting non-Abelian anyons [179] have been of wide interest, especially with the potential application in topological quantum computing [180, 181]. There are several system which have been investigated, such as superfluid ^{3}He-A [182], the layered superconductor $\mathrm{Sr_2Ru\,O_4}$ [183] and the fractional quantum Hall state at filling $\nu = 5/2$ [184, 185]. Further research has been conducted on semiconductor-superconductor heterostructures [186, 187] as well as systems where the semiconductor is a 1D quantum wire with spin-orbit coupling [188, 189]. Recently an additional candidate, namely indium antimonide nano-wires in contact with an s-wave superconductor, showed evidence of the elusive non-Abelian zero-energy Majorana states [190, 191]. For an overview of the research area of Majorana fermions in superconductors see [162]. Despite the progress in these fields there are still open questions to address:

In the last couple of years the focus on cold atomic gases was deepened and wide spread, establishing a different angle on p-wave superconductors. Cold

atomic gases have different strengths and shortcomings compared to solid state systems and might offer solutions to problems which are hard to address in solid state experiments. A prime example is the controllability of the spatial dimensions of a setup by optical lattices [30] and the high tunability of the interaction strengths in the system through Feshbach resonances [192]. A shortcoming in this field is the very limited lifetime of atomic p-wave resonant gases where the decay channels are well understood [193, 194]. This fact poses as a central challenge to identify possible realizations of p-wave superfluids with sufficient lifetimes. Ideas to circumvent the decay channels are, for example, Bose-Fermi mixtures in optical lattices [195–197], microwave dressed polar molecules [198], the quantum Zeno effect [199], and driven dissipation [200]. Even synthetic spin-orbit coupling with the use of s-wave interactions was proposed theoretically [201, 202], as well as the idea of coupling nanoplasmonic fields with synthetic gauge fields to design p-wave interactions [203]. The experimental implementation of synthetic spin-orbit coupling via ultracold atomic collisions was promising [204], but further experimental realizations to these previous theoretical proposals have so far been precluded by the complexity of the setups.

Here we present a proposal for an experimental realization of p-wave superfluids with the advantage of feasibility within contemporary experimental techniques in cold atomic gases setups. In the following we explain our system, the required calculations and the obtained phase diagrams.

4.2.1. Lattice Setup

We begin our considerations with the lattice setup and build up everything else from there. We consider a two-dimensional optical square lattice, created by counter propagating lasers. We tune the lattice system such that an additional minimum in the center of each lattice square appears, see fig. 4.4a). We refer to this minimum as *plaquette*. These plaquettes form a dual lattice of our lattice system. States within the plaquettes are labeled by $|...\rangle_p$.

In order to realize a system which exhibits Majorana modes and experiences topological properties, we propose fermionic alkaline-earth atoms such as ^{87}Sr or ^{171}Yb atoms in our lattice system. The metastable $^3P_2$ state of the alkaline-

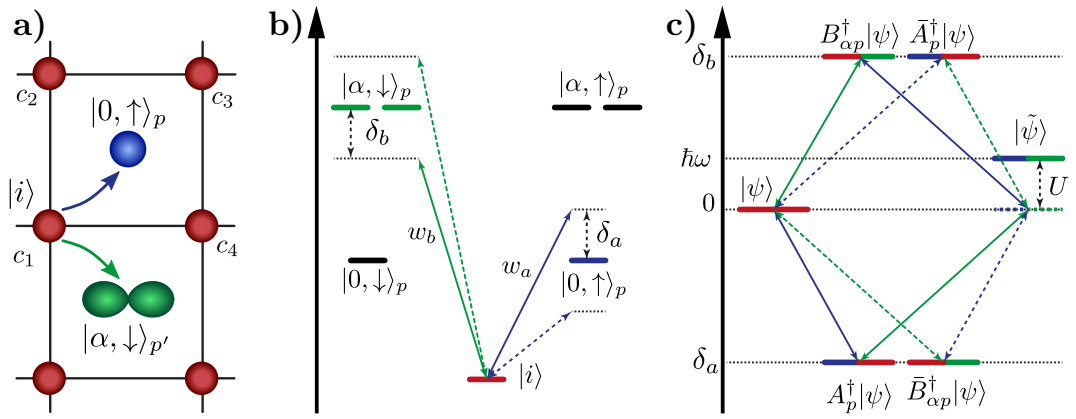

Fig. 4.4 Microscopic and experimental setup. **a)** The spinless fermions reside on the lattice sites i and are coupled to two different internal states which are trapped in the center of the plaquettes p. The lattice sites surround the plaquettes. The first state on the plaquette $|0,\uparrow\rangle_p$ exhibits an s-wave orbital symmetry, whereas the second state $|\alpha,\downarrow\rangle_p$ gives a p_α-wave symmetry and is twofold degenerate. **b)** Single particle energy level structure. The relevant transitions of the system are illustrated by solid lines. The dashed lines denote the additional transitions which are required for the design of the desired coupling Hamiltonian. **c)** Basic energy levels for the two-particle states with the two interfering paths to obtain the molecular state in the plaquette: The states on the lattice sites are described by $|\psi\rangle$, whereas the states with the near resonant repulsively bound molecule, exhibiting p-wave symmetry, are given by $|\tilde{\psi}\rangle = \left(A^\dagger_p B^\dagger_{\alpha p} - \bar{A}^\dagger_p \bar{B}^\dagger_{\alpha p}\right)|\psi\rangle$. For details see main text. Figure taken and adapted from [205].

earth atoms will be a key ingredient. The optical lattice is then created such that these metastable states are trapped at the sites of the optical lattice, whereas the ground state ${}^1S_0$ is trapped in the center of plaquettes, see fig. 4.4a). It is tuned close to the anti-magic wavelength, see section 2.2. This setup requires only *one* 2D optical lattice. In addition, light assisted two-particle losses from the metastable ${}^3P_2$ are quenched due to their fermionic statistics.

To simplify the investigations, we start with spinless fermionic atoms. We address the fermionic annihilation (creation) operators acting on states of the lattice sites i with $c_i^{(\dagger)}$. Next we introduce the operators for the states on the plaquettes. We are interested in two different hyperfine states of the electronic

ground state ${}^1S_0$ which will be denoted by a spin index $\sigma \in \{\uparrow, \downarrow\}$. The lowest lying states are then $|0, \sigma\rangle_p$. In particular, $a_p^\dagger$ creates $|0, \uparrow\rangle_p$ and exhibits s-wave symmetry, see fig. 4.4a). The first excited state $|\alpha, \sigma\rangle_p$ with $\alpha \in \{x, y\}$ is twofold degenerate and exhibits p-wave symmetry. The state $|\alpha, \downarrow\rangle_p$ is created by the operator $b_{\alpha p}^\dagger$, see fig. 4.4b). We focus on the details of the symmetry arguments in sec. 4.2.2. Similar setups for bosonic atoms have been previously proposed [206].
The coupling between the states on the lattice to the center of the plaquette is driven by two Raman transitions or alternatively by direct transitions. We have to investigate the two transitions further to give the corresponding Hamiltonians for the different processes. The first Raman transition couples to the plaquette state $|0, \uparrow\rangle_p$ through the Hamiltonian

$$\mathrm{H}_a = w_a \sum_p \left(A_p^\dagger + A_p \right) , \tag{4.20}$$

with the operator $A^\dagger = a_p^\dagger \left(c_1 + c_2 + c_3 + c_4\right)$. For the ordering of the operators c_i see fig. 4.4a). The coupling strength $w_a = E_a + \delta_a$ accounts for the coupling energy, the strength of the Rabi frequency and wave function overlap. It includes the energy of the excited state E_a as well as the detuning δ_a. The second coupling Hamiltonian is

$$\mathrm{H}_b = w_b \sum_{\alpha, p} \left(B_{\alpha p}^\dagger + B_{\alpha p} \right) , \tag{4.21}$$

where $B_{x/y\,p}^\dagger = b_{x/y\,p}^\dagger \left(c_1 \pm c_2 - c_3 \mp c_4\right)$ and $w_b = E_b + \delta_b$ is the coupling energy for the second transition. It also includes the detuning δ_b, see fig. 4.4b). Note, the energies $E_{b,\alpha}$ for the excited states created by $B_{\alpha p}^\dagger |\psi\rangle$ are the same such that we can solely write E_b for these energies, see fig. 4.4b). For sake of simplicity, we set $\delta_b = -\delta_a$ and $w_a = w_b$.

4.2.2. Symmetry of Operators

The symmetries of the involved states $|0, \sigma\rangle_p$ and $|\alpha, \sigma\rangle_p$ become clear when we investigate the behavior of the corresponding operators under a spatial rotation

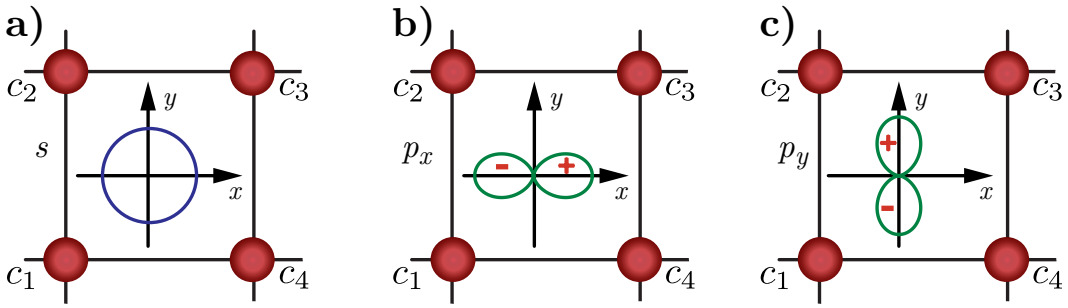

Fig. 4.5 The lattice sites are numbered as given by the operators c_i and contain a plaquette p, where one (two) fermion(s) can occupy a (molecular) state. **a)** A fermion occupying a state exhibiting s-wave symmetry in the center of the plaquette. **b)** Two lattice fermions form a molecular state with p_x-wave symmetry. **c)** Analogous molecular state with p_y-wave symmetry. Figure adapted from [205].

by $\pi/4$, in the mathematically positive direction. In fig. 4.5 we give a sketch of the different symmetries present. The operators of interest are

$$\begin{aligned} s-\text{wave:} \quad & A_p^\dagger = a_p^\dagger \, (c_1 + c_2 + c_3 + c_4) \, , \\ p_x-\text{wave:} \quad & B_{xp}^\dagger = b_{xp}^\dagger \, (c_1 + c_2 - c_3 - c_4) \, , \\ p_y-\text{wave:} \quad & B_{yp}^\dagger = b_{yp}^\dagger \, (c_1 - c_2 - c_3 + c_4) \, . \end{aligned}$$

Now we rotate every operator by $\pi/4$ counterclockwise to pinpoint its behavior

$$\begin{aligned} A_p^\dagger : \quad & (c_1 + c_2 + c_3 + c_4) \xrightarrow{\pi/4} (c_4 + c_1 + c_2 + c_3) \Rightarrow A_p^\dagger \, , \\ B_{xp}^\dagger : \quad & (c_1 + c_2 - c_3 - c_4) \xrightarrow{\pi/4} (c_4 + c_1 - c_2 - c_3) \\ & = (c_1 - c_2 - c_3 + c_4) \Rightarrow B_{yp}^\dagger \, , \\ B_{yp}^\dagger : \quad & (c_1 - c_2 - c_3 + c_4) \xrightarrow{\pi/4} (c_4 - c_1 - c_2 + c_3) \\ & = -\,(c_1 + c_2 - c_3 - c_4) \Rightarrow -B_{xp}^\dagger \, . \end{aligned}$$

Note that the operators $b_{\alpha p}^{(\dagger)}$ are only fixed up to a phase. This phase takes care of the appearing signs during the rotation and we can absorb those signs into the $b_{\alpha p}^{(\dagger)}$. Then the operators $B_{\alpha p}^\dagger$ behave as $B_{xp}^\dagger \to B_{yp}^\dagger$ and $B_{yp}^\dagger \to B_{xp}^\dagger$ characterizing their the p-wave symmetry.

4.2.3. Derivation of Microscopic Hamiltonian

After getting familiar with the lattice setup, the states, the involved operators, and the symmetries, we now turn to the actual derivation of the microscopic Hamiltonian.
The idea is to form repulsively bound states in the center of the plaquettes which consist of two orbital states. In order to induce strong p-wave interactions, we need a combination of the orbital degrees of freedom and s-wave interaction. The two fermions in the two orbital states have to be in different hyperfine states to profit from a stable s-wave interaction. This interaction can be tuned via conventional Feshbach resonances [30]. The repulsively bound state in the center of the plaquette thus contains one fermion with s-wave symmetry and another with p_α-wave symmetry resulting in a p_α-molecular state on the plaquette.
The interaction energy for a molecule is U due to the s-wave scattering between two different hyperfine states. The corresponding state is

$$|2\rangle = a_p^\dagger b_{\alpha p}^\dagger |0\rangle \,.$$

Within the rotating frame and the previously introduced simplifications the energy for the transition of two fermions is

$$\hbar\omega = w_a + w_b + U = \delta_a - \delta_a + U = U \,,$$

see fig. 4.4c) for an illustration of the relevant level scheme.
Following these ideas, we elaborate on the mechanisms behind the scenario. The generic hopping Hamiltonian H_t is

$$\mathrm{H}_t = -\sum_{\langle i,j\rangle} t_{ij} c_i^\dagger c_j \,, \tag{4.22}$$

where the sum runs over all lattice sites i and all nearest neighbors j, t_{ij} is the hopping amplitude. The details of the different hopping mechanisms are explained in section 4.2.5, after the introduction of the effective Hamiltonian (4.45).
The Hamiltonian for the chemical potential for the fermions on the lattice sites

is

$$\mathrm{H}_{\mu} = -\mu \sum_{i} c_i^{\dagger} c_i = -\mu \sum_{i} n_i \,. \tag{4.23}$$

For the plaquette the chemical potential is

$$\mathrm{H}_{\mu,p} = -\mu \sum_{\alpha,p} \left(a_p^{\dagger} a_p + b_{\alpha p}^{\dagger} b_{\alpha p} \right) \,, \tag{4.24}$$

to ensure no particle depletion of states of the lattice sites or plaquettes.
The interaction Hamiltonian H_{int} for the plaquette is

$$\mathrm{H}_{int} = U \sum_{\alpha,p} b_{\alpha p}^{\dagger} b_{\alpha p} \, a_p^{\dagger} a_p \,. \tag{4.25}$$

The full microscopic Hamiltonian thus reads

$$\begin{aligned} \mathrm{H} &= \mathrm{H}_t + \mathrm{H}_{\mu} + \mathrm{H}_{\mu,p} + \mathrm{H}_a + \mathrm{H}_b + \mathrm{H}_{int} \,, \\ &= -\sum_{\langle i,j \rangle} t_{ij} c_i^{\dagger} c_j - \mu \sum_{i} c_i^{\dagger} c_i - \mu \sum_{\alpha,p} \left(a_p^{\dagger} a_p + b_{\alpha p}^{\dagger} b_{\alpha p} \right) \\ &\quad + w_a \sum_{p} \left(A_p^{\dagger} + A_p \right) + w_b \sum_{\alpha,p} \left(B_{\alpha p}^{\dagger} + B_{\alpha p} \right) \\ &\quad + U \sum_{\alpha,p} b_{\alpha p}^{\dagger} b_{\alpha p} \, a_p^{\dagger} a_p \,. \end{aligned} \tag{4.26}$$

4.2.4. Derivation of Effective Hamiltonian

The microscopic Hamiltonian (4.26) describes all possible processes of the system. Here we are interested in reducing the complexity of the microscopic Hamiltonian to obtain an effective Hamiltonian describing the effective processes. In the following we extend the concepts given in section 2.4 to fit this setup.
For the derivation of an effective Hamiltonian we set the fermionic hopping to zero, i.e. $t_{ij} = 0$. In addition, we prohibit hopping between plaquettes. Furthermore we neglect the chemical potentials for the fermions. Thus the relevant Hamiltonians are $\mathrm{H} = \mathrm{H}_a + \mathrm{H}_b + \mathrm{H}_{int}$.
In order to derive the effective Hamiltonian, we refer to degenerate perturbation

theory. The high degeneracy of the system stems from the hopping of the fermions on the lattice sites. The basic procedure is described in section 2.4. We focus solely on the plaquettes. The lowest possible energy achievable on the plaquette is zero, if there is no fermion or molecule present. Hence in the ground state all plaquettes are empty. A slightly higher energy is achieved if two fermions form a p_α-symmetric molecule on a plaquette – since we made the simplification $\delta_a = -\delta_b$. A single fermion on a plaquette contributes the highest energy, namely $w_{a,b} = E_{a,b} + \delta_{a,b}$, thus $w_{a,b} \gg U$. Therefore the system will favor totally empty plaquettes or plaquettes filled with p_α-molecules.
The effective Hamiltonian is then obtained by a Schrieffer-Wolff transformation [106], see section 2.4. After this transformation we are left with the generic Hamiltonian H_T

$$\mathrm{H}_T = \mathrm{H}_0 - \frac{1}{2}\sum_{n,n'} |n'\rangle\langle n| \sum_m \langle n'|\mathrm{H}_1|m\rangle\langle m|\mathrm{H}_1|n\rangle \left(\frac{1}{E_m - E_n} - \frac{1}{E_{n'} - E_m}\right), \tag{4.27}$$

where H_0 is the unperturbed Hamiltonian, H_1 the perturbation, $|n\rangle$ is the initial state, E_n its energy, $|m\rangle$ is the intermediate state, E_m its energy, $|n'\rangle$ is the final state and $E_{n'}$ is the energy of the final state.
Now we discuss the consequences for the states. For the ground state of the system we know that no fermion is on a plaquette, hence the initial state is always the Fermi sea on the lattice sites: $|FS\rangle$. The plaquette contains a single fermion, which can have three possible symmetries, namely s-wave, p_x-wave and p_y-wave. This plaquette with a single fermion has a high energy penalty, resulting in an energy contribution of $w_{a,b}$. Clearly, the system prefers a lower energy contribution. This is caused through two possible processes: either through a hopping back of the fermion to the lattice site or by hopping of an additional fermion onto the plaquette (which then creates a molecule). The back hopping is forbidden, since a s-wave fermion cannot hop back as a p_α-wave symmetric and vice versa, i.e., a single fermion cannot change its symmetry while on a plaquette. An additional fermion hopping onto the plaquette is also forbidden. In order to form a molecule of p_α-wave, a s-wave symmetric fermion requires a p_α-wave fermion to create a p_α-molecule and vice versa.

With these initial considerations, we can derive the effective Hamiltonian. The Hamiltonian in perturbation theory is

$$\mathrm{H} = \mathrm{H}_0 + \mathrm{H}_1 \,, \tag{4.28}$$

with the unperturbed part being

$$\mathrm{H}_0 = \delta_a \sum_p a_p^\dagger a_p + \delta_b \sum_{\alpha,p} b_{\alpha p}^\dagger b_{\alpha p} + U \sum_{\alpha,p} b_{\alpha p}^\dagger b_{\alpha p}\, a_p^\dagger a_p \,, \tag{4.29}$$

where the first two parts are the energy offsets for a fermion on a plaquette. The perturbation is

$$H_1 = w_a \sum_p \left(A_p^\dagger + A_p\right) + w_b \sum_{\alpha,p} \left(B_{\alpha p}^\dagger + B_{\alpha p}\right) \,. \tag{4.30}$$

We now discuss the relevant processes. Here we only focus on the given states on the plaquette and not on the lattice sites, since we know that an additional/missing fermion on the lattice or plaquette will be considered by the neglected chemical potential μ. In fig. 4.6 we illustrate the possible processes, they are

a) Initial $|n\rangle$ empty, intermediate $|m\rangle$ one fermion s or p_α, final $|n'\rangle$ empty.

b) Initial $|n\rangle$ empty, intermediate $|m\rangle$ one fermion s or p_α, final $|n'\rangle$ two fermions, forming a p_α-molecule.

c) Initial $|n\rangle$ two fermions forming a p_α-molecule, intermediate $|m\rangle$ one fermion with either s or p_α, final $|n'\rangle$ empty.

d) Initial $|n\rangle$ two fermions forming a p_α-molecule, intermediate $|m\rangle$ one fermion p_α, final $|n'\rangle$ again two fermions forming again the p_α-molecule.

e) Initial $|n\rangle$ two fermions forming a p_α-molecule, intermediate $|m\rangle$ one fermion s, final $|n'\rangle$ again two fermions, forming the p_α-molecule.

f) Initial $|n\rangle$ two fermions forming a p_α-molecule, intermediate $|m\rangle$ one fermion s, final $|n'\rangle$ again two fermions forming $p_{\alpha'}$-molecule.

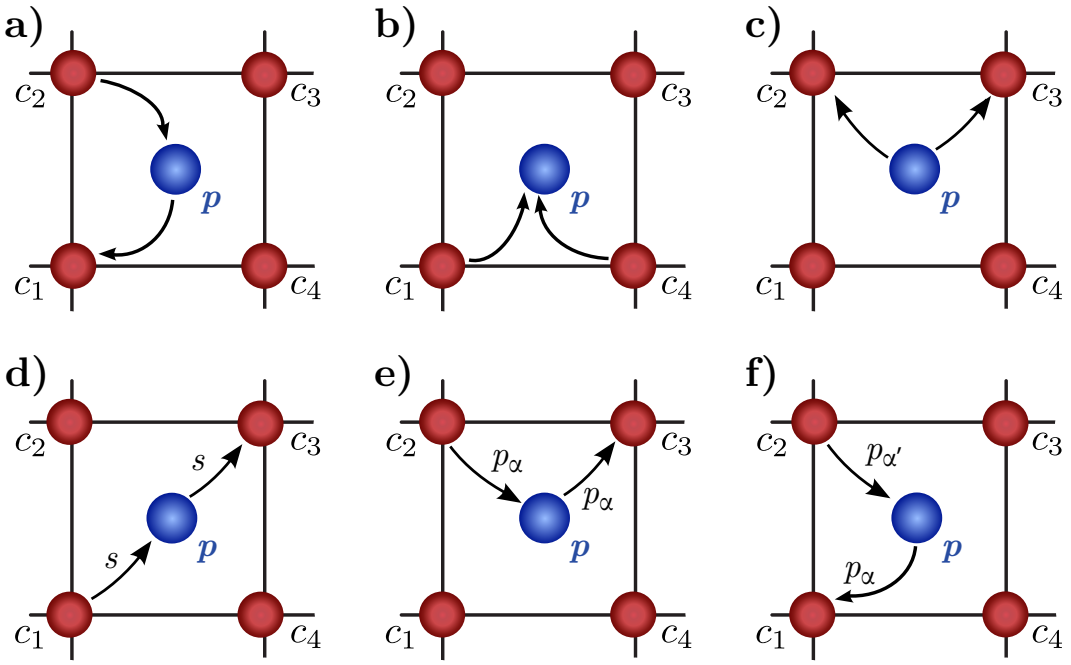

Fig. 4.6 Illustrations of the different processes, as described in the text. **a)** *In*: Fermion with s- or p_α-symmetry *Out*: corresponding fermion with s- or p_α-symmetry. **b)** *In*: Two fermions with s- and p_α-symmetry, respectively *Out*: Nothing. **c)** *In*: Nothing *Out*: Two fermions with s- and p_α-symmetry, respectively. **d)** *In*: Fermion with s-symmetry *Out*: Fermion with s-symmetry. **e)** *In*: Fermion with p_α-symmetry *Out*: Fermion with p_α-symmetry. **f)** *Out*: Fermion with p_α-symmetry *In*: Fermion with $p_{\alpha'}$-symmetry. Figure adapted from [205].

For the cases c) - f) we shift the energy ground level to E_a in order to measure all energies relative to this. Then the ground state energy is U since two fermions form a molecule. The introduced energy offset for the fermions vanishes, since $\delta_a = -\delta_b$.
Next we discuss one contribution of the matrix elements

$$\langle n'|\mathrm{H}_1|m\rangle\langle m|\mathrm{H}_1|n\rangle \left(\frac{1}{E_m - E_n} - \frac{1}{E_{n'} - E_m} \right) , \tag{4.31}$$

of the presented processes as an example and refer to appendix C.1 for the details.
The matrix elements are

a)i: $|n\rangle$: empty, $E_n = 0$, $|m\rangle$: s-wave fermion, $E_m = \delta_a$,
$|n'\rangle$: empty, $E_{n'} = 0$

$$\begin{aligned}
\mathrm{H}_{a)i} &= \frac{2}{\delta_a}\sum_p \langle n'|\ |w_a|^2 \left(A_p^\dagger A_p^\dagger + A_p^\dagger A_p + A_p A_p^\dagger + A_p A_p\right) \\
&\quad + w_a w_b \sum_\alpha \left(A_p^\dagger B_{\alpha p}^\dagger + A_p^\dagger B_{\alpha p} + A_p B_{\alpha p}^\dagger + A_p B_{\alpha p}\right) \\
&\quad + w_b w_a \sum_\alpha \left(B_{\alpha p}^\dagger A_p^\dagger + B_{\alpha p}^\dagger A_p + B_{\alpha p} A_p^\dagger + B_{\alpha p} A_p\right) \\
&\quad + |w_b|^2 \sum_{\alpha,\alpha'} \Bigg(B_{\alpha p}^\dagger B_{\alpha' p}^\dagger + B_{\alpha p}^\dagger B_{\alpha' p} \\
&\qquad\qquad + B_{\alpha p} B_{\alpha' p}^\dagger + B_{\alpha p} B_{\alpha' p} \Bigg) |n\rangle\,, \qquad (4.32)
\end{aligned}$$

where $A_p^{(\dagger)}$ and $B_{\alpha p}^{(\dagger)}$ are bosonic operators, $\left[A_p^{(\dagger)},\, B_{\alpha p}^{(\dagger)}\right] = 0$. However $\left[A_p,\, A_p^\dagger\right] \neq 1$ and $\left[B_{\alpha p},\, B_{\alpha p}^\dagger\right] \neq 1$, which can be easily proven by inserting the corresponding operators.

For sake of later convenience, we simplify the expression above by physically motivated argumentations. The combinations $A_p A_p$ and $A_p^\dagger A_p^\dagger$ directly vanish because of the Fermi statistics of $a_p^{(\dagger)}$ and $c_i^{(\dagger)}$, no two identical fermions can be created or annihilated on the same lattice site or plaquette. For $\alpha \neq \alpha'$ the combination $B_{\alpha p}^\dagger B_{\alpha' p}^\dagger$ and $B_{\alpha p} B_{\alpha' p}$ also vanishes. While a p_x- and p_y-fermion could be on a plaquette, the energy penalty is with $2w_b$ very large and thus not favorable for the system. For $\alpha = \alpha'$ the two combinations directly vanish, due to Fermi statistics.

Hence we are left with

$$\begin{aligned}
\mathrm{H}_{a)i} &= \frac{2}{\delta_a}\sum_p \langle n'| \, |w_a|^2 \left(A_p^\dagger A_p + A_p A_p^\dagger\right) \\
&\quad + w_a w_b \sum_\alpha \left(B_{\alpha p}^\dagger A_p^\dagger + A_p B_{\alpha p}\right) \\
&\quad + w_b w_a \sum_\alpha \left(A_p^\dagger B_{\alpha p}^\dagger + B_{\alpha p} A_p\right) \\
&\quad + w_a w_b \sum_\alpha \left(A_p^\dagger B_{\alpha p} + A_p B_{\alpha p}^\dagger + B_{\alpha p}^\dagger A_p + B_{\alpha p} A_p^\dagger\right) \\
&\quad + |w_b|^2 \sum_{\alpha,\alpha'} \left(B_{\alpha p}^\dagger B_{\alpha' p} + B_{\alpha p} B_{\alpha' p}^\dagger\right) |n\rangle \, . \qquad (4.33)
\end{aligned}$$

For the process in fig. 4.6a) there is only the

$$\mathrm{H}_{a)i} = \frac{2|w_a|^2}{\delta_a}\sum_p A_p A_p^\dagger \, , \qquad (4.34)$$

contribution relevant. All other terms directly drop out.

After the straightforward analysis given in appendix C.1 we can give the final form of the transformed Hamiltonian (with $\delta_b = -\delta_a$ and $w_a = w_b$) by summing all Hamiltonians H_i from before to give

$$\begin{aligned}
\mathrm{H}_T &= \mathrm{H}_0 - \frac{1}{2}\sum_{n,n'} |n'\rangle\langle n| \sum_m \langle n'|\mathrm{H}_1|m\rangle\langle m|\mathrm{H}_1|n\rangle \left(\frac{1}{E_m - E_n} - \frac{1}{E_{n'} - E_m}\right) \\
&= \mathrm{H}_0 - \sum_p \Bigg[\frac{|w_a|^2}{\delta_a} A_p A_p^\dagger - \frac{|w_a|^2}{\delta_a}\sum_\alpha B_{\alpha p} B_{\alpha p}^\dagger \\
&\quad - \frac{U|w_a|^2}{U^2 - \delta_a^2}\sum_\alpha \left(B_{\alpha p}^\dagger A_p^\dagger + A_p B_{\alpha p}\right) \\
&\quad - \frac{|w_a|^2}{U + \delta_a} A_p^\dagger A_p - \frac{|w_a|^2}{U - \delta_a}\sum_\alpha B_{\alpha p}^\dagger B_{\alpha p} \\
&\quad - \frac{|w_a|^2}{U - \delta_a}\sum_{\alpha,\alpha',p,\alpha\neq\alpha'} B_{\alpha' p}^\dagger B_{\alpha p} \Bigg] \, , \qquad (4.35)
\end{aligned}$$

where H_0 is the unperturbed Hamiltonian (4.29).
Next we discuss the nature of the individual terms of Hamiltonian (4.35)

- $\frac{|w_a|^2}{\delta_a} A_p A_p^\dagger - \frac{|w_a|^2}{\delta_a} B_{\alpha p} B_{\alpha p}^\dagger$
  These contributions are related to pure single fermionic hopping. If the states on the lattice sites are available, single site, nearest neighbor or next-nearest neighbor hopping can be achieved. This can be observed by writing down the operators in their fermionic form. In addition, the pre-factor can be related to the hopping amplitude t_{ij} of the Hubbard model. Hence $t_{ij} \sim \frac{|w_a|^2}{\delta_a}, \frac{|w_b|^2}{\delta_b}$.

- $-\frac{U|w_a|^2}{U^2-\delta_a^2} \sum_\alpha \left(B_{\alpha p}^\dagger A_p^\dagger + A_p B_{\alpha p} \right)$
  This is the relevant coupling term of our model, the molecule creation and annihilation.

- $-\frac{|w_a|^2}{U+\delta_a} A_p^\dagger A_p - \frac{|w_a|^2}{U-\delta_a} \sum_{\alpha,\alpha'} B_{\alpha' p}^\dagger B_{\alpha p}$
  This is again a single fermionic hopping contribution, but here the hopping leads from a state on the plaquette into a state on the lattice site and back into a state on the plaquette to form a p_α-molecule. We refer to this terms as correlated or induced hopping since they are a perturbation of the molecule.
  The latter can also be regarded as fermionic hopping. The fermions are indistinguishable and hopping occurs through the annihilation and creation of the molecules. A fermion leaves the molecular state and a different one enters this state. Regarding the lattice system, a fermion hopped.

Analysis of Coupling Operators

We investigate the contributions for the coupling Hamiltonian of the molecule in more detail. Using the molecular creation and annihilation operators in their fermionic representation reveals

$$B_{xp}^\dagger A_p^\dagger = 2 a_p^\dagger b_{xp}^\dagger \left[c_2 c_3 - c_4 c_1 + c_1 c_3 + c_2 c_4 \right] , \tag{4.36a}$$

$$B_{yp}^\dagger A_p^\dagger = 2 a_p^\dagger b_{yp}^\dagger \left[c_1 c_2 - c_3 c_4 + c_1 c_3 - c_2 c_4 \right] . \tag{4.36b}$$

For sake of convenience, we introduce new operators, $X_p^\dagger = a_p^\dagger b_{xp}^\dagger$ and $Y_p^\dagger = a_p^\dagger b_{yp}^\dagger$, which exhibit orbital p-wave symmetry. Then the coupling parts read

$$B_{xp}^\dagger A_p^\dagger = 2X_p^\dagger \left[c_2 c_3 - c_4 c_1 + c_1 c_3 + c_2 c_4\right] , \tag{4.37a}$$

$$B_{yp}^\dagger A_p^\dagger = 2Y_p^\dagger \left[c_1 c_2 - c_3 c_4 + c_1 c_3 - c_2 c_4\right] . \tag{4.37b}$$

The annihilation configuration $B_{\alpha p} A_p$ immediately follows from this.
Thus, in total we have four possibilities to create a molecule with p_α-wave symmetry in a state of the plaquette, as given by the operators c_i above. The problem with all four contributions is, that they cancel each other out when applying mean-field theory in a later step. In order to observe interesting phases and properties of our model, we need a scheme to quench the contributions $c_1^{(\dagger)} c_3^{(\dagger)}$ and $c_2^{(\dagger)} c_4^{(\dagger)}$ or the other ones in eq. (4.37a) and eq. (4.37b).
In the following we address a possible mechanism to select the desired operator configurations.

Quenching Unwanted Contributions

In the general concepts we introduced the concept of positive and negative optical lattices, see section 2.1. Here we apply this concept to this setup and introduce a positive and negative optical lattice as illustrated in fig. 4.7. If we use a positive optical lattice system, we encounter all of the discussed coupling operator contributions (4.37a) and (4.37b). Using the negative optical lattice reveals an alternative set of operators with

$$\begin{aligned} \overline{A}_p^\dagger &= a_p^\dagger \left(c_1 - c_2 + c_3 - c_4\right) , \\ \overline{B}_{xp}^\dagger &= b_{xp}^\dagger \left(c_1 - c_2 - c_3 + c_4\right) , \\ \overline{B}_{yp}^\dagger &= b_{yp}^\dagger \left(c_1 + c_2 - c_3 - c_4\right) , \end{aligned} \tag{4.38}$$

where the differing signs result from the bipartite lattice, see fig. 4.7b).

As before, we need to perform the degenerate perturbation approach to find the analogous forms of the involved Hamiltonians. After the calculation we

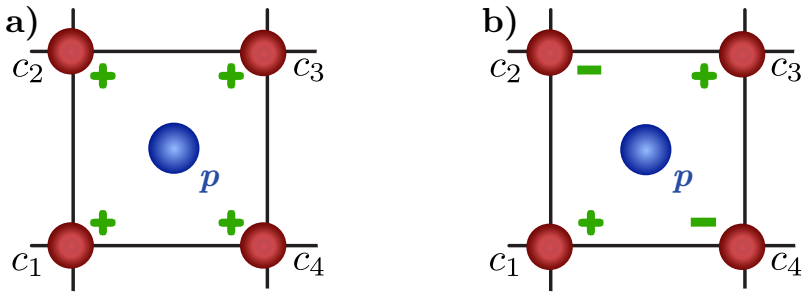

Fig. 4.7 a) Positive optical lattice where every lattice site is positive. The lattice sites are labeled as given by the operators c_i and the plaquettes by p. **b)** Negative optical lattice where every other lattice site is negative. Overlapping both optical lattices then quenches the unwanted terms of the Hamiltonian and reveals the effective model. Figure adapted from [205].

have

$$\begin{aligned}\overline{\mathrm{H}}_T &= \mathrm{H}_0 - \sum_p \Bigg[\frac{|w_a|^2}{\delta_a} \overline{A}_p \overline{A}_p^\dagger - \frac{|w_a|^2}{\delta_a} \sum_\alpha \overline{B}_{\alpha p} \overline{B}_{\alpha p}^\dagger \\ &\quad - \frac{U|w_a|^2}{U^2 - \delta_a^2} \sum_\alpha \left(\overline{B}_{\alpha p}^\dagger \overline{A}_p^\dagger + \overline{A}_p \overline{B}_{\alpha p} \right) \\ &\quad - \frac{|w_a|^2}{U + \delta_a} \overline{A}_p^\dagger \overline{A}_p - \frac{|w_a|^2}{U - \delta_a} \sum_\alpha \overline{B}_{\alpha p}^\dagger \overline{B}_{\alpha p} \\ &\quad - \frac{|w_a|^2}{U - \delta_a} \sum_{\alpha, \alpha', p, \alpha \neq \alpha'} \overline{B}_{\alpha' p}^\dagger \overline{B}_{\alpha p} \Bigg] , \end{aligned} \tag{4.39}$$

where H_0 is again the unperturbed Hamiltonian (4.29) as before.
Again we consider the part of the Hamiltonian in detail, which gives rise to the creation and annihilation processes of the molecule

$$\overline{B}_{xp}^\dagger \overline{A}_p^\dagger = 2X_p^\dagger \left[c_1 c_3 - c_1 c_4 - c_2 c_3 + c_2 c_4 \right] , \tag{4.40a}$$

$$\overline{B}_{yp}^\dagger \overline{A}_p^\dagger = 2Y_p^\dagger \left[-c_1 c_2 + c_1 c_3 - c_2 c_4 + c_3 c_4 \right] . \tag{4.40b}$$

The key idea to quench unwanted contributions is to use one set of lasers for the positive optical lattice and another for the negative one. Then both lattices are overlapped, resulting in the final bipartite lattice system. If the overlapping

is set up with a *negative* sign, we obtain as effective Hamiltonian

$$\begin{aligned}
\mathrm{H} &= \mathrm{H}_T - \overline{\mathrm{H}}_T \\
&= -\sum_p \Bigg[\frac{|w_a|^2}{\delta_a} \left(A_p A_p^\dagger - \overline{A}_p \overline{A}_p^\dagger - \sum_\alpha \left(B_{\alpha p} B_{\alpha p}^\dagger - \overline{B}_{\alpha p} \overline{B}_{\alpha p}^\dagger \right) \right) \\
&\qquad - \frac{U|w_a|^2}{U^2 - \delta_a^2} \sum_\alpha \left(B_{\alpha p}^\dagger A_p^\dagger - \overline{B}_{\alpha p}^\dagger \overline{A}_p^\dagger + A_p B_{\alpha p} - \overline{A}_p \overline{B}_{\alpha p} \right) \\
&\qquad - \frac{|w_a|^2}{U + \delta_a} \left(A_p^\dagger A_p - \overline{A}_p^\dagger \overline{A}_p \right) \\
&\qquad - \frac{|w_a|^2}{U - \delta_a} \sum_\alpha \left(B_{\alpha p}^\dagger B_{\alpha p} - \overline{B}_{\alpha p}^\dagger \overline{B}_{\alpha p} \right) \\
&\qquad - \frac{|w_a|^2}{U - \delta_a} \sum_{\alpha, \alpha', p, \alpha \neq \alpha'} \left(B_{\alpha' p}^\dagger B_{\alpha p} - \overline{B}_{\alpha' p}^\dagger \overline{B}_{\alpha p} \right) \Bigg] . \qquad (4.41)
\end{aligned}$$

With this mechanism, the molecular part of the above Hamiltonian reduces to

$$B_{xp}^\dagger A_p^\dagger - \overline{B}_{xp}^\dagger \overline{A}_p^\dagger = 4 X_p^\dagger \left[c_2 c_3 - c_4 c_1 \right] , \qquad (4.42a)$$

$$B_{yp}^\dagger A_p^\dagger - \overline{B}_{yp}^\dagger \overline{A}_p^\dagger = 4 Y_p^\dagger \left[c_1 c_2 - c_3 c_4 \right] . \qquad (4.42b)$$

The combinations for the annihilation processes directly follow from the above equations. In addition with the choice of detuning $\hbar|\omega| \ll |\delta_a|$ all states with a single fermion in a state on the plaquette can be eliminated adiabatically, see fig. 4.4b) and c). Furthermore, the induced hopping terms via a single excitation in the center of the plaquette reduces to an additional *conventional* hopping, as in the Hubbard model with the hopping strength $t_{ij} = 2|w_a|^2/\delta_a$. In contrast, if the overlapping of the two optical lattices is done with a *positive* sign, the coupling part of the Hamiltonian takes the form

$$B_{xp}^\dagger A_p^\dagger + \overline{B}_{xp}^\dagger \overline{A}_p^\dagger = 4 X_p^\dagger \left[c_1 c_3 + c_2 c_4 \right] , \qquad (4.43)$$

$$B_{yp}^\dagger A_p^\dagger + \overline{B}_{yp}^\dagger \overline{A}_p^\dagger = 4 Y_p^\dagger \left[c_1 c_3 - c_2 c_4 \right] . \qquad (4.44)$$

This scheme allows us to switch between the two types of molecular processes. For sure, both sets promise interesting physics. However, in the following we will concentrate on the first scheme, where the overlapping is done with a negative sign. The analysis of the second configuration then is straightforward

and was recently done [207]. For sake of completeness, the full Hamiltonian, expressed in fermionic and bosonic operators can be found in appendix C.2.

4.2.5. Effective Hamiltonian

In the previous section we investigated the structure of our lattice setup and derived the effective Hamiltonian from the physically relevant mechanisms. The effective Hamiltonian we will use for further analysis is

$$\mathrm{H}_{eff} = -\sum_{\langle i,j\rangle} t_{ij} c_i^\dagger c_j - \mu \sum_i c_i^\dagger c_i + \mathrm{H}_x + \mathrm{H}_y \,, \tag{4.45}$$

where $c_i^{(\dagger)}$ are the spinless fermionic annihilation (creation) operators acting on lattice site i, μ is the chemical potential fixing the average particle number and t_{ij} is the hopping amplitude between nearest neighbor sites $\langle i,j\rangle$. Here we consider two different hopping amplitudes t_x for hopping along the x-direction and t_y for hopping along the y-direction, see fig. 4.8. Since we use spinless fermions, the bound states on the plaquette must exhibit an odd parity symmetry for a non-vanishing interaction. The two coupling Hamiltonians $\mathrm{H}_{x,y}$, as derived before, then are

$$\mathrm{H}_x = \gamma \sum_p X_p^\dagger X_p + g \sum_p \left[X_p^\dagger \left(c_2 c_3 - c_4 c_1 \right) + \mathrm{h.c.} \right] , \tag{4.46a}$$

$$\mathrm{H}_y = \gamma \sum_p Y_p^\dagger Y_p + g \sum_p \left[Y_p^\dagger \left(c_1 c_2 - c_3 c_4 \right) + \mathrm{h.c.} \right] , \tag{4.46b}$$

where we sum over all plaquettes p. The lattice sites are labeled as given in fig. 4.8. The coupling strength to the lattice bound state is g and given in terms of the microscopic quantities: $g = 4|w_a|^2 U / \left(U^2 - \delta_a^2 \right)$. The detuning from resonance is $\gamma = \hbar\omega - 2\mu$ and includes the chemical potential, where $\hbar\omega$ is the energy difference between the molecular state and two free fermions.

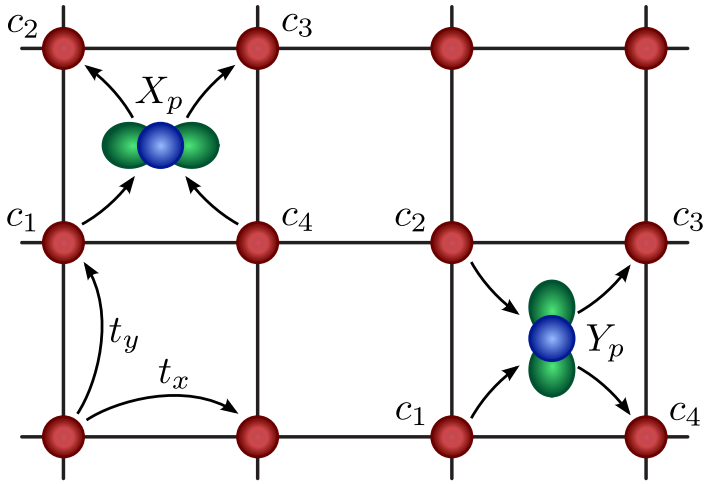

Fig. 4.8 Effective setup of the lattice system where spinless fermions reside on the lattice sites, labeled by operators c_i. The fermions are coupled to a molecular state in the center of each plaquette. The molecular states are labeled by X_p and Y_p, exhibit a p-wave symmetry and are doubly degenerate. The system can be tuned through the anisotropic hopping strengths t_y/t_x from a coupled wire setup to a 2D isotropic system. Figure taken from [205].

4.2.6. Fourier Transformation of Effective Hamiltonian

The first step to handle Hamiltonian (4.45) is to Fourier transform it, where we use the convention

$$c_i^\dagger = \frac{1}{\sqrt{N}} \sum_{\mathbf{q}} e^{-i\mathbf{q}\mathbf{r}_i} c_{\mathbf{q}}^\dagger \,, \quad X_p = \frac{1}{\sqrt{N}} \sum_{\mathbf{q}'} e^{i\mathbf{q}'\mathbf{r}_p} X_{\mathbf{q}} \,, \tag{4.47}$$

with N the total number of lattice sites and plaquettes. The kinetic part and chemical potential part of Hamiltonian (4.45) reads

$$\mathrm{H}_{kin} = \sum_{\mathbf{q}} \left(\varepsilon'_{\mathbf{q}} - \mu\right) n_{\mathbf{q}} = \sum_{\mathbf{q}} \varepsilon_{\mathbf{q}} n_{\mathbf{q}} \,, \tag{4.48}$$

with $\varepsilon'_{\mathbf{q}} = -2\left(t_x \cos\left(q_x a\right) + t_y \cos\left(q_y a\right)\right)$. Next we Fourier transform the coupling Hamiltonians $\mathrm{H}_{x,y}$. To this end, we use the following relations to address the lattice sites $\mathbf{r}_i$ relative to the plaquette site $\mathbf{r}_p$

$$\begin{aligned} \mathbf{r}_1 &= \mathbf{r}_p - \frac{a}{2}\mathbf{e}_x - \frac{a}{2}\mathbf{e}_y \,, & \mathbf{r}_2 &= \mathbf{r}_p - \frac{a}{2}\mathbf{e}_x + \frac{a}{2}\mathbf{e}_y \,, \\ \mathbf{r}_3 &= \mathbf{r}_p + \frac{a}{2}\mathbf{e}_x + \frac{a}{2}\mathbf{e}_y \,, & \mathbf{r}_4 &= \mathbf{r}_p + \frac{a}{2}\mathbf{e}_x - \frac{a}{2}\mathbf{e}_y \,, \end{aligned}$$

where $\mathbf{e}_{x,y}$ is the unity vector in x, y-direction, respectively and a the lattice spacing. The Fourier transformation of the coupling Hamiltonian H_x (4.46a) then gives

$$\begin{aligned}\mathrm{H}_x &= \gamma \sum_{\mathbf{q}} X^\dagger_{\mathbf{q}} X_{\mathbf{q}} \\ &\quad + \frac{2ig}{\sqrt{N}} \sum_{\mathbf{q},\mathbf{q}'} \Bigg[X^\dagger_{\mathbf{q}+\mathbf{q}'}\, c_{\mathbf{q}} c_{\mathbf{q}'} \sin\Big(\frac{a}{2} \big\{ q_y + q'_y - \big(q_x - q'_x \big) \big\} \Big) \\ &\qquad - X_{\mathbf{q}+\mathbf{q}'}\, c^\dagger_{\mathbf{q}} c^\dagger_{\mathbf{q}'} \sin\Big(\frac{a}{2} \big\{ q_y + q'_y + \big(q_x - q'_x \big) \big\} \Big) \Bigg], \end{aligned} \tag{4.49}$$

and for the other coupling Hamiltonian H_y (4.46b)

$$\begin{aligned}\mathrm{H}_y &= \gamma \sum_{\mathbf{q}} Y^\dagger_{\mathbf{q}} Y_{\mathbf{q}} \\ &\quad + \frac{2ig}{\sqrt{N}} \sum_{\mathbf{q},\mathbf{q}'} \Bigg[- Y^\dagger_{\mathbf{q}+\mathbf{q}'}\, c_{\mathbf{q}} c_{\mathbf{q}'} \sin\Big(\frac{a}{2} \big\{ q_x + q'_x + \big(q_y - q'_y \big) \big\} \Big) \\ &\qquad + Y_{\mathbf{q}+\mathbf{q}'}\, c^\dagger_{\mathbf{q}} c^\dagger_{\mathbf{q}'} \sin\Big(\frac{a}{2} \big\{ q_x + q'_x - \big(q_x - q'_x \big) \big\} \Big) \Bigg]. \end{aligned} \tag{4.50}$$

To simplify the above expressions further, we rename the summation indices and use the fermionic commutation relations to end up with the coupling Hamiltonian

$$\begin{aligned}\mathrm{H}_c &= \mathrm{H}_x + \mathrm{H}_y \\ &= \gamma \sum_{\mathbf{q}} \big[X^\dagger_{\mathbf{q}} X_{\mathbf{q}} + Y^\dagger_{\mathbf{q}} Y_{\mathbf{q}} \big] \\ &\quad + \frac{2ig}{\sqrt{N}} \sum_{\mathbf{q},\mathbf{q}'} \Bigg\{ \Big[X^\dagger_{\mathbf{q}+\mathbf{q}'}\, c_{\mathbf{q}} c_{\mathbf{q}'} + X_{\mathbf{q}+\mathbf{q}'}\, c^\dagger_{\mathbf{q}} c^\dagger_{\mathbf{q}'} \Big] \\ &\qquad \times \sin\Big(\frac{a}{2} \big\{ q_y + q'_y - \big(q_x - q'_x \big) \big\} \Big) \\ &\qquad + \Big[Y^\dagger_{\mathbf{q}+\mathbf{q}'}\, c_{\mathbf{q}} c_{\mathbf{q}'} + Y_{\mathbf{q}+\mathbf{q}'}\, c^\dagger_{\mathbf{q}} c^\dagger_{\mathbf{q}'} \Big] \\ &\qquad \times \sin\Big(\frac{a}{2} \big\{ q_x + q'_x - \big(q_y - q'_y \big) \big\} \Big) \Bigg\}. \end{aligned} \tag{4.51}$$

We split the summations into two parts, use the fact that $\sin(x)$ is an odd function and the relation

$$\sin\alpha - \sin\beta = 2\cos\left(\frac{\alpha+\beta}{2}\right)\sin\left(\frac{\alpha-\beta}{2}\right), \tag{4.52}$$

to calculate the final form of the coupling Hamiltonian

$$\begin{aligned}
\mathrm{H}_c =& \gamma \sum_{\mathbf{q}} \left[X^\dagger_{\mathbf{q}} X_{\mathbf{q}} + Y^\dagger_{\mathbf{q}} Y_{\mathbf{q}}\right] \\
&- \frac{2ig}{\sqrt{N}} \sum_{\mathbf{q},\mathbf{q}'} \Bigg\{ \left[X^\dagger_{\mathbf{q}+\mathbf{q}'}\, c_{\mathbf{q}} c_{\mathbf{q}'} + X_{\mathbf{q}+\mathbf{q}'}\, c^\dagger_{\mathbf{q}} c^\dagger_{\mathbf{q}'}\right] \\
&\qquad \times \cos\left(\frac{a}{2}\left\{q_y + q'_y\right\}\right) \sin\left(\frac{a}{2}\left\{q_x - q'_x\right\}\right) \\
&\quad + \left[Y^\dagger_{\mathbf{q}+\mathbf{q}'}\, c_{\mathbf{q}} c_{\mathbf{q}'} + Y_{\mathbf{q}+\mathbf{q}'}\, c^\dagger_{\mathbf{q}} c^\dagger_{\mathbf{q}'}\right] \\
&\qquad \times \cos\left(\frac{a}{2}\left\{q_x + q'_x\right\}\right) \sin\left(\frac{a}{2}\left\{q_y - q'_y\right\}\right) \Bigg\}.
\end{aligned} \tag{4.53}$$

Thus, the whole Fourier transformed Hamiltonian is

$$\begin{aligned}
\mathrm{H} =& \sum_{\mathbf{q}} \varepsilon_{\mathbf{q}} n_{\mathbf{q}} + \gamma \sum_{\mathbf{q}} \left[X^\dagger_{\mathbf{q}} X_{\mathbf{q}} + Y^\dagger_{\mathbf{q}} Y_{\mathbf{q}}\right] \\
&- \frac{2ig}{\sqrt{N}} \sum_{\mathbf{q},\mathbf{q}'} \Bigg\{ \left[X^\dagger_{\mathbf{q}+\mathbf{q}'}\, c_{\mathbf{q}} c_{\mathbf{q}'} + X_{\mathbf{q}+\mathbf{q}'}\, c^\dagger_{\mathbf{q}} c^\dagger_{\mathbf{q}'}\right] \\
&\qquad \times \cos\left(\frac{a}{2}\left\{q_y + q'_y\right\}\right) \sin\left(\frac{a}{2}\left\{q_x - q'_x\right\}\right) \\
&\quad + \left[Y^\dagger_{\mathbf{q}+\mathbf{q}'}\, c_{\mathbf{q}} c_{\mathbf{q}'} + Y_{\mathbf{q}+\mathbf{q}'}\, c^\dagger_{\mathbf{q}} c^\dagger_{\mathbf{q}'}\right] \\
&\qquad \times \cos\left(\frac{a}{2}\left\{q_x + q'_x\right\}\right) \sin\left(\frac{a}{2}\left\{q_y - q'_y\right\}\right) \Bigg\},
\end{aligned} \tag{4.54}$$

with $\varepsilon_{\mathbf{q}}$ given in eq. (4.48), γ being the detuning from resonance and g the coupling strength.

4.2.7. Mean-Field Calculations

We are interested in the zero temperature mean-field phase diagram before investigating the topological phases realized within our system. This mean-field analysis is well-justified as recent density matrix renormalization group

(DMRG) simulations verified the appearance of a p-wave superfluid exhibiting Majorana modes in a double wire setup [160]. Since our investigation goes beyond a double wire setup, we expect that the influence of thermal and quantum fluctuations are suppressed even further and the calculated phase diagram should capture the appearing transitions faithfully.
Next, we present the mean-field theory for our system. Previously we argued that there is a resonant coupling between the fermions on the lattice sites and the molecular states on the plaquettes. This gives rise to a p-wave paring for the fermions and leads to a p-wave superfluid in the system. Here the superfluid order parameters are of the form

$$\Delta_x = \frac{4g}{N}\Big\langle \sum_p X_p \Big\rangle = \frac{4g}{\sqrt{N}}\langle X_0\rangle\,, \tag{4.55a}$$

$$\Delta_y = \frac{4g}{N}\Big\langle \sum_p Y_p \Big\rangle = \frac{4g}{\sqrt{N}}\langle Y_0\rangle\,, \tag{4.55b}$$

and describe the macroscopic condensation of the $p_{x,y}$-molecules into the zero momentum mode. Applying this to the Hamiltonian (4.54) and inserting the order parameters reveals

$$\begin{aligned} \mathrm{H}_{mol} = \quad & \gamma\left[\langle X_0^\dagger\rangle\langle X_0\rangle + \langle Y_0^\dagger\rangle\langle Y_0\rangle\right] \\ & -\frac{2ig}{\sqrt{N}}\sum_{\mathbf{q}}\Bigg\{\left[\langle X_0^\dagger\rangle c_{\mathbf{q}}c_{-\mathbf{q}} + \langle X_0\rangle c_{\mathbf{q}}^\dagger c_{-\mathbf{q}}^\dagger\right]\sin(q_x a) \\ & \qquad + \left[\langle Y_0^\dagger\rangle c_{\mathbf{q}}c_{-\mathbf{q}} + \langle Y_0\rangle c_{\mathbf{q}}^\dagger c_{-\mathbf{q}}^\dagger\right]\sin(q_y a)\Bigg\}\,, \end{aligned} \tag{4.56}$$

where we focus on the molecular contribution of the Hamiltonian. In addition, we are interested in the modes $\mathbf{q} = 0$ and $\mathbf{q}' = -\mathbf{q}$, refer to Hamiltonian (4.54). Note that the first part – the summation over $\mathbf{q}$ of the detuning part with $X_{\mathbf{q}}^\dagger X_{\mathbf{q}}$ and $Y_{\mathbf{q}}^\dagger Y_{\mathbf{q}}$ – reduces to the above contribution, since only the $\mathbf{q} = 0$ part is relevant. In the coupling Hamiltonian the molecular operators $X^{(\dagger)}, Y^{(\dagger)}$ become relevant as soon as they act on the zero momentum mode, where we then are interested in the mean-field part $\langle X_0^{(\dagger)}\rangle$ and $\langle Y_0^{(\dagger)}\rangle$.
We rearrange the above Hamiltonian and introduce the superfluid order param-

eters (4.55a),(4.55b) which yield the full mean-field Hamiltonian

$$\begin{aligned}\mathrm{H_{MF}} &= \sum_{\mathbf{q}} \varepsilon_{\mathbf{q}} n_{\mathbf{q}} + \frac{N}{16}\frac{\gamma}{g^2}\left(|\Delta_x|^2 + |\Delta_y|^2\right) \\ &\quad -\frac{i}{2}\sum_{\mathbf{q}} \Big\{ \left[\Delta_x^* c_{\mathbf{q}} c_{-\mathbf{q}} + \Delta_x c_{\mathbf{q}}^\dagger c_{-\mathbf{q}}^\dagger\right] \sin(q_x a) \\ &\qquad + \left[\Delta_y^* c_{\mathbf{q}} c_{-\mathbf{q}} + \Delta_y c_{\mathbf{q}}^\dagger c_{-\mathbf{q}}^\dagger\right] \sin(q_y a) \Big\} . \end{aligned} \tag{4.57}$$

This quadratic Hamiltonian can be rearranged into a convenient matrix representation, namely

$$\begin{aligned}\mathrm{H_{MF}} = &\frac{1}{2}\sum_{\mathbf{q}} \begin{pmatrix} c_{\mathbf{q}}^\dagger \\ c_{-\mathbf{q}} \end{pmatrix} \begin{pmatrix} \varepsilon_{\mathbf{q}} & \Delta_{\mathbf{q}} \\ \Delta_{-\mathbf{q}}^* & -\varepsilon_{\mathbf{q}} \end{pmatrix} \begin{pmatrix} c_{\mathbf{q}} \\ c_{-\mathbf{q}}^\dagger \end{pmatrix} \\ &+ \frac{1}{2}\sum_{\mathbf{q}} \varepsilon_{\mathbf{q}} + \frac{N}{16}\frac{\gamma}{g^2}\left(|\Delta_x|^2 + |\Delta_y|^2\right) , \end{aligned} \tag{4.58}$$

where the gap parameter takes the form of a p-wave superfluid

$$\Delta_{\mathbf{q}} = -i\left[\Delta_x \sin(q_x a) + \Delta_y \sin(q_y a)\right] . \tag{4.59}$$

Diagonalizing the Hamiltonian through a Bogoliubov transformation is straightforward and gives the excitation spectrum

$$E_{\mathbf{q}}^{\pm} = \pm\sqrt{\varepsilon_{\mathbf{q}}^2 + |\Delta_{\mathbf{q}}|^2} , \tag{4.60}$$

and the diagonal Hamiltonian

$$\mathrm{H_{MF}} = \sum_{\mathbf{q}} E_{\mathbf{q}}\, \alpha_{\mathbf{q}}^\dagger \alpha_{\mathbf{q}} + F(\Delta_x, \Delta_y) , \tag{4.61}$$

where $\alpha_{\mathbf{q}}^{(\dagger)}$ are the Bogoliubov quasiparticle operators and $F(\Delta_x, \Delta_y)$ is the ground state energy functional. Note that we define $E_{\mathbf{q}} := E_{\mathbf{q}}^+$ and $-E_{\mathbf{q}} := E_{\mathbf{q}}^-$. We are interested in the ground state of the system. The ground state energy per unit cell is

$$\mathcal{F}(\Delta_x, \Delta_y) = \frac{F(\Delta_x, \Delta_y)}{N} = \frac{\gamma}{16 g^2}\left(|\Delta_x|^2 + |\Delta_y|^2\right) + \int \frac{\mathrm{d}\mathbf{q}}{v_0}\frac{\varepsilon_{\mathbf{q}} - E_{\mathbf{q}}}{2} , \tag{4.62}$$

with $v_0 = (2\pi)^2 / a^2$ denoting the volume of the first Brillouin zone. Here we used the fact that we consider a large lattice which justifies the transition from summation to integration. We can analyze the new ground state by minimizing the ground state energy with respect to the gap parameters

$$\partial_{\Delta_x} \mathcal{F}(\Delta_x, \Delta_y) = \partial_{\Delta_y} \mathcal{F}(\Delta_x, \Delta_y) = 0 \,. \tag{4.63}$$

This determines the gap parameters self-consistently and hence the global minima. The calculation is numerically demanding. In the following we avoid these complications by introducing the two gap parameters as

$$\Delta_x = e^{i\theta} \Delta \cos(\vartheta) \,, \tag{4.64a}$$

$$\Delta_y = e^{i\theta} \Delta \sin(\vartheta) \; e^{i\phi} \,, \tag{4.64b}$$

where $\exp(i\theta)$ is a global phase for both gaps. It can be set to $\exp(i\theta) = 1$ without loss of generality, in analogy to the superconducting case in the BCS scenario. The strength of the gap is Δ. The gaps also experience a relative strength ϑ and a relative phase ϕ.
There are in principle three types of superconductors, which can appear in our system:

- p_x (p_y) *superconducting phase*: $\Delta_y = 0$ ($\Delta_x = 0$), $\phi = 0$, ($\phi = \pi/2$). This phase is possible in our setup.

- $p_x + p_y$ *superconducting phase*: $\Delta_x = \Delta_y$ and $\vartheta = \pi/4$, $\phi = 0$, π. This superconductor does not appear in our system.

- $p_x + ip_y$ *superconducting phase*: $\Delta_x = \pm i \Delta_y$, there the angles are $\vartheta = \pi/4$ and $\phi = \pm\pi/2$. The numerical result is that the energy minimum is always at $\phi = \pm\pi/2$. The two order parameters are finite and obey a fixed phase relation $\Delta_x/\Delta_y = \pm i |\Delta_x/\Delta_y|$,. This phase is possible within our system.

If the strength of the gap Δ is zero, we end up with a common Fermi sea and no superfluidity. The analysis of the parameter range within mean-field theory then reveals the mean-field phase diagram of fig. 4.9. For the fully isotropic setup with $t_x = t_y$ we find a $p_x + ip_y$ superfluid, i.e. $\Delta_x = \pm i \Delta_y$. This phase breaks

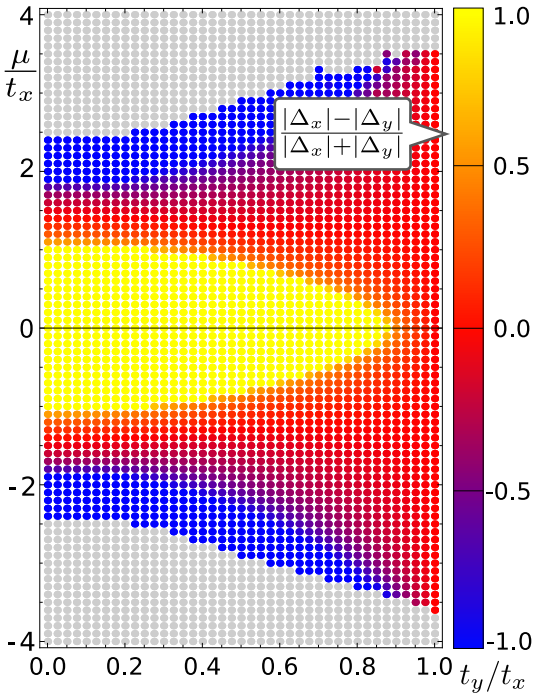

Fig. 4.9 Mean-field phase diagram for the parameter regime $\gamma t_x/g^2 = 1.5$. For isotropic hopping $t_x = t_y$ the ground state is a $p_x + ip_y$ superfluid, whereas for strong anisotropy $t_x \neq t_y$ a pure p_x or p_y superfluid order parameter prevails. The grey dots indicate the insufficient convergence of the gap parameters within the numerical calculations, thus the superfluid phase is inaccessible for experimentally realistic temperatures. On the right side of the diagram the color coding is given for the gap parameter $|\Delta_x| - |\Delta_y|/|\Delta_x|+|\Delta_y|$: yellow corresponds to a p_x, blue to a p_y and red to a $p_x + ip_y$ superfluid. Figure adapted from [205].

both, the $U(1)$ and the time-reversal symmetry. The $p_x + ip_y$ superfluid is also stable to a small anisotropy in the hopping for a finite interaction strength, see fig. 4.9. The anisotropic behavior is reflected in the order parameter $|\Delta_x| \neq |\Delta_y|$. If we increase the anisotropy $t_x \neq t_y$, we discover transitions into a p_x or p_y superfluid. This transition depends on the value of the chemical potential μ. Be aware, in our zero temperature scenario true long-range order survives, as predicted in mean-field theory. On the other hand, thermal fluctuations will lead to quasi long-range order in our 2D system [208]. In the following we investigate the topological properties of our system which are not affected by the phase fluctuations of the order parameter.

4.2.8. Topological Phase Transitions

In addition to the discussed mean-field phases, our lattice system also exhibits topological phases and transitions. The possible topological phases of quadratic

fermionic Hamiltonians have been classified exhaustively [209]. The topological quantum phase transitions analyzed in this system is captured in the classification discussed in [209]. In order to study the topological properties, the quadratic Hamiltonian (4.58) is investigated. The superfluid order parameters Δ_x and Δ_y then determine the symmetries. We characterize the topological properties of the system where the superfluid experiences an excitation gap. To this end, we need three topological indices [210]. In the methods section of [205], we give a method to calculate the required topological indices of the system.

The first index denotes the *strong topological index* ν given by the Chern number and can take values $\nu = 0, \pm 1$. It characterizes the 2D $p_x + ip_y$ superfluid. We denote the additional *weak topological indices* [211, 212] as $\nu_x = 0, 1$ and $\nu_y = 0, 1$. They describe the appearance of Majorana modes in Kitaev's Majorana wire [156]. The weak topological indices can be of finite value in the p_x and chiral $p_x + ip_y$ superfluids. Here we point out, that the topological phase transitions only depend on the topology of the Fermi surface. In addition, the boundaries for the topological phase transitions are independent of the values of the superfluid order parameters. We then divide the system into three different regions, see fig. 4.10:

- Region (I): Closed Fermi surface
- Region (II): Open Fermi surface
- Region (III): Strong pairing regime (trivial band insulating state, no interaction present)

In region (III) the superfluids have no topological order, $\nu = \nu_x = \nu_y = 0$, and hence are neglected in the following.

Next, we combine the introduced topological indices with the superfluid order parameters to describe the realized phases in the system. Time-reversal invariant superfluids are denoted as $\mathrm{SF}_{\nu:\nu_x\nu_y}$, chiral superfluids as $\mathrm{cSF}_{\nu:\nu_x\nu_y}$. For a review of time-reversal and chiral symmetry see [158, 161]. We begin with the chiral $p_x + ip_y$ superfluid. There are two topological phases present, which are fundamentally different, see fig. 4.10a).

In region (I), we have strong topological superfluids $\mathrm{cSF}_{-1:00}$ and $\mathrm{cSF}_{1:11}$ with a

finite Chern number $\nu = \pm 1$. Consulting the standard symmetry classification scheme [213–215], we find that these superfluids $\mathrm{cSF}_{\pm 1:\nu_x\nu_y}$ are in symmetry class D (particle-hole (PH) symmetry, broken time-reversal (TR) symmetry). Here the weak indices of the phase depend on the chemical potential, thus $\nu_x = \nu_y = 1$ for $\mu > 0$ and $\nu_x = \nu_y = 0$ for $\mu < 0$. This will strongly affect the appearance of Majorana modes, see section 4.2.9.
Next, we investigate region (II) and find a weak topological superfluid in the symmetry class D ($\mathrm{cSF}_{0:01}$), as well as a p_x weak topological superfluid ($\mathrm{SF}_{0:01}$) in the symmetry class BDI (PH + TR symmetry).
The superfluid phase in region (I) with the closed Fermi surface becomes gapless and exhibits no topological properties. The realized p_y superfluid is gapless in region (I) and (II).
In order to obtain to full phase diagram of the system, we have to combine the mean-field phase diagram with the topological properties of fig. 4.10b) and overlap them. The bold lines in fig. 4.10b) indicate the topological transitions, as illustrated in fig. 4.10a). The details of the full phase diagram strongly depend on the strength of the coupling parameters. In this scenario we are interested in a strong coupling regime, where $g^2/\gamma \sim t_x, t_y$ with large superfluid gaps. For a parameter range of $\gamma t_x/g^2 = 1.5$ all given cases for the topological phases can be nicely realized for varying values of the two parameters μ/t_x and t_y/t_x, for details see fig. 4.10 and [205]. We also point out, that the mean-field and topological phase transitions are decoupled from each other, see fig. 4.10c) and d).

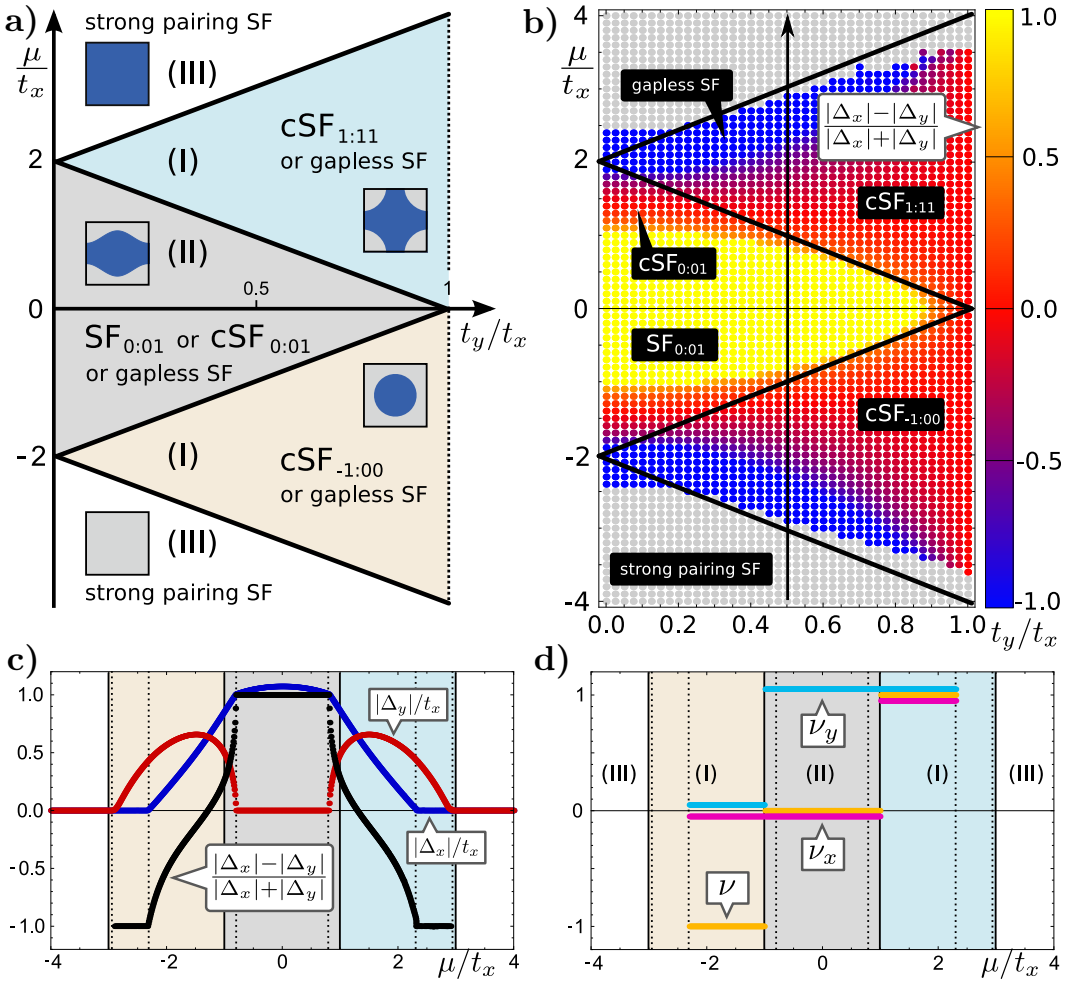

Fig. 4.10 a) Topological phase diagram showing the three different topological regions. The topological indices also depend on the superfluid order parameter. We denote a time-reversal invariant superfluid as $\mathrm{SF}_{\nu:\nu_x\nu_y}$ and a chiral superfluid as $\mathrm{cSF}_{\nu:\nu_x\nu_y}$, where ν is the strong topological index and $\nu_{x,y}$ the weak ones. The insets of the different phases illustrate the topology of the Fermi surface, for details see text. **b)** Mean-field phase diagram as before in fig. 4.9. Here the boundaries of the topological phase transitions are included. **c)**, **d)** Illustrations of the gap parameters $|\Delta_x|/t_x$, $|\Delta_y|/t_x$ and $|\Delta_x|-|\Delta_y|/|\Delta_x|+|\Delta_y|$ for a cut through the topological and mean-field phase diagram at $t_x = t_y/2$, indicated in **b)** by the arrow. The color shading directly corresponds to the classifications in **a)**. The solid (dashed) lines within the plots give the topological (mean-field) transitions. Note that the topological and mean-field transitions are decoupled: The topological index ν_y takes the value 1 at a different position than the vanishing gap Δ_y. Figure taken and adapted from [205].

4.2.9. Majorana Modes and Braiding

In our system we expect the appearance of Majorana modes at topological defects [210]. Topological defects can be vortices and lattice dislocations. Majorana modes are localized, doubly degenerate zero-energy modes of the excitation spectrum of the quadratic Hamiltonian

$$\mathrm{H} = -\sum_{\langle i,j\rangle} \Big(t_{ij} c_j^\dagger c_i + \Delta_{ij} c_i c_j + \mathrm{h.c.} \Big) - \mu \sum_i c_i^\dagger c_i \,, \tag{4.65}$$

with t_{ij} the hopping strengths, Δ_{ij} the (spatially varying) gap and μ the chemical potential. The gap Δ_{ij} needs to be determined self-consistently by the previous mean-field theory. Topological defects can be introduced into the system via spatial dependencies of the gap, to implement vortices, or directly into the lattice structure, to have dislocations. Diagonalizing the Hamiltonian (4.65) then verifies the presence of Majorana modes in the system:

- In the core of vortices for the $\mathrm{cSF}_{1:\nu_x\nu_y}$ phases.
- At edge dislocations in x- and y-direction for positive chemical potentials $\mu > 0$ with finite weak topological index $\nu_x = \nu_y = 1$, as well as in the superfluid phases $\mathrm{cSF}_{0:01}$ and $\mathrm{SF}_{0:01}$ in x-direction.

An example of a numerical solution of the diagonalized Hamiltonian is illustrated in fig. 4.11. For further details of Majorana modes at edge dislocations see [205].

The investigated system at hand now provides the possibility to implement a protocol for the observation of the experimentally elusive non-Abelian braiding statistics of Majorana modes. From before we know that Majorana modes can be created at edge dislocations in certain parameter regimes. Within the framework of cold atomic gases, a vortex in the optical field generating the optical lattice directly corresponds to an edge dislocation [216]. The next handy feature of cold gases is the local site addressability [217–219], which allows for arbitrary shapes of the lattice. This enables the generation of edge dislocations in a controlled fashion. This setup paves the way for the experimental observation of the non-Abelian statistics of Majorana modes by braiding the dislocations. Here we present the protocol for the braiding operation, see fig. 4.12. It is

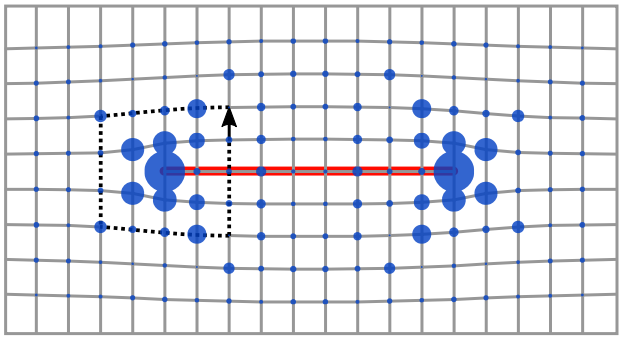

Fig. 4.11 Majorana modes at lattice dislocations. The edge dislocation forms a single quantum wire, indicated by the red line. Here the setup generates two Majorana modes at both ends of the quantum wire for a weak topological index $\nu_y = 1$. In this parameter regime the localized wave function of the two Majorana modes is computed by diagonalizing the Hamiltonian (4.65) through a Bogoliubov transformation. The radii of the blue circles represent the square of the wave function of the Majorana modes and are proportional to it. Figure taken and adapted from [205].

important to stress that all operations are performed adiabatically, i.e., slower than the characteristic time scale given by the superfluid gap:

1. Create two dislocation pairs at different positions on the lattice to initialize the system. This gives an unoccupied fermionic mode at each dislocation, with a finite single particle gap, described by the operators $c^\dagger_{r,b}$. At low temperatures all fermions are Cooper paired.

2. Separate the two dislocations along path 1, then along path 2, see fig. 4.12. The operations divide the created fermionic modes into four Majorana modes localized at the dislocation endpoints. The initial state is defined by $c_{r,b}|g\rangle = 0$.

3. The braiding is performed by recombining the two dislocations, first along path 3, afterwards along path 4. This procedure can be viewed as moving the two Majorana modes around each other on the lattice.

4. The general non-Abelian braiding rules for Majorana modes [169] state that this process transforms the initially unoccupied fermionic mode into

an occupied fermionic mode. The new state then is $c^\dagger_{r,b}|g\rangle$. We drop the appearing Abelian phase factor since it is not relevant in our procedure.

5. The energy difference of the molecular to the free fermionic state $\hbar\omega$ is now ramped to negative values. This drives the system into the strong pairing phase, where all paired fermions are in the center of the plaquettes.

6. Finally, the fermionic density on the original lattice is measured to probe for unpaired fermions. Successfully performing all the above operations then reveals one unpaired fermion at each lattice dislocation pair.

Further details to the braiding protocol and discussions, e.g. regarding induced noise or finite temperature influences, can be found in [205].

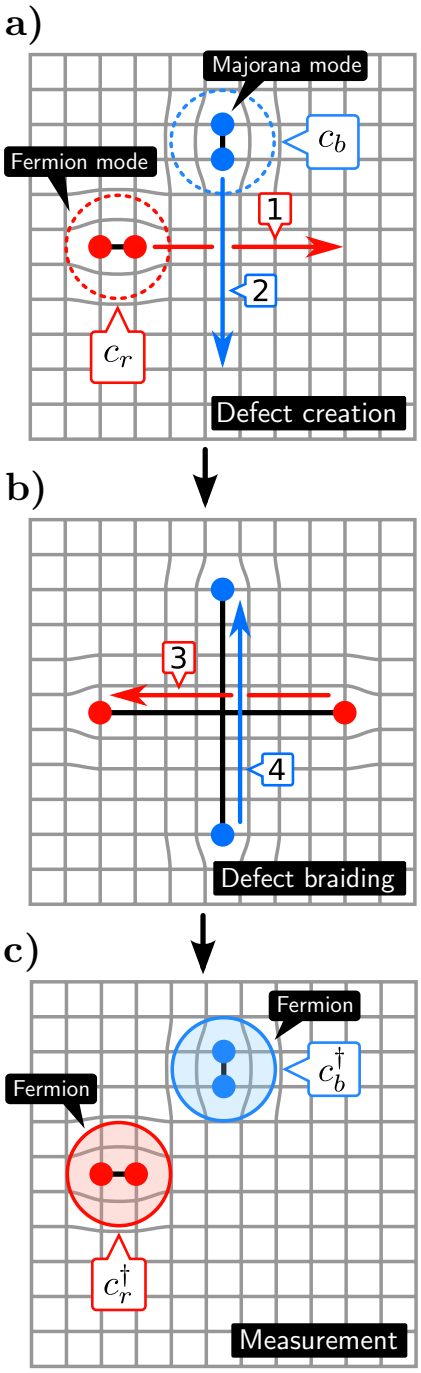

Fig. 4.12 Procedure for the braiding operation. **a)** Two dislocation pairs are formed in the lattice structure to generate four Majorana modes, indicated by the red and blue dots. Here two Majorana modes form an unoccupied fermion mode, as illustrated by the dashed circles in red and blue. The unoccupied fermionic modes are described by operators $c_{r,b}$. Next, the lattice dislocations are spatially separated first along path 1, afterwards along path 2. **b)** The braiding operation takes place by recombining the generated Majorana modes, first along path 3, then path 4. The paths are now intertwined. **c)** After the braiding operation, the initially unoccupied fermionic state at each dislocation pair transformed into an occupied fermion mode described by the operators $c_{r,b}^\dagger$. This is shown as full red and blue circles in the figure. Afterwards a measurement of all unpaired fermions takes place to show the unique signature of the non-Abelian braiding statistics of the Majorana modes. Figure taken and adapted from [205].

4.3. Conclusion and Outlook

We introduced a lattice setup for spinless fermions, where fermions occupy the lattice sites. A special feature of this setup are the plaquettes which are surrounded by the lattice sites. The setup was constructed in such a way, that the lattice sites were coupled to the plaquettes in order to produce molecular states in the center of the plaquettes with p-wave symmetry. Then a Schrieffer-Wolff transformation was applied to the microscopic Hamiltonian to end up at an effective Hamiltonian after quenching the undesired operator contributions. The effective Hamiltonian was analyzed on a mean-field level, which was justified based on DMRG calculations of a three wire setup [205]. We found the mean-field phase diagram and its superfluid phases such as the time-reversal invariant p_x, p_y and the chiral $p_x + ip_y$ superfluid. This lead to the investigation of the inherent topological properties of the system. In addition, we determined the topological phase diagram as well as the possibility of appearing Majorana modes at vortex cores and lattice dislocations. Afterwards we numerically diagonalized the Hamiltonian (4.65) and demonstrated the appearance of Majorana Modes in the system. In the last section we described how the setup enables efficient braiding of the Majorana modes and demonstrated their non-Abelian statistics.
We thus showed how cold atomic gases in optical lattices can quantum simulate p-wave superfluids and Majorana modes. In addition we give way towards an possible experimental observation for non-Abelian braiding statistics.
As a further step of the system, the operator set within the microscopic Hamiltonian, which was quenched due to the overlapping of the positive and negative optical lattice, should be considered to reveal the full possibilities and physics of the proposed setup. Recently, this analysis was carried out and the phase diagrams determined [207].
Additional steps for future work are: consider the system with full spin statistics, allow hopping between plaquettes, introduce interactions between occupied plaquettes and build an experiment to realize the spinless scenario in order to demonstrate the non-Abelian braiding statistics of the Majorana modes.

APPENDIX

ONE

SUPPLEMENTARY MATERIAL TO GENERAL CONCEPTS

For sake of completeness, we give the periodic table of elements [220].

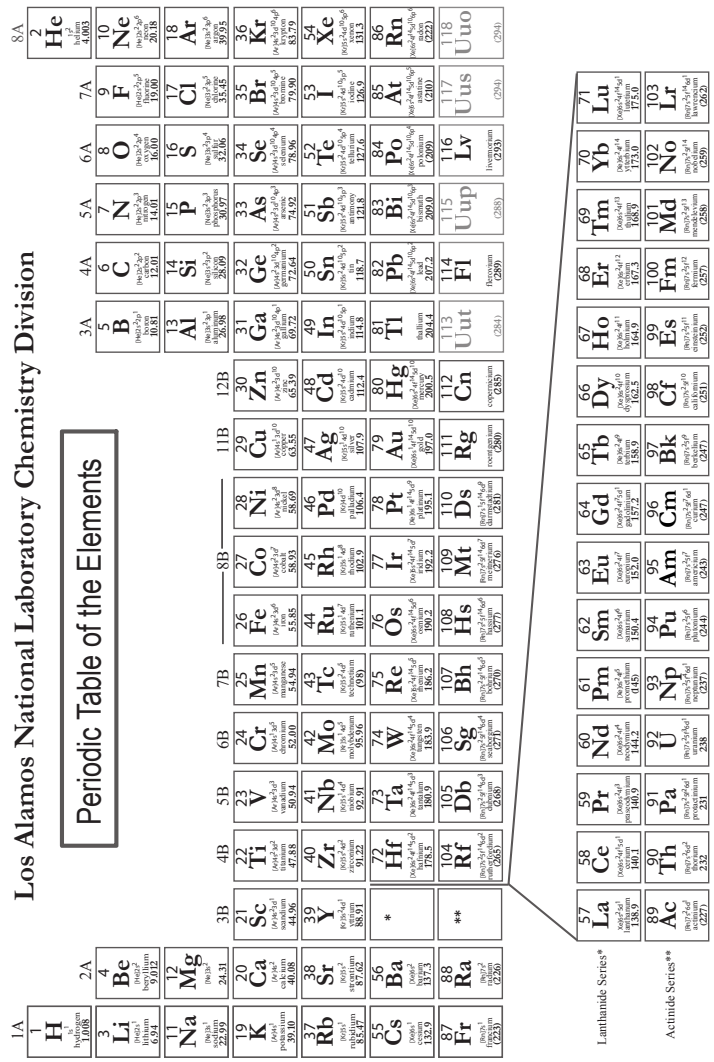

Fig. A.1 Periodic table of elements adapted and taken from [220].

APPENDIX

TWO

SUPPLEMENTARY MATERIAL TO QUANTUM SIMULATOR

B.1. Sommerfeld Expansion

For the presentation of the Sommerfeld expansion we follow the structure given in [141]. In the mean-field analysis of section 3.4 we will encounter integrals of the form

$$\int_{-\infty}^{\infty} \mathrm{d}\epsilon\, g(\epsilon)\, f(\epsilon)\ , \quad \text{with} \quad f(\epsilon) = \frac{1}{\exp\left[(\epsilon-\mu)/k_{\mathrm{B}}T\right]+1}\,, \tag{B.1}$$

where $g(\epsilon)$ is the density of states, $f(\epsilon)$ the Fermi-Dirac distribution as given above, k_{B} is the Boltzmann constant, T the temperature and μ the chemical potential. If we are interested in cases, where the temperature is very small compared to the Fermi temperature $T \ll T_F$, the integral can be expanded to make it manageable. The expansion is

$$\int_{-\infty}^{\infty} g(\epsilon)\, f(\epsilon)\, \mathrm{d}\epsilon = \int_{-\infty}^{\mu} g(\epsilon)\, \mathrm{d}\epsilon + \sum_{n=1}^{\infty} a_n\, (k_{\mathrm{B}}T)^{2n}\, \frac{\mathrm{d}^{2n-1}}{\mathrm{d}\epsilon^{2n-1}}\, g(\epsilon)\Big|_{\epsilon=\mu}\,, \tag{B.2}$$

where the dimensionless numbers a_n are given by

$$a_n = \int_{-\infty}^{\infty} \frac{x^{2n}}{(2n)!} \left(-\frac{\mathrm{d}}{\mathrm{d}x}\, \frac{1}{e^x+1}\right) \mathrm{d}x\,, \tag{B.3}$$

and $x = (\epsilon - \mu)/k_{\mathrm{B}}T$. For the most common cases, it is sufficient to only consider the $n = 1$ contribution in the expansion. Then we obtain

$$\int_{-\infty}^{\infty} g(\epsilon)\, f(\epsilon)\, \mathrm{d}\epsilon \approx \int_{-\infty}^{\mu} g(\epsilon)\, \mathrm{d}\epsilon + \frac{\pi^2}{6}\, (k_{\mathrm{B}}T)^2\, \frac{\mathrm{d}}{\mathrm{d}\epsilon}\, g(\epsilon)\Big|_{\epsilon=\mu} + \mathcal{O}\big(T^4\big)\ . \tag{B.4}$$

For details regarding the Sommerfeld expansion, its additional terms and limits, see [107, 108, 141].

B.2. Derivation of Microscopic Hamiltonian

The microscopic Hamiltonian (3.19) can be derived starting from the general Hamiltonian of second quantized form expressed through the field operators

$$\begin{aligned} \mathrm{H} = &\sum_{\alpha s} \int \mathrm{d}\mathbf{x} \left(-\frac{\hbar^2}{2m} \boldsymbol{\nabla} \Psi^{\dagger}_{\alpha s}(\mathbf{x})\, \boldsymbol{\nabla} \Psi_{\alpha s}(\mathbf{x}) + U(\mathbf{x})\, \Psi^{\dagger}_{\alpha s}(\mathbf{x})\, \Psi_{\alpha s}(\mathbf{x}) \right) \\ &+ \frac{1}{2} \sum_{\alpha\beta s s'} \int \mathrm{d}\mathbf{x}\, \mathrm{d}\mathbf{x}' \Psi^{\dagger}_{\alpha s}(\mathbf{x})\, \Psi^{\dagger}_{\beta s'}\big(\mathbf{x}'\big)\ V_{\alpha\beta}\big(\mathbf{x}, \mathbf{x}'\big)\ \Psi_{\beta s'}\big(\mathbf{x}'\big)\, \Psi_{\alpha s}(\mathbf{x})\ , \end{aligned} \tag{B.5}$$

where $\Psi^{(\dagger)}_{\alpha s}(\mathbf{x})$ is the field operator for annihilation (creation), s is the spin component $\uparrow\downarrow$, $U(\mathbf{x})$ is a possible single-particle potential, $V_{\alpha\beta}(\mathbf{x}, \mathbf{x}')$ is the two-particle potential and α, β consider the relevant orbitals p_x, p_y, where α and β have to be summed over all possible contributions. In the following we abbreviate the labeling for the considered orbital to $\alpha = x$, y and always write the orbital label as an index for the operators or quantities. To avoid confusion, we write spatial components as exponents ^{x,y,z}. The first part of the Hamiltonian is the kinetic part and the third part takes care of two-particle interactions. The general form of the Hamiltonian can be found in standard literature [72, 120, 121].

The next step is to find the Hamiltonian for the p-orbital system considered in chapter 3. We apply the common approach using Wannier functions

$w^*_{\alpha s}(\mathbf{x}-\mathbf{x}_{ij})$ for the field operators [30, 53, 95] and have

$$\Psi^\dagger_{\alpha s}(\mathbf{x}) = \sum_j w^*_{\alpha s}(\mathbf{x}-\mathbf{x}_j)\, c^\dagger_{j\alpha s} + \sum_i w^*_{\alpha s}(\mathbf{x}-\mathbf{x}_i)\, c^\dagger_{i\alpha s}\,, \tag{B.6a}$$

$$\Psi_{\beta s'}(\mathbf{x}) = \sum_j w_{\beta s'}(\mathbf{x}-\mathbf{x}_j)\, c_{j\beta s'} + \sum_i w_{\beta s'}(\mathbf{x}-\mathbf{x}_i)\, c_{i\beta s'}\,, \tag{B.6b}$$

as two examples of the required field operators. Here i and j consider the lattice sites. We then insert all field operators into the Hamiltonian (B.5) and expand it. The next step is to apply simplifications based on the setup of our system. Within the kinetic part we are only interested in nearest neighbor hopping, the summation becomes $\sum_{ij} \to \sum_{\langle i,j\rangle}$. The hopping strengths are introduced to be

- $t^{\parallel}_{\alpha s}$ for hopping possibilities along the σ-binding of the orbitals
- $t^{\perp}_{\alpha s}$ for π-bindings of the orbitals
- possible hopping possibilities along the δ-binding are neglected due to the weak strength of this binding, compared to the larger σ- and π-binding

For an illustration of the hopping strengths see fig. 3.2. Then, we set equal hopping strengths for both spin components and orbitals, such that

- $t^{\parallel}_{x\uparrow} = t^{\parallel}_{x\downarrow} = t^{\parallel}_{ys} = t^{\parallel}$,
- $t^{\perp}_{x\uparrow} = t^{\perp}_{x\downarrow} = t^{\perp}_{ys} = t^{\perp}$,

which is justified, since we do not encounter mechanisms in our system, which treat the hopping strengths differently. The hopping strengths, expressed through Wannier functions, then are

$$t^{\parallel} = \int \mathrm{d}\mathbf{x}\, \frac{\hbar^2}{2m} \boldsymbol{\nabla} w^*_{\alpha s}(\mathbf{x}-\mathbf{x}_j)\, \boldsymbol{\nabla} w_{\alpha s}(\mathbf{x}-\mathbf{x}_i)\,, \tag{B.7a}$$

$$t^{\perp} = \int \mathrm{d}\mathbf{x}\, \frac{\hbar^2}{2m} \boldsymbol{\nabla} w^*_{\alpha s}(\mathbf{x}-\mathbf{x}_{j'})\, \boldsymbol{\nabla} w_{\alpha s}(\mathbf{x}-\mathbf{x}_i)\,. \tag{B.7b}$$

The kinetic part of the Hamiltonian can then be reduced to

$$\begin{aligned} \mathrm{H}_{kin} = &- t^{\parallel} \sum_{\langle i,j,j' \rangle s} \left[c^{\dagger}_{jxs} c_{ix\sigma} + c^{\dagger}_{j'ys} c_{iys} + \mathrm{h.c.} \right] \\ &- t^{\perp} \sum_{\langle i,j,j' \rangle s} \left[c^{\dagger}_{j'xs} c_{ix\sigma} + c^{\dagger}_{jys} c_{iys} + \mathrm{h.c.} \right] , \end{aligned} \tag{B.8}$$

where $j' = i \pm a\,\mathbf{e}^{y}$ is the nearest neighbor in y-direction and $j = i \pm a\,\mathbf{e}^{x}$ in x-direction. The lattice spacing is a and the unit vector for the relevant directions $\mathbf{e}^{x,y}$. For the single-particle contribution we only consider a global chemical potential μ with the terms

$$\mathrm{H}_{\mu} = -\mu \sum_{i\alpha s} c^{\dagger}_{i\alpha s} c_{i\alpha s} \, . \tag{B.9}$$

The major task within this derivation now is the two-particle interaction and its Hamiltonian. Here we apply the following arguments to reduce the contributing terms

- only C_4 symmetric orbital terms are relevant,
- only keep terms, which are allowed by Pauli principle,
- neglect all contributions, that go beyond on-site interaction,
- allow terms with intra-orbital $\alpha = \beta$ and inter-orbital $\alpha \neq \beta$ contributions.

These arguments reduce the present terms even further. To obtain a more compact form for the interaction, we analyze the Wannier functions and find, that they can be chosen to be real $w^{*}_{\alpha s}(\mathbf{x} - \mathbf{x}_i) = w_{\alpha s}(\mathbf{x} - \mathbf{x}_i)$ [221–226]. In addition, we can choose the Wannier functions to be independent of spin $w_{\alpha\uparrow}(\mathbf{x} - \mathbf{x}_i) = w_{\alpha\downarrow}(\mathbf{x} - \mathbf{x}_i) = w_{\alpha}(\mathbf{x} - \mathbf{x}_i)$.
Next, we introduce a contact interaction [30, 227]

$$V\big(\mathbf{x}, \mathbf{x}'\big) = \frac{4\pi\hbar^2\, a_s}{m} \delta\big(\mathbf{x} - \mathbf{x}'\big) = g\, \delta\big(\mathbf{x} - \mathbf{x}'\big) \, , \tag{B.10}$$

where m is the atomic mass and a_s the s-wave scattering length. After these simplifications, based on the setup of the system, we are left with two interaction

potentials

$$\text{intra-orbital potential} \quad U = g \int \mathrm{d}\mathbf{x}\, |w_\alpha(\mathbf{x})|^4 \,, \tag{B.11a}$$

$$\text{inter-orbital potential} \quad V = g \int \mathrm{d}\mathbf{x}\, |w_x(\mathbf{x})|^2 \, |w_y(\mathbf{x})|^2 \,, \tag{B.11b}$$

with g from before. The Wannier functions can be approximated to be of Gaussian form, these considerations are done in sec. B.3.
The interaction Hamiltonian thus is

$$\begin{aligned} \mathrm{H}_{int} = \sum_i \Big[& U \left\{ c^\dagger_{iy\downarrow} c^\dagger_{iy\uparrow} c_{iy\uparrow} c_{iy\downarrow} + c^\dagger_{ix\downarrow} c^\dagger_{ix\uparrow} c_{ix\uparrow} c_{ix\downarrow} \right\} \\ & + V \Big\{ c^\dagger_{iy\downarrow} c^\dagger_{iy\uparrow} c_{ix\uparrow} c_{ix\downarrow} + c^\dagger_{ix\downarrow} c^\dagger_{ix\uparrow} c_{iy\uparrow} c_{iy\downarrow} \\ & \quad + c^\dagger_{iy\downarrow} c^\dagger_{ix\uparrow} c_{ix\uparrow} c_{iy\downarrow} + c^\dagger_{ix\downarrow} c^\dagger_{iy\uparrow} c_{iy\uparrow} c_{ix\downarrow} \\ & \quad + c^\dagger_{iy\downarrow} c^\dagger_{ix\uparrow} c_{iy\uparrow} c_{ix\downarrow} + c^\dagger_{ix\downarrow} c^\dagger_{iy\uparrow} c_{ix\uparrow} c_{iy\downarrow} \Big\} \Big] \,. \end{aligned} \tag{B.12}$$

Introducing the particle number operators as $n_{i\alpha s} = c^\dagger_{i\alpha s} c_{i\alpha s}$ gives

$$\begin{aligned} \mathrm{H}_{int} = \sum_i \Big[& U \left\{ n_{iy\downarrow} n_{iy\uparrow} + n_{ix\downarrow} n_{ix\uparrow} \right\} \\ & + V \Big\{ c^\dagger_{iy\downarrow} c^\dagger_{iy\uparrow} c_{ix\uparrow} c_{ix\downarrow} + c^\dagger_{ix\downarrow} c^\dagger_{ix\uparrow} c_{iy\uparrow} c_{iy\downarrow} \\ & \quad + n_{iy\downarrow} n_{ix\uparrow} + n_{ix\downarrow} n_{iy\uparrow} \\ & \quad + c^\dagger_{iy\downarrow} c^\dagger_{ix\uparrow} c_{iy\uparrow} c_{ix\downarrow} + c^\dagger_{ix\downarrow} c^\dagger_{iy\uparrow} c_{ix\uparrow} c_{iy\downarrow} \Big\} \Big] \,. \end{aligned} \tag{B.13}$$

Next, we use the representation of the spin operators $\vec{S}_{i\alpha} = \left(S^x_{i\alpha}, S^y_{i\alpha}, S^z_{i\alpha}\right)$, where the components are defined through

$$S^\gamma_{i\alpha} = \frac{1}{2} \sum_{s,s'} c^\dagger_{i\alpha\sigma}\, \sigma^\gamma_{s\,s'}\, c_{i\alpha s'} \quad \text{with} \quad \gamma = x, y, z \,, \tag{B.14}$$

with σ^γ being the Pauli matrices given by

$$\sigma^x = \begin{pmatrix} 0 & 1 \\ 1 & 0 \end{pmatrix} \,, \quad \sigma^y = \begin{pmatrix} 0 & -i \\ i & 0 \end{pmatrix} \,, \quad \sigma^z = \begin{pmatrix} 1 & 0 \\ 0 & -1 \end{pmatrix} \,. \tag{B.15}$$

These definitions can also be found in standard literature [72, 120, 121]. Inserting the spin operator into the Hamiltonian (B.13) then reveals

$$\begin{aligned} \mathrm{H}_{int} = \sum_i \Big[& U \left\{ n_{iy\downarrow} n_{iy\uparrow} + n_{ix\downarrow} n_{ix\uparrow} \right\} \\ & + V \Big\{ c^\dagger_{iy\downarrow} c^\dagger_{iy\uparrow} c_{ix\uparrow} c_{ix\downarrow} + c^\dagger_{ix\downarrow} c^\dagger_{ix\uparrow} c_{iy\uparrow} c_{iy\downarrow} \\ & - 2 \left(\vec{S}_{ix} \cdot \vec{S}_{iy} - \frac{1}{4} n_{ix} n_{iy} \right) \Big\} \Big] , \end{aligned} \tag{B.16}$$

where $n_{i\alpha}$ is the total particle number operator for orbital α. To compress the interaction Hamiltonian even further, we introduce in analogy to the spin operator, the orbital operator $\vec{T}_{is} = \left(\vec{T}^x_{is}, \vec{T}^y_{is}, \vec{T}^z_{is} \right)$ with its components

$$T^\gamma_{is} = \frac{1}{2} \sum_{\alpha,\beta} c^\dagger_{i\alpha s} \, \sigma^\gamma_{\alpha\,\beta} \, c_{i\beta s} \, , \quad \text{with} \quad \gamma = x, y, z \, , \tag{B.17}$$

where here the summation is carried out over the orbitals and the spin is kept fixed. In addition we give the orbital raising and lowering operator

$$T^\pm_{is} = T^x_{is} \pm T^y_{is} \, , \tag{B.18}$$

as in the common case for the spin operator. The interaction Hamiltonian then takes the convenient form

$$\begin{aligned} \mathrm{H}_{int} = \sum_i \Big[& U \left\{ n_{iy\downarrow} \, n_{iy\uparrow} + n_{ix\downarrow} \, n_{ix\uparrow} \right\} \\ & + V \left\{ T^+_{i\uparrow} \, T^+_{i\downarrow} + T^-_{i\uparrow} \, T^-_{i\downarrow} - 2 \left(\vec{S}_{ix} \cdot \vec{S}_{iy} - \frac{1}{4} n_{ix} n_{iy} \right) \right\} \Big] . \end{aligned} \tag{B.19}$$

This is the final form of the microscopic interaction Hamiltonian. In combination with the kinetic Hamiltonian (B.8) and the Hamiltonian of the chemical potential (B.9), we then obtain the desired form of Hamiltonian (3.19).

B.3. Approximation to Wannier Functions

In order to gain more insight to the interaction strengths U and V from eq. (B.11a),(B.11b), we approximate the Wannier functions $w_\alpha(\mathbf{x})$ to be of

Gaussian form. In addition we know, that the Wannier function for the p_x-orbital w_x is confined in y-direction and vice versa for the p_y-orbital Wannier function w_y. Both functions are confined in the z-direction due to the setup of the optical lattice. Hence, we approximate the Wannier functions through

$$w_x = A \exp\left[-\frac{\chi^2}{2}\left(\frac{x^2}{\sigma^{x\,2}} + \frac{y^2}{\sigma^{y\,2}} + \frac{z^2}{\sigma^{z\,2}}\right)\right], \tag{B.20a}$$

$$w_y = B \exp\left[-\frac{\zeta^2}{2}\left(\frac{x^2}{\sigma'^{x\,2}} + \frac{y^2}{\sigma'^{y\,2}} + \frac{z^2}{\sigma^{z\,2}}\right)\right], \tag{B.20b}$$

where A, B are normalization constants, χ, ζ are adjustable parameters and $\sigma^{x,y,z}$ are the sizes of the atomic cloud within the optical lattice setup. In addition, $\sigma^x > \sigma'^x$ and $\sigma^y < \sigma'^y$.

The first step is to normalize the Wannier functions to 1, thus

$$\int_{-\infty}^{\infty} |w_\alpha(\mathbf{x})|^2 \,\mathrm{d}\mathbf{x} \stackrel{!}{=} 1\,.$$

We compute for the individual Wannier functions

$$\int_{-\infty}^{\infty} |w_x(\mathbf{x})|^2 \,\mathrm{d}\mathbf{x} = A^2 \int_{-\infty}^{\infty} \exp\left[-\chi^2\left(\frac{x^2}{\sigma^{x\,2}} + \frac{y^2}{\sigma^{y\,2}} + \frac{z^2}{\sigma^{z\,2}}\right)\right] \mathrm{d}\mathbf{x} \tag{B.21}$$

$$= A^2 \left(\frac{\pi^{3/2}\sigma^x\,\sigma^y\,\sigma^z}{\chi^3}\right) \stackrel{!}{=} 1 \tag{B.22}$$

$$\Rightarrow A = \sqrt{\frac{\chi^3}{\pi^{3/2}\,\sigma^x\,\sigma^y\,\sigma^z}}\,, \tag{B.23}$$

and analogously for w_y to find

$$B = \sqrt{\frac{\zeta^3}{\pi^{3/2}\,\sigma'^x\,\sigma'^y\,\sigma^z}}\,. \tag{B.24}$$

The second step is to calculate the interaction strength U using w_x and w_y

$$\begin{aligned} U(w_x) &= g \int_{-\infty}^{\infty} |w_x|^4 \,\mathrm{d}\mathbf{x} \\ &= g \int \left(\frac{\chi^3}{\pi^{3/2}\,\sigma^x\,\sigma^y\,\sigma^z}\right)^2 \exp\left[-2\chi^2\left(\frac{x^2}{\sigma^{x\,2}} + \frac{y^2}{\sigma^{y\,2}} + \frac{z^2}{\sigma^{z\,2}}\right)\right] \mathrm{d}\mathbf{x} \\ &= g \left(\frac{\chi^3}{\pi^{3/2}\,\sigma^x\,\sigma^y\,\sigma^z}\right)^2 \left[\frac{\pi^{3/2}\,\sigma^x\,\sigma^y\,\sigma^z}{2\sqrt{2}\chi^3}\right] = \frac{g}{2\sqrt{2}} \frac{\chi^3}{\pi^{3/2}\sigma^x\,\sigma^y\,\sigma^z}\,, \end{aligned} \tag{B.25}$$

and

$$\begin{aligned} U(w_y) &= g \int_{-\infty}^{\infty} |w_y|^4 \, \mathrm{d}\mathbf{x} \\ &= g \int \left(\frac{\zeta^3}{\pi^{3/2}\, \sigma'^x\, \sigma'^y\, \sigma^z} \right)^2 \exp\left[-2\zeta^2 \left(\frac{x^2}{\sigma'^{x\,2}} + \frac{y^2}{\sigma'^{y\,2}} + \frac{z^2}{\sigma^{z\,2}} \right) \right] \mathrm{d}\mathbf{x} \\ &= g \left(\frac{\zeta^3}{\pi^{3/2}\, \sigma'^x\, \sigma'^y\, \sigma^z} \right)^2 \left[\frac{\pi^{3/2}\, \sigma'^x\, \sigma'^y\, \sigma^z}{2\sqrt{2}\zeta^3} \right] = \frac{g}{2\sqrt{2}} \frac{\zeta^3}{\pi^{3/2}\, \sigma'^x\, \sigma'^y\, \sigma^z} \,. \end{aligned} \tag{B.26}$$

Then we compare both results, since both interaction strengths have to be the same, based on the previous assumptions and requirements. Therefore

$$\begin{aligned} U(w_x) &\stackrel{!}{=} U(w_y) \\ \frac{g}{2\sqrt{2}} \frac{\chi^3}{\pi^{3/2}\, \sigma^x\, \sigma^y\, \sigma^z} &\stackrel{!}{=} \frac{g}{2\sqrt{2}} \frac{\zeta^3}{\pi^{3/2}\, \sigma'^x\, \sigma'^y\, \sigma^z} \\ \Rightarrow \zeta &= \left(\frac{\sigma'^x\, \sigma'^y}{\sigma^x\, \sigma^y} \right)^{1/3} \chi \,. \end{aligned} \tag{B.27}$$

The two Wannier functions hence are

$$w_x = \sqrt{\frac{\chi^3}{\pi^{3/2}\, \sigma^x\, \sigma^y\, \sigma^z}} \exp\left[-\frac{\chi^2}{2} \left(\frac{x^2}{\sigma^{x\,2}} + \frac{y^2}{\sigma^{y\,2}} + \frac{z^2}{\sigma^{z\,2}} \right) \right] , \tag{B.28a}$$

$$w_y = \sqrt{\frac{\chi^3}{\pi^{3/2}\, \sigma^x\, \sigma^y\, \sigma^z}} \exp\left[-\left(\frac{\sigma'^x\, \sigma'^y}{\sigma^x\, \sigma^y} \right)^{2/3} \frac{\chi^2}{2} \left(\frac{x^2}{\sigma'^{x\,2}} + \frac{y^2}{\sigma'^{y\,2}} + \frac{z^2}{\sigma^{z\,2}} \right) \right] . \tag{B.28b}$$

The third step is to compute the interaction strength V with the obtained Wannier functions and use $\gamma^2 = (\sigma'^x\, \sigma'^y / \sigma^x\, \sigma^y)^{2/3}$

$$V = g \int_{-\infty}^{\infty} |w_x|^2 \, |w_y|^2 \, \mathrm{d}\mathbf{x} \,. \tag{B.29}$$

We directly calculate

$$\begin{aligned} V = g \left(\frac{\chi^3}{\pi^{3/2}\, \sigma^x\, \sigma^y\, \sigma^z} \right)^2 \times \\ \int \exp\Big[-\chi^2 \Big(x^2 \left(\frac{1}{\sigma^{x\,2}} + \frac{\gamma^2}{\sigma'^{x\,2}} \right) \\ + y^2 \left(\frac{1}{\sigma^{y\,2}} + \frac{\gamma^2}{\sigma'^{y\,2}} \right) + \frac{z^2}{\sigma^{z\,2}} \left(1 + \gamma^2 \right) \Big) \Big] \, \mathrm{d}\mathbf{x} \\ = g \left(\frac{\chi^3}{\pi^{3/2}\, \sigma^x\, \sigma^y\, \sigma^z} \right)^2 \left[\frac{\pi^{3/2} \sigma^z}{\chi^3 \sqrt{(1+\gamma^2) \left(\frac{1}{\sigma^{x\,2}} + \frac{\gamma^2}{\sigma'^{x\,2}} \right) \left(\frac{1}{\sigma^{y2}} + \frac{\gamma^2}{\sigma'^{y\,2}} \right)}} \right] . \end{aligned} \tag{B.30}$$

Next, we bring the above expression in a convenient form by massaging the equation and have

$$V = \frac{g\, \chi^3}{\pi^{3/2}\, \sigma^x\, \sigma^y\, \sigma^z} \left[\left(1 + \gamma^2 \right) \left(1 + \gamma^2 \frac{\sigma^{x\,2}}{\sigma'^{x\,2}} \right) \left(1 + \gamma^2 \frac{\sigma^{y\,2}}{\sigma'^{y\,2}} \right) \right]^{-1/2} . \tag{B.31}$$

The fourth step is to investigate the ratio V/U of the interaction strengths

$$\frac{V}{U} = \frac{2\sqrt{2}}{\left[(1+\gamma^2) \left(1 + \gamma^2 \frac{\sigma^{x\,2}}{\sigma'^{x\,2}} \right) \left(1 + \gamma^2 \frac{\sigma^{y\,2}}{\sigma'^{y\,2}} \right) \right]^{1/2}} . \tag{B.32}$$

Next, we can simplify the expressions further by assuming that the expansion of the p_x-orbital in x-direction is the same as the p_y-orbital in y-direction, such that

$$\sigma^x = \sigma'^{y} \quad \text{and} \quad \sigma^y = \sigma'^{x} . \tag{B.33}$$

We can set the adjustable parameter to $\chi = 1$. The Wannier functions simplify to

$$w_x = \sqrt{\frac{1}{\pi^{3/2}\, \sigma^x\, \sigma^y\, \sigma^z}} \exp\left[-\frac{1}{2} \left(\frac{x^2}{\sigma^{x\,2}} + \frac{y^2}{\sigma^{y\,2}} + \frac{z^2}{\sigma^{z\,2}} \right) \right] , \tag{B.34a}$$

$$w_y = \sqrt{\frac{1}{\pi^{3/2}\, \sigma^x\, \sigma^y\, \sigma^z}} \exp\left[-\frac{1}{2} \left(\frac{x^2}{\sigma^{y\,2}} + \frac{y^2}{\sigma^{x\,2}} + \frac{z^2}{\sigma^{z\,2}} \right) \right] , \tag{B.34b}$$

and the interaction strengths become

$$U = \frac{g}{(2\pi)^{3/2}\,\sigma^x\,\sigma^y\,\sigma^z}\,, \tag{B.35a}$$

$$V = \frac{g}{2\pi^{3/2}\,\sigma^x\,\sigma^y\,\sigma^z}\left[1+\frac{\sigma^{x\,4}+\sigma^{y\,4}}{2\sigma^{x\,2}\,\sigma^{y\,2}}\right]^{-1/2}\,, \tag{B.35b}$$

whereas the ratio then is

$$\frac{V}{U} = \sqrt{2}\Bigg/\left[1+\frac{\sigma^{x\,4}+\sigma^{y\,4}}{2\sigma^{x\,2}\,\sigma^{y\,2}}\right]^{1/2}\,. \tag{B.36}$$

Hence, the ratio solely depends on the sizes of the clouds in x- and y-direction and can be tuned accordingly.

B.4. Behavior of Density of States Near van Hove Singularities

The density of states $g(\epsilon)$ can be calculated through [107, 141]

$$g_{n\alpha s}(\epsilon) = \frac{1}{N}\sum_{\mathbf{k}}\delta(\epsilon-\varepsilon_{n\mathbf{k}\alpha s})\,, \tag{B.37}$$

where n considers the energy band, α the orbital, s the spin, ϵ is the energy and N the number of lattice sites. In addition, the density of states can be computed by

$$g_{n\alpha s}(\epsilon) = \frac{1}{(2\pi)^d\,N}\int\frac{\mathrm{d}S}{|\boldsymbol{\nabla}\varepsilon_{n\mathbf{k}\alpha s}|}\,, \tag{B.38}$$

with d being the dimension and the integral has to be taken over the surface S. Since we are here interested in the non-interacting case, the dispersion relations are two-fold degenerate with respect to spin. In addition we restrict our considerations to the lowest energy band n. The two dispersion relations are

$$\varepsilon_{\mathbf{k}x} = -2\left(t^{\parallel}\cos(k^x a)+t^{\perp}\cos(k^y a)\right)\,, \tag{B.39a}$$

$$\varepsilon_{\mathbf{k}y} = -2\left(t^{\parallel}\cos(k^y a)+t^{\perp}\cos(k^x a)\right)\,. \tag{B.39b}$$

In order to find the characteristic points of the density of states we investigate

$$|\partial\varepsilon_{\mathbf{k}\alpha}/\partial\mathbf{k}| = 0\,, \tag{B.40}$$

and compute for the dispersion relation of the x-orbital

$$\begin{aligned}\frac{\partial\varepsilon_{\mathbf{k}x}}{\partial\mathbf{k}} &= \begin{pmatrix} -2t^{\parallel}a\,\sin(k^x a) \\ 2t^{\perp}a\,\sin(k^y a)\end{pmatrix} \\ \Rightarrow |\partial\varepsilon_{\mathbf{k}\alpha}/\partial\mathbf{k}| &= 2at^{\parallel}\sqrt{\sin^2(k^x a) + \left(t^{\perp\,2}/t^{\parallel\,2}\right)\sin^2(k^y a)} \stackrel{!}{=} 0\,.\end{aligned} \tag{B.41}$$

Thus, we find the characteristic points to be

$$\begin{aligned}&\textbf{1.)}\ k^x = 0\,,\ k^y = 0\,, && \textbf{2.)}\ k^x = \pm\pi/a\,,\ k^y = \pm\pi/a\,,\\ &\textbf{3.)}\ k^x = \pm\pi/a\,,\ k^y = 0\,, && \textbf{4.)}\ k^x = 0\,,\ k^y = \pm\pi/a\,.\end{aligned} \tag{B.42}$$

Here we are interested in the behavior of the dispersion relation at the critical k-values $k_1 = (\pm\pi/a, 0)$ and $k_2 = (0, \pm\pi/a)$, the characteristic points. These points are saddle points and signal the van Hove singularities. In fig. B.1 we give the plot of the dispersion relation (3.3) and the corresponding contour plot, where we have marked the characteristic points.

The proceeding calculations are in analogy to the two-dimensional tight-binding case discussed in [228]. In contrast to the common tight-binding scenario, we have two hopping parameters and here the Fermi surface is open, as shown in fig B.1. Thus, we expect two van Hove singularities. The idea for the calculations now is, that we focus on a small region Λ around the saddle points at $k_1 = (\pm\pi/a, 0)$ and $k_2 = (0, \pm\pi/a)$, since we are only interested in the behavior of the density of states near the van Hove singularities.

As a first step, we approach the van Hove singularities on the x-axis. For this, the dispersion relation becomes of the form

$$\begin{aligned}\varepsilon_{1\mathbf{k}x} &= -2\left(t^{\parallel}\cos(k^x a - k_1^x a) + t^{\perp}\cos(k^y a)\right) \\ &= -2\left(t^{\parallel}\cos(k^x a - \pi) + t^{\perp}\cos(k^y a)\right)\,.\end{aligned} \tag{B.43}$$

We expand the cosine to second order, $\cos(x) \approx 1 - \frac{1}{2}\,x^2$, and use the relation

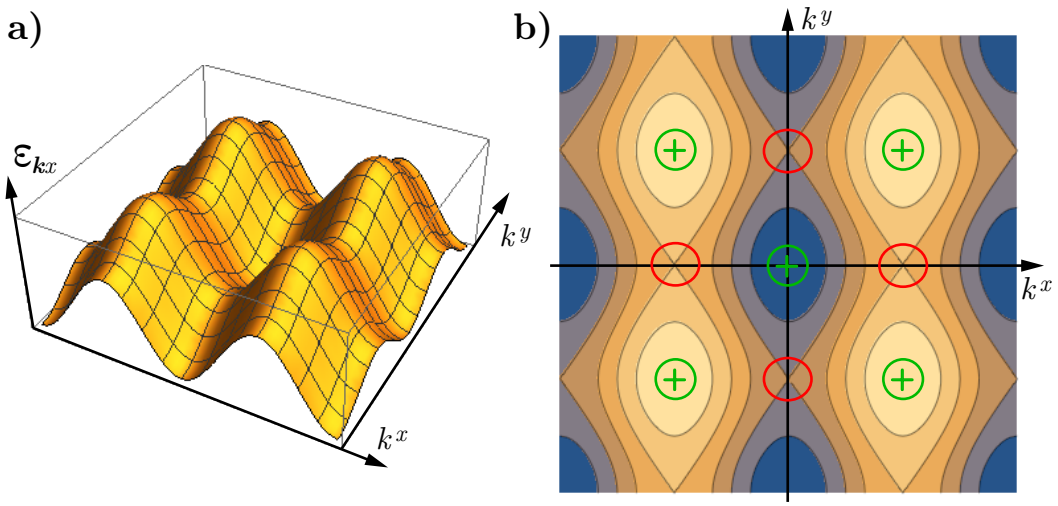

Fig. B.1 a) Three-dimensional plot of the dispersion relation of one orbital and one spin direction (3.3) for the hopping strengths $t^\perp/t^\parallel = 1/2$. **b)** Contour plot of the same dispersion relation, where the saddle points $k_1 = (\pm\pi/a, 0)$ and $k_2 = (0, \pm\pi/a)$ are marked red, the four maxima $k_3 = (\pm\pi/a, \pm\pi/a)$ and $k_4 = (\mp\pi/a, \pm\pi/a)$ and the minimum $k_5 = (0, 0)$ are in green.

$\cos(180° - \alpha) = -\cos(\alpha)$, to obtain

$$\begin{aligned}\varepsilon_{1\mathbf{k}x} &= -2\left(-t^\parallel\left(1 - \frac{1}{2}\left(k^x a - \pi\right)^2\right) + t^\perp\left(1 - \frac{1}{2}\left(k^y a\right)^2\right)\right) \\ &= 2\left(t^\parallel - t^\perp\right) - 2\left(\frac{t^\parallel}{2}\left(k^x a - \pi\right)^2 - \frac{t^\perp}{2}\left(k^y a\right)^2\right) . \end{aligned} \tag{B.44}$$

Next, we bring the above equation into a handy form for later calculations

$$\begin{aligned}\varepsilon_{1\mathbf{k}x} - 2\left(t^\parallel - t^\perp\right) &= -2\left(\frac{t^\parallel}{2}\left(k^x a - \pi\right)^2 - \frac{t^\perp}{2}\left(k^y a\right)^2\right) \\ -\frac{1}{2t^\parallel}\left(\varepsilon_{1\mathbf{k}x} - 2\left(t^\parallel - t^\perp\right)\right) &= \frac{1}{2}\left(k^x a - \pi\right)^2 - \frac{1}{2}\frac{t^\perp}{t^\parallel}\left(k^y a\right)^2 . \end{aligned} \tag{B.45}$$

Here we introduce new quantities to express equation (B.45) in a more conve-

nient form

$$\chi = -\frac{1}{2t^{\parallel}} \left(\varepsilon_{1\mathbf{k}x} - 2 \left(t^{\parallel} - t^{\perp} \right) \right) , \tag{B.46a}$$

$$\gamma = \frac{t^{\perp}}{t^{\parallel}} , \tag{B.46b}$$

$$\xi = \pi - k^x a , \tag{B.46c}$$

$$\eta = k^y a , \tag{B.46d}$$

$$\Rightarrow \text{for eq. (B.45):} \quad \chi = \frac{1}{2}\xi^2 - \frac{1}{2}\gamma\,\eta^2 . \tag{B.46e}$$

We calculate the density of states of the two-dimensional problem through

$$g_x(\varepsilon) \sim \oint \frac{\mathrm{d}l}{|\boldsymbol{\nabla}\varepsilon_{\mathbf{k}x}|} , \tag{B.47}$$

with $|\boldsymbol{\nabla}\varepsilon_{\mathbf{k}x}|$ being

$$\partial_{k^x}\, \varepsilon_{1\mathbf{k}x} = -2t^{\parallel} a\ (k^x a - \pi) = 2t^{\parallel} a\, \xi , \tag{B.48a}$$

$$\partial_{k^y}\, \varepsilon_{1\mathbf{k}x} = 2t^{\perp} a\ (k^y a) = 2t^{\perp} a\, \eta , \tag{B.48b}$$

$$\Rightarrow |\boldsymbol{\nabla}\varepsilon_{\mathbf{k}x}| = 2t^{\parallel} a \sqrt{\xi^2 + \gamma^2\eta^2} . \tag{B.48c}$$

Then the density of states becomes

$$g_x \sim \oint \frac{\mathrm{d}l}{2t^{\parallel} a \sqrt{\xi^2 + \gamma^2\eta^2}} . \tag{B.49}$$

Now we have to determine the line segment $\mathrm{d}l$

$$\mathrm{d}l = \sqrt{(\mathrm{d}k^x)^2 + (\mathrm{d}k^y)^2} = \frac{1}{a}\sqrt{(\mathrm{d}\xi)^2 + (\mathrm{d}\eta)^2} , \tag{B.50}$$

with $\mathrm{d}k^x = -\mathrm{d}\xi/a$ and $\mathrm{d}k^y = \mathrm{d}\eta/a$. We can then write the density of states as

$$g_x \sim \oint \frac{\sqrt{(\mathrm{d}\xi)^2 + (\mathrm{d}\eta)^2}}{\sqrt{\xi^2 + \gamma^2\,\eta^2}} , \tag{B.51}$$

where we have neglected all pre-factors, since we are only interested in the behavior of the density of states near the van Hove singularity. Now we

investigate the change in energy on the considered surface χ (B.46e), to further simplify the integral. The change in energy is zero, $\mathrm{d}\chi = 0$, because it is a surface of constant energy. Thus,

$$\begin{aligned} \mathrm{d}\chi = 0 = \mathrm{d}\left(\frac{1}{2}\xi^2 - \frac{1}{2}\gamma\,\eta^2\right) = \xi\,\mathrm{d}\xi - \gamma\,\eta\,\mathrm{d}\eta = 0 \\ \Rightarrow \quad \mathrm{d}\eta = \frac{\xi}{\gamma\,\eta}\,\mathrm{d}\xi\,, \end{aligned} \tag{B.52}$$

and hence the density of states (B.51) can be expressed as

$$g_x \sim \oint \frac{\sqrt{(\mathrm{d}\xi)^2 + \left(\frac{\xi}{\gamma\eta}\right)^2 (\mathrm{d}\xi)^2}}{\sqrt{\xi^2 + \gamma^2\,\eta^2}} \sim \oint \frac{\mathrm{d}\xi}{\gamma\,\eta}\,. \tag{B.53}$$

With the definition (B.46e) we can give the parameter η as

$$\eta = \sqrt{\frac{1}{\gamma}\left(\xi^2 - 2\chi\right)}\,. \tag{B.54}$$

Inserting this into equation (B.53) reveals

$$g_x \sim \frac{1}{\sqrt{\gamma}} \oint \frac{\mathrm{d}\xi}{\sqrt{\xi^2 - 2\chi}}\,. \tag{B.55}$$

The integration is carried out in the range from $\xi_1 = \sqrt{2\chi}$ to $\xi_2 \approx \pi/2$. The additional numerical factor, due to the closed line integral $\oint \mathrm{d}l$, is neglected, because we are just interested in the behavior. Keep in mind, that the expansion of the cosine to second order becomes invalid for such large values of ξ, but the integrand is small in the chosen region, such that the whole integral contribution is small [228]. The integral hence is

$$g_x \sim \int_{\xi_1}^{\xi_2} \frac{\mathrm{d}\xi}{\sqrt{\xi^2 - 2\chi}} = \left[\ln\left(\xi + \sqrt{-2\chi + \xi^2}\right)\right]_{\xi_1}^{\xi_2}\,, \tag{B.56}$$

where we only are interested in the qualitative behavior and have the desired result

$$g_x(\varepsilon) \sim -\frac{1}{2}\ln\left[\varepsilon_{1\,x} - 2\left(1 - \frac{t^\perp}{t^\parallel}\right)\right]\,. \tag{B.57}$$

The density of states experiences a logarithmic behavior near the van Hove singularities, characterized through the two hopping parameters $t^{\parallel}$ and $t^{\perp}$. In the special case for isotropic hopping, $t^{\parallel} = t^{\perp}$, the above behavior reduces to the common behavior of the density of states for the two-dimensional tight-binding model $g \sim -\frac{1}{2} \ln \varepsilon$ [107, 228].
Investigating the remaining characteristic k-values for the p_x-orbital dispersion relation reveals the analog results and especially the analog behaviors near the two van Hove singularities.
In fig. B.2 we sketch the behavior of the density of states near the van Hove singularities $\varepsilon = \pm 1$, as calculated in equation (B.57). The analysis of the dispersion relation for the p_y-orbital and its characteristic points gives the analog results.

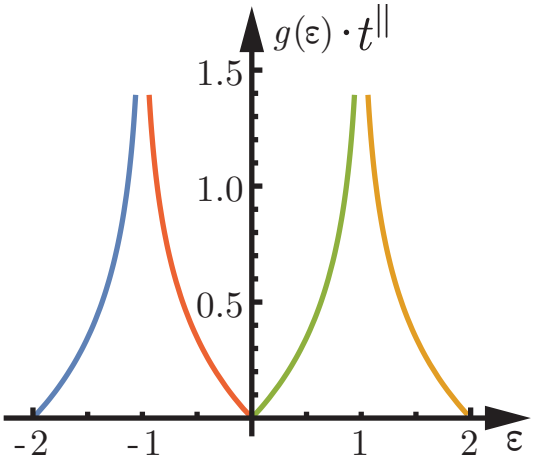

Fig. B.2 Behavior of the density of states $g(\varepsilon)$ for the p-orbital scenario near the van Hove singularities $\varepsilon = \pm 1$ as calculated in eq. (B.57) for all four possible contributions of the characteristic points (B.42).

B.5. Analysis of Single-Site with Two Fermions

Here we investigate the ground state for the single-site. We encounter two degrees of freedom from spin ($\uparrow\downarrow$) and orbital ($p_{x,y}$). Constraints are due to the Pauli principle, i.e. the anti-symmetric total wave function. If the spin contribution is symmetric, the orbital contribution has to be anti-symmetric and vice versa. To find the possible ground state configuration we refer to the

Clebsch-Gordan series for the addition of angular momenta [69, 229]. It reads

$$|J,\, M\rangle = \sum_{m_1=-j_1}^{j_1} \sum_{m_2=-j_2}^{j_2} |j_1,\, j_2; m_1,\, m_2\rangle \, \langle j_1,\, j_2; m_1,\, m_2 | J,\, M\rangle \,, \tag{B.58}$$

where $\langle ... | ... \rangle$ are the Clebsch-Gordan coefficients, J is the total angular momentum with

$$-|j_1 - j_2| \leq J \leq j_1 + j_2 \,, \tag{B.59}$$

in this case it can take the values $J = 0,\, 1$ and M is

$$M = -J \,...\, J \quad \text{i.e.} \quad -1,\, 0,\, 1 \,, \tag{B.60}$$

with the constraint $M = m_1 + m_2$ and $m_i = -1/2,\, 0,\, 1/2$. Thus we are interested in introducing a total angular momentum for the site, which then characterizes the possible ground state. This total angular momentum is constructed out of two angular momenta, one for each orbital, $\vec{J} = \vec{J}_x + \vec{J}_y$. The next step is to evaluate all the possible Clebsch-Gordan coefficients. Here we restrict the considerations only to those cases, where we obtain a spin singlet $|S_i\rangle$ or spin triplet $|T_i\rangle$ configuration. We label those states in the final representation as $|p_x\,;\, p_y\rangle = |S_i \,/\, T_i\rangle$ and begin with the possible spin triplet states.

- $J = 1\,, M = 1$:

$$|J = 1\,, M = 1\rangle = \sum_{m_1=-j_1}^{j_1} \sum_{m_2=-j_2}^{j_2} |j_1,\, j_2; m_1,\, m_2\rangle \, \langle j_1,\, j_2; m_1,\, m_2 | J = 1,\, M = 1\rangle \,, \tag{B.61}$$

  here we only compute a non-zero contribution for $\langle ... | ... \rangle$, if $j_1 = 1/2$, $j_2 = 1/2$ and $m_1 = 1/2$, $m_2 = 1/2$. This then reveals the state

$$\begin{aligned} |J = 1,\, M = 1\rangle &= |p_x = \uparrow\,; p_y = \uparrow\rangle \\ &\Rightarrow |T_1\rangle = c^\dagger_{ix\uparrow}\, c^\dagger_{iy\uparrow} |0\rangle \,, \end{aligned} \tag{B.62}$$

  the first spin triplet state.

- $J = 1,\ M = 0$:

$$|J = 1,\ M = 0\rangle = \sum_{m_2} \sum_{m_1} |m_1,\ m_2\rangle \langle m_1,\ m_2|M\rangle\,, \tag{B.63}$$

in this scenario there are two possibilities $m_1 = 1/2,\ m_2 = -1/2$ or $m_1 = -1/2,\ m_2 = 1/2$, thus

$$\begin{aligned} |J = 1,\ M = 0\rangle &= \frac{1}{\sqrt{2}} \left(|p_x =\uparrow;\ p_y =\downarrow\rangle + |p_x =\downarrow;\ p_y =\uparrow\rangle\right) \\ \Rightarrow |T_3\rangle &= \frac{1}{\sqrt{2}} \left(c^\dagger_{ix\uparrow}\, c^\dagger_{iy\downarrow} + c^\dagger_{ix\downarrow}\, c^\dagger_{iy\uparrow}\right) |0\rangle\,, \end{aligned} \tag{B.64}$$

the second spin triplet state.

- $J = 1,\ M = -1$:
Here we obtain only non-zero contributions when $m_1 = m_2 = -1/2$ and thus

$$\begin{aligned} |J = 1,\ M = -1\rangle &= |p_x =\downarrow;\ p_y =\downarrow\rangle \\ \Rightarrow |T_2\rangle &= c^\dagger_{ix\downarrow}\, c^\dagger_{iy\downarrow}|0\rangle\,, \end{aligned} \tag{B.65}$$

which is the third spin triplet state.

After the discussion for the spin triplet states, we turn to the corresponding investigations for the spin singlet states. In contrast to the coupling of two spin-1/2 particles, we encounter additional coupling mechanisms for the spin singlet state, which result in additional possible states. We only give the states fulfilling the previous requirements. They are

- $J = 0,\ M = (1/2 - 1/2) + 0$:

$$\begin{aligned} &|J = 0,\ M = (1/2 - 1/2) + 0\rangle = \\ &\sum_{m_1} \sum_{m_2} |m_1,\ m_2\rangle \langle m_1,\ m_2|M = (1/2 - 1/2) + 0\rangle\,, \end{aligned} \tag{B.66}$$

here we have to couple two spins, $\uparrow + \downarrow$, within one orbital and leave the other orbital empty. This coupling can be done in both orbitals,

combined symmetrically and anti-symmetrically, resulting in the states

$$|J=0,\, M=0\rangle = \frac{1}{\sqrt{2}}\left(|\downarrow\uparrow;\, 0\rangle \pm |0;\, \downarrow\uparrow\right)$$
$$\Rightarrow |S_{1,2}\rangle = \frac{1}{\sqrt{2}}\left(c^\dagger_{ix\downarrow}\, c^\dagger_{ix\uparrow} \pm c^\dagger_{iy\downarrow}\, c^\dagger_{iy\uparrow}\right)|0\rangle\,, \tag{B.67}$$

two of the spin singlet states.

- $J=0,\, M=1/2-1/2=0$:
  In this possibility one orbital has to have spin $\uparrow$, the other $\downarrow$, such that

$$|J=0,\, M=1/2-1/2\rangle = \frac{1}{\sqrt{2}}\left(|\uparrow;\downarrow\rangle - |\downarrow;\uparrow\rangle\right)$$
$$\Rightarrow |S_3\rangle = \frac{1}{\sqrt{2}}\left(c^\dagger_{ix\uparrow}\, c^\dagger_{iy\downarrow} - c^\dagger_{ix\downarrow}\, c^\dagger_{iy\uparrow}\right)|0\rangle\,. \tag{B.68}$$

  the third spin singlet state.

An illustration of all possible configuration is given in fig. 3.4.

B.6. Calculations of Mean-Field Section

The following sections are dedicated to calculations of section 3.4, which were neglected for sake of readability.

B.6.1. Mean-Particle Density p_y-Orbital

The mean-particle density of the p_y-orbital is calculated through the general relation

$$\bar{n}_{ys} = \int_{-\infty}^{\infty} g_{ys}(\varepsilon)\, f_{ys}(\varepsilon)\,\mathrm{d}\varepsilon = \frac{1}{2}\int_{-\infty}^{\infty} g_y(\varepsilon)\, f_{ys}(\varepsilon)\,\mathrm{d}\varepsilon\,, \tag{B.69}$$

and gives

$$\bar{n}_y = \bar{n}_{y\uparrow} + \bar{n}_{y\downarrow} = \frac{1}{2}\int_{-\infty}^{\infty} g_y(\varepsilon)\, f_{y\uparrow}(\varepsilon)\,\mathrm{d}\varepsilon + \frac{1}{2}\int_{-\infty}^{\infty} g_y(\varepsilon)\, f_{y\downarrow}(\varepsilon)\,\mathrm{d}\varepsilon\,. \tag{B.70}$$

Using the Sommerfeld expansion (3.39) results in

$$\begin{aligned}\bar{n}_y &\approx \frac{1}{2}\left\{\int_{-\infty}^{\mu_{y\uparrow}} g_y(\varepsilon)\,\mathrm{d}\varepsilon + \frac{\pi^2}{6}\left(k_\mathrm{B}T\right)^2 g_y'\left(\mu_{y\uparrow}\right)\right\} \\ &\quad + \frac{1}{2}\left\{\int_{-\infty}^{\mu_{y\downarrow}} g_y(\varepsilon)\,\mathrm{d}\varepsilon + \frac{\pi^2}{6}\left(k_\mathrm{B}T\right)^2 g_y'\left(\mu_{y\downarrow}\right)\right\} \\ &= \frac{1}{2}\int_{-\infty}^{\bar{E}_{F,y}+\Delta\mu_y} g_y(\varepsilon)\,\mathrm{d}\varepsilon + \frac{1}{2}\int_{-\infty}^{\bar{\bar{E}}_{F,y}+\Delta\mu_y} g_y(\varepsilon)\,\mathrm{d}\varepsilon \\ &\quad + \frac{1}{2}\frac{\pi^2}{6}\left(k_\mathrm{B}T\right)^2\left[g_y'\big(\mu_{y\uparrow}\big) + g_y'\big(\mu_{y\downarrow}\big)\right]\,, \end{aligned} \tag{B.71}$$

where

$$\begin{aligned}\bar{E}_{F,y} &= E_{F,y} + \frac{1}{2}\left(Um_y + Vm_x + g_J\mu_\mathrm{B}H\right)\,, \\ \bar{\bar{E}}_{F,y} &= E_{F,y} - \frac{1}{2}\left(Um_y + Vm_x + g_J\mu_\mathrm{B}H\right)\,, \end{aligned} \tag{B.72}$$

and the Fermi energy is close to the chemical potential such that $\mu = E_F + \Delta\mu$ holds. Next, we split the integral limits and add a zero, which gives

$$\begin{aligned}\bar{n}_y &= \frac{1}{2}\int_{-\infty}^{E_{F,y}} g_y(\varepsilon)\,\mathrm{d}\varepsilon + \frac{1}{2}\int_{E_{F,y}}^{\bar{E}_{F,y}} g_y(\varepsilon)\,\mathrm{d}\varepsilon + \frac{1}{2}\int_{\bar{E}_{F,y}}^{\bar{E}_{F,y}+\Delta\mu_y} g_y(\varepsilon)\,\mathrm{d}\varepsilon \\ &\quad + \frac{1}{2}\int_{-\infty}^{\bar{\bar{E}}_{F,y}} g_y(\varepsilon)\,\mathrm{d}\varepsilon + \frac{1}{2}\int_{\bar{\bar{E}}_{F,y}}^{\bar{\bar{E}}_{F,y}+\Delta\mu_y} g_y(\varepsilon)\,\mathrm{d}\varepsilon \pm \frac{1}{2}\int_{\bar{\bar{E}}_{F,y}}^{E_{F,y}} g_y(\varepsilon)\,\mathrm{d}\varepsilon \\ &\quad + \frac{1}{2}\frac{\pi^2}{6}\left(k_\mathrm{B}T\right)^2\left[g_y'\big(\mu_{y\uparrow}\big) + g_y'\big(\mu_{y\downarrow}\big)\right]\,. \end{aligned} \tag{B.73}$$

The first term of the first and second line can be combined to $\int_{-\infty}^{E_{F,y}} g_y(\varepsilon)\,\mathrm{d}\varepsilon = \bar{n}_{0y}$. Integrating the remaining parts computes

$$\begin{aligned}\bar{n}_y &= \bar{n}_{0y} + \frac{1}{2}\Big[G_y(\varepsilon)\Big]_{E_{F,y}}^{\bar{E}_{F,y}} - \frac{1}{2}\Big[G_y(\varepsilon)\Big]_{\bar{\bar{E}}_{F,y}}^{E_{F,y}} + \frac{1}{2}\Big[G_y(\varepsilon)\Big]_{\bar{E}_{F,y}}^{\bar{E}_{F,y}+\Delta\mu_y} \\ &\quad + \frac{1}{2}\Big[G_y(\varepsilon)\Big]_{\bar{\bar{E}}_{F,y}}^{\bar{\bar{E}}_{F,y}+\Delta\mu_y} + \frac{1}{2}\frac{\pi^2}{6}\left(k_\mathrm{B}T\right)^2\left[g_y'\big(\mu_{y\uparrow}\big) + g_y'\big(\mu_{y\downarrow}\big)\right]\,. \end{aligned} \tag{B.74}$$

We expand the integrated density of states $G_y(\varepsilon)$ around the Fermi energy $E_{F,y}$ up to third order in the magnetizations m_α, in addition we expand the

temperature dependent term around $\bar{E}_{F,y}$, $\bar{\bar{E}}_{F,y}$ up to first order in $\Delta\mu_y$ to then compute

$$\begin{aligned}
\bar{n}_y \approx \bar{n}_{0y} &+ \frac{1}{2}\Big\{ G_y\big(E_{F,y}\big) + \frac{1}{2}\left(Um_y + Vm_x + g_J\mu_{\mathrm{B}}H\right) g_y\big(E_{F,y}\big) \\
&\quad + \frac{1}{8}\left(Um_y + Vm_x\right)^2 g_y'\big(E_{F,y}\big) \\
&\quad + \frac{1}{2}\,\frac{1}{4!}\left(Um_y + Vm_x\right)^3 g_y''\big(E_{F,y}\big) - G_y\big(E_{F,y}\big) \Big\} \\
&- \frac{1}{2}\Big\{ G_y\big(E_{F,y}\big) - \Big[G_y\big(E_{F,y}\big) - \frac{1}{2}\left(Um_y + Vm_x + g_J\mu_{\mathrm{B}}H\right) g_y\big(E_{F,y}\big) \\
&\quad + \frac{1}{8}\left(Um_y + Vm_x\right)^2 g_y'\big(E_{F,y}\big) \\
&\quad - \frac{1}{2}\,\frac{1}{4!}\left(Um_y + Vm_x\right)^3 g_y''\big(E_{F,y}\big) \Big] \Big\} \\
&+ \frac{1}{2}\left\{ G_y\big(\bar{E}_{F,y}\big) + \Delta\mu_y\, g_y\big(\bar{E}_{F,y}\big) - G_y\big(\bar{E}_{F,y}\big) \right\} \\
&+ \frac{1}{2}\left\{ G_y\big(\bar{\bar{E}}_{F,y}\big) + \Delta\mu_y\, g_y\big(\bar{\bar{E}}_{F,y}\big) - G_y\big(\bar{\bar{E}}_{F,y}\big) \right\} \\
&+ \frac{1}{2}\,\frac{\pi^2}{6}\left(k_{\mathrm{B}}T\right)^2 \Big[g_y'\big(\bar{E}_{F,y}\big) + \Delta\mu_y\, g_y''\big(\bar{E}_{F,y}\big) \\
&\qquad\qquad + g_y'\big(\bar{\bar{E}}_{F,y}\big) + \Delta\mu_y\, g_y''\big(\bar{\bar{E}}_{F,y}\big) \Big] .
\end{aligned} \tag{B.75}$$

The mean-particle density thus reduces to

$$\begin{aligned}
\bar{n}_y = \bar{n}_{0y} &+ \frac{1}{2}\left\{ \frac{1}{4}\,\left(Um_y + Vm_x\right)^2 g_y'\big(E_{F,y}\big) + \frac{\pi^2}{6}\left(k_{\mathrm{B}}T\right)^2 \bar{g}_y'\big(E_{F,y}\big) \right\} \\
&+ \frac{1}{2}\,\Delta\mu_y \left\{ \bar{g}_y\big(E_{F,y}\big) + \frac{\pi^2}{6}\left(k_{\mathrm{B}}T\right)^2 \bar{g}_y''\big(E_{F,y}\big) \right\} ,
\end{aligned} \tag{B.76}$$

with

$$\begin{aligned}
\bar{g}_y\big(E_{F,y}\big) &= g_y\big(\bar{E}_{F,y}\big) + g_y\big(\bar{\bar{E}}_{F,y}\big) \ , \\
\bar{g}_y'\big(E_{F,y}\big) &= g_y'\big(\bar{E}_{F,y}\big) + g_y'\big(\bar{\bar{E}}_{F,y}\big) \ , \\
\bar{\bar{g}}_y''\big(E_{F,y}\big) &= g_y''\big(\bar{E}_{F,y}\big) + g_y''\big(\bar{\bar{E}}_{F,y}\big) \ .
\end{aligned} \tag{B.77}$$

Here we assume, that $\bar{n}_y - \bar{n}_{0y} \approx 0$, which is justified, since the magnetizations and the magnetic field is small, the deviation $\Delta\mu_y$ then is

$$\Delta\mu_y = -\frac{\frac{1}{4}\,\left(Um_y + Vm_x\right)^2 g_y'\big(E_{F,y}\big) + \frac{\pi^2}{6}\left(k_{\mathrm{B}}T\right)^2 \bar{g}_y'\big(E_{F,y}\big)}{\bar{g}_y\big(E_{F,y}\big) + \frac{\pi^2}{6}\left(k_{\mathrm{B}}T\right)^2 \bar{g}_y''\big(E_{F,y}\big)} . \tag{B.78}$$

B.6.2. Expansions for Density of States

The expansions for the density of states $\bar{g}_\alpha$, $\bar{\bar{g}}_\alpha$ and their derivatives, around the Fermi energy $E_{F,\alpha}$ in orders of the magnetizations m_α are performed, where terms higher than the second derivative in the density of states are neglected. We start with

$$\begin{aligned} g_\alpha\big(\bar{E}_{F,\alpha}\big) &\approx g_\alpha\big(E_{F,\alpha}\big) + \frac{1}{2}\left(Um_\alpha + Vm_{\alpha'} + g_J\mu_\mathrm{B}H\right) g'_\alpha\big(E_{F,\alpha}\big) \\ &\quad + \frac{1}{8}\left(Um_\alpha + Vm_{\alpha'}\right)^2 g''_\alpha\big(E_{F,\alpha}\big) \ , \\ g_\alpha\big(\bar{\bar{E}}_{F,\alpha}\big) &\approx g_\alpha\big(E_{F,\alpha}\big) - \frac{1}{2}\left(Um_\alpha + Vm_{\alpha'} + g_J\mu_\mathrm{B}H\right) g'_\alpha\big(E_{F,\alpha}\big) \\ &\quad + \frac{1}{8}\left(Um_\alpha + Vm_{\alpha'}\right)^2 g''_\alpha\big(E_{F,\alpha}\big) \ , \end{aligned} \tag{B.79}$$

where $\alpha, \alpha' = x, y$ and $\alpha' \neq \alpha$. As before, here only the linear contribution of the magnetic field is relevant. The resulting equations for the different density of states are

$$\begin{aligned} \bar{g}_\alpha\big(E_{F,\alpha}\big) &= g_\alpha\big(\bar{E}_{F,\alpha}\big) + g_\alpha\big(\bar{\bar{E}}_{F,\alpha}\big) \\ &\approx 2g_\alpha\big(E_{F,\alpha}\big) + \frac{1}{4}\left(Um_\alpha + Vm_{\alpha'}\right)^2 g''_\alpha\big(E_{F,\alpha}\big) \ , \\ \bar{\bar{g}}_\alpha\big(E_{F,\alpha}\big) &= g_\alpha\big(\bar{E}_{F,\alpha}\big) - g_\alpha\big(\bar{\bar{E}}_{F,\alpha}\big) \\ &\approx \left(Um_\alpha + Vm_{\alpha'} + g_J\mu_\mathrm{B}H\right) g'_\alpha\big(E_{F,\alpha}\big) \ . \end{aligned} \tag{B.80}$$

For the first derivative

$$\begin{aligned} g'_\alpha\big(\bar{E}_{F,\alpha}\big) &\approx g'_\alpha\big(E_{F,\alpha}\big) + \frac{1}{2}\left(Um_\alpha + Vm_{\alpha'} + g_J\mu_\mathrm{B}H\right) g''_\alpha\big(E_{F,\alpha}\big) \ , \\ g'_\alpha\big(\bar{\bar{E}}_{F,\alpha}\big) &\approx g'_\alpha\big(E_{F,\alpha}\big) - \frac{1}{2}\left(Um_\alpha + Vm_{\alpha'} + g_J\mu_\mathrm{B}H\right) g''_\alpha\big(E_{F,\alpha}\big) \ , \end{aligned} \tag{B.81}$$

thus

$$\begin{aligned} \bar{g}'_\alpha\big(E_{F,\alpha}\big) &= g'_\alpha\big(\bar{E}_{F,\alpha}\big) + g'_\alpha\big(\bar{\bar{E}}_{F,\alpha}\big) \approx 2g'_\alpha\big(E_{F,\alpha}\big) \ , \\ \bar{\bar{g}}'_\alpha\big(E_{F,\alpha}\big) &= g'_\alpha\big(\bar{E}_{F,\alpha}\big) - g'_\alpha\big(\bar{\bar{E}}_{F,\alpha}\big) \\ &\approx \left(Um_\alpha + Vm_{\alpha'} + g_J\mu_\mathrm{B}H\right) g''_\alpha\big(E_{F,\alpha}\big) \ . \end{aligned} \tag{B.82}$$

And for the second derivative

$$
\begin{aligned}
&g''_\alpha\big(\bar{E}_{F,\alpha}\big) \approx g''_\alpha\big(E_{F,\alpha}\big) + \mathcal{O}\left(g'''_\alpha\right) \,, \\
&g''_\alpha\big(\bar{\bar{E}}_{F,\alpha}\big) \approx g''_\alpha\big(E_{F,\alpha}\big) + \mathcal{O}\left(g'''_\alpha\right) \,, \\
&\bar{g}''_\alpha\big(E_{F,\alpha}\big) = g''_\alpha\big(\bar{E}_{F,\alpha}\big) + g''_\alpha\big(\bar{\bar{E}}_{F,\alpha}\big) \approx 2g''_\alpha\big(E_{F,\alpha}\big) \,, \\
&\bar{\bar{g}}''_\alpha\big(E_{F,\alpha}\big) = g''_\alpha\big(\bar{E}_{F,\alpha}\big) - g''_\alpha\big(\bar{\bar{E}}_{F,\alpha}\big) \approx 0 \,.
\end{aligned} \tag{B.83}
$$

B.6.3. Magnetization p_y-Orbital

The magnetization of the p_y-orbital is computed through

$$
m_y = \bar{n}_{y\uparrow} - \bar{n}_{y\downarrow} = \frac{1}{2}\int_{-\infty}^{\infty} g_y(\varepsilon)\, f_{y\uparrow}(\varepsilon)\,\mathrm{d}\varepsilon - \frac{1}{2}\int_{-\infty}^{\infty} g_y(\varepsilon)\, f_{y\downarrow}(\varepsilon)\,\mathrm{d}\varepsilon \,, \tag{B.84}
$$

applying the Sommerfeld expansion (3.39) results in

$$
\begin{aligned}
m_y \approx{}& \frac{1}{2}\left\{\int_{-\infty}^{\mu_{y\uparrow}} g_y(\varepsilon)\,\mathrm{d}\varepsilon + \frac{\pi^2}{6}\left(k_\mathrm{B}T\right)^2 g'_y\big(\mu_{y\uparrow}\big)\right\} \\
&- \frac{1}{2}\left\{\int_{-\infty}^{\mu_{y\downarrow}} g_y(\varepsilon)\,\mathrm{d}\varepsilon + \frac{\pi^2}{6}\left(k_\mathrm{B}T\right)^2 g'_y\big(\mu_{y\downarrow}\big)\right\} \,.
\end{aligned} \tag{B.85}
$$

Splitting the limits of the integrals and adding a zero reveals

$$
\begin{aligned}
m_y ={}& \frac{1}{2}\int_{-\infty}^{E_{F,y}} g_y(\varepsilon)\,\mathrm{d}\varepsilon + \frac{1}{2}\int_{E_{F,y}}^{\bar{E}_{F,y}} g_y(\varepsilon)\,\mathrm{d}\varepsilon + \frac{1}{2}\int_{\bar{E}_{F,y}}^{\bar{E}_{F,y}+\Delta\mu_y} g_y(\varepsilon)\,\mathrm{d}\varepsilon \\
&- \frac{1}{2}\int_{-\infty}^{\bar{\bar{E}}_{F,y}} g_y(\varepsilon)\,\mathrm{d}\varepsilon - \frac{1}{2}\int_{\bar{\bar{E}}_{F,y}}^{\bar{\bar{E}}_{F,y}+\Delta\mu_y} g_y(\varepsilon)\,\mathrm{d}\varepsilon \pm \frac{1}{2}\int_{\bar{\bar{E}}_{F,y}}^{E_{F,y}} g_y(\varepsilon)\,\mathrm{d}\varepsilon \\
&+ \frac{1}{2}\frac{\pi^2}{6}\left(k_\mathrm{B}T\right)^2\left[g'_y\big(\mu_{y\uparrow}\big) - g'_y\big(\mu_{y\downarrow}\big)\right] \\
={}& \frac{1}{2}\int_{\bar{\bar{E}}_{F,y}}^{\bar{E}_{F,y}} g_y(\varepsilon)\,\mathrm{d}\varepsilon + \frac{1}{2}\int_{\bar{E}_{F,y}}^{\bar{E}_{F,y}+\Delta\mu_y} g_y(\varepsilon)\,\mathrm{d}\varepsilon - \frac{1}{2}\int_{\bar{\bar{E}}_{F,y}}^{\bar{\bar{E}}_{F,y}+\Delta\mu_y} g_y(\varepsilon)\,\mathrm{d}\varepsilon \\
&+ \frac{1}{2}\frac{\pi^2}{6}\left(k_\mathrm{B}T\right)^2\left[g'_y\big(\mu_{y\uparrow}\big) - g'_y\big(\mu_{y\downarrow}\big)\right] \,,
\end{aligned} \tag{B.86}
$$

with $\bar{E}_{F,y}$ and $\bar{\bar{E}}_{F,y}$ from before, equation (B.72). As the next step, we integrate the individual terms and compute

$$\begin{aligned} m_y = \frac{1}{2}\Big[G_y(\varepsilon)\Big]_{\bar{\bar{E}}_{F,y}}^{\bar{E}_{F,y}} + \frac{1}{2}\Big[G_y(\varepsilon)\Big]_{\bar{E}_{F,y}}^{\bar{E}_{F,y}+\Delta\mu_y} - \frac{1}{2}\Big[G_y(\varepsilon)\Big]_{\bar{\bar{E}}_{F,y}}^{\bar{\bar{E}}_{F,y}+\Delta\mu_y} \\ + \frac{1}{2}\,\frac{\pi^2}{6}\,(k_\mathrm{B}T)^2\left[g_y'\big(\mu_{y\uparrow}\big) - g_y'\big(\mu_{y\downarrow}\big)\right] . \end{aligned} \tag{B.87}$$

We expand the integrated density of states $G_y(\varepsilon)$ around the Fermi energy $E_{F,y}$ up to third order in the magnetizations and we expand the temperature dependent term around the modified Fermi energies $\bar{E}_{F,y}$, $\bar{\bar{E}}_{F,y}$ in orders of the deviation $\Delta\mu_y$ up to first order. The magnetization then becomes

$$\begin{aligned} m_y \approx \frac{1}{2}\Big\{ & G_y\big(E_{F,y}\big) + \frac{1}{2}\left(Um_y + Vm_x + g_J\mu_\mathrm{B}H\right) g_y\big(E_{F,y}\big) \\ & + \frac{1}{8}\left(Um_y + Vm_x\right)^2 g_y'\big(E_{F,y}\big) \\ & + \frac{1}{2}\,\frac{1}{4!}\left(Um_y + Vm_x\right)^3 g_y''\big(E_{F,y}\big) \\ & - \Big[G_y\big(E_{F,y}\big) - \frac{1}{2}\left(Um_y + Vm_x + g_J\mu_\mathrm{B}H\right) g_y\big(E_{F,y}\big) \\ & + \frac{1}{8}\left(Um_y + Vm_x\right)^2 g_y'\big(E_{F,y}\big) \\ & - \frac{1}{2}\,\frac{1}{4!}\left(Um_y + Vm_x\right)^3 g_y''\big(E_{F,y}\big)\Big]\Big\} \\ & + \frac{1}{2}\left\{G_y\big(\bar{E}_{F,y}\big) + \Delta\mu_y\, g_y\big(\bar{E}_{F,y}\big) - G_y\big(\bar{E}_{F,y}\big)\right\} \\ & - \frac{1}{2}\left\{G_y\big(\bar{\bar{E}}_{F,y}\big) + \Delta\mu_y\, g_y\big(\bar{\bar{E}}_{F,y}\big) - G_y\big(\bar{\bar{E}}_{F,y}\big)\right\} \\ & + \frac{1}{2}\,\frac{\pi^2}{6}\,(k_\mathrm{B}T)^2\Big[g_y'\big(\bar{E}_{F,y}\big) + \Delta\mu_y\, g_y''\big(\bar{E}_{F,y}\big) \\ & \qquad - \big(g_y'\big(\bar{\bar{E}}_{F,y}\big) + \Delta\mu_y\, g_y''\big(\bar{\bar{E}}_{F,y}\big)\big)\Big] , \end{aligned} \tag{B.88}$$

this then reduces to

$$\begin{aligned} m_y = \frac{1}{2}\Big\{ & \left(U m_y + V m_x + g_J \mu_\mathrm{B} H\right) g_y\big(E_{F,y}\big) \\ & + \frac{1}{4!}\left(U m_y + V m_x\right)^3 g_y''\big(E_{F,y}\big) \Big\} \\ & + \frac{1}{2}\,\Delta\mu_y \left\{ \bar{\bar{g}}_y\big(E_{F,y}\big) + \frac{\pi^2}{6}\left(k_\mathrm{B}T\right)^2 \bar{\bar{g}}_y''\big(E_{F,y}\big) \right\} \\ & + \frac{1}{2}\,\frac{\pi^2}{6}\left(k_\mathrm{B}T\right)^2 \bar{\bar{g}}_y'\big(E_{F,y}\big) \ , \end{aligned} \tag{B.89}$$

where we have introduced

$$\begin{aligned} \bar{\bar{g}}_y\big(E_{F,y}\big) &= g_y\big(\bar{E}_{F,y}\big) - g_y\big(\bar{\bar{E}}_{F,y}\big) \ , \\ \bar{\bar{g}}_y'\big(E_{F,y}\big) &= g_y'\big(\bar{E}_{F,y}\big) - g_y'\big(\bar{\bar{E}}_{F,y}\big) \ , \\ \bar{\bar{g}}_y''\big(E_{F,y}\big) &= g_y''\big(\bar{E}_{F,y}\big) - g_y''\big(\bar{\bar{E}}_{F,y}\big) \ . \end{aligned} \tag{B.90}$$

Then, we use the expansions of sec. B.6.2 to reduce and simplify equation (B.89) further such that

$$\begin{aligned} m_y \approx \frac{1}{2}\Big\{ & \left(U m_y + V m_x + g_J \mu_\mathrm{B} H\right) g_y\big(E_{F,y}\big) \\ & + \frac{\pi^2}{6}\left(k_\mathrm{B}T\right)^2 \left(U m_y + V m_x + g_J \mu_\mathrm{B} H\right) g_y''\big(E_{F,y}\big) \\ & + \frac{1}{4!}\left(U m_y + V m_x\right)^3 g_y''\big(E_{F,y}\big) \Big\} \\ & + \frac{1}{2}\,\Delta\mu_y \left\{ \left(U m_y + V m_x + g_J \mu_\mathrm{B} H\right) g_y'\big(E_{F,y}\big) \right\} \ . \end{aligned} \tag{B.91}$$

We insert the deviation $\Delta\mu_y$ of eq. (B.78), where we also apply the expansions of sec. B.6.2 to $\Delta\mu_y$, into the above equation and have

$$\begin{aligned} m_y = \frac{1}{2}\Big\{ & \left(U m_y + V m_x + g_J \mu_\mathrm{B} H\right) \left[g_y\big(E_{F,y}\big) + \frac{\pi^2}{6}\left(k_\mathrm{B}T\right)^2 g_y''\big(E_{F,y}\big) \right] \\ & + \frac{1}{4!}\left(U m_y + V m_x\right)^3 g_y''\big(E_{F,y}\big) \Big\} \\ & + \frac{1}{2}\Big\{ - \frac{1}{8}\left(U m_y + V m_x\right)^2 - \frac{\pi^2}{6}\left(k_\mathrm{B}T\right)^2 \Big\} \frac{g_y'\big(E_{F,y}\big)}{g_y\big(E_{F,y}\big)} \\ & \quad \times \left(U m_y + V m_x + g_J \mu_\mathrm{B} H\right) g_y'\big(E_{F,y}\big) \ . \end{aligned} \tag{B.92}$$

Here we have neglected a small contribution within the denominator of the deviation $\Delta\mu_y$. The magnetization then becomes

$$\begin{aligned} m_y = \frac{1}{2}\left(U m_y + V m_x + g_J \mu_\mathrm{B} H\right) g_y\big(E_{F,y}\big) \\ \times \left\{ 1 - \frac{\pi^2}{6} \left(k_\mathrm{B} T\right)^2 \left[\frac{g_y'^2\big(E_{F,y}\big)}{g_y^2\big(E_{F,y}\big)} - \frac{g_y''\big(E_{F,y}\big)}{g_y\big(E_{F,y}\big)} \right] \right\} \\ + \frac{3}{2} \frac{1}{4!} \left(U m_y + V m_x\right)^3 \left[\frac{g_y''\big(E_{F,y}\big)}{3} - \frac{g_y'^2\big(E_{F,y}\big)}{g_y\big(E_{F,y}\big)} \right] . \end{aligned} \tag{B.93}$$

Ginzburg-Landau Theory for Magnetization

Within the magnetization (B.93) we have neglected higher contributions of the magnetic field than linear order. This is based on the principle form of the energy functional within the Ginzburg-Landau theory of phase transitions [100, 101], it reads

$$F[m] \sim a_2\, m^2 + a_4\, m^4 - m \cdot H\,, \tag{B.94}$$

where $a_{2,4}$ are some tuning parameters and m the corresponding order parameter. Minimizing the energy functional with respect to the order parameter then reveals

$$\frac{\mathrm{d}F[m]}{\mathrm{d}m} \stackrel{!}{=} 0 = 2a_2\, m + 4a_4\, m^3 - H\,, \tag{B.95}$$

and thus only the linear order in the magnetic field is relevant.

Magnetization of p_y-Orbital

For sake of convenience we introduce

$$\begin{aligned} \xi\big(T, E_{F,y}\big) &= 1 - \frac{\pi^2}{6} \left(k_\mathrm{B} T\right)^2 \left[\frac{g_y'^2\big(E_{F,y}\big)}{g_y^2\big(E_{F,y}\big)} - \frac{g_y''\big(E_{F,y}\big)}{g_y\big(E_{F,y}\big)} \right] \\ &= 1 - \frac{\pi^2}{6} \left(k_\mathrm{B} T\right)^2 \Lambda\big(E_{F,y}\big)\,, \\ \zeta\big(E_{F,y}\big) &= \left[\frac{g_y''\big(E_{F,y}\big)}{3} - \frac{g_y'^2\big(E_{F,y}\big)}{g_y\big(E_{F,y}\big)} \right] , \end{aligned} \tag{B.96}$$

and the magnetization takes the convenient form

$$m_y = \frac{1}{2}\left(U m_y + V m_x + g_J \mu_\mathrm{B} H\right) g_y\big(E_{F,y}\big)\, \xi\big(T, E_{F,y}\big) + \frac{3}{2}\frac{1}{4!}\left(U m_y + V m_x\right)^3 \zeta\big(E_{F,y}\big)\,. \tag{B.97}$$

B.6.4. Eigenvalue Problem of Magnetization

We determine the eigenvalues and eigenvectors for the tensor representation (3.60) of the magnetization, for the special case of vanishing magnetic field, $H = 0$. The tensor representation then is

$$\begin{pmatrix} m_x \\ m_y \end{pmatrix} = \frac{1}{2}\begin{pmatrix} U g_x\big(E_{F,x}\big)\, \xi\big(T, E_{F,x}\big) & V g_x\big(E_{F,x}\big)\, \xi\big(T, E_{F,x}\big) \\ V g_y\big(E_{F,y}\big)\, \xi\big(T, E_{F,y}\big) & U g_y\big(E_{F,y}\big)\, \xi\big(T, E_{F,y}\big) \end{pmatrix} \begin{pmatrix} m_x \\ m_y \end{pmatrix}, \tag{B.98}$$

for sake of brevity, we introduce

$$\begin{aligned} g_x\big(E_{F,x}\big) &= g_x\,, & g_y\big(E_{F,y}\big) &= g_y\,, \\ \xi\big(T, E_{F,x}\big) &= \xi_x\,, & \xi\big(T, E_{F,y}\big) &= \xi_y\,. \end{aligned} \tag{B.99}$$

The representation takes the form

$$\begin{pmatrix} m_x \\ m_y \end{pmatrix} = \frac{1}{2}\begin{pmatrix} U g_x \xi_x & V g_x \xi_x \\ V g_y \xi_y & U g_y \xi_y \end{pmatrix} \begin{pmatrix} m_x \\ m_y \end{pmatrix}. \tag{B.100}$$

We compute the eigenvalues through the standard procedure $\det(A - \lambda \mathrm{E}) \stackrel{!}{=} 0$, this leads to

$$\begin{aligned} &\left| \begin{pmatrix} \frac{1}{2} U g_x \xi_x - \lambda & \frac{1}{2} V g_x \xi_x \\ \frac{1}{2} V g_y \xi_y & \frac{1}{2} U g_y \xi_y - \lambda \end{pmatrix} \right| \stackrel{!}{=} 0 \\ \Rightarrow\ &\lambda^2 - \frac{\lambda}{2} U\left(g_x \xi_x + g_y \xi_y\right) + \frac{1}{4} g_x g_y \xi_x \xi_y \left(U^2 - V^2\right) = 0\,, \end{aligned} \tag{B.101}$$

solving for λ then yields

$$\begin{aligned} \lambda_{1,2} &= \frac{U}{4}\left(g_x \xi_x + g_y \xi_y\right) \pm \frac{1}{2}\sqrt{\frac{U^2}{4}\left(g_x \xi_x + g_y \xi_y\right)^2 - g_x g_y \xi_x \xi_y \left(U^2 - V^2\right)} \\ &= \frac{U}{4}\left(g_x \xi_x + g_y \xi_y\right)\left[1 \pm \sqrt{1 + \frac{4 g_x g_y \xi_x \xi_y \left(V^2 - U^2\right)^2}{U^2 \left(g_x \xi_x + g_y \xi_y\right)^2}}\right], \end{aligned} \tag{B.102}$$

the desired eigenvalues. We are interested in a setup, where the two density of states are identical, with the same Fermi energy

$$\begin{aligned} g_x &= g_y = g(E_F) \ , \\ \xi_x &= \xi_y = \xi(T, E_F) \ , \end{aligned} \tag{B.103}$$

the eigenvalues then become

$$\lambda_{1,2} = \frac{1}{2}\, g(E_F)\, \xi(T, E_F)\, [U \pm V] \ . \tag{B.104}$$

The eigenvalues directly lead to two self-consistency equations

$$\begin{aligned} &\begin{pmatrix} m_x \\ m_y \end{pmatrix} = \begin{pmatrix} \lambda_1 & 0 \\ 0 & \lambda_2 \end{pmatrix} \begin{pmatrix} m_x \\ m_y \end{pmatrix} \\ \Rightarrow \quad & 1 = \frac{1}{2}\, g(E_F)\, \xi(T, E_F)\, [U + V] \\ \text{and} \quad & 1 = \frac{1}{2}\, g(E_F)\, \xi(T, E_F)\, [U - V] \ . \end{aligned} \tag{B.105}$$

Fulfilling one of the self-consistency equations signals the instability of the system and thus a phase transition. The next task is to compute the eigenvectors to determine the principle structure of the phase after the transition. The eigenvectors are calculated through $(A - \lambda_i \mathrm{E})\,(\mathrm{EV}_i) = 0$, where we find the first set of eigenvectors for the first eigenvalue

$$\begin{aligned} &\begin{pmatrix} \frac{1}{2}U g(E_F)\, \xi(T, E_F) - \lambda_1 & \frac{1}{2}V g(E_F)\, \xi(T, E_F) \\ \frac{1}{2}V g(E_F)\, \xi(T, E_F) & \frac{1}{2}U g(E_F)\, \xi(T, E_F) - \lambda_1 \end{pmatrix} \begin{pmatrix} \mathrm{EV}_{11} \\ \mathrm{EV}_{12} \end{pmatrix} \stackrel{!}{=} \begin{pmatrix} 0 \\ 0 \end{pmatrix} \\ &\qquad \frac{1}{2}V g(E_F)\, \xi(T, E_F) \begin{pmatrix} -1 & 1 \\ 1 & -1 \end{pmatrix} \begin{pmatrix} \mathrm{EV}_{11} \\ \mathrm{EV}_{12} \end{pmatrix} \stackrel{!}{=} \begin{pmatrix} 0 \\ 0 \end{pmatrix} \\ &\qquad\qquad \Rightarrow \qquad \mathrm{EV}_1 = \begin{pmatrix} 1 \\ 1 \end{pmatrix} \quad \vee \quad \begin{pmatrix} -1 \\ -1 \end{pmatrix} \ . \end{aligned} \tag{B.106}$$

These eigenvectors correspond to the common ferromagnet, where the majority of spins are $\uparrow$ or $\downarrow$ in both orbitals, depending on the eigenvector. The order

parameter here thus is $m = m_x + m_y$. The second set of eigenvectors is

$$\begin{pmatrix} \frac{1}{2}Ug(E_F)\,\xi(T,E_F) - \lambda_2 & \frac{1}{2}Vg(E_F)\,\xi(T,E_F) \\ \frac{1}{2}Vg(E_F)\,\xi(T,E_F) & \frac{1}{2}Ug(E_F)\,\xi(T,E_F) - \lambda_2 \end{pmatrix} \begin{pmatrix} \mathrm{EV}_{21} \\ \mathrm{EV}_{22} \end{pmatrix} \stackrel{!}{=} \begin{pmatrix} 0 \\ 0 \end{pmatrix}$$

$$\frac{1}{2}Vg(E_F)\,\xi(T,E_F) \begin{pmatrix} 1 & 1 \\ 1 & 1 \end{pmatrix} \begin{pmatrix} \mathrm{EV}_{21} \\ \mathrm{EV}_{22} \end{pmatrix} \stackrel{!}{=} \begin{pmatrix} 0 \\ 0 \end{pmatrix}$$

$$\Rightarrow \qquad \mathrm{EV}_2 = \begin{pmatrix} 1 \\ -1 \end{pmatrix} \quad \vee \quad \begin{pmatrix} -1 \\ 1 \end{pmatrix}. \tag{B.107}$$

Here the majority of spins point $\uparrow$ within the p_x-orbitals and $\downarrow$ in the p_y-orbitals or vice versa. This configuration relates to a ferromagnetic phase with orbital symmetry breaking. Here, the order parameter can be given as $\tilde{m} = m_x - m_y$.

Note that we have the same set of eigenvectors, if we use the tensor representation

$$\begin{pmatrix} 0 \\ 0 \end{pmatrix} = \begin{pmatrix} \frac{1}{2}Ug_x\xi_x - 1 & \frac{1}{2}Vg_x\xi_x \\ \frac{1}{2}Vg_y\xi_y & \frac{1}{2}Ug_y\xi_y - 1 \end{pmatrix} \begin{pmatrix} m_x \\ m_y \end{pmatrix}. \tag{B.108}$$

B.6.5. Susceptibility of Mean-Field System

In general, the magnetic susceptibility is calculated through

$$\chi = \frac{\partial M}{\partial H} \qquad \text{or} \qquad \chi = \frac{\partial^2 F}{\partial H^2}\,, \tag{B.109}$$

where M is the thermodynamic magnetization of the system, H the magnetic field and $F = G(T,H)$ is the energy functional, here the Gibbs free energy. The susceptibility χ represents the magnetic moment induced by a magnetic field H. If the relation

$$\vec{M} = \chi \vec{H}\,, \tag{B.110}$$

holds, then the material is called to be linear. In addition, if $\chi > 0$, the material is dominated by paramagnetism, for $\chi < 0$ by diamagnetism, [141, 146]. The two relevant equations, deduced from eq. (3.58) and eq. (3.63), are

$$\begin{aligned} 0 &= \frac{1}{2}\,g_J\mu_\mathrm{B}Hg(E_F)\,\xi(T,E_F) + \left[\frac{1}{2}\,g(E_F)\,\xi(T,E_F)\,(U+V)\right] m\,, \\ 0 &= \frac{1}{2}\,g_J\mu_\mathrm{B}Hg(E_F)\,\xi(T,E_F) + \left[\frac{1}{2}\,g(E_F)\,\xi(T,E_F)\,(U-V)\right] \tilde{m}\,, \end{aligned} \tag{B.111}$$

where we have also introduced the order parameters $m = m_x + m_y$ for the ferromagnetic phase and $\tilde{m} = m_x - m_y$ for the ferromagnetic phase with orbital symmetry breaking, as before. We can solve both equations for m, $\tilde{m}$ and compute

$$\begin{aligned} m &= \frac{\frac{1}{2}\, g_J \mu_\mathrm{B}\, g(E_F)\, \xi(T, E_F)\ H}{1 - \frac{1}{2}\, g(E_F)\, \xi(T, E_F)\, (U + V)}\,, \\ \tilde{m} &= \frac{\frac{1}{2}\, g_J \mu_\mathrm{B}\, g(E_F)\, \xi(T, E_F)\ H}{1 - \frac{1}{2}\, g(E_F)\, \xi(T, E_F)\, (U - V)}\,. \end{aligned} \tag{B.112}$$

Hence, the system always has a finite magnetization for an applied magnetic field, even before the instability condition is reached. Our system depends linearly on the magnetic field, thus the susceptibility can be calculated as

$$\begin{aligned} \chi &= \frac{M}{H} = \frac{\mu_\mathrm{B} m}{H} \\ \Rightarrow \chi &= \frac{\frac{1}{2}\, g_J \mu_\mathrm{B}^2\, g(E_F)\, \xi(T, E_F)}{1 - \frac{1}{2}\, g(E_F)\, \xi(T, E_F)\, (U \pm V)}\,. \end{aligned} \tag{B.113}$$

The susceptibility diverges at the same critical condition as found for the self-consistency equations (3.64a) and (3.64b). Fulfilling the self-consistency equations, the susceptibility diverges and signals a phase transition leading to additional solutions for the magnetizations m, $\tilde{m}$. In fig. B.3 we give the susceptibilities for the dominant order parameter m for three different reduced Fermi energies $\epsilon_F > 0$ and two temperatures, the same parameters as in fig. 3.10, in order to compare the behavior. Again, we only give the $\epsilon_F > 0$ sector, since we obtain the analog results for $\epsilon_F < 0$. From the plot B.3 we find that the susceptibility diverges at the same values as the phase transition occurs in the plot for the solutions of the magnetization fig. 3.10. This holds for the zero temperature scenario as well as for $k_\mathrm{B}T/t^{\parallel} = 1$. Increasing the temperature shifts the divergence of the susceptibility to larger values of the interaction strengths, as in the vanishing magnetic field case.

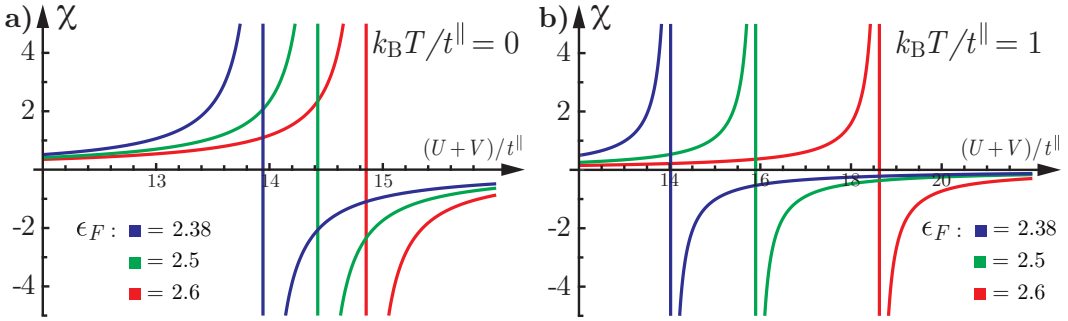

Fig. B.3 Susceptibility χ of eq. (B.113) for three different reduced Fermi energies $\epsilon_F > 0$ as given in the plot and two different temperatures $k_B T/t^{\parallel}$, plotted over the reduced interaction strengths $(U+V)/t^{\parallel}$. The parameters are chosen to be identical to fig. 3.10, to observe the diverging susceptibility at the same critical condition, as the magnetic field free scenario. **a)** Zero temperature susceptibility. **b)** Here the temperature is $k_B T/t^{\parallel} = 1$ and we see, that the functions are shifted to larger interaction strengths, as before.

B.6.6. Solutions of Magnetization for Finite Magnetic Field

The self-consistency equation (3.58) can be transformed by using the eigenvectors $\mathrm{EV}_1 = (1,1)$ and $\mathrm{EV}_2 = (1,-1)$, thus the order parameters $m = m_x + m_y$ and $\tilde{m} = m_x - m_y$, as well as the simplification of identical density of state (3.62). The equation becomes

$$0 = m\left[1 + \frac{\frac{3}{2}\,\frac{1}{4!}\,(U \pm V)^3\,\zeta(E_F)}{\frac{1}{2}\,(U \pm V)\,g(E_F)\,\xi(T,E_F) - 1}\,m^2\right] + \frac{\frac{1}{2}\,g_J\,\mu_B\,g(E_F)\,\xi(T,E_F)\,H}{\frac{1}{2}\,(U \pm V)\,g(E_F)\,\xi(T,E_F) - 1}\,, \tag{B.114}$$

where the plus sign within the interaction strengths $U+V$ relates to the dominant order parameter m and the minus sign in $U-V$ to the sub-leading order parameter $\tilde{m}$. Solving this equation by hand for the magnetization is

tedious, therefore we introduce new parameters

$$\begin{aligned} a &= \frac{3}{2}\,\frac{1}{4!}\,(U \pm V)^3\,\zeta(E_F)\ , \\ b &= \frac{1}{2}\,(U \pm V)\,g(E_F)\ \xi(T, E_F) - 1\,, \\ c &= \frac{1}{2}\,g_J\,\mu_{\mathrm{B}}\,g(E_F)\ \xi(T, E_F)\ H\,, \end{aligned} \tag{B.115}$$

and the equation to solve then takes the convenient form

$$0 = m\left[1 + \frac{a}{b}\,m^2\right] + \frac{c}{b} \quad . \tag{B.116}$$

We insert this equation into the software "Mathematica" and find the three possible solutions as

$$\begin{aligned} m_1 &= \frac{2 \times 3^{1/3} a\,b - 2^{1/3}\,[d(a,b,c)]^{2/3}}{6^{2/3}\,a\ [d(a,b,c)]^{1/3}}\,, \\ m_2 &= \frac{-2\left(3i + \sqrt{3}\right) a\,b + 2^{1/3}\,3^{1/6}\left(1 - i\sqrt{3}\right)[d(a,b,c)]^{2/3}}{2 \times 2^{2/3}\,3^{5/6}\,a\ [d(a,b,c)]^{1/3}}\,, \\ m_3 &= \frac{-2\left(-3i + \sqrt{3}\right) a\,b + 2^{1/3}\,3^{1/6}\left(1 + i\sqrt{3}\right)[d(a,b,c)]^{2/3}}{2 \times 2^{2/3}\,3^{5/6}\,a\ [d(a,b,c)]^{1/3}}\,, \end{aligned} \tag{B.117}$$

with

$$d(a,b,c) = 9a^2 c + \sqrt{3}\sqrt{a^3\,(4b^3 + 27a\,c^2)}\,. \tag{B.118}$$

The solutions (B.117) are plotted in fig. 3.11 for three different reduced Fermi energies $\epsilon_F > 0$, two different temperatures as well as two different magnetic fields. For further details and explanations of the behavior, see main text within sec. 3.4.6.

B.7. Derivations of Strong Coupling Section

We present here additional calculations and considerations of the strong coupling section, which were neglected in the main text.

B.7.1. Representation of Projected Equations in Strong Coupling Limit

The full Hamiltonian of our system is

$$\begin{aligned}\mathrm{H} = &-\sum_{\alpha s}\left\{t^{\parallel}\sum_{\langle i,j\rangle_{\alpha}^{\parallel}}\left(c_{j\alpha s}^{\dagger}c_{i\alpha s}+\mathrm{h.c.}\right)+t^{\perp}\sum_{\langle i,j\rangle_{\bar{\alpha}}^{\perp}}\left(c_{j\alpha s}^{\dagger}c_{i\alpha s}+\mathrm{h.c.}\right)\right\}\\ &-\mu\sum_{i\alpha s}c_{i\alpha s}^{\dagger}c_{i\alpha s}+U\sum_{i}\left(n_{ix\uparrow}\,n_{ix\downarrow}+n_{iy\uparrow}\,n_{iy\downarrow}\right)\\ &+V\sum_{i}\left[T_{i\uparrow}^{+}\,T_{i\downarrow}^{+}+T_{i\uparrow}^{-}\,T_{i\downarrow}^{-}-2\left(\vec{S}_{ix}\cdot\vec{S}_{iy}-\frac{1}{4}\,n_{ix}\,n_{iy}\right)\right]\\ =&\mathrm{H}_{kin}+\mathrm{H}_{int}=\tilde{\mathrm{T}}+\tilde{\mathrm{V}}\,,\end{aligned}\tag{B.119}$$

where the chemical potential μ directly vanishes, since we are interested in half-filling.

Before we get into the detailed analysis of the different projections, we give the form of the projectors P_m. The P_0 projector makes sure, that no double-occupancy occurs for a certain lattice site, despite the initial configuration of the state within the considered site. On the other hand, the projector P_1 acts to have a site with one double-occupancy of one of the orbitals, where as P_2 acts to have two double-occupancies. The projectors then are of the form

$$\begin{aligned}P_0&=\left(1-n_{i\alpha s}\,n_{i\alpha\bar{s}}\right)\left(1-n_{i\bar{\alpha}\bar{s}}\right)\,,\\ P_1&=\left(1-n_{i\alpha s}\,n_{i\alpha\bar{s}}\right)n_{i\bar{\alpha}\bar{s}}\,,\\ P_2&=n_{i\alpha s}\,n_{i\alpha\bar{s}}\,n_{i\bar{\alpha}\bar{s}}\,,\end{aligned}\tag{B.120}$$

where $n_{i\alpha s}$ is the number operator, $\alpha = x, y$, $\alpha \neq \bar{\alpha}$ considers the orbital and $s = \uparrow, \downarrow$, $s \neq \bar{s}$ the spin. Since there are two orbitals present in our system, instead of one [111], the projectors thus consider this.

Step by step we now analyze the different projections $P_0\,\mathrm{H}\,P_0$, $P_1\,\mathrm{H}\,P_0$, $P_0\,\mathrm{H}\,P_1$, $P_1\,\mathrm{H}\,P_1$, $P_2\,\mathrm{H}\,P_1$, $P_1\,\mathrm{H}\,P_2$, $P_2\,\mathrm{H}\,P_2$ and investigate, how they act on the different Hilbert subspaces.

1.) $P_0\,\mathrm{H}\,P_0$: Here we know, hopping is solely from a half-filled site i into an empty or singly filled neighboring site j. No interaction term appears here,

because double-occupancy does not occur. Only $\tilde{\mathrm{T}}$ is relevant.

$$
\begin{aligned}
&P_0\,\mathrm{H}\,P_0 = P_0\,\tilde{\mathrm{T}}\,P_0 \\
&= -P_0 \sum_{\alpha s} \left\{ t^{\parallel} \sum_{\langle i,j\rangle^{\parallel}_{\alpha}} \left(c^{\dagger}_{j\alpha s} c_{i\alpha s} + \mathrm{h.c.} \right) + t^{\perp} \sum_{\langle i,j\rangle^{\perp}_{\alpha}} \left(c^{\dagger}_{j\alpha s} c_{i\alpha s} + \mathrm{h.c.} \right) \right\} P_0 \\
&= -\sum_{\langle i,j\rangle^{\parallel}_{\alpha},s} \Big[\left(1 - n_{jys}\, n_{jy\bar{s}}\right) \left(1 - n_{jx\bar{s}}\right) t^{\parallel}\, c^{\dagger}_{jxs} c_{ixs} \left(1 - n_{ix\bar{s}}\right) \left(1 - n_{iys}\, n_{iy\bar{s}}\right) \\
&\qquad + \left(1 - n_{jxs}\, n_{jx\bar{s}}\right) \left(1 - n_{jy\bar{s}}\right) t^{\parallel}\, c^{\dagger}_{jys} c_{iys} \left(1 - n_{iy\bar{s}}\right) \left(1 - n_{ixs}\, n_{ix\bar{s}}\right) \Big] \\
&\quad - \sum_{\langle i,j\rangle^{\perp}_{\alpha},s} \Big[\left(1 - n_{jys}\, n_{jy\bar{s}}\right) \left(1 - n_{jx\bar{s}}\right) t^{\perp}\, c^{\dagger}_{jxs} c_{ixs} \left(1 - n_{ix\bar{s}}\right) \left(1 - n_{iys}\, n_{iy\bar{s}}\right) \\
&\qquad + \left(1 - n_{jxs}\, n_{jx\bar{s}}\right) \left(1 - n_{jy\bar{s}}\right) t^{\perp}\, c^{\dagger}_{jys} c_{iys} \left(1 - n_{iy\bar{s}}\right) \left(1 - n_{ixs}\, n_{ix\bar{s}}\right) \Big] .
\end{aligned}
\tag{B.121}
$$

2.) $P_1\,\mathrm{H}\,P_0$: This combination of operators projects the half-filled orbitals onto a single double-occupied subspace. No interaction term appears here, because the double-occupied subspace is already projected out by P_0. Thus, we only have hopping from a half-filled site i to a neighboring half-filled site j to make

an orbital double-occupied. The projection then is

$$
\begin{aligned}
&P_1 \,\mathrm{H}\, P_0 = P_1 \,\tilde{\mathrm{T}}\, P_0 \\
&= -P_1 \sum_{\alpha s} \left\{ t^{\parallel} \sum_{\langle i,j\rangle^{\parallel}_{\alpha}} \left(c^{\dagger}_{j\alpha s} c_{i\alpha s} + \mathrm{h.c.} \right) + t^{\perp} \sum_{\langle i,j\rangle^{\perp}_{\alpha}} \left(c^{\dagger}_{j\alpha s} c_{i\alpha s} + \mathrm{h.c.} \right) \right\} P_0 \\
&= - \sum_{\langle i,j\rangle^{\parallel}_{\alpha},s} \Big[\left(1 - n_{jys}\, n_{jy\bar{s}}\right) n_{jx\bar{s}}\; t^{\parallel}\, c^{\dagger}_{jxs} c_{ixs} \left(1 - n_{ix\bar{s}}\right) \left(1 - n_{iys}\, n_{iy\bar{s}}\right) \\
&\qquad + \left(1 - n_{jxs}\, n_{jx\bar{s}}\right) n_{jy\bar{s}}\; t^{\parallel}\, c^{\dagger}_{jys} c_{iys} \left(1 - n_{iy\bar{s}}\right) \left(1 - n_{ixs}\, n_{ix\bar{s}}\right) \Big] \\
&\quad - \sum_{\langle i,j\rangle^{\perp}_{\alpha},s} \Big[\left(1 - n_{jys}\, n_{jy\bar{s}}\right) n_{jx\bar{s}}\; t^{\perp}\, c^{\dagger}_{jxs} c_{ixs} \left(1 - n_{ix\bar{s}}\right) \left(1 - n_{iys}\, n_{iy\bar{s}}\right) \\
&\qquad + \left(1 - n_{jxs}\, n_{jx\bar{s}}\right) n_{jy\bar{s}}\; t^{\perp}\, c^{\dagger}_{jys} c_{iys} \left(1 - n_{iy\bar{s}}\right) \left(1 - n_{ixs}\, n_{ix\bar{s}}\right) \Big] .
\end{aligned}
\tag{B.122}
$$

3.) $P_0 \,\mathrm{H}\, P_1$: For this configuration of projectors, the interaction term is cancelled out by P_0. In this process hopping starts at site i, where one orbital is double-occupied and ends in an empty site j to make this half-filled or singly occupied.

$$
\begin{aligned}
&P_0 \,\mathrm{H}\, P_1 = P_0 \,\tilde{\mathrm{T}}\, P_1 \\
&= -P_0 \sum_{\alpha s} \left\{ t^{\parallel} \sum_{\langle i,j\rangle^{\parallel}} \left(c^{\dagger}_{j\alpha s} c_{i\alpha s} + \mathrm{h.c.} \right) + t^{\perp} \sum_{\langle i,j\rangle^{\perp}} \left(c^{\dagger}_{j\alpha s} c_{i\alpha s} + \mathrm{h.c.} \right) \right\} P_1
\end{aligned}
$$

$$
\begin{aligned}
= - \sum_{\langle i,j\rangle^{\parallel},s} \Big[& (1 - n_{jys}\, n_{jy\bar{s}})\, (1 - n_{jx\bar{s}})\, t^{\parallel}\, c^{\dagger}_{jxs} c_{ixs}\; n_{ix\bar{s}}\, (1 - n_{iys}\, n_{iy\bar{s}}) \\
& + (1 - n_{jxs}\, n_{jx\bar{s}})\, (1 - n_{jy\bar{s}})\, t^{\parallel}\, c^{\dagger}_{jys} c_{iys}\; n_{iy\bar{s}}\, (1 - n_{ixs}\, n_{ix\bar{s}}) \Big] \\
- \sum_{\langle i,j\rangle^{\perp},s} \Big[& (1 - n_{jys}\, n_{jy\bar{s}})\, (1 - n_{jx\bar{s}})\, t^{\perp}\, c^{\dagger}_{jxs} c_{ixs}\; n_{ix\bar{s}}\, (1 - n_{iys}\, n_{iy\bar{s}}) \\
& + (1 - n_{jxs}\, n_{jx\bar{s}})\, (1 - n_{jy\bar{s}})\, t^{\perp}\, c^{\dagger}_{jys} c_{iys}\; n_{iy\bar{s}}\, (1 - n_{ixs}\, n_{ix\bar{s}}) \Big] .
\end{aligned}
\tag{B.123}
$$

4.) $P_1\, \mathrm{H}\, P_1$: With this combination we encounter for the first time the interaction part, since we start in a single double-occupied site i and the process makes the neighboring site j double-occupied for one orbital. The correct form of the projected interaction part will be the task of a later step within the derivation. Here we first concentrate on the hopping mechanism.

$$
\begin{aligned}
& P_1\, \mathrm{H}\, P_1 = P_1\, \tilde{\mathrm{T}}\, P_1 + P_1\, \tilde{\mathrm{V}}\, P_1 \,, \\
& P_1\, \tilde{\mathrm{T}}\, P_1 = \\
& - P_1 \sum_{\alpha s} \Big\{ t^{\parallel} \sum_{\langle i,j\rangle^{\parallel}_{\alpha}} \Big(c^{\dagger}_{j\alpha s} c_{i\alpha s} + \mathrm{h.c.} \Big) + t^{\perp} \sum_{\langle i,j\rangle^{\perp}_{\alpha}} \Big(c^{\dagger}_{j\alpha s} c_{i\alpha s} + \mathrm{h.c.} \Big) \Big\} P_1 \\
& \quad = - \sum_{\langle i,j\rangle^{\parallel}_{\alpha},s} \Big[(1 - n_{jys}\, n_{jy\bar{s}})\, n_{jx\bar{s}}\; t^{\parallel}\, c^{\dagger}_{jxs} c_{ixs}\; n_{ix\bar{s}}\, (1 - n_{iys}\, n_{iy\bar{s}}) \\
& \qquad + (1 - n_{jxs}\, n_{jx\bar{s}})\, n_{jy\bar{s}}\; t^{\parallel}\, c^{\dagger}_{jys} c_{iys}\; n_{iy\bar{s}}\, (1 - n_{ixs}\, n_{ix\bar{s}}) \Big] \\
& \quad - \sum_{\langle i,j\rangle^{\perp}_{\alpha},s} \Big[(1 - n_{jys}\, n_{jy\bar{s}})\, n_{jx\bar{s}}\; t^{\perp}\, c^{\dagger}_{jxs} c_{ixs}\; n_{ix\bar{s}}\, (1 - n_{iys}\, n_{iy\bar{s}}) \\
& \qquad + (1 - n_{jxs}\, n_{jx\bar{s}})\, n_{jy\bar{s}}\; t^{\perp}\, c^{\dagger}_{jys} c_{iys}\; n_{iy\bar{s}}\, (1 - n_{ixs}\, n_{ix\bar{s}}) \Big] ,
\end{aligned}
$$

$$P_1\,\tilde{\mathrm{V}}\,P_1 = P_1 \sum_{\langle j\rangle^{\parallel}} \left[\left\{ U\left(n_{jx\uparrow}\,n_{jx\downarrow} + n_{jy\uparrow}\,n_{jy\downarrow}\right) + \frac{1}{2}\,V\; n_{jx}\,n_{jy} \right\} \right] P_1$$
$$+\, P_1 \sum_{\langle j\rangle^{\perp}} \left[\left\{ U\left(n_{jx\uparrow}\,n_{jx\downarrow} + n_{jy\uparrow}\,n_{jy\downarrow}\right) + \frac{1}{2}\,V\; n_{jx}\,n_{jy} \right\} \right] P_1\,. \tag{B.124}$$

Be aware, for this process the orbital operators ($T^{\pm}_{is}$) as well as the spin operator contribution ($\vec{S}_{i\alpha}\,\vec{S}_{i\beta}$) vanishes in the interaction Hamiltonian.
5.) $P_2\,\mathrm{H}\,P_1$: Here we start at a site i, where one orbital is double-occupied, and one fermion hops into a site j, where already one orbital is double-occupied. For this configuration we also encounter the interaction term.

$$P_2\,\mathrm{H}\,P_1 = P_2\,\tilde{\mathrm{T}}\,P_1 + P_2\,\tilde{\mathrm{V}}\,P_1\,,$$
$$P_2\,\tilde{\mathrm{T}}\,P_1 =$$
$$- P_2 \sum_{\alpha s} \left\{ t^{\parallel} \sum_{\langle i,j\rangle^{\parallel}_{\alpha}} \left(c^{\dagger}_{j\alpha s} c_{i\alpha s} + \mathrm{h.c.} \right) + t^{\perp} \sum_{\langle i,j\rangle^{\perp}_{\alpha}} \left(c^{\dagger}_{j\alpha s} c_{i\alpha s} + \mathrm{h.c.} \right) \right\} P_1$$
$$= - \sum_{\langle i,j\rangle^{\parallel}_{\alpha},s} \Big[n_{jys}\,n_{jy\bar{s}}\,n_{jx\bar{s}}\; t^{\parallel}\, c^{\dagger}_{jxs} c_{ixs}\; n_{ix\bar{s}}\,(1 - n_{iys}\,n_{iy\bar{s}})$$
$$+ n_{jxs}\,n_{jx\bar{s}}\,n_{jy\bar{s}}\; t^{\parallel}\, c^{\dagger}_{jys} c_{iys}\; n_{iy\bar{s}}\,(1 - n_{ixs}\,n_{ix\bar{s}}) \Big]$$
$$- \sum_{\langle i,j\rangle^{\perp}_{\alpha},s} \Big[n_{jys}\,n_{jy\bar{s}}\,n_{jx\bar{s}}\; t^{\perp}\, c^{\dagger}_{jxs} c_{ixs}\; n_{ix\bar{s}}\,(1 - n_{iys}\,n_{iy\bar{s}})$$
$$+ n_{jxs}\,n_{jx\bar{s}}\,n_{jy\bar{s}}\; t^{\perp}\, c^{\dagger}_{jys} c_{iys}\; n_{iy\bar{s}}\,(1 - n_{ixs}\,n_{ix\bar{s}}) \Big]\,,$$
$$P_2\,\tilde{\mathrm{V}}\,P_1 = P_2 \sum_{\langle j\rangle^{\parallel}} \left[\left\{ U\left(n_{jx\uparrow}\,n_{jx\downarrow} + n_{jy\uparrow}\,n_{jy\downarrow}\right) + \frac{1}{2}\,V\; n_{jx}\,n_{jy} \right\} \right] P_1$$
$$+\, P_2 \sum_{\langle j\rangle^{\perp}} \left[\left\{ U\left(n_{jx\uparrow}\,n_{jx\downarrow} + n_{jy\uparrow}\,n_{jy\downarrow}\right) + \frac{1}{2}\,V\; n_{jx}\,n_{jy} \right\} \right] P_1\,. \tag{B.125}$$

6.) $P_1\,\mathrm{H}\,P_2$: For this configuration, we start at a fully filled lattice site i and one fermion hops into a neighboring half-filled site j in order to achieve one

orbital to be occupied by two fermions. Again we encounter the interaction term, which takes on the similar form as before.

$$
\begin{aligned}
&P_1\,\mathrm{H}\,P_2 = P_1\,\tilde{\mathrm{T}}\,P_2 + P_1\,\tilde{\mathrm{V}}\,P_2\,,\\
&P_1\,\tilde{\mathrm{T}}\,P_2 = \\
&-P_1 \sum_{\alpha s}\left\{ t^{\parallel} \sum_{\langle i,j\rangle^{\parallel}_{\alpha}} \left(c^{\dagger}_{j\alpha s} c_{i\alpha s} + \mathrm{h.c.} \right) + t^{\perp} \sum_{\langle i,j\rangle^{\perp}_{\alpha}} \left(c^{\dagger}_{j\alpha s} c_{i\alpha s} + \mathrm{h.c.} \right) \right\} P_2 \\
&\quad = -\sum_{\langle i,j\rangle^{\parallel}_{\alpha},s} \Big[(1 - n_{jys}\, n_{jy\bar{s}})\, n_{jx\bar{s}}\; t^{\parallel}\, c^{\dagger}_{jxs} c_{ixs}\; n_{ix\bar{s}}\, n_{iys}\, n_{iy\bar{s}} \\
&\qquad\quad + (1 - n_{jxs}\, n_{jx\bar{s}})\, n_{jy\bar{s}}\; t^{\parallel}\, c^{\dagger}_{jys} c_{iys}\; n_{iy\bar{s}}\, n_{ixs}\, n_{ix\bar{s}} \Big] \\
&\quad - \sum_{\langle i,j\rangle^{\perp}_{\alpha},s} \Big[(1 - n_{jys}\, n_{jy\bar{s}})\, n_{jx\bar{s}}\; t^{\perp}\, c^{\dagger}_{jxs} c_{ixs}\; n_{ix\bar{s}}\, n_{iys}\, n_{iy\bar{s}} \\
&\qquad\quad + (1 - n_{jxs}\, n_{jx\bar{s}})\, n_{jy\bar{s}}\; t^{\perp}\, c^{\dagger}_{jys} c_{iys}\; n_{iy\bar{s}}\, n_{ixs}\, n_{ix\bar{s}} \Big]\,, \\
&P_1\,\tilde{\mathrm{V}}\,P_2 = P_1 \sum_{\langle j\rangle^{\parallel}} \left[\left\{ U \left(n_{jx\uparrow}\, n_{jx\downarrow} + n_{jy\uparrow}\, n_{jy\downarrow} \right) + \frac{1}{2}\, V\; n_{jx}\, n_{jy} \right\} \right] P_2 \\
&\qquad + P_1 \sum_{\langle j\rangle^{\perp}} \left[\left\{ U \left(n_{jx\uparrow}\, n_{jx\downarrow} + n_{jy\uparrow}\, n_{jy\downarrow} \right) + \frac{1}{2}\, V\; n_{jx}\, n_{jy} \right\} \right] P_2\,.
\end{aligned}
\tag{B.126}
$$

7.) $P_2\,\mathrm{H}\,P_2$: Here we start at a fully filled lattice site i and the hopping process reveals a fully filled neighboring site j.

$$P_2\,\mathrm{H}\,P_2 = P_2\,\tilde{\mathrm{T}}\,P_2 + P_2\,\tilde{\mathrm{V}}\,P_2\,,$$

$$
\begin{aligned}
&P_2\,\tilde{\mathrm{T}}\,P_2 = \\
&-P_2\sum_{\alpha s}\left\{t^{\parallel}\sum_{\langle i,j\rangle^{\parallel}_{\alpha}}\left(c^{\dagger}_{j\alpha s}c_{i\alpha s}+\mathrm{h.c.}\right)+t^{\perp}\sum_{\langle i,j\rangle^{\perp}_{\alpha}}\left(c^{\dagger}_{j\alpha s}c_{i\alpha s}+\mathrm{h.c.}\right)\right\}P_2 \\
&\quad=-\sum_{\langle i,j\rangle^{\parallel}_{\alpha},s}\Big[n_{jys}\,n_{jy\bar{s}}\,n_{jx\bar{s}}\;t^{\parallel}\,c^{\dagger}_{jxs}c_{ixs}\;n_{ix\bar{s}}\,n_{iys}\,n_{iy\bar{s}} \\
&\qquad\quad+n_{jxs}\,n_{jx\bar{s}}\,n_{jy\bar{s}}\;t^{\parallel}\,c^{\dagger}_{jys}c_{iys}\;n_{iy\bar{s}}\,n_{ixs}\,n_{ix\bar{s}}\Big] \\
&\quad-\sum_{\langle i,j\rangle^{\perp}_{\alpha},s}\Big[n_{jys}\,n_{jy\bar{s}}\,n_{jx\bar{s}}\;t^{\perp}\,c^{\dagger}_{jxs}c_{ixs}\;n_{ix\bar{s}}\,n_{iys}\,n_{iy\bar{s}} \\
&\qquad\quad+n_{jxs}\,n_{jx\bar{s}}\,n_{jy\bar{s}}\;t^{\perp}\,c^{\dagger}_{jys}c_{iys}\;n_{iy\bar{s}}\,n_{ixs}\,n_{ix\bar{s}}\Big]\,, \\
&P_2\,\tilde{\mathrm{V}}\,P_2 = P_2\sum_{\langle j\rangle^{\parallel}}\left[\left\{U\left(n_{jx\uparrow}\,n_{jx\downarrow}+n_{jy\uparrow}\,n_{jy\downarrow}\right)+\frac{1}{2}\,V\;n_{jx}\,n_{jy}\right\}\right]P_2 \\
&\quad+P_2\sum_{\langle j\rangle^{\perp}}\left[\left\{U\left(n_{jx\uparrow}\,n_{jx\downarrow}+n_{jy\uparrow}\,n_{jy\downarrow}\right)+\frac{1}{2}\,V\;n_{jx}\,n_{jy}\right\}\right]P_2\,.
\end{aligned}
\tag{B.127}
$$

B.7.2. Two-Site Investigation of Effective Hamiltonian

For the effective Hamiltonian (3.84) we encounter additional coupling mechanisms, compared to the previous spin-1/2 scenario of the original Hamiltonian (B.119). For the two-site model, the effective Hamiltonian reduces to

$$
\mathrm{H}_{SC}=\left[\tilde{J}^{\parallel}\left(\vec{S}_{1x}\cdot\vec{S}_{2x}-\frac{1}{4}\,n_{1x}\,n_{2x}\right)+\tilde{J}^{\perp}\left(\vec{S}_{1y}\cdot\vec{S}_{2y}-\frac{1}{4}\,n_{1y}\,n_{2y}\right)\right]\,,
\tag{B.128}
$$

with the new parameters $\tilde{J}^{\parallel}=4t^{\parallel\,2}/\left(U+V\right)$ and $\tilde{J}^{\perp}=4t^{\perp\,2}/\left(U+V\right)$. To calculate the energies, we introduce the total x- and y-spin operators, namely

$$
\vec{S}_{12\,\alpha}=\vec{S}_{1\alpha}+\vec{S}_{2\alpha}\,,
\tag{B.129}
$$

where α considers the orbital p_x, p_y. Thus, we couple the two spin-1/2 to a spin-1 operator such that the quantum numbers of it are

$$S_{12\,\alpha} = 0, 1 \quad \text{with} \quad m_{S\,12\,\alpha} = 0, \pm 1\,. \tag{B.130}$$

With this, we have to consider a new basis with

$$|\alpha, S_{12\,\alpha}, m_{S\,12\,\alpha}\rangle = A\,|\alpha_1\,\alpha_2\rangle + B\,|\alpha_1\,\alpha_2\rangle\,. \tag{B.131}$$

We can write for the different couplings

$$\begin{aligned}
S_{12\,\alpha} = 0\,: \quad & m_{S\,12\,\alpha} = 0 \quad \Rightarrow \quad |\alpha, 0, 0\rangle = \frac{1}{2}\left(\,|\uparrow\downarrow\rangle - |\downarrow\uparrow\rangle\,\right)\,, \\
S_{12\,\alpha} = 1\,: \quad & m_{S\,12\,\alpha} = 1 \quad \Rightarrow \quad |\alpha, 1, 1\rangle = |\uparrow\uparrow\rangle\,, \\
& m_{S\,12\,\alpha} = 0 \quad \Rightarrow \quad |\alpha, 1, 0\rangle = \frac{1}{2}\left(\,|\uparrow\downarrow\rangle + |\downarrow\uparrow\rangle\,\right)\,, \\
& m_{S\,12\,\alpha} = -1 \quad \Rightarrow \quad |\alpha, 1, -1\rangle = |\downarrow\downarrow\rangle\,,
\end{aligned} \tag{B.132}$$

After the introduction of the spin operator, we can re-express the two-site Hamiltonian as

$$\begin{aligned}
H_{SC} = \tilde{J}^{\parallel} & \left\{\frac{1}{2}\left(S^2_{12\,x} - S^2_{1x} - S^2_{2x}\right) - \frac{1}{4}\,n_{1x}\,n_{2x}\right\} \\
& + \tilde{J}^{\perp}\left\{\frac{1}{2}\left(S^2_{12\,y} - S^2_{1y} - S^2_{2y}\right) - \frac{1}{4}\,n_{1y}\,n_{2y}\right\}\,,
\end{aligned} \tag{B.133}$$

We directly find, that only the spin singlet configuration computes a non-zero energy and thus delivers the lowest energy. Hence, the two-site strong coupling ground state is described by the spin singlet, an antiferromagnet.

B.7.3. Introduction of Spin-1 Operator Representation

To further reduce the representation of the effective Hamiltonian (3.84), we consider a spin-1 scenario. Each lattice site is described by a spin triplet configuration, as given in the initial steps of the strong coupling derivation. The possible spin triplet states $|T_i\rangle$ for a single site are given in equation (3.20). This initial configuration of the lattice sites then suggests to introduce a spin-1 representation. The reduced effective Hamiltonian then should take a form as

$$\mathrm{H}_J \sim \vec{S}_i \cdot \vec{S}_j\,, \tag{B.134}$$

where the spin-1 operators are constructed through

$$\vec{S}_i = \vec{S}_{ix} + \vec{S}_{iy} \quad \text{and} \quad \vec{S}_j = \vec{S}_{jx} + \vec{S}_{jy}\,. \tag{B.135}$$

Coupling these spin operators together reveals for the Hilbert subspaces

$$(\mathcal{H}_1)_i \otimes (\mathcal{H}_1)_j = (\mathcal{H}_0 \oplus \mathcal{H}_1 \oplus \mathcal{H}_2)_{ij}\ , \tag{B.136}$$

and thus

- $S = 2$: quintet, 5 states,
- $S = 1$: triplet, 3 states,
- $S = 0$: singlet, 1 state,

in total 9 possible configurations.

Representation of Spin-1 States

For these different coupling mechanisms (B.136) we refer to the Clebsch-Gordan framework and its coupling table for different angular momenta [69]. In the following we give these states and write them as

$$|S_{total}\,,\, m_{total}\rangle = A\,|m_i\,;\, m_j\rangle + B\,|m_i\,;\, m_j\rangle + C\,|m_i\,;\, m_j\rangle\,, \tag{B.137}$$

on the other hand we know for the initial configuration

$$|\text{site } i\rangle = |S = 1\,,\, m = 0, \pm 1\rangle_i\,, \tag{B.138}$$

which were spin triplets. This is why we only give the m quantum number in equation (B.137) for the individual sites.
We begin by giving the singlet case

$$\begin{aligned} &S = 0, \quad m = 0: \\ &|0,0\rangle = \frac{1}{\sqrt{3}}\Big(|1;-1\rangle - |0;0\rangle + |-1;1\rangle\Big) \\ &\quad = \frac{1}{\sqrt{3}}\Bigg[|x\uparrow y\uparrow; x\downarrow y\downarrow\rangle - \frac{1}{2}\Big(|x\uparrow y\downarrow; x\uparrow y\downarrow\rangle + |x\uparrow y\downarrow; x\downarrow y\uparrow\rangle \\ &\qquad + |x\downarrow y\uparrow; x\uparrow y\downarrow\rangle + |x\downarrow y\uparrow; x\downarrow y\uparrow\rangle\Big) + |x\downarrow y\downarrow; x\uparrow y\uparrow\rangle\Bigg]\,, \end{aligned} \tag{B.139}$$

where we write the different configurations within the individual orbitals and sites in the second and third row.
The triplet case is

$$
\begin{aligned}
&S=1, \quad m=1: \\
&|1,1\rangle = \frac{1}{\sqrt{2}}\Big(|1\,;\,0\rangle - |0\,;\,1\rangle\Big) \\
&\qquad = \frac{1}{2}\Big[|x\uparrow y\uparrow; x\uparrow y\downarrow\rangle + |x\uparrow y\uparrow; x\downarrow y\uparrow\rangle \\
&\qquad\qquad - |x\uparrow y\downarrow; x\uparrow y\uparrow\rangle - |x\downarrow y\uparrow; x\uparrow y\uparrow\rangle\Big]\,, \\
&S=1, \quad m=0: \\
&|1,0\rangle = \frac{1}{\sqrt{2}}\Big(|1\,;\,-1\rangle - |-1\,;\,1\rangle\Big) \\
&\qquad = \frac{1}{\sqrt{2}}\left(|x\uparrow y\uparrow; x\downarrow y\downarrow\rangle - |x\downarrow y\downarrow; x\uparrow y\uparrow\rangle\right)\,, \\
&S=1, \quad m=-1: \\
&|1;-1\rangle = \frac{1}{\sqrt{2}}\Big(|0\,;\,-1\rangle - |-1\,;\,0\rangle\Big) \\
&\qquad = \frac{1}{2}\Big[|x\uparrow y\downarrow; x\downarrow y\downarrow\rangle + |x\downarrow y\uparrow; x\downarrow y\downarrow\rangle \\
&\qquad\qquad - |x\downarrow y\downarrow; x\uparrow y\downarrow\rangle - |x\downarrow y\downarrow; x\downarrow y\uparrow\rangle\Big]\,.
\end{aligned}
\tag{B.140}
$$

As the last step we give the quintet states

$$
\begin{aligned}
&S=2, \quad m=2: \\
&|2,2\rangle = |1\,;\,1\rangle = |x\uparrow y\uparrow; x\uparrow y\uparrow\rangle \\
&S=2, \quad m=1: \\
&|2,1\rangle = \frac{1}{\sqrt{2}}\Big(|1\,;\,0\rangle + |0\,;\,1\rangle\Big) \\
&\qquad = \frac{1}{2}\Big[|x\uparrow y\uparrow; x\uparrow y\downarrow\rangle + |x\uparrow y\uparrow; x\downarrow y\uparrow\rangle \\
&\qquad\qquad + |x\uparrow y\downarrow; x\uparrow y\uparrow\rangle + |x\downarrow y\uparrow; x\uparrow y\uparrow\rangle\Big] \\
&S=2, \quad m=0: \\
&|2,0\rangle = \frac{1}{\sqrt{6}}\,|1\,;\,-1\rangle + \sqrt{\frac{2}{3}}\,|0\,;\,0\rangle + \frac{1}{\sqrt{6}}\,|-1\,;\,1\rangle \\
&\qquad = \frac{1}{\sqrt{6}}\Big[|x\uparrow y\uparrow; x\downarrow y\downarrow\rangle + |x\uparrow y\downarrow; x\uparrow y\downarrow\rangle + |x\uparrow y\downarrow; x\downarrow y\uparrow\rangle \\
&\qquad\qquad + |x\downarrow y\uparrow; x\uparrow y\downarrow\rangle + |x\downarrow y\uparrow; x\downarrow y\uparrow\rangle + |x\downarrow y\downarrow; x\uparrow y\uparrow\rangle\Big] \\
&S=2, \quad m=-1: \\
&|2,-1\rangle = \frac{1}{\sqrt{2}}\Big(|0\,;\,-1\rangle + |-1\,;\,0\rangle\Big) \\
&\qquad = \frac{1}{2}\Big[|x\uparrow y\downarrow; x\downarrow y\downarrow\rangle + |x\downarrow y\uparrow; x\downarrow y\downarrow\rangle \\
&\qquad\qquad + |x\downarrow y\downarrow; x\uparrow y\downarrow\rangle + |x\downarrow y\downarrow; x\downarrow y\uparrow\rangle\Big] \\
&S=2, \quad m=2: \\
&|2,2\rangle = |-1\,;\,-1\rangle = |x\downarrow y\downarrow; x\downarrow y\downarrow\rangle\,.
\end{aligned}
\tag{B.141}
$$

Reduction of Effective Hamiltonian

After giving all possible states for the coupling of spins and their representations, we focus on the reduction of the effective Hamiltonian. As the first step, we consider the application of the spin operators $S^{\pm}_{i\alpha} = S^{x}_{i\alpha} \pm S^{y}_{i\alpha}, S^{z}_{i\alpha}$ onto the

pre-coupled states $|S\,,\,m\rangle_i$ (B.138). The next step is then to find a translation of the spin operators $S_{i\alpha}$ towards the spin-1 operators.
From basic quantum mechanics [69, 72, 121, 229] we know

$$\begin{aligned} S^z_{i\alpha}\,|S\,,\,m\rangle_i &= m\,|S\,,\,m\rangle_i \\ \langle j_1\,j_2\,m_1\,m_2|J^{\pm}|j_1\,j_2\,J\,m\rangle &= \sqrt{J\,(J+1)-m\,(m\pm 1)} \\ &\quad\times\langle j_1\,j_2\,m_1\,m_2|j_1\,j_2\,j\,m\pm 1\rangle\,, \end{aligned} \tag{B.142}$$

where we give the relation and action of the raising and lowering spin operator for a general angular momentum operator, in addition $J^{\pm}=J^{\pm}_1+J^{\pm}_2$.
We then calculate

$$\begin{aligned} \langle m'_i|S^+_{i\alpha}|m_i\rangle &= \begin{pmatrix}\langle 1|\\ \langle 0|\\ \langle -1|\end{pmatrix}\begin{pmatrix}0 & 1/\sqrt{2} & 0\\ 0 & 0 & 1/\sqrt{2}\\ 0 & 0 & 0\end{pmatrix}\begin{pmatrix}|1\rangle\\ |0\rangle\\ |-1\rangle\end{pmatrix}\,, \\ \langle m'_i|S^-_{i\alpha}|m_i\rangle &= \begin{pmatrix}\langle 1|\\ \langle 0|\\ \langle -1|\end{pmatrix}\begin{pmatrix}0 & 0 & 0\\ 1/\sqrt{2} & 0 & 0\\ 0 & 1/\sqrt{2} & 0\end{pmatrix}\begin{pmatrix}|1\rangle\\ |0\rangle\\ |-1\rangle\end{pmatrix}\,, \\ \langle m'_i|S^z_{i\alpha}|m_i\rangle &= \begin{pmatrix}\langle 1|\\ \langle 0|\\ \langle -1|\end{pmatrix}\begin{pmatrix}1/2 & 0 & 0\\ 0 & 0 & 0\\ 0 & 0 & -1/2\end{pmatrix}\begin{pmatrix}|1\rangle\\ |0\rangle\\ |-1\rangle\end{pmatrix}\,. \end{aligned} \tag{B.143}$$

Note, the initial – pre-coupled – states on every lattice site i are spin triplets, as given in equation (3.20). The additional configurations of states follow after the coupling of $(\mathcal{H}_1)_i\otimes(\mathcal{H}_1)_j$.
Next, we determine the actions of the newly introduced spin-1 operators of

equation (B.135) for the pre-coupled states $|S\,,\,m\rangle_i$. We compute

$$\begin{aligned}
\langle m_i'|S_i^+|m_i\rangle &= \begin{pmatrix} \langle 1| \\ \langle 0| \\ \langle -1| \end{pmatrix} \begin{pmatrix} 0 & \sqrt{2} & 0 \\ 0 & 0 & \sqrt{2} \\ 0 & 0 & 0 \end{pmatrix} \begin{pmatrix} |1\rangle \\ |0\rangle \\ |-1\rangle \end{pmatrix} , \\
\langle m_i'|S_i^-|m_i\rangle &= \begin{pmatrix} \langle 1| \\ \langle 0| \\ \langle -1| \end{pmatrix} \begin{pmatrix} 0 & 0 & 0 \\ \sqrt{2} & 0 & 0 \\ 0 & \sqrt{2} & 0 \end{pmatrix} \begin{pmatrix} |1\rangle \\ |0\rangle \\ |-1\rangle \end{pmatrix} , \\
\langle m_i'|S_i^z|m_i\rangle &= \begin{pmatrix} \langle 1| \\ \langle 0| \\ \langle -1| \end{pmatrix} \begin{pmatrix} 1 & 0 & 0 \\ 0 & 0 & 0 \\ 0 & 0 & -1 \end{pmatrix} \begin{pmatrix} |1\rangle \\ |0\rangle \\ |-1\rangle \end{pmatrix} .
\end{aligned} \tag{B.144}$$

Now we compare the results of equation (B.143) and equation (B.144) closely, in order to find the translation from the spin operators $S_{i\alpha}^{\pm\,,z}$ towards the new spin-1 operators $S_i^{\pm\,,z}$ as

$$\begin{aligned}
&S_{i\alpha}^{\pm} \;\rightarrow\; \frac{1}{2}\,S_i^{\pm} \quad \text{and} \quad S_{i\alpha}^{z} \;\rightarrow\; S_i^{z} \\
&\Rightarrow\; \vec{S}_{i\alpha} \;\rightarrow\; \frac{1}{2}\,\vec{S}_i\,,
\end{aligned} \tag{B.145}$$

for our half-filled strong coupling scenario. In addition we can translate the particle number operators to $n_{i\alpha} \rightarrow n_i/2$.
Then we are able to evaluate the translation for the effective Hamiltonian

$$\begin{aligned}
\mathrm{H}_{SC} = \sum_{\alpha} \Bigg[& J^{\parallel} \sum_{\langle i,j\rangle_{\alpha}^{\parallel}} \Big(\vec{S}_{i\alpha} \cdot \vec{S}_{j\alpha} - \frac{1}{4}\, n_{i\alpha} n_{j\alpha} \Big) \\
& + J^{\perp} \sum_{\langle i,j\rangle_{\alpha}^{\perp}} \Big(\vec{S}_{i\alpha} \cdot \vec{S}_{j\alpha} - \frac{1}{4}\, n_{i\alpha} n_{j\alpha} \Big) \Bigg] ,
\end{aligned} \tag{B.146}$$

into the spin-1 representation and directly obtain

$$\mathrm{H}_J = \frac{1}{4} \Big(J^{\parallel} + J^{\perp} \Big) \sum_{\langle i,j\rangle} \Big(\vec{S}_i \cdot \vec{S}_j - \frac{1}{4} n_i n_j \Big) \,. \tag{B.147}$$

Be aware, now the summation runs over all lattice sites i as well as every neighboring site j regardless of the previously restricted directions indicated

through $\langle i,j\rangle_{\alpha}^{\parallel,\perp}$. The reduced effective Hamiltonian H_J is again of the well-known Heisenberg form and has the desired spin operator contribution of $\vec{S}_i \cdot \vec{S}_j$. The new ground state is again an antiferromagnetic configuration, as we can calculate through the different coupled states $|S=0,\,1,\,2\rangle_{ij}$ with

$$\begin{aligned} &\vec{S}_i \cdot \vec{S}_j = \frac{1}{2}\left(S_{ij}^2 - S_i^2 - S_j^2\right) , \\ &\Rightarrow \mathrm{H}_J = \frac{1}{8}\left(J^{\parallel} + J^{\perp}\right) \sum_{\langle i,j\rangle} \left(S_{ij}^2 - S_i^2 - S_j^2 - \frac{1}{2} n_i n_j\right) . \end{aligned} \tag{B.148}$$

For our half-filled strong coupling case with the initial spin triplet configuration we know

$$n_i \,|S=1\,,\, m\rangle_i = 2\,|S=1\,,m\rangle_i \,, \tag{B.149}$$

and $S_{i,j}=1$. The Hamiltonian H_J can be reduced to

$$\mathrm{H}_J = \frac{1}{8}\left(J^{\parallel} + J^{\perp}\right) \sum_{\langle i,j\rangle} \left(S_{ij}^2 - 6\right) , \tag{B.150}$$

where we find the lowest energy for the Hamiltonian for the singlet configuration. Hence, the ground state is ordered in an antiferromagnet, to maximize the virtual hopping processes, as illustrated in the example in fig. 3.15.

APPENDIX

THREE

SUPPLEMENTARY MATERIAL TO MAJORANA MODES

C.1. Analysis Possible Processes

We present in detail the relevant processes given in section 4.2.4 of the derivation of the effective Hamiltonian. The individual processes refer to fig. 4.6.

a) i: $|n\rangle$: empty, $E_n = 0$, $|m\rangle$: s-wave fermion, $E_m = \delta_a$,
$|n'\rangle$: empty, $E_{n'} = 0$

$$\mathrm{H}_{a)i} = \frac{2|w_a|^2}{\delta_a} \sum_p A_p A_p^\dagger \,, \tag{C.1}$$

as discussed in detail in section 4.2.4.

For sake of readability and convenience, we will only give the relevant contribution to the total Hamiltonian for the given configuration.

a) ii: $|n\rangle$: empty, $E_n = 0$, $|m\rangle$: p_α-wave fermion, $E_m = \delta_b$,
$|n'\rangle$: empty, $E_{n'} = 0$

$$\mathrm{H}_{a)ii} = \frac{2\,|w_b|^2}{\delta_b} \sum_{\alpha,p} B_{\alpha p} B_{\alpha p}^\dagger \,. \tag{C.2}$$

After these scenarios – where the final state remains empty – we consider the cases where the initial state is empty and the final state is occupied with a molecule.

b) i: $|n\rangle$: empty, $E_n = 0$, $|m\rangle$: s-wave fermion, $E_m = \delta_a$,
$|n'\rangle$: p_α-molecule, $E_{n'} = U + \delta_a + \delta_b$

$$\mathrm{H}_{b)i} = w_b w_a \sum_{\alpha,p} B^\dagger_{\alpha p} A^\dagger_p \left(\frac{1}{\delta_a} - \frac{1}{U + \delta_b} \right) . \tag{C.3}$$

b) ii: $|n\rangle$: empty, $E_n = 0$, $|m\rangle$: p_α-wave fermion, $E_m = \delta_b$,
$|n'\rangle$: p_α-molecule, $E_{n'} = U + \delta_a + \delta_b$

$$\mathrm{H}_{b)ii} = w_a w_b \sum_{\alpha,p} A^\dagger_p B^\dagger_{\alpha p} \left(\frac{1}{\delta_b} - \frac{1}{U + \delta_a} \right) . \tag{C.4}$$

b): With $\left[A^\dagger_p,\, B^\dagger_{\alpha p} \right] = 0$, we can sum eq. (C.3) and eq. (C.4) and compute for the condition $\delta_b = -\delta_a$

$$\mathrm{H}_{b)} = -\frac{2 w_a w_b U}{U^2 - \delta_a^2} \sum_{\alpha,p} B^\dagger_{\alpha p} A^\dagger_p . \tag{C.5}$$

Next we investigate the scenarios, where the initial state is occupied by a molecule, but the final state is empty.

c) i: $|n\rangle$: p_α-molecule, $E_n = U + \delta_a + \delta_b$,
$|m\rangle$: s-wave fermion, $E_m = \delta_a$, $|n'\rangle$: empty, $E_{n'} = 0$

$$\mathrm{H}_{c)i} = w_a w_b \sum_{\alpha,p} A_p B_{\alpha p} \left(\frac{1}{\delta_a} - \frac{1}{U + \delta_b} \right) . \tag{C.6}$$

c) ii: $|n\rangle$: p_α-molecule, $E_n = U + \delta_a + \delta_b$,
$|m\rangle$: p_α-wave fermion, $E_m = \delta_b$, $|n'\rangle$: empty, $E_{n'} = 0$

$$\mathrm{H}_{c)ii} = w_a w_b \sum_{\alpha,p} B_{\alpha p} A_p \left(\frac{1}{\delta_b} - \frac{1}{U + \delta_a} \right) . \tag{C.7}$$

c): We again combine eq. (C.6) and eq. (C.5) and use $\delta_b = -\delta_a$, to find

$$\mathrm{H}_{c)} = -\frac{2U w_a w_b}{U^2 - \delta_a^2} \sum_{\alpha,p} A_p B_{\alpha p} \,. \tag{C.8}$$

The process in fig. 4.6d) is again a hopping process of fermions on the lattice sites and thus covered in the contributions of **a)** above. Now we turn our attention the the processes where the initial state is occupied by a molecule and the final state is again a molecule.

e) i: $|n\rangle$: p_α-molecule, $E_n = U + \delta_a + \delta_b$,
$|m\rangle$: p_α-wave fermion, $E_m = \delta_b$,
$|n'\rangle$: p_α-molecule, $E_{n'} = U + \delta_a + \delta_b$

$$\mathrm{H}_{e)i} = -\frac{2|w_a|^2}{U + \delta_a} \sum_{p} A_p^\dagger A_p \,. \tag{C.9}$$

e) ii: $|n\rangle$: p_α-molecule, $E_n = U + \delta_a + \delta_b$,
$|m\rangle$: s-wave fermion, $E_m = \delta_a$,
$|n'\rangle$: p_α-molecule, $E_{n'} = U + \delta_a + \delta_b$

$$\mathrm{H}_{e)ii} = -\frac{2|w_b|^2}{U + \delta_b} \sum_{\alpha,p} B_{\alpha p}^\dagger B_{\alpha p} \,. \tag{C.10}$$

f): $|n\rangle$: p_α-molecule, $E_n = U + \delta_a + \delta_b$,
$|m\rangle$: s-wave fermion, $E_m = \delta_a$,
$|n'\rangle$: $p_{\alpha'}$-molecule, $E_{n'} = U + \delta_a + \delta_b$

$$\mathrm{H}_{f)} = -\frac{2|w_b|^2}{U + \delta_b} \sum_{\alpha,\alpha',p,\alpha\neq\alpha'} B_{\alpha' p}^\dagger B_{\alpha p} \,. \tag{C.11}$$

For sake of completeness, we investigate row 4 of the Hamiltonian (4.33) for the general case, in addition also the operator configuration $B_{\alpha p} B_{\alpha' p}^\dagger$, for $\alpha \neq \alpha'$. The Hamiltonian of interest reads

$$\mathrm{H}_3 = w_a w_b \sum_{\alpha,p} \left(\underbrace{A_p^\dagger B_{\alpha p}}_{\beta} + \underbrace{B_{\alpha p} A^\dagger}_{\epsilon} + \underbrace{A_p B_{\alpha p}^\dagger}_{\chi} + \underbrace{B_{\alpha p}^\dagger A_p}_{\xi} \right) \,. \tag{C.12}$$

Parts β and ξ require one corresponding fermion to be in a state of the plaquette in order to be able to act. Since the energy penalty for one fermion is high, the system will not be in a state, with one fermion on a plaquette as the ground state. Hence, these parts drop out, based on energy scale reasoning. In addition, we give the calculations for these cases

$\boldsymbol{\beta}$: $E_n = \delta_b$, $E_m = 0$, $E_{n'} = \delta_a$

$$\mathrm{H}_\beta = -w_a w_b \sum_{\alpha,p} A_p^\dagger B_{\alpha p} \left(\frac{1}{\delta_b} + \frac{1}{\delta_a} \right) = 0 \,, \text{ since } \delta_b = -\delta_a \,. \tag{C.13}$$

$\boldsymbol{\xi}$: $E_n = \delta_a$, $E_m = 0$, $E_{n'} = \delta_b$

$$\mathrm{H}_\xi = -w_a w_b \sum_{\alpha,p} B_{\alpha p}^\dagger A_p \left(\frac{1}{\delta_a} + \frac{1}{\delta_b} \right) = 0 \,. \tag{C.14}$$

The fermions do not change their symmetry while being in a state on the plaquette. Thus, parts ϵ and χ also drop out. These parts require a change of symmetry from s-wave to p_α-wave and vice versa. We present the calculations for both cases

$\boldsymbol{\epsilon}$: We have to have a fermion in a state on the plaquette, namely p_α-wave fermion, in order to avoid divergence within the energy term. Then $E_n = \delta_b$, $E_m = U + \delta_a + \delta_b$, $E_{n'} = \delta_a$

$$\mathrm{H}_\epsilon = w_a w_b \sum_{\alpha,p} B_{\alpha p} A_p^\dagger \left(\frac{1}{U + \delta_a} + \frac{1}{U + \delta_b} \right) \,, \tag{C.15}$$

since no interaction term can be present, this reduces to

$$\mathrm{H}_\epsilon = w_a w_b \sum_{\alpha,p} B_{\alpha p} A_p^\dagger \left(\frac{1}{\delta_a} + \frac{1}{\delta_b} \right) = 0 \,. \tag{C.16}$$

$\boldsymbol{\chi}$: Here we also have to have an initial state with an s-wave fermion on the plaquette to avoid divergence.

$E_n = \delta_a$, $E_m = U + \delta_a + \delta_b$, $E_{n'} = \delta_b$

$$\begin{aligned} \mathrm{H}_\chi &= w_a w_b \sum_{\alpha,p} A_p B^\dagger_{\alpha p} \left(\frac{1}{U+\delta_b} + \frac{1}{U+\delta_a} \right) \text{ since } U = 0 \\ &= w_a w_b \sum_{\alpha,p} A_p B^\dagger_{\alpha p} \left(\frac{1}{\delta_b} + \frac{1}{\delta_a} \right) = 0\,. \end{aligned} \tag{C.17}$$

The symmetry change reason also holds for the last term, $B_{\alpha p} B^\dagger_{\alpha' p}$, $\alpha \neq \alpha'$. A p_α-wave fermion does not change symmetry to $p_{\alpha'}$-wave by its own, only through a rotation by $\pi/4$. Therefore this term drops out too.

C.2. Transformed Hamiltonian

Here we give the full transformed Hamiltonian of the p-wave section, with all operators inserted. The Hamiltonian then reads

$$\begin{aligned} \mathrm{H}_T = \mathrm{H}_0 - \sum_p \Bigg\{ & \frac{|w_a|^2}{\delta_a} \left(A_p A^\dagger_p - \overline{A}_p \overline{A}^\dagger_p - \sum_\alpha \left(B_{\alpha p} B^\dagger_{\alpha p} - \overline{B}_{\alpha p} \overline{B}^\dagger_{\alpha p} \right) \right) \\ & - \frac{U|w_a|^2}{U^2 - \delta_a^2} \sum_\alpha \left(B^\dagger_{\alpha p} A^\dagger_p - \overline{B}^\dagger_{\alpha p} \overline{A}^\dagger_p + A_p B_{\alpha p} - \overline{A}_p \overline{B}_{\alpha p} \right) \\ & - \frac{|w_a|^2}{U+\delta_a} \left(A^\dagger_p A_p - \overline{A}^\dagger_p \overline{A}_p \right) - \frac{|w_a|^2}{U-\delta_a} \sum_{\alpha',\alpha} \left(B^\dagger_{\alpha' p} B_{\alpha p} - \overline{B}^\dagger_{\alpha' p} \overline{B}_{\alpha p} \right) \Bigg\}, \end{aligned}$$

with

$$\mathrm{H}_0 = \delta_a \sum_p a^\dagger_p a_p + \delta_b \sum_{\alpha,p} b^\dagger_{\alpha p} b_{\alpha p} + U \sum_{\alpha,p} b^\dagger_{\alpha p} b_{\alpha p}\, a^\dagger_p a_p\,.$$

Then

$$
\begin{aligned}
\mathrm{H}_T = \mathrm{H}_0 + \sum_p \Bigg\{ \quad & -\tfrac{2|w_a|^2}{\delta_a} \quad \Big[a_p a_p^\dagger \big(c_1^\dagger c_2 + c_1^\dagger c_4 + c_2^\dagger c_1 + c_2^\dagger c_3 \\
& \qquad\qquad + c_3^\dagger c_2 + c_3^\dagger c_4 + c_4^\dagger c_1 + c_4^\dagger c_3 \big) \\
& \quad - b_{xp} b_{xp}^\dagger \big(c_1^\dagger c_2 - c_1^\dagger c_4 + c_2^\dagger c_1 - c_2^\dagger c_3 \\
& \qquad\qquad - c_3^\dagger c_2 + c_3^\dagger c_4 - c_4^\dagger c_1 + c_4^\dagger c_3 \big) \\
& \quad - b_{yp} b_{yp}^\dagger \big(- c_1^\dagger c_2 + c_1^\dagger c_4 - c_2^\dagger c_1 + c_2^\dagger c_3 \\
& \qquad\qquad + c_3^\dagger c_2 - c_3^\dagger c_4 + c_4^\dagger c_1 - c_4^\dagger c_3 \big) \Big] \\
& + \tfrac{4U|w_a|^2}{U^2 - \delta_a^2} \quad \Big[X_p^\dagger \left(c_2 c_3 - c_4 c_1 \right) + X_p \left(c_3^\dagger c_2^\dagger - c_1^\dagger c_4^\dagger \right) \\
& \quad + Y_p^\dagger \left(c_1 c_2 - c_3 c_4 \right) + Y_p \left(c_2^\dagger c_1^\dagger - c_4^\dagger c_3^\dagger \right) \Big] \\
& + \tfrac{2|w_a|^2}{U + \delta_a} \quad \Big[a_p^\dagger a_p \big(c_1 c_2^\dagger + c_1 c_4^\dagger + c_2 c_1^\dagger + c_2 c_3^\dagger \\
& \qquad\qquad + c_3 c_2^\dagger + c_3 c_4^\dagger + c_4 c_1^\dagger + c_4 c_3^\dagger \big) \Big] \\
& + \tfrac{2|w_a|^2}{U - \delta_a} \quad \Big[b_{xp}^\dagger b_{xp} \big(c_1 c_2^\dagger - c_1 c_4^\dagger + c_2 c_1^\dagger - c_2 c_3^\dagger \\
& \qquad\qquad - c_3 c_2^\dagger + c_3 c_4^\dagger - c_4 c_1^\dagger + c_4 c_3^\dagger \big) \\
& \quad + b_{yp}^\dagger b_{yp} \big(- c_1 c_2^\dagger + c_1 c_4^\dagger - c_2 c_1^\dagger + c_2 c_3^\dagger \\
& \qquad\qquad + c_3 c_2^\dagger - c_3 c_4^\dagger + c_4 c_1^\dagger - c_4 c_3^\dagger \big) \\
& \quad + b_{xp}^\dagger b_{yp} \big(- c_1 c_2^\dagger + c_1 c_4^\dagger + c_2 c_1^\dagger - c_2 c_3^\dagger \\
& \qquad\qquad + c_3 c_2^\dagger - c_3 c_4^\dagger - c_4 c_1^\dagger + c_4 c_3^\dagger \big) \\
& \quad + b_{yp}^\dagger b_{xp} \big(c_1 c_2^\dagger - c_1 c_4^\dagger - c_2 c_1^\dagger + c_2 c_3^\dagger \\
& \qquad\qquad - c_3 c_2^\dagger + c_3 c_4^\dagger + c_4 c_1^\dagger - c_4 c_3^\dagger \big) \Big] \Bigg\} .
\end{aligned}
$$

BIBLIOGRAPHY

[1] H. Bethe. "Zur Theorie der Metalle". German. In: *Zeitschrift für Physik* 71.3-4 (1931), pp. 205–226. DOI: 10.1007/BF01341708 (cit. on p. 1).

[2] F. Bloch. "Über die Quantenmechanik der Elektronen in Kristallgittern". German. In: *Zeitschrift für Physik* 52.7-8 (1929), pp. 555–600. DOI: 10.1007/BF01339455 (cit. on p. 1).

[3] F. Bloch. "Bemerkung zur Elektronentheorie des Ferromagnetismus und der elektrischen Leitfähigkeit". German. In: *Zeitschrift für Physik* 57.7-8 (1929), pp. 545–555. DOI: 10.1007/BF01340281 (cit. on p. 1).

[4] F. Bloch. "Zur Theorie des Ferromagnetismus". German. In: *Zeitschrift für Physik* 61.3-4 (1930), pp. 206–219. DOI: 10.1007/BF01339661 (cit. on p. 1).

[5] E. Teller. "Bemerkung zur Theorie des Ferromagnetismus". German. In: *Zeitschrift für Physik* 62.1-2 (1930), pp. 102–105. DOI: 10.1007/BF01340408 (cit. on p. 1).

[6] E. C. Stoner. "LXXX. Atomic moments in ferromagnetic metals and alloys with non-ferromagnetic elements". In: *The London, Edinburgh, and Dublin Philosophical Magazine and Journal of Science* 15.101 (1933), pp. 1018–1034. DOI: 10.1080/14786443309462241 (cit. on pp. 1, 30).

[7] F. Bloch. "Zur Theorie des Austauschproblems und der Remanenzerscheinung der Ferromagnetika". German. In: *Zeitschrift für Physik* 74.5-6 (1932), pp. 295–335. DOI: 10.1007/BF01337791 (cit. on p. 1).

[8] C. Møller. "Zur Theorie des Austauschproblems und des Ferromagnetismus bei tiefen Temperaturen". German. In: *Zeitschrift für Physik* 82.9-10 (1933), pp. 559–567. DOI: 10.1007/BF01338329 (cit. on p. 1).

[9] L. Landau. "Diamagnetismus der Metalle". German. In: *Zeitschrift für Physik* 64.9-10 (1930), pp. 629–637. DOI: 10.1007/BF01397213 (cit. on p. 1).

[10] T. Nagamiya, K. Yosida, and R. Kubo. "Antiferromagnetism". In: *Advances in Physics* 4.13 (1955), pp. 1–112. DOI: 10 . 1080 / 00018735500101154 (cit. on p. 1).

[11] G. H. Wannier. "Antiferromagnetism. The Triangular Ising Net". In: *Phys. Rev.* 79 (2 1950), pp. 357–364. DOI: 10.1103/PhysRev.79.357 (cit. on p. 1).

[12] J. C. Slater and G. F. Koster. "Simplified LCAO Method for the Periodic Potential Problem". In: *Phys. Rev.* 94.6 (1954), pp. 1498–1524. DOI: 10.1103/PhysRev.94.1498 (cit. on p. 1).

[13] J. B. Goodenough. "Theory of the Role of Covalence in the Perovskite-Type Manganites $[La,\ M(II)]MnO_3$". In: *Phys. Rev.* 100.2 (1955), pp. 564–573. DOI: 10.1103/PhysRev.100.564 (cit. on p. 1).

[14] E. Lieb and D. Mattis. "Theory of Ferromagnetism and the Ordering of Electronic Energy Levels". In: *Phys. Rev.* 125 (1 1962), pp. 164–172. DOI: 10.1103/PhysRev.125.164 (cit. on p. 1).

[15] P. W. Anderson. "Antiferromagnetism. Theory of Superexchange Interaction". In: *Phys. Rev.* 79 (2 1950), pp. 350–356. DOI: 10.1103/PhysRev.79.350 (cit. on p. 1).

[16] P. W. Anderson. "New Approach to the Theory of Superexchange Interactions". In: *Phys. Rev.* 115.1 (1959), p. 2. DOI: 10.1103/PhysRev.115.2 (cit. on p. 1).

[17] W. S. Fyfe and V. J. "Covalent Super-Exchange in Solid State Physics". In: *Nature* 187 (4743 1960), pp. 1108–1108. DOI: 10.1038/1871108a0 (cit. on p. 1).

[18] J. Hubbard. "Electron Correlations in Narrow Energy Bands". In: *Proceedings of the Royal Society of London A: Mathematical, Physical and Engineering Sciences* 276.1365 (1963), pp. 238–257. DOI: 10.1098/rspa.1963.0204 (cit. on pp. 1, 8, 9, 27).

[19] M. Imada, A. Fujimori, and Y. Tokura. "Metal-insulator transitions". In: *Rev. Mod. Phys.* 70.4 (1998), pp. 1039–1263. DOI: 10.1103/RevModPhys.70.1039 (cit. on pp. 1, 8, 9).

[20] G. Khaliullin and S. Okamoto. "Quantum Behavior of Orbitals in Ferromagnetic Titanates: Novel Orderings and Excitations". In: *Phys. Rev. Lett.* 89.16 (2002), p. 167201. DOI: 10.1103/PhysRevLett.89.167201 (cit. on p. 1).

[21] J. Chaloupka, G. Jackeli, and G. Khaliullin. "Kitaev-Heisenberg Model on a Honeycomb Lattice: Possible Exotic Phases in Iridium Oxides $A2IrO3$". In: *Phys. Rev. Lett.* 105.2 (2010), p. 027204. DOI: 10.1103/PhysRevLett.105.027204 (cit. on p. 1).

[22] S. Sachdev. "Quantum magnetism and criticality". In: *Nat. Phys.* 4.3 (2008), pp. 1745–2473. DOI: 10.1038/nphys894 (cit. on pp. 1, 9).

[23] S. Sachdev and B. Keimer. "Quantum criticality". In: *Physics Today* 64.2 (2011), pp. 29–35. DOI: http://dx.doi.org/10.1063/1.3554314 (cit. on pp. 1, 9).

[24] J. Bardeen, L. N. Cooper, and J. R. Schrieffer. "Theory of Superconductivity". In: *Phys. Rev.* 108 (5 1957), pp. 1175–1204. DOI: 10.1103/PhysRev.108.1175 (cit. on pp. 1, 75).

[25] J. G. Bednorz and K. A. Müller. "Possible high T_c superconductivity in the $Ba-La-Cu-O$ system". In: *Zeitschrift für Physik B - Condensed Matter* 64 (2 1986). DOI: 10.1007/BF01303701 (cit. on p. 1).

[26] B. Keimer, S. A. Kivelson, M. R. Norman, S. Uchida, and J. Zaanen. "From quantum matter to high-temperature superconductivity in copper oxides". In: *Nature* 518 (7538 2015), pp. 179–186. DOI: 10.1038/nature14165 (cit. on p. 1).

[27] D. Jaksch, C. Bruder, J. I. Cirac, C. W. Gardiner, and P. Zoller. "Cold Bosonic Atoms in Optical Lattices". In: *Phys. Rev. Lett.* 81.15 (1998), pp. 3108–3111. DOI: 10.1103/PhysRevLett.81.3108 (cit. on pp. 1, 8, 9, 27).

[28] D. Jaksch and P. Zoller. "The cold atom Hubbard toolbox". In: *Annals of Physics* 315.1 (2005). Special Issue, pp. 52 –79. DOI: http://dx.doi.org/10.1016/j.aop.2004.09.010 (cit. on pp. 1, 9).

[29] M. Greiner, O. Mandel, T. Esslinger, T. W. Hänsch, and I. Bloch. "Quantum phase transition from a superfluid to a Mott insulator in a gas of ultracold atoms". In: *Nature* 415.6867 (2002), pp. 39–33. DOI: 10.1038/415039a (cit. on pp. 1, 9).

[30] I. Bloch, J. Dalibard, and W. Zwerger. "Many-body physics with ultracold gases". In: *Rev. Mod. Phys.* 80.3 (2008), pp. 885–964. DOI: 10.1103/RevModPhys.80.885 (cit. on pp. 2, 5, 6, 9, 78, 82, 113, 114).

[31] W. Hofstetter, J. I. Cirac, P. Zoller, E. Demler, and M. D. Lukin. "High-Temperature Superfluidity of Fermionic Atoms in Optical Lattices". In: *Phys. Rev. Lett.* 89 (22 2002), p. 220407. DOI: 10.1103/PhysRevLett.89.220407 (cit. on p. 2).

[32] W. V. Liu, F. Wilczek, and P. Zoller. "Spin-dependent Hubbard model and a quantum phase transition in cold atoms". In: *Phys. Rev. A* 70 (3 2004), p. 033603. DOI: 10.1103/PhysRevA.70.033603 (cit. on pp. 2, 9).

[33] M. Köhl, H. Moritz, T. Stöferle, K. Günter, and T. Esslinger. "Fermionic Atoms in a Three Dimensional Optical Lattice: Observing Fermi Surfaces, Dynamics, and Interactions". In: *Phys. Rev. Lett.* 94 (8 2005), p. 080403. DOI: 10.1103/PhysRevLett.94.080403 (cit. on pp. 2, 9, 20).

[34] T. Rom, T. Best, D. van Oosten, U. Schneider, S. Fölling, B. Paredes, and I. Bloch. "Free fermion antibunching in a degenerate atomic Fermi gas released from an optical lattice". In: *Nature* 444 (7120 2006), pp. 733 –736. DOI: 10.1038/nature05319 (cit. on p. 2).

[35] J. K. Chin, D. E. Miller, Y. Liu, C. Stan, W. Setiawan, C. Sanner, K. Xu, and W. Ketterle. "Evidence for superfluidity of ultracold fermions in an optical lattice". In: *Nature* 443 (7114 2006), pp. 961 –964. DOI: 10.1038/nature05224 (cit. on pp. 2, 9).

[36] U. Schneider, L. Hackermüller, S. Will, T. Best, I. Bloch, T. A. Costi, R. W. Helmes, D. Rasch, and A. Rosch. "Metallic and Insulating Phases of Repulsively Interacting Fermions in a 3D Optical Lattice". In: *Science* 322.5907 (2008), pp. 1520–1525. DOI: 10.1126/science.1165449 (cit. on pp. 2, 9, 20).

[37] R. W. Helmes, T. A. Costi, and A. Rosch. "Mott Transition of Fermionic Atoms in a Three-Dimensional Optical Trap". In: *Phys. Rev. Lett.* 100 (5 2008), p. 056403. DOI: 10.1103/PhysRevLett.100.056403 (cit. on p. 2).

[38] R. Jördens, N. Strohmaier, K. Gunter, H. Moritz, and T. Esslinger. "A Mott insulator of fermionic atoms in an optical lattice". In: *Nature* 455.7210 (2008), pp. 204–207. DOI: 10.1038/nature07244 (cit. on pp. 2, 9, 20).

[39] G.-B. Jo, Y.-R. Lee, J.-H. Choi, C. A. Christensen, T. H. Kim, J. H. Thywissen, D. E. Pritchard, and W. Ketterle. "Itinerant Ferromagnetism in a Fermi Gas of Ultracold Atoms". In: *Science* 325.5947 (2009), pp. 1521–1524. DOI: 10.1126/science.1177112 (cit. on p. 2).

[40] D. M. Weld and W. Ketterle. "Towards quantum magnetism with ultracold atoms". In: *Journal of Physics: Conference Series* 264.1 (2011), p. 012017 (cit. on p. 2).

[41] S. Trotzky, P. Cheinet, S. Fölling, M. Feld, U. Schnorrberger, A. M. Rey, A. Polkovnikov, E. A. Demler, M. D. Lukin, and I. Bloch. "Time-Resolved Observation and Control of Superexchange Interactions with Ultracold Atoms in Optical Lattices". In: *Science* 319.5861 (2008), p. 295. DOI: 10.1126/science.1150841 (cit. on pp. 2, 9).

[42] R. C. Brown, R. Wyllie, S. B. Koller, E. A. Goldschmidt, M. Foss-Feig, and J. V. Porto. "Two-dimensional superexchange-mediated magnetization dynamics in an optical lattice". In: *Science* 348.6234 (2015), pp. 540–544. DOI: 10.1126/science.aaa1385 (cit. on p. 2).

[43] L. De Leo, C. Kollath, A. Georges, M. Ferrero, and O. Parcollet. "Trapping and Cooling Fermionic Atoms into Mott and Néel States". In: *Phys. Rev. Lett.* 101 (21 2008), p. 210403. DOI: 10.1103/PhysRevLett.101.210403 (cit. on p. 2).

[44] A. Koetsier, R. A. Duine, I. Bloch, and H. T. C. Stoof. "Achieving the Néel state in an optical lattice". In: *Phys. Rev. A* 77 (2 2008), p. 023623. DOI: 10.1103/PhysRevA.77.023623 (cit. on pp. 2, 9).

[45] S. Fuchs, E. Gull, L. Pollet, E. Burovski, E. Kozik, T. Pruschke, and M. Troyer. "Thermodynamics of the 3D Hubbard Model on Approaching the Néel Transition". In: *Phys. Rev. Lett.* 106 (3 2011), p. 030401. DOI: 10.1103/PhysRevLett.106.030401 (cit. on p. 2).

[46] T. A. Corcovilos, S. K. Baur, J. M. Hitchcock, E. J. Mueller, and R. G. Hulet. "Detecting antiferromagnetism of atoms in an optical lattice via optical Bragg scattering". In: *Phys. Rev. A* 81 (1 2010), p. 013415. DOI: 10.1103/PhysRevA.81.013415 (cit. on p. 2).

[47] J. Simon, W. S. Bakr, R. Ma, M. E. Tai, P. M. Preiss, and M. Greiner. "Quantum simulation of antiferromagnetic spin chains in an optical lattice". In: *Nature* 472.7343 (2011), pp. 307–312. DOI: 10.1038/nature09994 (cit. on p. 2).

[48] T. Paiva, Y. L. Loh, M. Randeria, R. T. Scalettar, and N. Trivedi. "Fermions in 3D Optical Lattices: Cooling Protocol to Obtain Antiferromagnetism". In: *Phys. Rev. Lett.* 107 (8 2011), p. 086401. DOI: 10.1103/PhysRevLett.107.086401 (cit. on p. 2).

[49] F. Cordobes Aguilar, A. F. Ho, and J. Ruostekoski. "Optical Signatures of Antiferromagnetic Ordering of Fermionic Atoms in an Optical Lattice". In: *Phys. Rev. X* 4 (3 2014), p. 031036. DOI: 10.1103/PhysRevX.4.031036 (cit. on p. 2).

[50] R. G. Hulet, P. M. Duarte, R. A. Hart, and T.-L. Yang. "Antiferromagnetism with Ultracold Atoms". In: *ArXiv* arXiv:1512.05311 (1 2015), p. 013415 (cit. on p. 2).

[51] D. Greif, T. Uehlinger, G. Jotzu, L. Tarruell, and T. Esslinger. "Short-Range Quantum Magnetism of Ultracold Fermions in an Optical Lattice". In: *Science* 340.6138 (2013), pp. 1307–1310. DOI: 10.1126/science.1236362 (cit. on pp. 2, 20).

[52] I. Bloch, J. Dalibard, and S. Nascimbene. "Quantum simulations with ultracold quantum gases". In: *Nat. Phys.* 8.4 (2012), pp. 267–276. DOI: 10.1038/nphys2259 (cit. on p. 2).

[53] T. Esslinger. "Fermi-Hubbard Physics with Atoms in an Optical Lattice". In: *Annual Review of Condensed Matter Physics* 1.1 (2010), pp. 129–152. DOI: 10.1146/annurev-conmatphys-070909-104059 (cit. on pp. 2, 6, 9, 113).

[54] J. V. Porto. "Cold-Atom Magnetism". In: *Science* 340.6138 (2013), pp. 1297–1298. DOI: 10.1126/science.1239873 (cit. on p. 2).

[55] R. Grimm, M. Weidemüller, and Y. B. Ovchinnikov. "Optical Dipole Traps for Neutral Atoms". In: Advances In Atomic, Molecular, and Optical Physics 42 (2000). Ed. by B. Bederson and H. Walther, pp. 95–170. DOI: http://dx.doi.org/10.1016/S1049-250X(08)60186-X (cit. on p. 5).

[56] M. Lewenstein, A. Sanpera, and V. Ahufinger. *Ultracold Atoms in Optical Lattices: Simulating quantum many-body systems*. first. Oxford University Press, 2012 (cit. on pp. 5, 6, 9).

[57] D. Jaksch and P. Zoller. "Creation of effective magnetic fields in optical lattices: the Hofstadter butterfly for cold neutral atoms". In: *New J. Phys.* 5 (2003), p. 56 (cit. on p. 5).

[58] H. Katori. "Optical lattice clocks and quantum metrology". In: *Nat. Photon.* 5.4 (2011), pp. 203–210. DOI: 10.1038/nphoton.2011.45 (cit. on pp. 6, 7, 65).

[59] N. Hinkley, J. A. Sherman, N. B. Phillips, M. Schioppo, N. D. Lemke, K. Beloy, M. Pizzocaro, C. W. Oates, and A. D. Ludlow. "An Atomic Clock with 10^{18} Instability". In: *Science* 341.6151 (2013), pp. 1215–1218. DOI: 10.1126/science.1240420 (cit. on p. 6).

[60] M. D. Swallows, M. J. Martin, M. Bishof, C. Benko, Y. Lin, S. Blatt, A. M. Rey, and J. Ye. "Operating a ^{87}Sr optical lattice clock with high precision and at high density". In: *IEEE Transactions on Ultrasonics, Ferroelectrics, and Frequency Control* 59 (59 2012), pp. 416–625 (cit. on p. 6).

[61] T. L. Nicholson, M. J. Martin, J. R. Williams, B. J. Bloom, M. Bishof, M. D. Swallows, S. L. Campbell, and J. Ye. "Comparison of Two Independent Sr Optical Clocks with 1×10^{-17} Stability at 10^3 s". In: *Phys. Rev. Lett.* 109 (23 2012), p. 230801. DOI: 10.1103/PhysRevLett.109.230801 (cit. on p. 6).

[62] T. Nicholson et al. "Systematic evaluation of an atomic clock at 2×10^{-18} total uncertainty". In: *Nat Commun* 6 (2015). DOI: 10.1038/ncomms7896 (cit. on p. 6).

[63] J. Ye, H. J. Kimble, and H. Katori. "Quantum State Engineering and Precision Metrology Using State-Insensitive Light Traps". In: *Science* 320.5884 (2008), pp. 1734–1738. DOI: 10.1126/science.1148259 (cit. on pp. 7, 65).

[64] G. K. Campbell et al. "Probing Interactions Between Ultracold Fermions". In: *Science* 324.5925 (2009), pp. 360–363. DOI: 10.1126/science.1169724 (cit. on p. 7).

[65] R. Ciuryło, E. Tiesinga, and P. S. Julienne. "Optical tuning of the scattering length of cold alkaline-earth-metal atoms". In: *Phys. Rev. A* 71 (3 2005), p. 030701. DOI: 10.1103/PhysRevA.71.030701 (cit. on p. 7).

[66] M. Bishof, Y. Lin, M. D. Swallows, A. V. Gorshkov, J. Ye, and A. M. Rey. "Resolved Atomic Interaction Sidebands in an Optical Clock Transition". In: *Phys. Rev. Lett.* 106 (25 2011), p. 250801. DOI: 10.1103/PhysRevLett.106.250801 (cit. on p. 7).

[67] A. D. Ludlow et al. "Sr Lattice Clock at 1×10^{-16} Fractional Uncertainty by Remote Optical Evaluation with a *Ca* Clock". In: *Science* 319.5871 (2008), pp. 1805–1808. DOI: 10.1126/science.1153341 (cit. on p. 7).

[68] S. Falke et al. "A strontium lattice clock with 3×10^{-17} inaccuracy and its frequency". In: *New Journal of Physics* 16.7 (2014), p. 073023 (cit. on p. 7).

[69] C. Cohen-Tannoudji, B. Diu, and F. Laloë. *Quantenmechanik Band 1 & 2*. fourth. Walter de Gruyter GmbH & Co. KG, 2009 (cit. on pp. 7, 126, 150, 153).

[70] C. Cohen-Tannoudji, J. Dunpont-Roc, and G. Grynberg. *Atom-Photon Interactions: Basic Process and Applications: Basic Processes and Applications*. first. Wiley-VCH, 2010 (cit. on p. 7).

[71] H. Haken and H. C. Wolf. *Atom- und Quantenphysik: Einführung in die experimentellen und theoretischen Grundlagen*. Eight. Springer, 2004 (cit. on pp. 7, 30).

[72] L. D. Landau and E. M. Lifshitz. *Quantum Mechanics: Non-Relativistic Theory*. Third Revised. Butterworth-Heinemann, 1981 (cit. on pp. 7, 112, 116, 153).

[73] M. Takamoto, F.-L. Hong, R. Higashi, and H. Katori. "An optical lattice clock". In: *Nature* 435.7040 (2005), p. 321. DOI: 10.1038/nature03541 (cit. on pp. 7, 65).

[74] H. Katori, K. Hashiguchi, E. Y. Il'inova, and V. D. Ovsiannikov. "Magic Wavelength to Make Optical Lattice Clocks Insensitive to Atomic Motion". In: *Phys. Rev. Lett.* 103.15 (2009), p. 153004. DOI: 10.1103/PhysRevLett.103.153004 (cit. on p. 7).

[75] M. J. Martin, M. Bishof, M. D. Swallows, X. Zhang, C. Benko, J. von Stecher, A. V. Gorshkov, A. M. Rey, and J. Ye. "A Quantum Many-Body Spin System in an Optical Lattice Clock". In: *Science* 341.6146 (2013), pp. 632–636. DOI: 10.1126/science.1236929 (cit. on p. 8).

[76] A. J. Daley, M. M. Boyd, J. Ye, and P. Zoller. "Quantum Computing with Alkaline-Earth-Metal Atoms". In: *Phys. Rev. Lett.* 101.17 (2008), p. 170504. DOI: 10.1103/PhysRevLett.101.170504 (cit. on pp. 8, 20).

[77] A. V. Gorshkov, A. M. Rey, A. J. Daley, M. M. Boyd, J. Ye, P. Zoller, and M. D. Lukin. "Alkaline-Earth-Metal Atoms as Few-Qubit Quantum Registers". In: *Phys. Rev. Lett.* 102.11 (2009), p. 110503. DOI: 10.1103/PhysRevLett.102.110503 (cit. on p. 8).

[78] A. D. Ludlow, N. D. Lemke, J. A. Sherman, C. W. Oates, G. Quéméner, J. von Stecher, and A. M. Rey. "Cold-collision-shift cancellation and inelastic scattering in a Yb optical lattice clock". In: *Phys. Rev. A* 84 (5 2011), p. 052724. DOI: 10.1103/PhysRevA.84.052724 (cit. on pp. 8, 65).

[79] M. M. Boyd, T. Zelevinsky, A. D. Ludlow, S. Blatt, T. Zanon-Willette, S. M. Foreman, and J. Ye. "Nuclear spin effects in optical lattice clocks". In: *Phys. Rev. A* 76.2 (2007), p. 022510. DOI: 10.1103/PhysRevA.76.022510 (cit. on p. 8).

[80] M. D. Swallows, M. Bishof, Y. Lin, S. Blatt, M. J. Martin, A. M. Rey, and J. Ye. "Suppression of Collisional Shifts in a Strongly Interacting Lattice Clock". In: *Science* 331.6020 (2011), pp. 1043–1046. DOI: 10.1126/science.1196442 (cit. on p. 8).

[81] A. M. Rey, A. V. Gorshkov, and C. Rubbo. "Many-Body Treatment of the Collisional Frequency Shift in Fermionic Atoms". In: *Phys. Rev. Lett.* 103 (26 2009), p. 260402. DOI: 10.1103/PhysRevLett.103.260402 (cit. on pp. 8, 65).

[82] A. V. Gorshkov, M. Hermele, V. Gurarie, C. Xu, P. S. Julienne, J. Ye, P. Zoller, E. Demler, M. D. Lukin, and A. M. Rey. "Two-orbital SU(N) magnetism with ultracold alkaline-earth atoms". In: *Nat. Phys.* 6.4 (2010), pp. 289–295. DOI: 10.1038/nphys1535 (cit. on pp. 8, 20).

[83] X. Zhang, M. Bishof, S. L. Bromley, C. V. Kraus, M. S. Safronova, P. Zoller, A. M. Rey, and J. Ye. "Spectroscopic observation of SU(N)-symmetric interactions in Sr orbital magnetism". In: *Science* 345.6203

(2014), pp. 1467–1473. DOI: 10.1126/science.1254978 (cit. on pp. 8, 20).

[84] F. Scazza, M. Hofrichter C. Hofer, P. C. De Groot, I. Bloch, and S. Fölling. "Observation of two-orbital spin-exchange interactions with ultracold SU(N)-symmetric fermions". In: *Nat. Phys.* 10.10 (2015), pp. 779–784. DOI: 10.1038/nphys3061 (cit. on pp. 8, 20).

[85] M. Aidelsburger, M. Atala, S. Nascimbène, S. Trotzky, Y.-A. Chen, and I. Bloch. "Experimental Realization of Strong Effective Magnetic Fields in an Optical Lattice". In: *Phys. Rev. Lett.* 107 (25 2011), p. 255301. DOI: 10.1103/PhysRevLett.107.255301 (cit. on p. 8).

[86] S. Stellmer. "Degenerate quantum gases of strontium". PhD thesis. Universität Innsbruck, 2013 (cit. on p. 8).

[87] F. Gerbier and J. Dalibard. "Gauge fields for ultracold atoms in optical superlattices". In: *New Journal of Physics* 12.3 (2010), p. 033007 (cit. on p. 8).

[88] N. F. Mott. *Metal-insulator Transitions*. First. Taylor & Francis Ltd, 1974 (cit. on pp. 8, 9).

[89] B. H. Brandow. "Theory of mott insulators". In: *International Journal of Quantum Chemistry* 10.S10 (1976), pp. 417–434. DOI: 10.1002/qua.560100845 (cit. on p. 8).

[90] E. H. Lieb. "Two theorems on the Hubbard model". In: *Phys. Rev. Lett.* 62 (10 1989), pp. 1201–1204. DOI: 10.1103/PhysRevLett.62.1201 (cit. on p. 9).

[91] E. H. Lieb and F. Wu. "The one-dimensional Hubbard model: a reminiscence". In: *Physica A: Statistical Mechanics and its Applications* 321.1-2 (2003). Statphys-Taiwan-2002: Lattice Models and Complex Systems, pp. 1 –27. DOI: http://dx.doi.org/10.1016/S0378-4371(02)01785-5 (cit. on p. 9).

[92] A. E. Ruckenstein, P. J. Hirschfeld, and J. Appel. "Mean-field theory of high-T_c superconductivity: The superexchange mechanism". In: *Phys. Rev. B* 36 (1 1987), pp. 857–860. DOI: 10.1103/PhysRevB.36.857 (cit. on p. 9).

[93] S. K. Pati, R. R. P. Singh, and D. I. Khomskii. "Alternating Spin and Orbital Dimerization and Spin-Gap Formation in Coupled Spin-Orbital Systems". In: *Phys. Rev. Lett.* 81.24 (1998), pp. 5406–5409. DOI: 10.1103/PhysRevLett.81.5406 (cit. on p. 9).

[94] A. Bühler and H. P. Büchler. "Supersolid phase in atomic gases with magnetic dipole interaction". In: *Phys. Rev. A* 84 (2 2011), p. 023607. DOI: 10.1103/PhysRevA.84.023607 (cit. on p. 9).

[95] S. Giorgini, L. P. Pitaevskii, and S. Stringari. "Theory of ultracold atomic Fermi gases". In: *Rev. Mod. Phys.* 80.4 (2008), pp. 1215–1274. DOI: 10.1103/RevModPhys.80.1215 (cit. on pp. 9, 113).

[96] M Snoek, I Titvinidze, C Tőke, K Byczuk, and W Hofstetter. "Antiferromagnetic order of strongly interacting fermions in a trap: real-space dynamical mean-field analysis". In: *New Journal of Physics* 10.9 (2008), p. 093008 (cit. on p. 9).

[97] C. Honerkamp and W. Hofstetter. "Ultracold Fermions and the $SU(N)$ Hubbard Model". In: *Phys. Rev. Lett.* 92.17 (2004), p. 170403. DOI: 10.1103/PhysRevLett.92.170403 (cit. on p. 9).

[98] S. Chiesa, C. N. Varney, M. Rigol, and R. T. Scalettar. "Magnetism and Pairing of Two-Dimensional Trapped Fermions". In: *Phys. Rev. Lett.* 106.3 (2011), p. 035301. DOI: 10.1103/PhysRevLett.106.035301 (cit. on p. 9).

[99] A. Rapp, W. Hofstetter, and G. Zaránd. "Trionic phase of ultracold fermions in an optical lattice: A variational study". In: *Phys. Rev. B* 77.14 (2008), p. 144520. DOI: 10.1103/PhysRevB.77.144520 (cit. on p. 9).

[100] K. Huang. *Statistical Mechanics*. second. John Wiley & Sons, 1987 (cit. on pp. 9, 36, 44, 45, 135).

[101] L. D. Landau and E. M. Lifshitz. *Statistical Physics 1 & 2*. Third. Butterworth-Heinemann, 1981 (cit. on pp. 9, 36, 44, 135).

[102] M. Fähnle. *Lecture notes: Theory of Phase Transitions 1 & 2*. 2012 (cit. on p. 9).

[103] S. Sachdev. *Quantum Phase Transitions*. first. Cambridge University Press, 1999 (cit. on p. 9).

[104] M. Vojta. "Quantum phase transitions". In: *Reports on Progress in Physics* 66.12 (2003), p. 2069 (cit. on p. 9).

[105] F. H. L. Essler, H. Frahm, F. Göhmann, A. Klümper, and V. E. Korepin. *The One-Dimensional Hubbard Model*. First. Cambridge University Press, 2010 (cit. on pp. 9, 11, 12, 15).

[106] J. R. Schrieffer and P. A. Wolff. "Relation between the Anderson and Kondo Hamiltonians". In: *Phys. Rev.* 149 (2 1966), pp. 491–492. DOI: 10.1103/PhysRev.149.491 (cit. on pp. 11, 84).

[107] G. Czycholl. *Theoretische Festkörperphysik*. Third. Springer, 2007 (cit. on pp. 11, 15, 16, 24, 62, 112, 120, 125).

[108] G.Grosso and G. P. Parravicini. *Solid State Physics*. Sixth. Academic Pr Inc, 2000 (cit. on pp. 11, 15, 16, 112).

[109] J. Lapuszanski. *Magnetism in Metals and Metallic Compounds*. First. Springer US, 1976 (cit. on pp. 11, 15).

[110] S. Bravyi, D. P. DiVincenzo, and D. Loss. "Schrieffer–Wolff transformation for quantum many-body systems". In: *Annals of Physics* 326.10 (2011), pp. 2793 –2826. DOI: http://dx.doi.org/10.1016/j.aop.2011.06.004 (cit. on p. 11).

[111] J. Spałek. "t-J model then and now: A personal perspective from the pioneering times". In: *arXiv:0706.4236* (2007) (cit. on pp. 11, 12, 15, 16, 52, 61, 142).

[112] M. M. Salomaa. "Schrieffer-Wolff transformation for the Anderson Hamiltonian in a superconductor". In: *Phys. Rev. B* 37 (16 1988), pp. 9312–9317. DOI: 10.1103/PhysRevB.37.9312 (cit. on p. 11).

[113] A. L. Chernyshev, D. Galanakis, P. Phillips, A. V. Rozhkov, and A.-M. S. Tremblay. "Higher order corrections to effective low-energy theories for strongly correlated electron systems". In: *Phys. Rev. B* 70 (23 2004), p. 235111. DOI: 10.1103/PhysRevB.70.235111 (cit. on p. 11).

[114] K. A. Chao, J. Spałek, and A. M. Ole ś. "Kinetic exchange interaction in a narrow S-band". In: *Journal of Physics C: Solid State Physics* 10.10 (1977), p. L271 (cit. on pp. 11, 15).

[115] J. Spałek, A. M. Ole ś, and K. A. Chao. "Kinetic exchange interaction for magnetic impurities in metals: Nondegenerate Wolff model". In: *Phys. Rev. B* 18 (7 1978), pp. 3748–3752. DOI: 10.1103/PhysRevB.18.3748 (cit. on p. 11).

[116] A. Auerbach. *Interacting Electrons and Quantum Magnetism*. Corrected 2nd. Springer, 1998 (cit. on pp. 11, 16).

[117] M. Potthoff. *Lecture notes: Vielteilchentheorie*. 2008 (cit. on pp. 11, 15).

[118] W. Nolting and A. Ramakanth. *Quantum Theory of Magnetism*. First. Springer, 2010 (cit. on pp. 11, 15).

[119] J. Spałek. "Effect of pair hopping and magnitude of intra-atomic interaction on exchange-mediated superconductivity". In: *Phys. Rev. B* 37 (1 1988), pp. 533–536. DOI: 10.1103/PhysRevB.37.533 (cit. on p. 16).

[120] F. Schwabl. *Quantenmechanik für Fortgeschrittene*. Fifth. Springer, 2008 (cit. on pp. 16, 112, 116).

[121] G. Blatter. *Lecture notes: Quantenmechanik I*. 2005 (cit. on pp. 16, 112, 116, 153).

[122] A. Bühler and H. P. Büchler. *In preparation*. 2015 (cit. on p. 19).

[123] K. I. Kugel' and D. I. Khomskii. "Crystal structure and magnetic properties of substances with orbital degeneracy". In: *Soviet Physics JETP* 37.4 (1973), pp. 725–730 (cit. on p. 19).

[124] K. I. Kugel' and D. I. Khomskii. "The Jahn-Teller effect and magnetism: transition metal compounds". In: *Soviet Physics Uspekhi* 25.4 (1982), pp. 231–256. DOI: 10.1070/PU1982v025n04 (cit. on p. 19).

[125] Y. Tokura and N. Nagaosa. "Orbital Physics in Transition-Metal Oxides". In: *Science* 288.5465 (200), pp. 462–468. DOI: 10.1126/science.288.5465.462 (cit. on p. 19).

[126] G. Khaliullin. "Orbital Order and Fluctuations in Mott Insulators". In: *Progress of Theoretical Physics Supplement* 160 (2005), pp. 155–202. DOI: 10.1143/PTPS.160.155 (cit. on p. 19).

[127] K. Wu and H. Zhai. "Theory of quantum antiferromagnetism of fermions in an optical lattice with a half-filled p band". In: *Phys. Rev. B* 77 (17 2008), p. 174431. DOI: 10.1103/PhysRevB.77.174431 (cit. on p. 20).

[128] P. Hauke, E. Zhao, K. Goyal, I. H. Deutsch, W. V. Liu, and M. Lewenstein. "Orbital order of spinless fermions near an optical Feshbach resonance". In: *Phys. Rev. A* 84 (5 2011), p. 051603. DOI: 10.1103/PhysRevA.84.051603 (cit. on p. 20).

[129] T. Müller, S. Fölling, A. Widera, and I. Bloch. "State Preparation and Dynamics of Ultracold Atoms in Higher Lattice Orbitals". In: *Phys. Rev. Lett.* 99 (20 2007), p. 200405. DOI: 10.1103/PhysRevLett.99.200405 (cit. on p. 20).

[130] C. Xu and M. P. A. Fisher. "Bond algebraic liquid phase in strongly correlated multiflavor cold atom systems". In: *Phys. Rev. B* 75 (10 2007), p. 104428. DOI: 10.1103/PhysRevB.75.104428 (cit. on p. 20).

[131] R. B. Diener and T.-L. Ho. "Fermions in Optical Lattices Swept across Feshbach Resonances". In: *Phys. Rev. Lett.* 96 (1 2006), p. 010402. DOI: 10.1103/PhysRevLett.96.010402 (cit. on p. 20).

[132] L. Wang, X. Dai, S. Chen, and X. C. Xie. "Magnetism of cold fermionic atoms on the p band of an optical lattice". In: *Phys. Rev. A* 78 (2 2008), p. 023603. DOI: 10.1103/PhysRevA.78.023603 (cit. on p. 20).

[133] S. Zhang, H.-h. Hung, and C. Wu. "Proposed realization of itinerant ferromagnetism in optical lattices". In: *Phys. Rev. A* 82 (5 2010), p. 053618. DOI: 10.1103/PhysRevA.82.053618 (cit. on p. 20).

[134] E. Zhao and W. V. Liu. "Orbital Order in Mott Insulators of Spinless p-Band Fermions". In: *Phys. Rev. Lett.* 100 (16 2008), p. 160403. DOI: 10.1103/PhysRevLett.100.160403 (cit. on p. 20).

[135] N. Gemelke, E. Sarajlic, Y. Bidel, S. Hong, and S. Chu. "Parametric Amplification of Matter Waves in Periodically Translated Optical Lattices". In: *Phys. Rev. Lett.* 95 (17 2005), p. 170404. DOI: 10.1103/PhysRevLett.95.170404 (cit. on p. 20).

[136] H. Lignier, C. Sias, D. Ciampini, Y. Singh, A. Zenesini, O. Morsch, and E. Arimondo. "Dynamical Control of Matter-Wave Tunneling in Periodic Potentials". In: *Phys. Rev. Lett.* 99 (22 2007), p. 220403. DOI: 10.1103/PhysRevLett.99.220403 (cit. on p. 20).

[137] G. Wirth, M. Ölschläger, and A. Hemmerich. "Evidence for orbital superfluidity in the P-band of a bipartite optical square lattice". In: *Nat. Phys.* 7 (2 2011), pp. 147–153. DOI: 10.1038/nphys1857 (cit. on p. 20).

[138] C. V. Parker, L.-C. Ha, and C. Chin. "Direct observation of effective ferromagnetic domains of cold atoms in a shaken optical lattice". In: *Nat. Phys.* 9.12 (2013), pp. 769–774. DOI: 10.1038/nphys2789 (cit. on p. 20).

[139] M. Di Liberto, D. Malpetti, G. I. Japaridze, and C. Morais Smith. "Ultracold fermions in a one-dimensional bipartite optical lattice: Metal-insulator transitions driven by shaking". In: *Phys. Rev. A* 90 (2 2014), p. 023634. DOI: 10.1103/PhysRevA.90.023634 (cit. on p. 20).

[140] X. Li and W. V. Liu. "Physics of higher orbital bands in optical lattices: a review". In: *arXiv:1508.06285* (2015) (cit. on p. 20).

[141] N. W. Ashcroft and N. D. Mermin. *Solid State Physics*. International. Harcourt Brace College Publishers, 1975 (cit. on pp. 24, 43, 59, 62, 111, 112, 120, 138).

[142] D. Y. Xing, M Liu, and C. D. Gong. "Van Hove singularity and isotope effect in high-T_c copper oxides". In: *Phys. Rev. B* 44.33 (1991), pp. 525–530 (cit. on p. 24).

[143] S. Noorani. "Magnetism with fermionic atoms in optical lattices with orbital degree of freedom". Bachelor thesis. Universität Stuttgart, 2015 (cit. on pp. 30, 69).

[144] M. Sigrist. *Lecture notes: Solid State Theory*. 2014 (cit. on pp. 36, 43, 45, 59).

[145] K. Kopitzki and P. Herzog. *Einführung in die Festkörperphysik*. sixth. Teubner Studienbücher, 2007 (cit. on pp. 43, 59).

[146] S. Blundell. *Magnetism In Condensed Matter*. first. Oxford University Press, 2000 (cit. on pp. 43, 138).

[147] K. A. Chao, J. Spałek, and A. M. Ole ś. "Canonical perturbation expansion of the Hubbard model". In: *Phys. Rev. B* 18 (7 1978), pp. 3453–3464. DOI: 10.1103/PhysRevB.18.3453 (cit. on pp. 52, 61).

[148] J. Spałek. "Microscopic model of hybrid pairing: A common approach to heavy-fermion and high-T_c superconductivity". In: *Phys. Rev. B* 38 (1 1988), pp. 208–212. DOI: 10.1103/PhysRevB.38.208 (cit. on pp. 52, 61).

[149] L.-G. Levy. *Magnetism and Superconductivity*. first. Springer, 2000 (cit. on pp. 59, 77).

[150] P. M. Chaikin and T. C. Lubensky. *Principles of condensed matter physics*. first. Cambridge University Press, 1995 (cit. on p. 62).

[151] F. Werner, O. Parcollet, A. Georges, and S. R. Hassan. "Interaction-Induced Adiabatic Cooling and Antiferromagnetism of Cold Fermions in Optical Lattices". In: *Phys. Rev. Lett.* 95 (5 2005), p. 056401. DOI: 10.1103/PhysRevLett.95.056401 (cit. on p. 62).

[152] S. Fölling, S. Trotzky, P. Cheinet, R. Feld M.and Saers, A. Widera, T. Müller, and I. Bloch. "Direct observation of second-order atom tunnelling". In: *Nature* 448 (7157 2007), pp. 1029–1032. DOI: 10.1038/nature06112 (cit. on p. 65).

[153] A. Rey et al. "Probing many-body interactions in an optical lattice clock". In: *Annals of Physics* 340.1 (2014), pp. 311 –351. DOI: http://dx.doi.org/10.1016/j.aop.2013.11.002 (cit. on p. 65).

[154] N. D. Lemke, J. von Stecher, J. A. Sherman, A. M. Rey, C. W. Oates, and A. D. Ludlow. "p-Wave Cold Collisions in an Optical Lattice Clock". In: *Phys. Rev. Lett.* 107 (10 2011), p. 103902. DOI: 10.1103/PhysRevLett.107.103902 (cit. on p. 65).

[155] M. Bishof, M. J. Martin, M. D. Swallows, C. Benko, Y. Lin, G. Quéméner, A. M. Rey, and J. Ye. "Inelastic collisions and density-dependent excitation suppression in a ^{87}Sr optical lattice clock". In: *Phys. Rev. A* 84 (5 2011), p. 052716. DOI: 10.1103/PhysRevA.84.052716 (cit. on p. 65).

[156] A. Y. Kitaev. "Unpaired Majorana fermions in quantum wires". In: *Physics-Uspekhi* 44.10S (2001), pp. 131–136 (cit. on pp. 71, 73, 75, 101).

[157] D. A. Ivanov. "Non-Abelian Statistics of Half-Quantum Vortices in p-Wave Superconductors". In: *Phys. Rev. Lett.* 86 (2 2001), pp. 268–271. DOI: 10.1103/PhysRevLett.86.268 (cit. on p. 71).

[158] S.-Q. Shen. *Topological Insulators*. first. Springer, 2012 (cit. on pp. 72–74, 101).

[159] N. Lang. "Phase transitions and topological phases by driven dissipation". Master thesis. Universität Stuttgart, 2013 (cit. on p. 75).

[160] C. V. Kraus, M. Dalmonte, M. A. Baranov, A. M. Läuchli, and P. Zoller. "Majorana Edge States in Atomic Wires Coupled by Pair Hopping". In: *Phys. Rev. Lett.* 111 (17 2013), p. 173004 (cit. on pp. 75, 97).

[161] B. A. Bernevig and T. L. Hughes. *Topological Insulators and Topological Superconductors*. first. Cambridge University Press, 2013 (cit. on pp. 75, 101).

[162] C. W. J. Beenakker. "Search for Majorana Fermions in Superconductors". In: *Annu. Rev. Con. Mat. Phys.* 4 (2013), p. 113 (cit. on pp. 75, 77).

[163] F. Wilczek. "Majorana returns". In: *Nat. Phys.* 5.9 (2009), pp. 614–618. DOI: 10.1038/nphys1380 (cit. on p. 75).

[164] R. F. Service. "Search for Majorana Fermions Nearing Success at Last?" In: *Science* 332.6026 (2011), pp. 193–195. DOI: 10.1126/science.332.6026.193 (cit. on pp. 75, 76).

[165] N. Lang and H. P. Büchler. "Topological states in a microscopic model of interacting fermions". In: *Phys. Rev. B* 92 (4 2015), p. 041118. DOI: 10.1103/PhysRevB.92.041118 (cit. on p. 75).

[166] A. Stern. "Non-Abelian states of matter". In: *Nature* 464.7286 (2010), pp. 187–193. DOI: 10.1038/nature08915 (cit. on p. 75).

[167] J. Alicea, Y. Oreg, G. Refael, F. von Oppen, and M. P. A. Fisher. "Non-Abelian statistics and topological quantum information processing in 1D wire networks". In: *Nat. Phys.* 7.5 (2011), pp. 412–217. DOI: 10.1038/nphys1915 (cit. on p. 75).

[168] M. Z. Hasan and C. L. Kane. "*Colloquium* : Topological insulators". In: *Rev. Mod. Phys.* 82 (4 2010), pp. 3045–3067. DOI: 10.1103/RevModPhys.82.3045 (cit. on p. 75).

[169] A. Kitaev. "Anyons in an exactly solved model and beyond". In: *Ann. Phys.* 321.1 (2006), pp. 2 –111 (cit. on pp. 75, 105).

[170] S. Bosch. *Algebra*. sixth. Springer-Verlag, 2005 (cit. on p. 75).

[171] J. Kramer. *Zahlen für Einsteiger*. first. Friedr. Vieweg & Sohn Verlag, 2008 (cit. on p. 75).

[172] V. Heine. *Group Theory in Quantum Mechanics*. first. Pergamon Press, 1964 (cit. on p. 75).

[173] M. Tinkham. *Group Theory and Quantum Mechanics*. first Dover. Dover Publications, 2004 (cit. on p. 75).

[174] S. Sternberg. *Group Theory and Physics*. first. Cambridge University Press, 1995 (cit. on p. 75).

[175] M. Tinkham. *Introduction to Superconductivity*. second. Dover Publications, 2004 (cit. on pp. 75–77).

[176] P. G. de Gennes. *Superconductivity Of Metals And Alloys*. revised. Westview Press, 1999 (cit. on pp. 76, 77).

[177] A. J. Leggett. *Lecture notes: Superconductivity, Ancient and Modern*. 2008 (cit. on p. 77).

[178] A. Abrikosov, L. Gorkov, and I. Dzyaloshinski. *Methods Of Quantum Field Theory In Statistical Physics*. Revised English. Dover Publications, 1963 (cit. on p. 77).

[179] G Moore and N Read. "Nonabelions in the fractional quantum Hall effect". In: *Nucl. Phys. B* 360.2-3 (1991), pp. 362–396 (cit. on p. 77).

[180] A. Kitaev. "Fault-tolerant quantum computation by anyons". In: *Ann. Phys.* 303.1 (2003), pp. 2–30 (cit. on p. 77).

[181] C. Nayak, S. H. Simon, A. Stern, M. H. Freedman, and S. DasSarma. "Non-Abelian anyons and topological quantum computation". In: *Rev. Mod. Phys.* 80 (2008), p. 1083 (cit. on p. 77).

[182] G. E. Volovik. *Exotic properties of superfluid ^{3}He*. Singapore ; London: World Scientific, 1992 (cit. on p. 77).

[183] K Ishida, H Mukuda, Y Kitaoka, K Asayama, Z. Q. Mao, Y Mori, and Y Maeno. "Spin-triplet superconductivity in Sr2RuO4 identified by 17O Knight shift". In: *Nature* 396.6712 (1998), pp. 658–660 (cit. on p. 77).

[184] P Jiang, H Choi, W Kang, S. H. Simon, L. N. Pfeiffer, K. W. West, and K. W. Baldwin. "Braiding of Abelian and Non-Abelian Anyons in the Fractional Quantum Hall Effect". In: *arXiv:1112.3400* (2011) (cit. on p. 77).

[185] R. L. Willett, C Nayak, K Shtengel, L. N. Pfeiffer, and K. W. West. "Magnetic-Field-Tuned Aharonov-Bohm Oscillations and Evidence for Non-Abelian Anyons at ν=5/2". In: *Phys. Rev. Lett.* 111.18 (2013), p. 186401 (cit. on p. 77).

[186] J. D. Sau, R. M. Lutchyn, S. Tewari, and S. DasSarma. "Generic New Platform for Topological Quantum Computation Using Semiconductor Heterostructures". In: *Phys. Rev. Lett.* 104.4 (2010), p. 040502 (cit. on p. 77).

[187] J. Alicea. "Majorana fermions in a tunable semiconductor device". In: *Phys. Rev. B* 81.12 (2010), p. 125318 (cit. on p. 77).

[188] Y. Oreg, G. Refael, and F. von Oppen. "Helical Liquids and Majorana Bound States in Quantum Wires". In: *Phys. Rev. Lett.* 105 (17 2010), p. 177002. DOI: 10.1103/PhysRevLett.105.177002 (cit. on p. 77).

[189] R. M. Lutchyn, J. D. Sau, and S. Das Sarma. "Majorana Fermions and a Topological Phase Transition in Semiconductor-Superconductor Heterostructures". In: *Phys. Rev. Lett.* 105 (7 2010), p. 077001. DOI: 10.1103/PhysRevLett.105.077001 (cit. on p. 77).

[190] V Mourik, K Zuo, S. M. Frolov, S. R. Plissard, E. P. A. M. Bakkers, and L. P. Kouwenhoven. "Signatures of Majorana Fermions in Hybrid Superconductor-Semiconductor Nanowire Devices". In: *Science* 336.6084 (2012), pp. 1003–1007 (cit. on p. 77).

[191] A. Das, Y. Ronen, Y. Most, Y. Oreg, M. Heiblum, and H. Shtrikman. "Zero-bias peaks and splitting in an Al-InAs nanowire topological superconductor as a signature of Majorana fermions". In: *Nature Phys.* 8.12 (2012), pp. 887 –895 (cit. on p. 77).

[192] V Gurarie and L Radzihovsky. "Resonantly paired fermionic superfluids". In: *Ann. Phys.* 322.1 (2007), pp. 2–119 (cit. on p. 78).

[193] J Zhang, E. G. M. van Kempen, T Bourdel, L Khaykovich, J Cubizolles, F Chevy, M Teichmann, L Tarruell, S. J. J. M. F. Kokkelmans, and C Salomon. "P -wave Feshbach resonances of ultracold ^{6}Li". In: *Phys. Rev. A* 70.3 (2004), p. 030702 (cit. on p. 78).

[194] J. P. Gaebler, J. T. Stewart, J. L. Bohn, and D. S. Jin. "p-Wave Feshbach Molecules". In: *Phys. Rev. Lett.* 98.20 (2007), p. 200403 (cit. on p. 78).

[195] D. V. Efremov and L. Viverit. "p-wave Cooper pairing of fermions in mixtures of dilute Fermi and Bose gases". In: *Phys. Rev. B* 65 (13 2002), p. 134519. DOI: 10.1103/PhysRevB.65.134519 (cit. on p. 78).

[196] D. W. Wang, M Lukin, and E Demler. "Engineering superfluidity in Bose-Fermi mixtures of ultracold atoms". In: *Phys. Rev. A* 72.5 (2005), p. 051604 (cit. on p. 78).

[197] P Massignan, A Sanpera, and M Lewenstein. "Creating p-wave superfluids and topological excitations in optical lattices". In: *Phys. Rev. A* 81.3 (2010), p. 031607 (cit. on p. 78).

[198] N. R. Cooper and G. V. Shlyapnikov. "Stable Topological Superfluid Phase of Ultracold Polar Fermionic Molecules". In: *Phys. Rev. Lett.* 103.15 (2009), p. 155302 (cit. on p. 78).

[199] Y. J. Han, Y. H. Chan, W Yi, A Daley, S Diehl, P Zoller, and L. M. Duan. "Stabilization of the p-Wave Superfluid State in an Optical Lattice". In: *Phys. Rev. Lett.* 103.7 (2009), p. 070404 (cit. on p. 78).

[200] C.-E. Bardyn, M. A. Baranov, E. Rico, A. İmamo ğlu, P. Zoller, and S. Diehl. "Majorana Modes in Driven-Dissipative Atomic Superfluids with a Zero Chern Number". In: *Phys. Rev. Lett.* 109 (13 2012), p. 130402. DOI: 10.1103/PhysRevLett.109.130402 (cit. on p. 78).

[201] C. Zhang, S. Tewari, R. M. Lutchyn, and S. Das Sarma. "$p_x + ip_y$ Superfluid from s-Wave Interactions of Fermionic Cold Atoms". In: *Phys. Rev. Lett.* 101 (16 2008), p. 160401. DOI: 10.1103/PhysRevLett.101.160401 (cit. on p. 78).

[202] M. Sato, Y. Takahashi, and S. Fujimoto. "Non-Abelian Topological Order in s-Wave Superfluids of Ultracold Fermionic Atoms". In: *Phys. Rev. Lett.* 103.2 (2009), p. 020401 (cit. on p. 78).

[203] B. Juliá-Díaz, T. Graß, O. Dutta, D. E. Chang, and M. Lewenstein. "Engineering p-wave interactions in ultracold atoms using nanoplasmonic traps". In: *Nature Commun.* 4 (2013), p. 2046 (cit. on p. 78).

[204] R. A. Williams, L. J. LeBlanc, K. Jimenez-Garcia, M. C. Beeler, A. R. Perry, W. D. Phillips, and I. B. Spielman. "Synthetic Partial Waves in Ultracold Atomic Collisions". In: *Science* 335.6066 (2012), pp. 314 –317 (cit. on p. 78).

[205] A. Bühler, N. Lang, C. Kraus, G. Möller, S. Huber, and H. Büchler. "Majorana modes and p-wave superfluids for fermionic atoms in optical lattices". In: *Nat. Commun.* 5 (2014). DOI: 10.1038/ncomms5504 (cit. on pp. 79, 81, 86, 91, 94, 100–108).

[206] H. P. Büchler, M. Hermele, S. D. Huber, M. P. A. Fisher, and P. Zoller. "Atomic Quantum Simulator for Lattice Gauge Theories and Ring Exchange Models". In: *Phys. Rev. Lett.* 95 (4 2005), p. 040402 (cit. on p. 80).

[207] K.-S. Guther. "Majorana Modes in p-wave Superfluids". Bachelor thesis. Universität Stuttgart, 2014 (cit. on pp. 93, 108).

[208] N. D. Mermin and H. Wagner. "Absence of Ferromagnetism or Antiferromagnetism in One- or Two-Dimensional Isotropic Heisenberg Models". In: *Phys. Rev. Lett.* 17 (22 1966), pp. 1133–1136. DOI: 10.1103/PhysRevLett.17.1133 (cit. on p. 100).

[209] N Read and D. Green. "Paired states of fermions in two dimensions with breaking of parity and time-reversal symmetries and the fractional quantum Hall effect". In: *Phys. Rev. B* 61.15 (2000), pp. 10267–10297 (cit. on p. 101).

[210] D. Asahi and N. Nagaosa. "Topological indices, defects, and Majorana fermions in chiral superconductors". In: *Phys. Rev. B* 86 (10 2012), p. 100504 (cit. on pp. 101, 104).

[211] L. Fu, C. Kane, and E. Mele. "Topological Insulators in Three Dimensions". In: *Phys. Rev. Lett.* 98.10 (2007), p. 106803. DOI: 10.1103/PhysRevLett.98.106803 (cit. on p. 101).

[212] L. Fu and C. Kane. "Topological insulators with inversion symmetry". In: *Phys. Rev. B* 76.4 (2007), p. 045302. DOI: 10.1103/PhysRevB.76.045302 (cit. on p. 101).

[213] A. Altland and M. R. Zirnbauer. "Nonstandard symmetry classes in mesoscopic normal-superconducting hybrid structures". In: *Phys. Rev. B* 55.2 (1997), pp. 1142–1161. DOI: 10.1103/PhysRevB.55.1142 (cit. on p. 102).

[214] A. Schnyder, S. Ryu, A. Furusaki, and A. Ludwig. "Classification of topological insulators and superconductors in three spatial dimensions". In: *Phys. Rev. B* 78.19 (2008), p. 195125. DOI: 10.1103/PhysRevB.78.195125 (cit. on p. 102).

[215] A. Kitaev, V. Lebedev, and M. Feigel'man. "Periodic table for topological insulators and superconductors". In: *AIP Conference Proceedings* 22 (2009), pp. 22–30. DOI: 10.1063/1.3149495 (cit. on p. 102).

[216] E. Schonbrun and R. Piestun. "Optical vortices for localized optical lattice site manipulation". In: *Opt. Eng.* 45.2 (2006), pp. 028001–028001–5 (cit. on p. 104).

[217] W. S. Bakr, J. I. Gillen, A. Peng, S. Folling, and M. Greiner. "A quantum gas microscope for detecting single atoms in a Hubbard-regime optical lattice". In: *Nature* 462.7269 (Nov. 2009), pp. 74–77 (cit. on p. 104).

[218] J. F. Sherson, C. Weitenberg, M. Endres, M. Cheneau, I. Bloch, and S. Kuhr. "Single-atom-resolved fluorescence imaging of an atomic Mott insulator". In: *Nature* 467.7311 (Sept. 2010), pp. 68–72 (cit. on p. 104).

[219] F. Nogrette, H. Labuhn, S. Ravets, D. Barredo, L. Beguin, A. Vernier, T. Lahaye, and A. Browaeys. "Single-atom trapping in holographic 2D arrays of microtraps with arbitrary geometries". In: *arXiv:1402.5329* (2014) (cit. on p. 104).

[220] *Periodic Table of Elements*. Los Alamos National Laboratory Chemistry Division, 2015. DOI: http://periodic.lanl.gov/images/periodictable_bw.pdf (cit. on pp. 109, 110).

[221] G. H. Wannier. "The Structure of Electronic Excitation Levels in Insulating Crystals". In: *Phys. Rev.* 52.3 (1937), pp. 191–197. DOI: 10.1103/PhysRev.52.191 (cit. on p. 114).

[222] W. Kohn. "Analytic Properties of Bloch Waves and Wannier Functions". In: *Phys. Rev.* 115.4 (1959), pp. 809–821. DOI: 10.1103/PhysRev.115.809 (cit. on p. 114).

[223] W. Kohn. "Construction of Wannier Functions and Applications to Energy Bands". In: *Phys. Rev. B* 7.10 (1973), pp. 4388–4398. DOI: 10.1103/PhysRevB.7.4388 (cit. on p. 114).

[224] N. Marzari and D. Vanderbilt. "Maximally localized generalized Wannier functions for composite energy bands". In: *Phys. Rev. B* 56.20 (1997), pp. 12847–12865. DOI: 10.1103/PhysRevB.56.12847 (cit. on p. 114).

[225] L. He and D. Vanderbilt. "Exponential Decay Properties of Wannier Functions and Related Quantities". In: *Phys. Rev. Lett.* 86.23 (2001), pp. 5341–5344. DOI: 10.1103/PhysRevLett.86.5341 (cit. on p. 114).

[226] I. Souza, N. Marzari, and D. Vanderbilt. "Maximally localized Wannier functions for entangled energy bands". In: *Phys. Rev. B* 65.3 (2001), p. 035109. DOI: 10.1103/PhysRevB.65.035109 (cit. on p. 114).

[227] T. Lahaye, C. Menotti, L. Santos, M. Lewenstein, and T. Pfau. "The physics of dipolar bosonic quantum gases". In: *Reports on Progress in Physics* 72.12 (2009), p. 126401. DOI: 10.1088/0034-4885/72/12/126401 (cit. on p. 114).

[228] L. Mihaly and M. C. Martin. *Solid State Physics: Problems and Solutions*. Second. Wiley-VCH Verlag GmbH & Co. KGaA, 2008 (cit. on pp. 121, 124, 125).

[229] J. J. Sakurai. *Modern Quantum Mechanics*. Revised. Addison Wesley Longman Publishing Company, 1994 (cit. on pp. 126, 153).

ACKNOWLEDGEMENTS

First of all, I want to thank my supervisor Prof. Dr. H. P. Büchler for the opportunity to write this thesis, for his support through it and for all the discussions about one of the most exciting hobby there is.
Then I want to thank Prof. Dr. G. Wunner for taking care of the second report of my thesis and Prof. Dr. T. Pfau for being Head of the Exam Committee.
A special thanks to Nicolai Lang, David Peter and H. P. Büchler for viable comments regarding this thesis, in addition to Thomas Klumpp for the extended sessions optimizing the layout.
I thank Ildiko Poljak and Oliver Nagel for the nice conversations, all the help with administration and taking care of the daily business in the institute.
During my stay at the institute, I had the pleasure to meet a lot of people and those I thank: Jürgen Falb, Lars Bonnes, Thorsten Beck, Elke and Steffen Klug, Jan Gukelberger, Andreas Hehn, Jens Honer, Karim Bouadim, Eliane Epple, Emanuel Gavartin, the Schildbürger (Michael Hauber, Thorsten Treffon, David Peter), Nicolai Lang, Przemek Bienias, Krzysztof Jachymski, Sebastian Weber and Jan Kumlin.
Last but not least, my extraordinary thanks go to my girlfriend, my family and all my friends for the support throughout this time.